Polygonal Patterned Ground in the Terrestrial Arctic and Mars' Northern Plains: A Study of Quantitative Similarities and Mechanisms of Formation

Tracy E. Allen

Department of Earth Sciences, Dalhousie University,

Halifax, Nova Scotia, Canada B3H 3J5

Submitted in partial fulfillment of the requirements for the degree of Bachelor of Science (Honours) at Dalhousie University, March 22, 2004

Dalhousie University

Department of Earth Sciences
Halifax, Nova Scotia
Canada B3H 3J5
(902) 494-2358
FAX (902) 494-6889

DATE Apr 27, 2004

AUTHOR Tracy E. Allen

TITLE Polygonal Patterned Ground in the Terrestrial Arctic and Mars: Northern Plains: A Study of Quantitative Similarities and Mechanisms of Formation

Degree BSc Convocation Oct 2004 Year 2004

Permission is herewith granted to Dalhousie University to circulate and to have copied for non-commercial purposes, at its discretion, the above title upon the request of individuals or institutions.

ABSTRACT

Polygonal features of diameter 20–200 m, recently identified at mid-high latitudes of Mars in high resolution (1.5-13 m/pixel) digital images, are visually similar to ice-wedge patterns that form by seasonal cooling of ice-rich permafrost in Earth's arctic regions. Other hypotheses for Mars networks include desiccation, structural bending, or deep climatic cooling. Here I investigate these hypotheses by applying quantitative comparisons of Mars' networks from Utopia Planitia (43.5˚N, 269.3ºW) with terrestrial ice-wedge patterns located at the mouth of the Sagavanirktok River, near Prudhoe Bay, Alaska (70ºN-147ºW), as well as with experimental desiccation fracture patterns. Statistical metrics include intersection types, polygon size, relative orientation between neighboring fracture segments, and degree of orderliness. I find that Utopia Planitia networks a) are qualitatively similar to terrestrial ice wedge networks with respect to intersection types and degree of orderliness, but have larger spacing; b) are distinctively different from fracture patterns that form by a single fracture event, such as desiccation patterns in mud; and c) display a strong north-northeast orientation over large regions, approximately parallel to the regional topographic slope into the Utopia basin. I conclude that Mars networks formed by recent and multiple fracture events, likely caused by seasonal cooling similar to terrestrial permafrost patterns, and not by other proposed mechanisms.

Acknowledgements

I gratefully acknowledge the help and support of several individuals, first and foremost my supervisor Dr. Lawrence Plug, whose support and knowledge has proven invaluable. Special thank you to Carl Helmick and Sheila Ballantyne for their hard work and input, and Rebecca Brunt for always understanding.

Also, to my family and friends who have lived through this with me, thank you! Especially to Jon, without whom I wouldn't be where I am today.

"As in most complicated problems... the best we can hope, from a theoretical approach, is that pertinent, simple, idealized models can be selected, and that studying them will yield insight into the natural processes."

– A. H. Lachenbruch, 1962.

TABLE OF CONTENTS

Abstract ……..…… ii

Acknowledgements ……. iv

List of Figures ……. vii

List of Tables …….. viii

Chapter 1: Introduction to Polygonal Patterns and Definition of Objectives 10

1.1 General Statement …….....…. 10

1.2 Hypothesis ……..... 11

1.3 Practical Implications …….....…. 11

1.4 Previous Work Completed ……. 12

Chapter 2: Martian Climate, Geology, and Evidence for Water …… 13

2.1 Introduction to Mars ..…… 13

2.2 The Martian Atmosphere and Climate ……. 13

2.2.1 The Martian Atmosphere ……. 13

2.2.2 Obliquity and Climate Change ……. 14

2.2.3 Temperature …….. 16

2.2.4 Martian Albedo and Thermal Inertia ……..…… 17

2.3 Martian Geology …….. 20

2.3.1 Relative Age …… 20

2.3.2 Surface Topography and MOLA Data …… 21

2.3.3 Martian Volcanism …….. 24

2.3.4 Martian Tectonics …… 24

2.3.5 Martian Stratigraphy …… 24

2.4 Water on Mars ……. 28
2.4.1 Water in the Martian Atmosphere …….. 28
2.4.2 Ground Ice Stability …… 29
2.4.3 The Megaregolith, a Possible Reservoir? …… 30
2.4.4 Indications of Ground Ice from Neutron Flux Measurements 31
2.4.5 Surface Features …… 32
2.5 Utopia Planitia Field Area ……. 33

Chapter 3: Permafrost and Related Processes on Earth …… 36
3.1 Introduction to Permafrost …… 36
3.1.1 Temperature of Formation ……..... 36
3.1.2 Thickness and Distribution …… 37
3.1.3 Permafrost Composition and Association ……. 39
3.1.4 Surface Features of Permafrost …… 40
3.2 Introduction to Ground Ice …… 40
3.2.1 Classification of Ground Ice …… 40
3.2.2 Wedge Ice …… 42
3.2.3 Segregation Ice …… 42
3.2.4 Intrusive Ice …… 43

Chapter 4: Polygonal Patterns ……..…… 44
4.1 Small scale polygons on Mars …….. 44
4.1.1 Qualitative Description …… 44
4.2 Earth Analogue …… 46
4.2.1 Known mechanisms of formation …… 46
4.2.2 Principal Controls Over Network Patterns and Spacing ….. 48

Chapter 5: Methods ……..…… 50

5.1 Collection/Search of Images ..…… 50

5.1.1 Martian Images …….. 50

5.1.2 Terrestrial Images …… 52

5.1.3 Mudcrack Images …… 57

5.2 Digitizing Process …….. 59

5.3 Statistical Comparison of Networks ……..…… 59

Chapter 6: Results …… 64

6.1 Introduction …… 64

6.2 Qualitative Description of Martian Networks ……. 64

6.2.1 Distribution of Martian Polygonal Networks ……. 64

6.2.2 Region 1 Polygonal Networks …… 66

6.2.3 Region 2 Polygonal Networks …… 73

6.2.4 Region 3 Polygonal Networks …… 79

6.2.5 Region 4 Polygonal Networks …… 84

6.2.6 Region 5 Polygonal Networks …… 89

6.3 Qualitative Description of Terrestrial Networks …… 94

6.3.1 Distribution and Characteristics of Terrestrial Networks … 94

6.4 Qualitative Description of Mudcrack Networks …….. 98

6.4.1 Characteristics of Mudcrack Networks …… 98

Chapter 7: Discussion …… 101

7.1 Discussion of Martian Polygonal Networks ……. 101

7.1.1 Variations in Spacing, *D* ……. 101

7.1.2 Orthogonal versus Non-orthogonal Intersections ……... 102

7.1.3 Three-Way and Four-Way Intersections ……. 102

7.1.4 North-South Network Orientation ……..…… 103

7.1.5 Network Exposure …….. 108

7.1.6 Thermokarst Features ……. 108

7.2 Comparison of Martian and Terrestrial Networks …….. 109

7.2.1 Qualitative Comparison …… 109

Chapter 8: Conclusions …… 111

Appendix A …… 112

Appendix B …… 161

Appendix C …… 169

References …… 191

List of Figures

Fig. 1: Thermal Inertia Map of Mars 19

Fig. 2: MOLA Map of Mars 23

Fig. 3: Mars Global Stratigraphy 27

Fig. 4: Sources and Reservoirs 29

Fig. 5: Model of the Megaregolith 33

Fig. 6: Epithermal Neutron Flux Map of Mars 35

Fig. 7: Representation of Permafrost Distribution 38

Fig. 8: Schematical representation of Permafrost Terminology 39

Fig. 9: Classification Scheme for Ground Ice 41

Fig. 10: Martian Polygonal Pattern 45

Fig. 11: Schematic Representation of Ice-Wedge Formation 47

Fig. 12: Orthogonal versus Non-orthogonal Classification Scheme 49

Fig. 13: Small-scale Polygons on Mars 52

Fig. 14: Terrestrial Location Map 53

Fig. 15: Aerial Location Map 54

Fig. 16: Terrestrial Polygon Digitized for Pattern Analysis. 55

Fig. 17: Example of Mudcrack Images 58

Fig. 18: Spacing and Relative Orientation Measurements 60

Fig. 19: Two-dimensional Distributions 62

Fig. 20: Mars Network Basemap 65

Fig. 21: Region 1 Networks 67

Fig. 22: Region 1 Surface Plots 69

Fig. 23: Region 1 Rose Diagram 72

Fig. 24: Region 2 Networks 74

Fig. 25: Region 2 Surface Plots 75

Fig. 26: Thermokarst Feature 77
Fig. 27: Region 2 Rose Diagram 78
Fig. 28: Region 3 Networks 80
Fig. 29: Region 3 Surface Plots 82
Fig. 30: Region 3 Rose Diagram 83
Fig. 31: Region 4 Networks 85
Fig. 32: Region 4 Surface Plots 86
Fig. 33: Region 4 Rose Diagram 88
Fig. 34: Region 5 Networks 90
Fig. 35: Region 5 Surface Plots 91
Fig. 36: Region 5 Rose Diagram 93
Fig. 37: Earth Network 95
Fig. 38: Earth Surface Plot 1 96
Fig. 39: Earth Surface Plot 2 96
Fig. 40: Earth Rose Diagram 97
Fig. 41: Mud Surface Plot 20030824 100
Fig. 42: Mud Surface Plot 20030915 100
Fig. 43: Representation of Oceanus Borealis 106

List of Tables

Table 1: Time Stratigraphic System for Mars 21

Table 2: Average Monthly Max / Min Temp (Prudhoe Bay, Alaska) 56

Table 3: Monthly Precipitation Fluctuations (Prudhoe Bay, Alaska) 56

Table 4: Region 1 Values 66

Table 5: Region 2 Values 73

Table 6: Region 3 Values 79

Table 7: Region 4 Values 84

Table 8: Region 5 Values 89

Table 9: Terrestrial Values 94

Table 10: Mud Values 98

CHAPTER 1: INTRODUCTION

1.1 GENERAL STATEMENT

Polygonal networks resulting from ice wedge formation, are a striking and widespread feature of Arctic landscapes. Qualitatively similar patterns, perhaps of similar origin, have been recognized in imagery of Mars' surface. Terrestrial patterns, which require permafrost for their existence, form as a result of tension caused by thermal contraction, a process originally proposed by Leffingwell (1915). When soil temperatures reach -15 to -20ºC, the ice-rich frozen ground shrinks and vertical fractures develop (French, 1996). Melting of the overlying material the following spring, results in water filling the crack and producing a vertical vein of ice. The vein penetrates the permafrost layer, which undergoes horizontal compression the following summer due to re-expansion (Lachenbruch, 1962). This causes strata within the permafrost layer to be upturned through plastic deformation. The following winter, the initial vertical crack may re-open, allowing for more water to seep in and thus repeating the cycle. Over many years, this leads to the development of ice wedges on the order of 1.0-1.5 meters wide at the surface, extending to depths of 3.0-4.0 meters (French, 1996).

The visually similar polygonal patterns on the surface of Mars have been observed through high resolution (1.5 to 12.4 metres per pixel) digital images provided by the Mars Orbiter Camera (MOC) during the Mars Global Surveyor (MGS) mission. The qualitative similarities between terrestrial and Martian patterns are noteworthy, motivating the hypothesis that Mars' patterns may also be the result of past or present ice wedge formation (Seibert and Kargel, 2001).

This is a potentially enormous discovery, as it may establish the presence of a subsurface reservoir of water, which would allow for the sequestering of organic material and possibly life on Mars. Network patterns may also hold information regarding the substrate and climate under which networks formed.

1.2 HYPOTHESIS

Here I investigate the distribution of small-scale polygons within the Utopia Planitia region of Mars as a function of surface properties, and test the hypothesis that Mars and terrestrial polygonal patterns are quantitatively similar and, by inference, have formed by similar mechanisms. Using high-resolution, narrow angle images obtained by the Mars Orbiter Camera (MOC), polygonal patterns of Utopia Planitia in Mars' northern plains, and aerial photographs of similar networks in terrestrial regions located at the mouth of the Sagavanirktok River near Prudhoe Bay, Alaska (70ºN-147ºW), are compared based on geometrical properties such as intersection types, spacing and degree of orderliness. To investigate whether Martian patterns may have formed by differing tension fracture mechanisms, Mars patterns are also compared to a time series of experimental mudcrack polygonal networks.

1.3 PRACTICAL IMPLICATIONS

This study poses practical implications in that it addresses the question of whether or not terrestrial and Martian polygonal patterns are quantitatively similar. Because terrestrial patterns often are associated with thermal contraction crack mechanisms in cold-climate regions containing an ice-rich subsurface, the possibility that Martian patterns formed by similar mechanisms would provide information regarding the existence of liquid water or ground ice at or near the Martian surface. The presence of water or ground ice may reveal practical information with regards to its latitudinal distribution and/or seasonal or episodic dependence. Evidence for water on Mars may also provide valuable information, in that the presence of water would permit the sequestering of organic material and possibly life on Mars.

1.4 PREVIOUS WORK COMPLETED

Small scale polygonal patterns on the Martian surface were first identified by high-resolution Viking Orbiter images and Viking Lander 2 data, and were described by Mutch et al., (1977) and Luchitta (1981). Significant research has been conducted since this time in which a thermal contraction crack origin, resembling that known to be responsible for polygonal patterns formed by ice wedge networks on Earth, has been proposed for the Martian patterns (Mellon, 1997). Seibert and Kargel (2001) favour a model involving the growth of ice wedges under altered climatic and atmospheric conditions, but do not rule out the possibly of an origin similar to the formation of desiccation cracks in mud. The polygonal patterns may represent the net effect of long-term orbital variations on subsurface ice-rich deposits (Head et al., 2003) or, as proposed by Yoshikawa (2003), may have a structural origin, with their formation related to bending in the centre of the Utopia basin.

The exact mechanisms by which Martian polygonal patterns form remains unknown, however it is the aim of this study to investigate the proposed hypotheses by applying quantitative comparisons of terrestrial and Martian networks.

CHAPTER 2: MARTIAN CLIMATE, GEOLOGY, and EVIDENCE FOR WATER

2.1 INTRODUCTION TO MARS

Mars is the fourth planet from the Sun, having the shape of a triaxial ellipsoid, with equatorial radii of 3394 and 3399 km (Carr, 1996). The Martian year consists of ~687 Earth days, with each solar day being 24 hours and 39.6 minutes in length. The result is a Martian year with 669 sols (Mars solar days). Owing to its greater distance from the sun (~1.5 Aμ), Mars' mean solar flux at the top of the atmosphere is 0.43 times that of Earth, resulting in an average Martian surface temperature of 210 K (-63ºC). Mars' elliptical orbit has an eccentricity of 0.093 compared with that of Earth which is 0.0167. This results in very strong seasonality on Mars. Obliquity values for Mars and Earth are also significantly different at 25.19º and 23.45º respectively, further amplifying seasonality (de Pater and Lissauer, 2001). Long term variations in orbital motions and rotation are suggested to have effected the distribution and stability of water at the Martian surface (Head et al., 2003).

2.2 THE MARTIAN ATMOSPHERE AND CLIMATE

2.2.1 The Martian Atmosphere

Mars' atmosphere is remarkably thin (6 MPa at surface or 6‰ that of Earth's), composed primarily of CO_2 (95.3%). Also present, in considerably lesser amounts, are N_2 (2.7%), Ar (1.6%), O_2 (0.13%), and H_2O (0.03%). Water fraction varies significantly with seasonal latitude, ranging from <1 precipitable micron (pr mm) at the winter pole, to 100 pr mm at the summer pole (de Pater and Lissauer, 2001). The average amount of water present is ~ 10 pr mm, meaning that if all water present in the Martian atmosphere was to precipitate out, it would form a layer only 10 mm deep over the surface of the planet.

CO_2, the most abundant atmospheric constituent, condenses around the winter

pole to form a seasonal CO_2 cap. The longer southern winter results in a more extensive cap, extending from 50-60ºS, whereas the northern seasonal cap extends to ~65ºN (Carr, 1996). During northern hemisphere summer, CO_2 present at the northern pole evaporates and exposes a small water-ice cap in which the maximum observed water content equals 100 pr mm. No residual water cap has yet been identified at the southern pole (Carr, 1996). The seasonal condensation of CO_2 at the poles results in approximately 30% seasonal variation in mean atmospheric pressure, reaching a minimum of 5.6 mbar during southern hemisphere winter (Leovy, 2001).

2.2.2 Obliquity and Climate Change

Obliquity refers to the angle between the spin axis and the normal to the orbit plane, currently at 25.19º for Mars (de Pater and Lissauer, 2001). During the current epoch, oscillations in obliquity are suggested to have ranged between 13º and 42º, displaying a mean value of 24º, and a period of 1.2×10^5 years (Carr, 1996). Obliquities are thought to be inherently chaotic on time scales greater than 10^7 years, as a result of secular changes in orbital parameters. Variations in obliquity affect the insolation regime of polar regions, and are suggested to be particularly important for the history of water on Mars (Head et al., 2003).

At low obliquities (<30º), little to no solar insolation falls on high latitudes, resulting in the sequestering of volatiles, such as water, in the cold polar regions (Carr, 1996). At high obliquities (>30º) an increase in solar insolation results in the release of volatiles, such as water vapour, from the polar caps. Deposition of layered sediments observed at the north and south Martian poles are believed to be associated with changes in obliquity throughout Mars' history. The size of the CO_2 cap, atmospheric pressure, and ability of the regolith to retain absorbed CO_2 are suspected to vary as a result of oscillations in obliquity (Carr, 1996). These changes may subsequently influence dust storm activity, global wind regimes, and sedimentation at the poles.

The effects of obliquity on water are less clear; however, it has been suggested that evaporation of water at the poles may significantly increase the amount of water in the atmosphere, effectively causing variations in the frost-point temperature and stability of ice (Carr, 1996). Large amounts of water may subsequently be transported equatorward and deposited in mid to low latitudes as ice (Jakosky and Carr, 1985).

Recently, Head et al., (2003) suggest that a geologically recent ice age (~2.1-0.4 Myr ago) is responsible in the formation of water-ice-rich mantling deposits present poleward of ~30º. They suggest that emplacement of the deposits was in response to stability changes of water ice and dust driven by variations in obliquity. Variations in Mars' obliquity over the past 10 Myr resulted in changes in insolation and seasonality at mid to high latitudes, causing Mars to experience significant quasi-periodic variations in climatic conditions during this time (Head et al., 2003). Surficial deposits thought to have been formed as a result of quasi-periodic variations and occurring at latitudes poleward of ~30º include: 1.) smooth, metres-thick, formerly ice-rich dust mantle interpreted to have been deposited as a thin airfall layer that is now experiencing dissection and removal, 2.) polygons and patterned ground, and 3.) water-carved gullies. Head et al., (2003) suggest that increased atmospheric dust content, increased atmospheric water vapour content, and shifting of the surface ice stability zone toward the equator operate in conjunction to produce the latitude-dependant deposits during periods of high obliquity. A decrease in obliquity results in the lowering of the surface ice stability zone towards the polar caps, and an increase in ice sublimation. This increase in sublimation leaves behind a "weakly cemented, porous surface lag" which then acts to retard further sublimation. Head et al., (2003) also suggest that widespread desiccation occurs between 30º-60º latitude as obliquity lowers since water remains isolated predominantly in cold polar regions, thus causing the atmospheric humidity to decrease.

2.2.3 Temperature

The temperature in the lower part of Mars' atmosphere decreases with elevation at a rate of ~45 K/km within the convective boundary layer under clear atmospheric conditions (Leovy, 2001). Up to an elevation of ~45 km, Martian temperature is controlled by heat exchange with the ground because latent heat is negligible due to the minute amount of water present. Between 45-110 km elevation (therefore up to the mesopause), the temperature continues to decrease, but is dominated by CO_2 absorption and radiative emission. Above the mesopause (>110 km) the temperature gradient reverses due to absorption of ultraviolet radiation (de Pater and Lissauer, 2001). The homopause exists above the mesopause at ~125 km. It is at this elevation that atmospheric gases diffusively separate until reaching the exosphere, in which atoms and molecules slowly escape the planet's gravitational field.

The Martian atmosphere has a low heat capacity, absorbing little incoming radiation (when clear) as a result of its composition (abundant CO_2), thinness, and minute amounts of water present (Carr, 1996). Mars' atmosphere has a weak greenhouse, elevating the planet's temperature to only ~7ºC above what it would be if the atmosphere were not present. Consequently, the mean daily temperature at the equator is ~215 K (-58ºC), with ground temperatures ranging from ~260–280 K (-13ºC to +7ºC) during the day, to ~160-180 K (-113ºC to -93ºC) at night. Large diurnal surface variations are due to the low heat capacity of Mars atmosphere during most times. Temperatures vary with latitude, albedo and thermal inertia of surface molecules.

Suspended dust strongly influences atmospheric temperature. When 'clear' (i.e. when the optical depth at visible wavelengths «1) the maximum diurnal near-surface atmospheric temperature range is ~60ºC on Mars (Leovy, 2001). The amount of dust present in the atmosphere increases during the winter solstice, causing increased absorption of solar radiation and an increase in daily mean temperature and diurnal temperature range above the surface. It is important to note however, that the daytime

convective layer collapses at night, causing a strong temperature inversion to develop and a decrease in the range of surface diurnal temperature. As such, the daily average temperature near the Martian surface is not affected by increases in atmospheric dust (Leovy, 2001).

The transport of dust particles by wind has sufficiently modified the Martian surface through erosion and deposition, leading to difficulties in its geological interpretation. The Martian wind system is driven by horizontal variations in temperature and pressure. Similar to Earth, asymmetric Hadley circulation prevails on Mars, and is associated with northeasterly trade winds in the northern hemisphere and southeasterlies in the southern hemisphere. Winds extend up to 50º latitude in the northern winter, and during solstice seasons cut across the equator, curving to the east and forming an easterly jet stream in the summer subtropics (Leovy, 2001). Strong surface winds can suspend particles ~100 mm in diameter and create the aforementioned dust storms.

2.2.4 Martian Albedo and Thermal Inertia

Albedo refers to the fraction of the total incident solar radiation not absorbed by the surface, and is designated *A*. Martian values range from 0.095-0.415, preferentially between 0.135-0.275 (Carr, 1996).

Thermal inertia, designated *I* and defined as $(Krc)^{1/2}$ is a measure of the responsiveness of a material to changes in temperature (Cattermole, 2001). *K* refers to the thermal conductivity, *r* the density, and *c* the specific heat of the material. Variations in thermal conductivity cause most variations in thermal inertia since *r* and *c* of the materials do not display much variation. High thermal inertias occur in solid rocks and reflect a slow response to changes in temperature, whereas low values occur in loose granular materials with numerous voids, and reflect a faster response to temperature changes (Mellon et al., 2000). Variations in thermal inertias result because *I* is strongly

dependant on the physical properties of the near surface materials, such as particle size, degree of induration, exposure of bedrock, and abundance of material. Thermal inertia range from 1-15 thermal inertia units (=10^{-3} cal cm^{-2} $s^{-1/2}$) on the Martian surface, with values clustering around 6 and 2.5. These clusters correspond to albedo values of 0.135 and 0.275 respectively.

The values of thermal inertia vary across the Martian surface, with high thermal inertias occurring in the northern and southern hemispheres. In the northern hemisphere they are found within Chryse Planitia, Mare Acidalium, Utopia, western Elysium Planitia, and within the canyons, whereas in the southern hemisphere high values are noted within Argyre and the Hellas basin (Carr, 1996). Low thermal inertias occur in the uplands of Arabia, and a broad zone covering large areas of the Amazonis, Tharsis, and Arcadia Planitiae.

Surfaces with lower thermal inertias, therefore finer-grained uncemented material, heat up quicker in the day and cool quicker at night. These surface temperature however, “damp out” more quickly with depth (Carr, 1996). The result of this is that maps of thermal inertia, which essentially imply surface materials and induration present (i.e. fine or coarse grained), only apply to the upper few centimeters of the material, and do not pertain to materials at greater depth (Figure 1).

Low thermal inertias are represented by purple to dark blue colours, and likely represent loose, fine surface dust with very few rocks present. Medium thermal inertias (green to yellow in colour) represent a combination of coarser loose particles, scattered rocks, and/or a minimal number of scattered bedrock outcrops. High thermal inertias (red to white in colour) suggest a combination of coarse sand, dune sand, abundant rocks, and/or scattered bedrock exposures (Mellon et al., 2000).

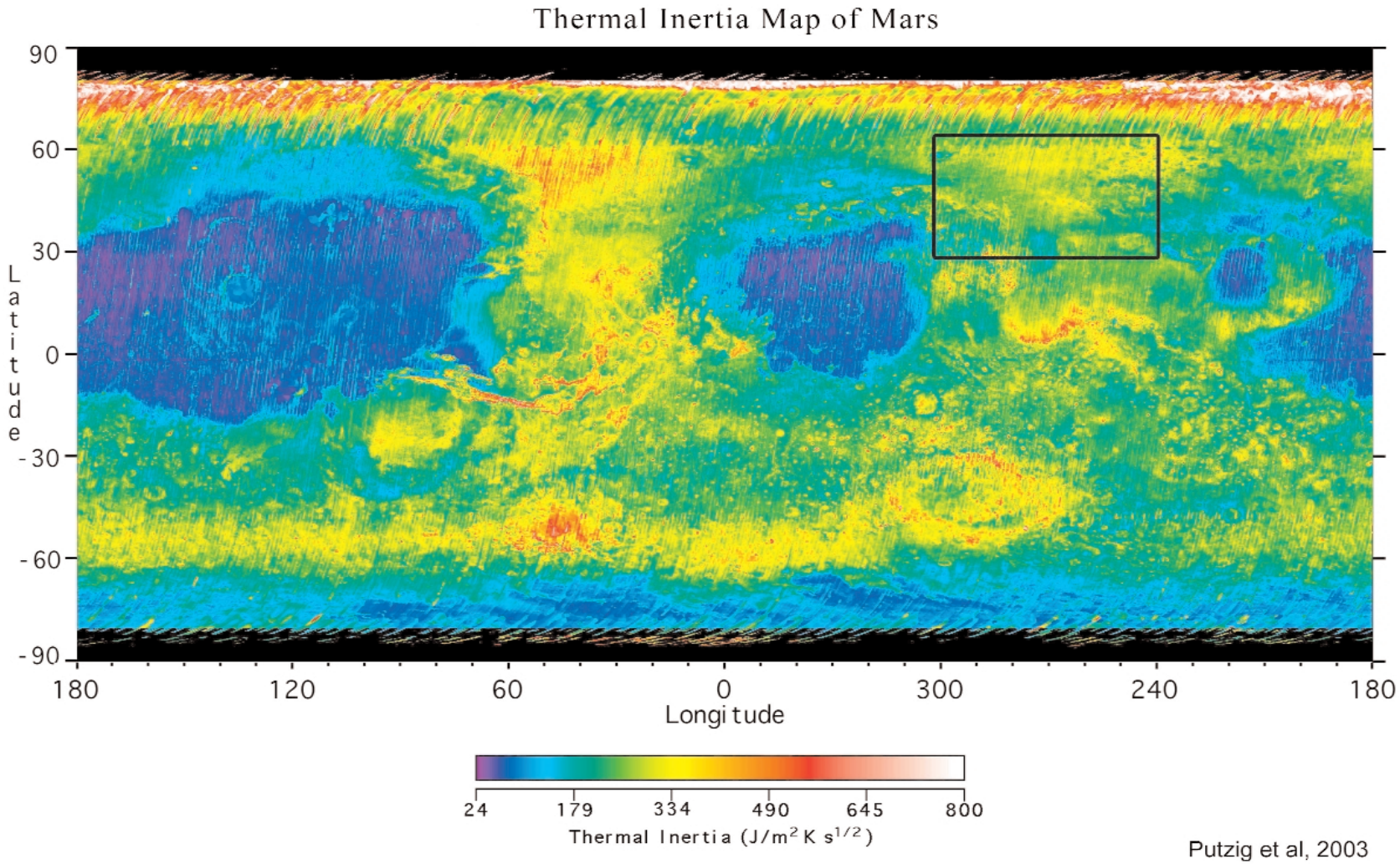

Figure 1: Thermal Inertia Map of Mars, displaying high thermal inertias occurring in the northern and southern hemispheres, and low thermal inertias in the uplands of Arabia, and a broad zone covering large areas of the Amazonis, Tharsis, and Arcadia Planitiae. After: Putzig et al., 2003.

2.3 MARTIAN GEOLOGY

The geology of Mars is greatly limited to interpretation of surface morphology, and some properties of the upper surface such as thermal inertia and albedo.

2.3.1 Relative Age

The relative age of Mars' different regions is determined based on the frequency of superimposed impact craters and cross-cutting relationships among surficial features. The method of crater-counting is commonly used, in which older surfaces display a greater number of superimposed impact craters (de Pater and Lissauer, 2001). Absolute ages determined from this method are very approximate because the impact history for Mars is unknown and is generally extrapolated from the impact history of the moon, which is located at a different position in the solar system.

The Martian geological record is divided into three time stratigraphic systems calibrated against the numbers of superimposed impact craters (Tanaka, 1986). Relative ages apply to the age of the surface, and not necessarily to the rocks themselves. The Noachian epoch relates to a period of immense crater bombardment which ended ~3.8 Gyr ago. During this period volcanism and crustal deformation was prominent, and the Tharsis bulge developed. The Hesperian epoch reflects the oldest surfaces postdating the end of heavy bombardment, and includes the period from 3.5-1.8 Gyr ago. The Amazonian epoch, reflecting the last 1.8 Gyr up to the present, saw a gradual decrease in volcanism and increase in erosional processes. Unfortunately absolute ages are poorly constrained, as the rate of change of cratering is itself poorly known (Tanaka, 1986). As such, several different time stratigraphic systems have been proposed (Table 1), such as that of Carr (1981).

Time-Stratigraphic Boundary	Crater Density	Absolute Age
Noachian-Hesperian	200>5 km in diameter/10^6 km^2 25>16 km in diameter/10^6 km^2	3.5-3.8 Gyr
Hesperian-Amazonian	400>2 km in diameter/10^6 km^2 67>5 km in diameter/10^6 km^2	1.8-3.5 Gyr

Table 1: Time-stratigraphic system based on crater density. After: Carr, 1981.

2.3.2 Surface Topography and MOLA Data

Martian elevations are referenced to the triple point of water datum, namely the level at which the average atmospheric pressure equals 6.1 mbar (Carr, 1996). The Martian surface is broadly divided into heavily and sparsely cratered regions, covering ~2/3 and 1/3 of the surface respectively. The division between these two regions is referred to as the global dichotomy, which describes a great circle inclined at ~35º to the equator. Heavily cratered regions lie to the south of the dichotomy and sparsely cratered regions to the north (Cattermole, 2001). Slopes generally lie between 1º - 3º, but reach values of up to 20º in isolated areas, and a general tendency for slopes to be oriented south-north exists. This factor is often suggested as evidence for the south-north flow of water on Mars in the past (Cattermole, 2001). Heavily cratered regions are located in the southern hemisphere at elevations of 2-5 km above the datum, and sparsely cratered regions at elevations 1-3 km below the datum, most of which are located at high northern latitudes. The dichotomy is superimposed by two broad bulges, the Tharsis bulge which is centered on the equator at 110ºW, is 10 km high and 6000 km wide, and a second bulge centered in Elysium at 30ºN, 210ºW (Carr, 1996). Both bulges are associated with previously active volcanism.

The northern hemisphere consists of extensive plains with substantial variation

in the number of superimposed craters. The origins of the plains is diverse, with those around Tharsis and Elysium dominated by lava flows, whereas those in the northern lowlands lack volcanic features, displaying fractures, textures, and patterns that have been attributed to water and ground ice processes, such as small-scale polygonal patterns (Carr, 1996).

Recently, very high-resolution topographic shade maps of Mars have been produced using laser altimeter instruments aboard the Mars Global Surveyor (MGS) spacecraft (Figure 2). Mars Orbiter Laser Altimeter (MOLA) transmits infrared laser pulses towards Mars at a rate of 10 Hz, measuring the time of flight and allowing for the determination of range of the MGS spacecraft to the Martian surface. The resulting range measurements have been used to construct a precise topographic map of Mars (Malin, 2003).

Figure 2 displays the pole-to-pole slope of 0.036°, which results in the south pole having a higher elevation than the north pole by ~6 km. This global-scale slope is suggested to have likely been present throughout most of the Martian history (Carr, 1996), and controlled surface and subsurface water transport.

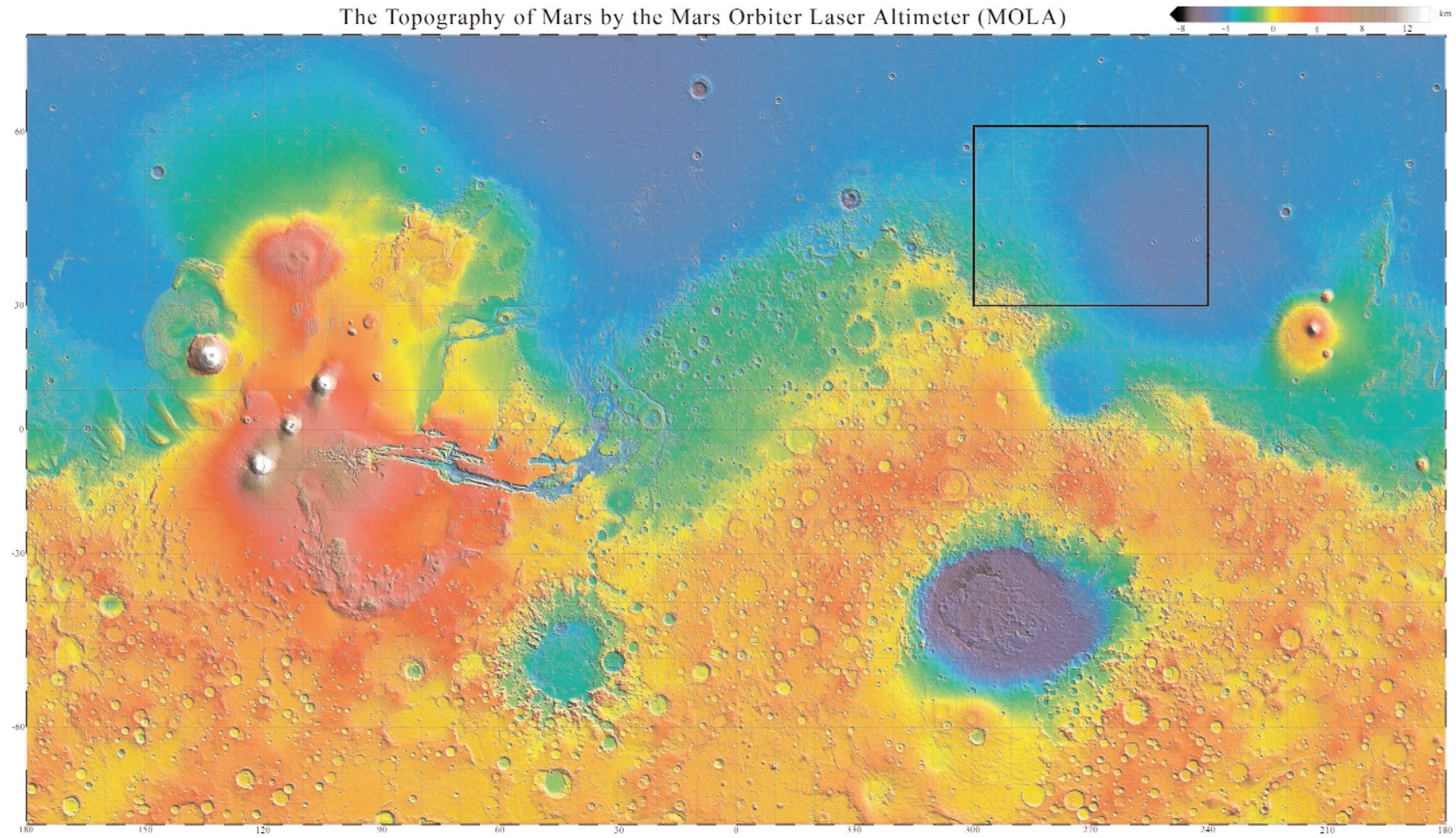

Figure 2: MOLA Map of Mars depicting topographic elevations. Warm colors correspond to high elevations and cold colors to low elevations, noting particularly the exceedingly flat northern hemisphere. After: Malin Space Science Systems.

2.3.3 Martian Volcanism

Elysium and Tharsis represent the two most prominent volcanic provinces on the Martian surface (Carr, 1996). The tallest volcano, Olympus Mons, resides on the northwest flank of the Tharsis bulge, and is ~550 km in diameter, and stand ~27 km high. Martian volcanoes are suggested to have formed by eruption of fluid lava accompanied by little pyroclastic activity, and their enormous size may reflect the buoyancy of the magmas and lack of Martian plate tectonics (Carr, 1996).

2.3.4 Martian Tectonics

The majority of the Martian surface lacks obvious evidence for plate tectonics, such as orogenic belts and subduction zones. Surface deformation is however indicated by the presence of wrinkle ridges, suggesting compression, and normal faults representing extensional processes (Carr, 1996). These features are believed to be the result of lithospheric stresses in response to the development of the Tharsis bulge. Crustal deformation is most easily recognized as the resulting Valles Marineris, an equatorial canyon system extending from ~30ºW-110ºW, and displaying a total length of ~4500 km (Cattermole, 2001).

2.3.5 Martian Stratigraphy

The first global geological map of Mars was produced in 1978, at which time a broad time-stratigraphic classification into the Noachian, Hesperian, and Amazonian epochs, was made (Scott and Carr, 1978). Analysis of Mariner 9 and Viking orbiter images, along with crater counting of geological units has since permitted the division of the epochs into eight series (Tanaka, 1986), in which series names are depicted by "Upper," "Middle," and "Lower." The Lower Noachian Series consists of material previously mapped as "basin rim" and "mountain material" (Scott and Carr, 1978). It type area includes Nereidum and Charitum Montes, surrounding Argyre Planitia

(Tanaka, 1986). The material displays a rugged appearance, is heavily cratered and faulted, and comprises hills, ridges, and massifs. This series reflects a period of major impact-basin formation, and development of the northern lowlands. The Middle Noachian Series consists of cratered terrain, in which the Noachis area west of the Hellas impact structure is the type area. The cratered terrain consists of rugged surfaces with moderate to high relief, and is marked by secondary craters, wrinkle ridges, erosional scarps, and channels (Tanaka, 1986). The Upper Noachian Series defines the flat and smooth intercrater plains material, in which the type area lies to the east of the Argyre impact basin. This series is marked by intense erosion, and development of runoff-channels.

The Lower Hesperian Series is identified as the base of the "ridged plains material" (Scott and Carr, 1978). The type section is located in Hesperian Planum, in which plains material displays a smooth surface marked by a pattern of wrinkle ridges. This series is hypothesized to reflects a period of burial and degradation of lowland cratered terrain, extensive faulting, major rifting, and formation of the Lowell impact basin (Tanaka, 1986). The Upper Hesperian Series consists of smooth and ridged plains material, reflecting resurfacing and erosion of the northern plains. The type area for this series, the Vastitas Borealis Formation, spans the majority of the lowland region north of 40ºN. The formation is characterized by troughs arranged in crude polygons, ranging from 5-20 km in diameter, ridges in polygonal and concentric patterns, mottled albedo patterns, and small knobs of varying density (Tanaka, 1986). This series may record a late Hesperian period of active volcanism, development of outflow channels, waning of Tharsis tectonism, deposition of unconsolidated material in the south polar region, and deposition of layered deposits in Valles Marineris.

The Lower Amazonian Series consists of smooth plains material composed of lava flows, fluvial deposits, and possible eolian material. The series signifies the

formation of the Olympus Mons aureoles, Lyot impact basin, and local volcanism at Tharsis Montes, Alba Patera, and Elysium Mons (Tanaka, 1986). The Middle Amazonian Series reflects the continued accumulation of lava flows in the northern plains, particularly Amazonis Planitia. It is marked by the deposition of poorly consolidated, thick material of the Medusae Fossae Formation, continued volcanism at Tharsis Montes and Olympus Mons, and development of debris flows and aprons. The Upper Amazonian Series consists of smooth flood-plain material, suggested to have been deposited by floods emanating from its type area in western Cerberus Rupes (Tanaka, 1986). The unit is sparsely cratered, and consists of low-albedo material, reflecting its relative youth.

The stratigraphy and geological activity (Figure 3) presented by Tanaka (1986) suggest that volcanism, tectonism, and bombardment by meteorites has decreased throughout Mars' history, whereas surficial processes have dominated in recent geological time. The Noachian epoch was dominated by fluvial activity, owing to a warmer climate and thicker atmosphere. The Hesperian epoch saw a cessation in the formation of runoff channels, and an increase in outflow channels that drained into the northern lowlands. Ground ice is thought to be responsible for the formation of debris flows, landslides, channels, etc. during the Hesperian and Amazonian (Tanaka, 1986). Eolian processes currently dominate the resurfacing of the Martian surface, particularly by dust storms and seasonal frost.

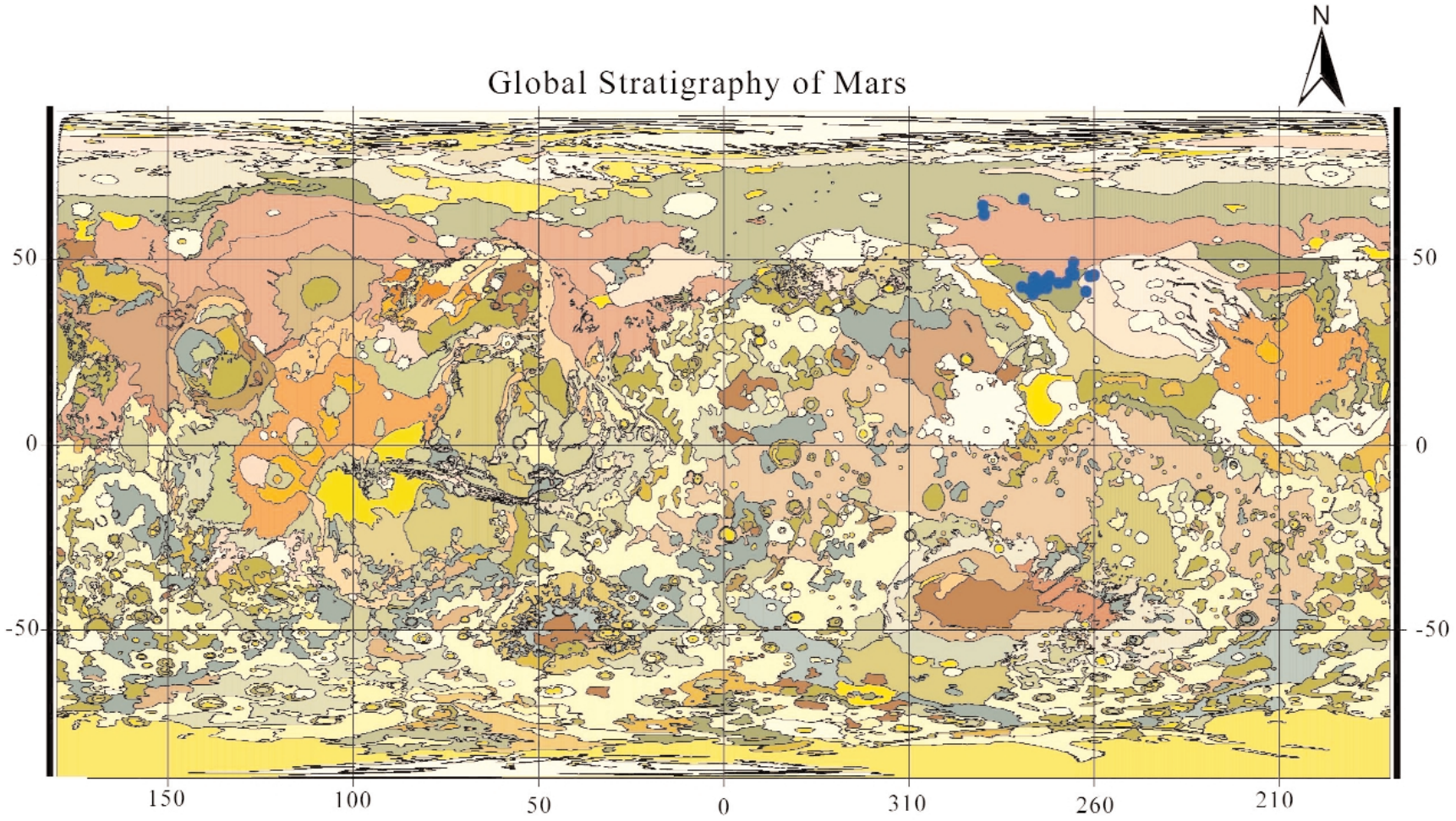

Figure 3: Mars global stratigraphy as described by Tanaka and Scott (1986). Accompanying legend and formation descriptions can be found in Appendix C.

2.4 WATER ON MARS

The presence and state of water on Mars has been a persistent topic of scientific discussion and investigation, since Schiaparelli first described linear albedo features as "canali" in 1877 (Carr, 1996). Mariner 9 first returned images of the Martian surface to Earth in 1972, in which large erosional features such as channels and small valleys were noted. These were followed by Viking orbiter images in 1975, which provided greater detail of these features and indicated the presence of many flow-like characteristics thought to have been formed by running water (Masson et al., 2001). Since this time, numerous landforms thought to be indicative of extensive water and/or ice activity on the Martian surface have been identified (Baker, 2001, Mustard et al., 2001).

2.4.1 Water in the Martian Atmosphere

Water comprises ~0.03% of the thin, cold Martian atmosphere under present climatic conditions (Carr, 1996). The Mars Atmospheric Water Detection (MAWD) apparatus aboard the Viking orbiter provided abundant information regarding circulation of water in the atmosphere (Jakosky and Farmer, 1982). The instrument inferred the amount of water vapour in the Martian atmosphere by comparing the absorption of solar radiation, with theoretical predictions based on a certain amount of water vapour. Results of this experiment indicated variation in atmospheric water content both seasonally and spatially. The northern spring and summer saw a transfer of water from the northern regolith and residual cap to the atmosphere surrounding the northern hemisphere (Carr, 1996). Water condenses onto the southern seasonal and residual caps prior to the onset of the northern winter, in which water vapour recondenses on the northern seasonal and residual caps and is resorbed into the regolith (Figure 4). The inability of the northern residual cap to supply the amount of water vapour present in the atmosphere at high latitudes has led to the suggestion that the Martian regolith is acting as a sink for additional water (Mustard et al., 2001).

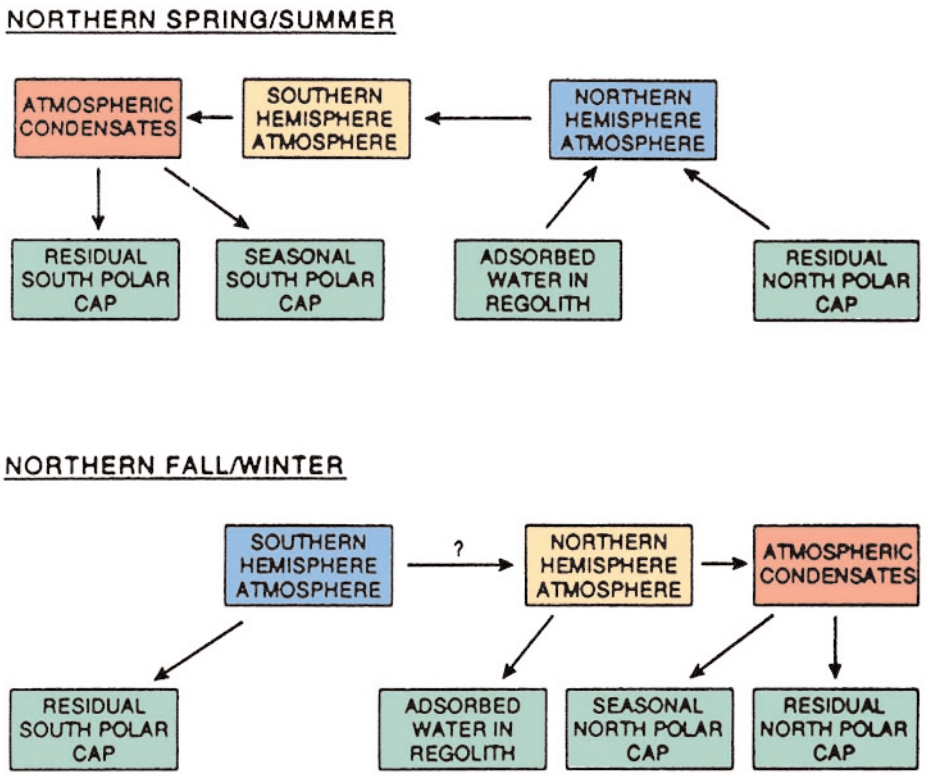

Figure 4: Sources and reservoirs for annually exchangeable water on Mars. After: Jakosky and Haberle, 1992.

2.4.2 Ground Ice Stability

The thermodynamic stability of ground ice is a function of the vapour pressure of water at the surface and ground temperature. Under current climatic conditions ground ice is unstable on the Martian surface at latitudes less than 30-40º as a result of the mean annual temperature existing above the frost point (~197 K, -76ºC). As such, the only reservoirs in which water has been directly observed are the atmosphere and the north pole residual cap. At low latitudes, ice present within near-surface materials will preferentially sublimate and diffuse into the atmosphere at rates of $\sim 10^{-5}$cm/yr, subsequently condensing at the poles (Carr, 1996). At latitudes >30º sublimation rates are dependant upon obliquity. Sublimation will only occur at high latitudes, at a rate of $\sim 10^{-5}$ - 10^{-6} cm/yr, if the corresponding obliquity is high (Carr, 1996). Mid-latitude

water varies on a 100 000 year timescale with respect to climatic changes (Mustard et al., 2001). Uncertainties exist however, in the extent to which this near-surface ground ice exists today and how it might be changing with time. Local albedo, thermal inertias, and changes in climate owing to variations in obliquity might also significantly effect the stability of near-surface ground ice.

2.4.3 The Megaregolith, a Possible Reservoir?

Abundant evidence exists to suggest that water existed close to the Martian surface at some point in the geological past. The question remains as to whether Mars has retained any of this water, and if so it must be located in the ground where it is inaccessible to direct observation. By analogy with the Moon, Clifford (1993) suggests that the heavily cratered terrain, which encompasses two thirds of the Martian surface, is likely underlain by a brecciated megaregolith formed by heavy bombardment of impact craters. The overlying near-surface materials are thought to consist of an assortment of impact ejecta, volcanics, and sediment (Figure 5). Younger terrains may also be underlain by similar materials. Based on reasonable assumptions for porosity of the megaregolith, capacity to hold water ranges from the equivalent of 0.5-1.5 km of water, if spread evenly over the planet (Carr, 1996). Unfortunately, whether or not water exists as ice in the shallow megaregolith or as groundwater in the deeper megaregolith is still unknown.

2.4.4 Indications of Ground Ice from Neutron Flux Measurements

Recently, neutron spectrometer measurements have been used to detail the distribution of water-equivalent hydrogen on Mars. The epithermal neutron energy range (0.4 eV to ~500 keV) is often employed for this purpose, as it is the most sensitive (Feldman et. al, 2003). The Neutron Spectrometer (aboard Mars Odyssey) detects the neutrons generated by atoms on the planet's surface when their nuclei are struck by cosmic rays. Elements create a unique distribution of neutron energy, either fast, thermal or epithermal. The signature of the neutron flux is a result of the elements composing the soil, and their distribution with depth. The near-surface composition of Martian regolith, believed to be composed of a mixture of weathered (fine-grained material, possible palagonite and clays), and unweathered (coarse-grained, likely of igneous origin) materials, also affects the epithermal neutron flux received (Feldman et al., 2002). Hydrogen in the soil absorbs energy from cosmic rays, thereby reducing the neutron flux that is emitted to the spectrometer. Reductions in epithermal neutron flux, as detected by orbiting spectrometers in MGS, indicate an abundance of hydrogen in the upper 1-2 m of the subsurface.

First results of subsurface hydrogen distribution were described in 2002 (Boynton et al., 2002) showing discrete regions of low flux in the south-polar and north-polar regions. The south-polar region exists poleward of -60º latitude, but extends equatorward to ~50º between 75º and 130º east longitude (Feldman et al., 2002). The majority of the north-polar region displays low epithermal flux values, however a minimum exists near +60º latitude between ~205º and 275º east longitude. Increase in epithermal flux intensities towards the poles is attributed to the overlying of hydrogen-rich soil by CO_2 ice caps (Feldman et al., 2002).

Variations in hydrogen concentration at low to mid latitudes are suggested to reflect geographic variations in the amount of physically and/or chemically bound H_2O and/or OH by minerals underlying a 15-20 cm thick hydrogen-poor dust layer (Feldman

et al., 2002). Boynton et al., (2002) suggest that hydrogen in the upper layer is likely in the form of physically or chemically bound H_2O, whereas it likely exists as ice in the lower layer. Strong correlations exist between regions in which ice is predicted to be stable under current Martian conditions at a depth of ~80 cm, and regions displaying low epithermal neutrons flux values (Boynton et al., 2002). Although results from the neutron spectrometer cannot confirm the presence of ice within the Martian regolith, they do suggest that the surface may represent a substantial reservoir for water on Mars (Boynton et al., 2002).

The Los Alamos National Laboratory has recently (July 2003) released new maps indicating the concentration of sub-surface hydrogen on Mars (Figure 6), from data collected over a time period of more than half a Martian year (687 Earth days). Low epithermal neutron flux values are indicative of high hydrogen concentration (red), and high flux values of low hydrogen concentration (blue).

2.4.5 Surface Features

Landforms suggested to be indicative of a past hydrologic cycle on Mars were first noted in Mariner 9 photographs released in 1972, which displayed features interpreted as giant channels and valleys (Masson et al., 2001). The Viking orbiter images of 1975 provided additional details of the channels and valleys, and noted the presence of many flow-like features believed to have been formed by running water. Recent MOC images allow for greater interpretation of these features suggesting the presence of outflow channels and valley networks indicative of a past environment in which running water was prevalent, terminal lakes located at the end of outflow channels, mass wasting features, and surface features with origins attributed to periglacial or permafrost processes such as debris flows, thermokarst, and polygons (Masson et al., 2001).

2.5 UTOPIA PLANITIA FIELD AREA

The Utopia Planitia region of Mars is located within the northern plains, which were emplaced during the Late Hesperian and Amazonian epochs. Deposition of the northern plains is believed to have involved volcanic, aeolian, and alluvial processes, possibly associated with widespread glaciation (Cattermole, 2001). The plains are broadly defined on the basis of their smooth or knobby appearance, composed of aeolian and relict material of older units respectively. Most of the flat, smooth material composing the northern plains belongs to the Vastitas Borealis Formation of Amazonian age. The Vastitas Borealis Formation consists of subpolar plain deposits within the northern lowlands, and its members are distinguished on the basis of morphology and albedo contrast (Scott and Tanaka, 1986).

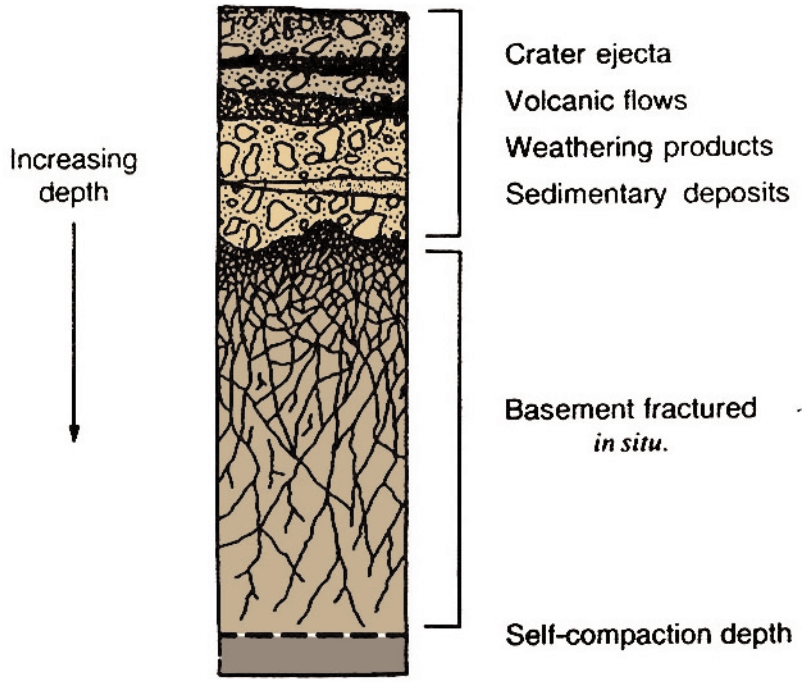

Figure 5: Model of the megaregolith, displaying interbedded crater ejecta, volcanics, and sediment, overlying a highly fractured basement unit. After: Clifford, 1981.

The small-scale polygonal patterns considered in this study are located within the Casius region of Utopia Planitia, located between 30º-65ºN latitude and 240º-300ºW

longitude. The higher-latitude plains (located above 30º-45ºN) are suggested to be covered by a vast layer of aeolian debris, displaying minimal evidence for primary volcanic deposition (Cattermole, 2001). Mottled and knobby plains comprise extensive areas within Utopia. The Mottled member (Hvm) consist of crater-ejecta blankets, displaying higher albedo than adjacent terrain, and is interpreted to represent lava flows erupted from fissures, or possibly deposits of alluvial or eolian origin (Scott and Tanaka, 1986). The Knobby member (Hvk) is similar in appearance to the Mottled member, but displays higher albedo and abundant small, dark, knob-like hills, some with summit craters. Scott and Tanaka (1986) have interpreted the unit to be of diverse origins including volcanic lava flows and eolian mantle.

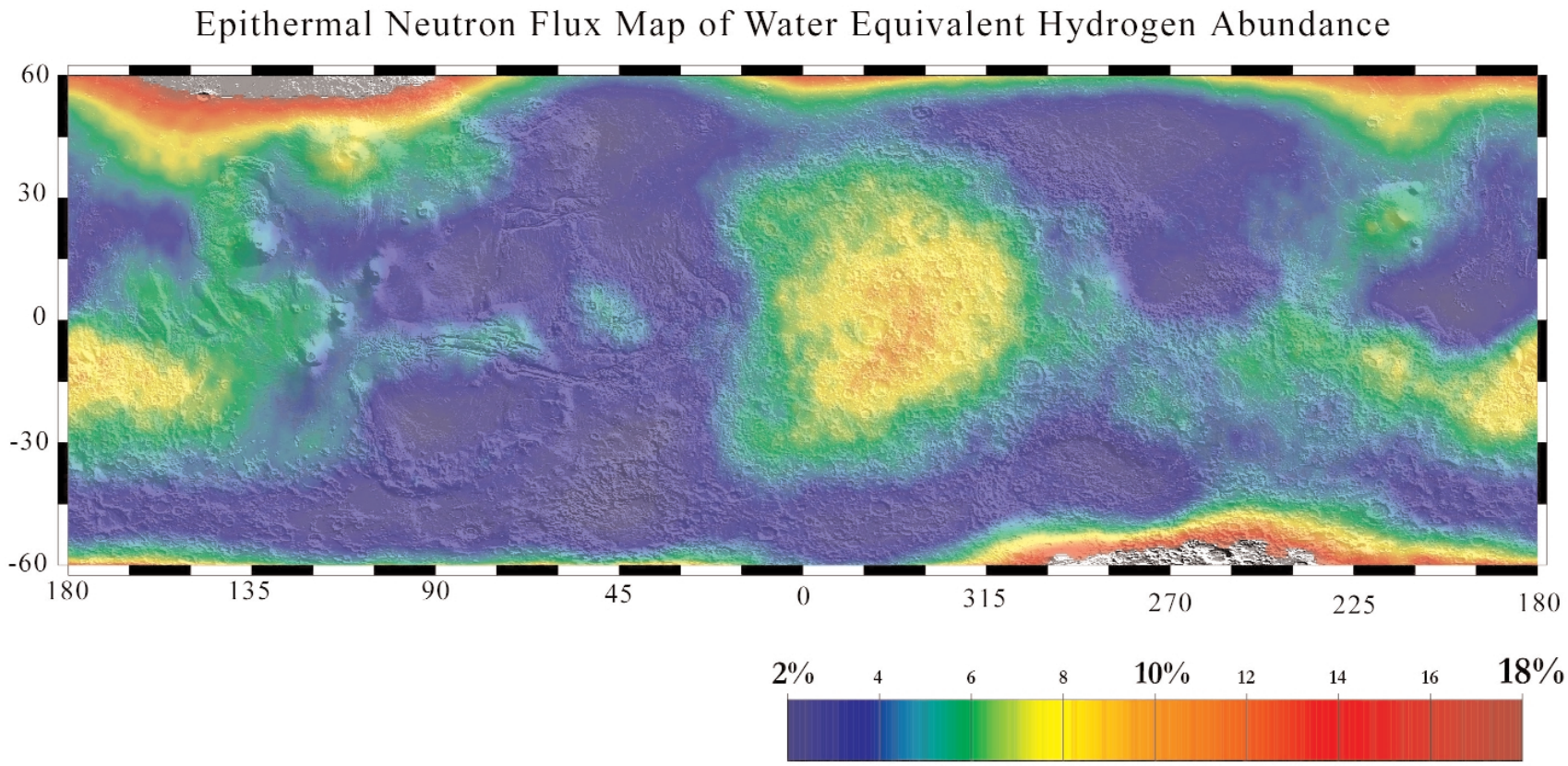

Figure 6: Epithermal neutron flux map of Mars, displaying water-equivalent hydrogen abundance. Courtesy: Los Alamos National Laboratory, 2003.

CHAPTER 3: PERMAFROST AND RELATED PROCESSES ON EARTH

3.1 INTRODUCTION TO PERMAFROST

First coined by Simeon W. Muller (1945), the term permafrost describes ground, whether rock or soil, that remains below 0°C continuously for two or more years. This time constraint is emplaced to avoid the inclusion of the overlying layer, which freezes every winter and thaws every summer termed the active layer. Permafrost is defined solely by temperature, and is independent of lithology or type of earth material, water content, or degree of induration (Black, 1954). The thickness of permafrost and the overlying active layer depend on local climatic conditions, soil properties, and vegetation cover. Permafrost thickness is also a function of ground surface temperatures and the geothermal gradient. Black (1954) suggests that permafrost exists in areas totaling ~26% of Earth's land area.

3.1.1 Temperature of Formation

Permafrost forms where the net heat balance at the surface of the Earth produces a mean annual air temperature below 0ºC over a period of several years (Black, 1954). This negative heat balance results in incomplete thawing of ground (consolidated by ice or not) that was frozen during the previous winter (French, 1996).

Mean annual air temperatures may vary greatly from mean annual ground temperatures, leading to uncertainty in the prediction of permafrost occurrence (Williams and Smith, 1989). Determination of mean annual ground temperature is dependent upon heat and mass exchange processes external to the formation material. As such, factors affecting the ground surface (vegetation, snow cover, etc.), along with climate influence permafrost development. Permafrost, or perennially frozen ground as it is often referred, typically develops in periglacial environments and areas in which the temperature prerequisite is fulfilled, such as at high altitudes, high latitudes, and submerged sea bottoms.

3.1.2 Thickness and Distribution

Under steady state conditions when permafrost is neither aggrading nor melting, an equilibrium exists between the internal heat gain with depth (the geothermal gradient) and heat loss from the surface (French, 1996). This balance determines the thickness to which permafrost develops. The lower limit of permafrost is defined when the amount by which the freezing point exceeds the mean surface temperature, is offset by the geothermal gradient.

The thickness of permafrost may also be altered by disturbances of the surface or changes in the climate, with an increase in mean surface temperature in the summer months resulting in a decrease in thickness and vise versa. Local variations in permafrost conditions also are dependant upon relief, aspect, and physical properties of the material, including thermal conductivity and heat capacity (Williams and Smith, 1989).

Permafrost is often classified on the basis of spatial continuity, and is divided into the continuous, discontinuous, and sporadic permafrost zones. The zone of continuous permafrost is the area in which "Permafrost occur(s) everywhere beneath the exposed land surface throughout a geographic region with the exception of widely scattered sites, such as newly deposited unconsolidated sediments, where the climate has just begun to influence the ground's thermal regime causing the formation of continuous permafrost" NRCC (1988). This classification encompasses the northern halves of Alaska and Canada, two-thirds of Greenland, and considerable parts of Tibet, Siberia, and China (Figure 7). Permafrost within the continuous zone of northern Alaska is on the order of 245-365 metres thick (Black, 1954), with maximum thicknesses of 610 metres recorded at some locations, including Prudhoe Bay, Alaska (French, 1996).

The zone of discontinuous permafrost is defined by the NRCC (1988) as the area in which "Permafrost occur(s) in some areas beneath the exposed land surface throughout a geographic region where other areas are free of permafrost." This zone

covers the majority of Alaska and Canada, all of Greenland, central Iceland, northern Scandinavia and Europe, and extensive areas of Tibet, Siberia, and China (Figure 5). The thickness of permafrost within the discontinuous zone is broadly variable ranging, for example, from 0-120 m in Alaska (Black, 1954).

Permafrost underlies 50-90% of the land area in the widespread permafrost zone, and occurs predominantly in peatlands underlying 10-50% of the land area in the sporadic zone at the southern region of discontinuous permafrost (Black, 1954). Localized permafrost also exists, where it is found in small isolated lenses in peat and affects less than 10% of the land area.

Broadly governing the distribution of the continuous and discontinuous zones of permafrost is climate, in which the boundary between the two roughly coincides with the -6 to -8°C mean annual air temperature isotherm (French, 1996).

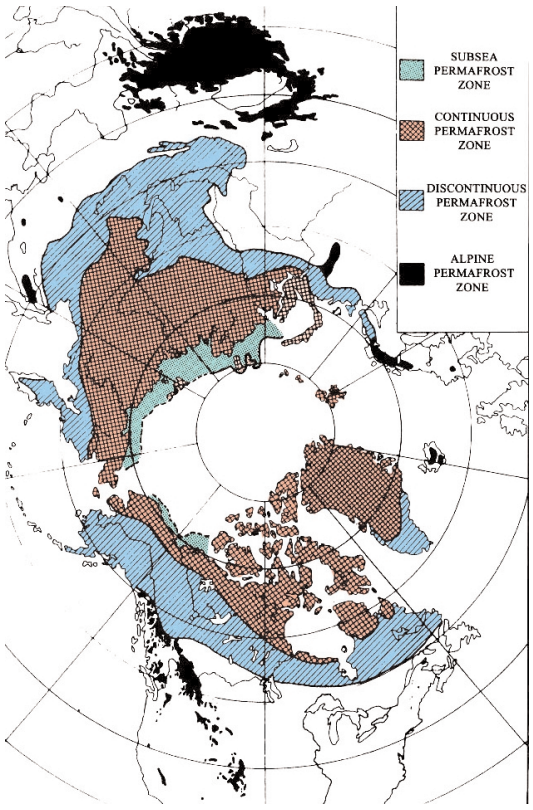

Figure 7: Representation of permafrost distribution in the terrestrial northern hemisphere, displaying the zones of continuous, discontinuous, subsea, and alpine permafrost. After: Péwé, 1975.

3.1.3 Permafrost Composition and Association

Permafrost may be composed of any type of material, regardless of consolidation (Williams and Smith, 1989). Moisture, in the form of water or ice, is an important component and is referred to by Black (1954) in terms of available pore space when unfrozen. Supersaturated, saturated, and undersaturated refers to the presence of more ice than pore space, an equal amount, or less ice than pore space, respectively.

The upper surface of the permafrost termed the permafrost table, is overlain by the supra-permafrost layer (French, 1996). The supra-permafrost layer includes the active layer, referring to the seasonal freeze-and-thaw layer present in the continuous and discontinuous permafrost zones (Figure 8). The active layer may be in contact with the permafrost table, or it may directly overlie unfrozen ground termed talik. The term 'talik' is used to describe unfrozen layers below the permafrost (sub-permafrost taliks) or within the permafrost (intra-permafrost taliks). Open and closed taliks may also exist if the talik is completely enclosed by permafrost (open talik), or if it is in contact with the active layer (closed talik), (French, 1996).

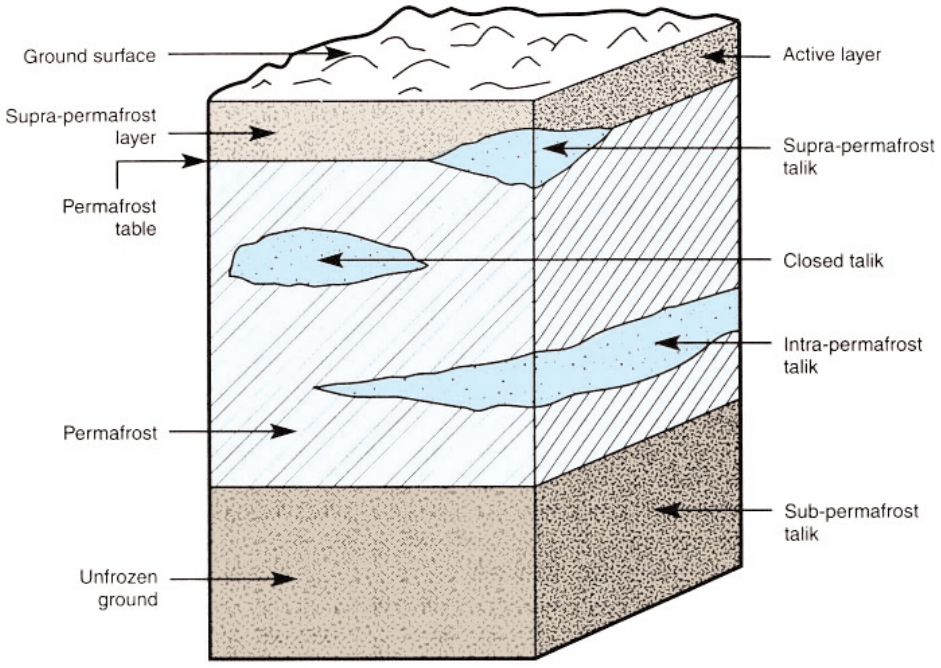

Figure 8: Schematical representation of permafrost terminology.
After: Ferrians et al., 1969.

3.1.4 Surface Features of Permafrost

Numerous surface expressions exists that are either directly or indirectly related to the presence of permafrost. Divided into two categories, these features reflect those associated with the aggradation of permafrost, and those with the degradation of permafrost (French, 1996). Although the development of many of these features is exceptional in permafrost regions, not necessarily all are limited to these environments and may form in non-permafrost regions as well. Examples of such features include; cryoturbation steps, palsas, thermokarst landforms, and patterned ground (including sorted/nonsorted circles and stripes).

3.2 INTRODUCTION TO GROUND ICE

Ground ice is defined by Pihlainen and Johnston (1963) as "a body of more of less clear ice within frozen ground." It is a term generally applied to all forms of ice that develop in frozen ground and during the freezing process. Ground ice may be present in pore spaces, voids, cavities, or other available openings in the ground material (French, 1996).

3.2.1 Classification of Ground Ice

Ground ice is quantitatively defined on the basis of ice content, and amount of excess ice (French, 1996). Defined as the weight of ice to dry soil, the ice content is expressed as a percentage, with values of less than 40-50% considered low. French (1996) states that excess ice pertains to "the volume of supernatant water present if a vertical column of frozen sediment were thawed."

Ground ice may be classified as epigenetic (forms as the average annual climate cools down) or syngenetic (results from a change in vegetation or an increase in deposition of soil) in the most general case. Mackay (1972) has suggested a

classification scheme dependent upon the source of the water prior to freezing, and the principal transfer process by which the water is moved. Three broad types of ground ice are recognized when employing this classification scheme (Figure 9), namely; 1.) wedge ice (including vein ice, ice wedges, and tension crack ice), 2.) segregated ice (i.e. epigenetic and aggradational ice), and 3.) intrusive ice (i.e. sill and pingo ice). Péwé (1966) expands this classification scheme to include pore ice, buried ice, and ice existing in caves, shafts, and other various openings.

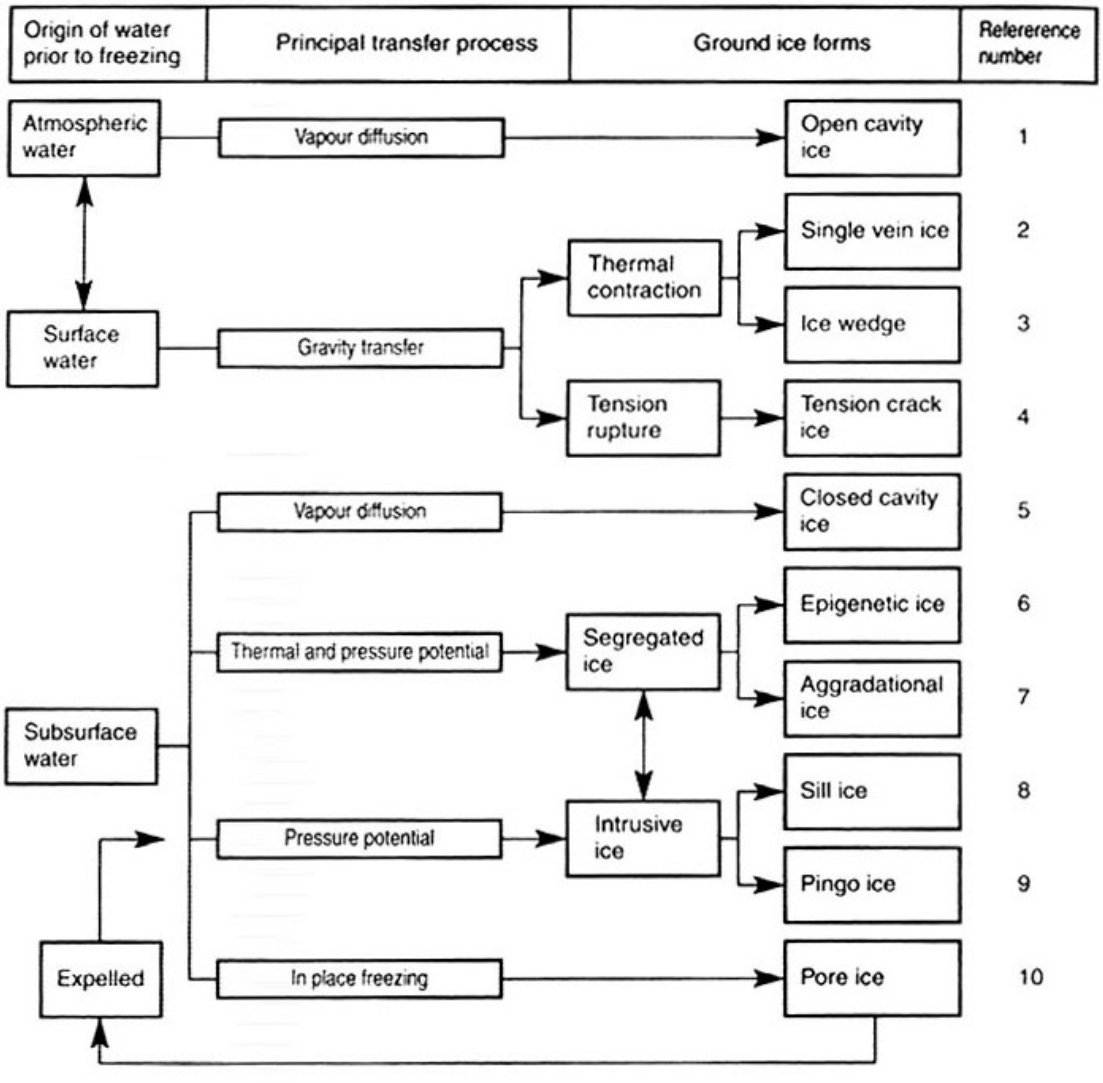

Figure 9: Classification scheme used to depict types of ground ice.
After: Mackay, 1972.

3.2.2 Wedge Ice

Wedge ice refers to large masses of ice which develop in thermal contraction cracks over many years (Péwé, 1966). Although discussed in detailed in Chapter 4, ice wedges require permafrost for their existence, and often occur in the continuous permafrost zone and poorly drained tundra lowlands where conditions of formation are favourable (French, 1996). Ice wedges form by the successive, annual accumulation of vein ice where water penetrates open tension fissures in the ground surface. Water that forms ice is derived from meltwater or rainfall, or release of unfrozen water in permafrost at the newly exposed crack surface. The fissures in which vein ice develops, form by thermal contraction of the tundra surface (Lachenbruch, 1962), generally within the upper 60cm of permafrost. Vein ice displays characteristic vertical foliation planes, identified by films of organic or inorganic matter, and air bubbles (Péwé, 1966). The formation of ice wedges from vein ice are an important feature in permafrost regions, and they often produce distinctive surface expressions such as polygonal networks, discussed in detail in Chapter 4.

3.2.3 Segregation Ice

Also referred to as Taber ice (Péwé, 1966), segregated ice occurs in both permafrost and seasonally frozen ground. Referring to soil in which the ice content is high (greater than 40-50%), segregated ice forms as the soil begins to freeze, causing water that is present to segregate into ice lenses. Unconsolidated substrates with grain size of 0.1 mm diameter or less are favoured for ice segregation, and the resulting ice crystals tend to develop in the direction of rapid heat conduction away from the surface (French, 1996). The thickness of ice lenses is on the order of centimeters to metres, and segregated ice may be identified by the presence of soil particles and air bubbles oriented normal to the plane of freezing.

3.2.4 Intrusive Ice

Originating from ground water supplied by increased hydrostatic pressure (Péwé, 1966), intrusive ice develops in both the seasonally and perennially frozen zones. The resulting ice body is relatively pure, with pingo and sill ice being the two types commonly identified (French, 1996). Pingo ice generally occurs in horizontal or lens-shaped masses, ranging from 50-100 m in diameter in Alaska, and up to 300 m elsewhere (Péwé, 1966). Pingos may form either by the intrusion and freezing of water under increased hydrostatic pressure, or as a result of segregated ice lenses. Sill ice forms as a tabular mass along the base of the active layer when a confining material is intruded by water that subsequently freezes (French, 1996).

CHAPTER 4: POLYGONAL PATTERNS

4.1 SMALL-SCALE POLYGONS ON MARS

Landforms indicative of an environment dominated by permafrost were recognized as long ago as the 1960s. Images from orbit and the Viking orbiter missions provided evidence of geomorphic features suggested to have formed as a result of ground ice and permafrost, such as patterned ground (Baker, 2001).

Carr (1996) suggests that ground ice in the crust and soil may represent one of the largest reservoirs of water on Mars. Ground ice in the subsurface is predicted to be stable, under current Martian conditions, at latitudes poleward of 40^{o} (Fanale et al., 1986), with exact latitudes dependant on local thermophysical properties (Mustard et al., 2001).

4.1.1 Qualitative Description

Small-scale polygonal patterns on the Martian surface, were first described based on Viking Lander 2 panoramic images and Viking Orbiter images (Kuzmin et al., 2003). The polygonal terrains are located in both the Northern and Southern hemispheres, particularly at latitudes greater than 40^{o}, thus where ground ice is predicted to be stable. Martian polygons on the order of tens to hundreds of metres in diameter are recognized, and their origin attributed to the contraction of ice-rich soil (Mellon, 1997). It is important to note that giant polygons several kilometres in diameter have also been observed. Their formation; however, is attributed to the tectonic uplift of basin floors, possibly related to the removal of a load which represents a former standing body of water, or as a result of the freezing and expansion of residual water near the subsurface (Hiesinger and Head, 2000).

Small-scale polygons within the region of Utopia Planitia (43.5^{o}N, 269.3^{o}W) within the Northern Plains of Mars, vary in size from 20 –200 metres in diameter, having an average size of ~80-90 m based on observations by Kuzmin et al., (2002).

Abundant polygons have been noted to occur on crater floors (Figure 10); however, the polygonal terrains themselves are essentially uncratered, indicating a relatively young phase of water-related activity on Mars (Baker, 2001). Kuzmin et al., (2002) also reports that the polygons are predominantly orthogonal in form and display 3-way and 4-way intersections.

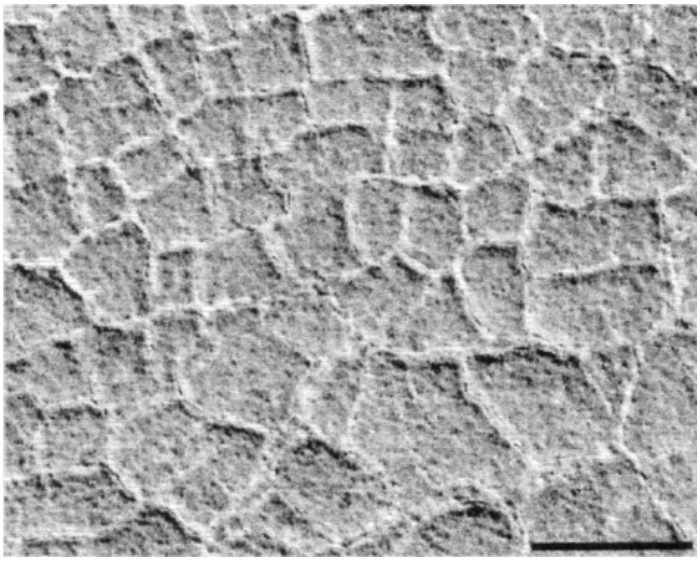

Figure 10: Polygonal pattern discovered on the floor of a crater in Mars' northern plains. Approximate location: 67.5ºN, 312.5ºW. MOC image M01-00294. Scale bar = 200m.

Relating the observed small-scale polygons to a thermal contraction process similar to that responsible for terrestrial polygons, is primarily based on visual morphological evidence (Mellon, 1997). In an attempt to ascertain the origin of the Martian polygons, Mellon (1997) developed a time-dependent viscoelastic model of thermal stress to test the hypothesis that small-scale Martian polygons are the result of thermal contraction cracking, as is often the cause of polygonal patterns in terrestrial permafrost. Using a time-dependent Maxwellian viscoelastic model, similar to the steady-state model of Lachenbruch (1962) used to study terrestrial polygons, an examination of seasonal tensile stress owing to seasonal temperature variations were

conducted for Martian soils. For the purpose of this study Mellon (1997) assumed that the Martian subsurface was ice-cemented and that approximately all pore space was filled. Results of this study indicate that seasonal variations in ground temperature might cause the tensile stress sufficient to fracture ice-cemented permafrost at depths of 1.5 m or less. Mellon (1997) suggests that these fractures could then propagate to greater depths due to the added stress in subsequent layers caused by the fracture strain of layers above. Using a tensile stress of 2 – 3 MPa, appropriate for ice at low temperatures (Mellon, 1997), fractures might readily form in ice-cemented permafrost poleward of 20º to 30º latitude as the tensile stress should exceed the tensile strength at this point.

4.2 EARTH ANALOGUE

4.2.1 Known Mechanisms of Formation

Ice-wedge networks, long recognized in areas of terrestrial permafrost, are the product of ice wedges interconnected to form closed polygons (French, 1996). These networks are widespread in Arctic and subarctic landscapes, especially in ice-rich lowlands of unconsolidated terrain. A clear understanding of mechanisms for the development of ice wedge networks is crucial for their comparison with visually similar features on Mars.

By definition, ice wedges require permafrost for their existence (French, 1996). The contraction theory of ice wedge development, originally proposed by Leffingwell (1915), states that fractures develop where cooling-derived tensile stress exceeds the tensile strength of frozen ground. Conditions for cracking may differ; however, for soils with varying ice contents (French, 1996), and the absolute temperature and rate of temperature change is also suggested by French (1996) to be important in the formation of fractures. The primary fracture initiates at or near the ground surface, and has the ability to spread in either horizontal or vertical directions (Mackay, 1986). When the

temperature rises the following spring, the water from melting snow infiltrates the crack and subsequently freezes. Along with the accumulation of frost hoar on crack walls, this produces a vertical vein of ice that penetrates the permafrost and prevents the closing of the fracture the following summer when temperatures rise and the ground expands. The re-expansion of frozen soil during the summer months causes horizontal compression, resulting in plastic deformation of surrounding frozen soil (Lachenbruch, 1962). The deformation may lead to the development of distinct ridges at the ground surface, separated by a central depression over the wedge (French, 1996). The vertical ice vein is a plane of weakness, which reopens during following winters due to renewed thermal tension (Lachenbruch, 1962). Additional melt water and/or ice is deposited into the fracture the following spring, which subsequently freezes, and over many years produces a vertical ice-wedge (Figure 11).

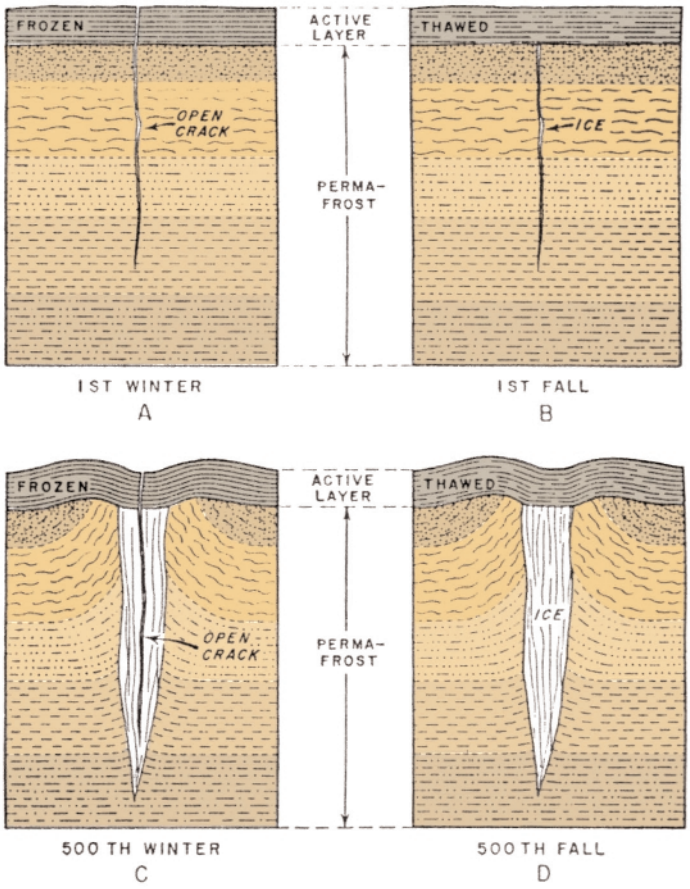

Figure 11: Schematic representation of ice-wedge formation based on the contraction crack theory set forth by Leffingwell (1915).
11A Formation of vertical fracture during the Arctic winter as a result of tension stress caused by thermal contraction of the surface.
11B Melting of snow in the spring results in the accumulation of water in the crack. This water subsequently freezes with the accumulation of hoarfrost, producing a vertical vein of ice.
11C Re-expansion of the permafrost the following summer produces horizontal compression, leading to the upturning of strata by plastic deformation.
The crack reopens the following winter as a result of renewed thermal tension, and meltwater again enters and freezes in the crack.
11D Repetition of this cycle over hundreds of years leads to the formation of vertical wedge-shaped masses of ice.
After: Lachenbruch, 1962.

4.2.2 Principal Controls Over Network Patterns and Spacing

The formation of numerous ice-wedges eventually leads to their surface expression as a network of polygonal patterns. Ice-wedges join predominantly at right angles and range in diameter from 15 to 80 metres (Black, 1976). Intersections within most polygonal networks display a tendency towards orthogonality (Leffingwell, 1915; French, 1996; Black, 1976). These have been proposed to form by sequential emplacement of fractures in which the gradual build up of stress results in primary fractures forming where strength is low (a flaw) or stress is high. The first fracture imposes an anisotropic residual stress that constrains the angle of propagation of a second fracture to the perpendicular to the first (Lachenbruch, 1965). This proposed mechanism, although rarely observed in nature because of a lack of measurements, is observed to occur in numerical models of fracture network development (Plug and Werner, 2001), which reproduces the planview geometry of natural ice wedge networks.

Orthogonal networks have been classified into "random" orthogonal systems in which the cracks display no preferred direction of orientation, and "oriented" orthogonal systems in which they do (Figure 12) (Lachenbruch, 1965). Oriented orthogonal systems are thought to result from horizontal stress differences generated by horizontal thermal gradients, which create anisotropic stress that constrain the initial fracture to follow a straight, coherent path perpendicular to the axis of principal stress. One natural location where thermal gradients occur is near receding bodies of water (Lachenbruch, 1965).

Non-orthogonal intersections, also referred to as hexagonal or angular junctions, display equiangular intersection angles of 120º. These have been proposed to form by several different mechanisms. One hypothesis is that equiangular intersections form where cracks develop in a homogeneous, nonplastic media subjected to uniform cooling (Lachenbruch, 1965). An alternative hypothesis is that branching of rapidly propagating fractures may form 3-way equiangular intersections; however all measurements of crack

propagation in frozen ground have shown that cracks propagate at rates far below the speed of an elastic shear wave, which is the minimum "speed limit" for branching to occur (Plug and Werner, 2001; Lawn, 1993). Lastly, 3-way equiangular intersections have also been proposed to develop where initial fractures follow sinuous paths under heterogeneous stress and/or substrate rheology. In this case, secondary fractures propagate toward the outer, convex side of bends in primary fractures and adopt an orientation perpendicular to the tangent of the primary fracture. This produces an intersection that appears to be 3-way equiangular, especially when the sub-meter scale details of the intersection are observed by subsequent growth of the ice wedge and deformation of surrounding permafrost (Plug and Werner, 2001). This model cannot account for polygonal networks in which the majority of intersections are 3-way equiangular; however, measurements or intersection statistics that show such networks exist in nature are not available (Plug and Werner, 2001).

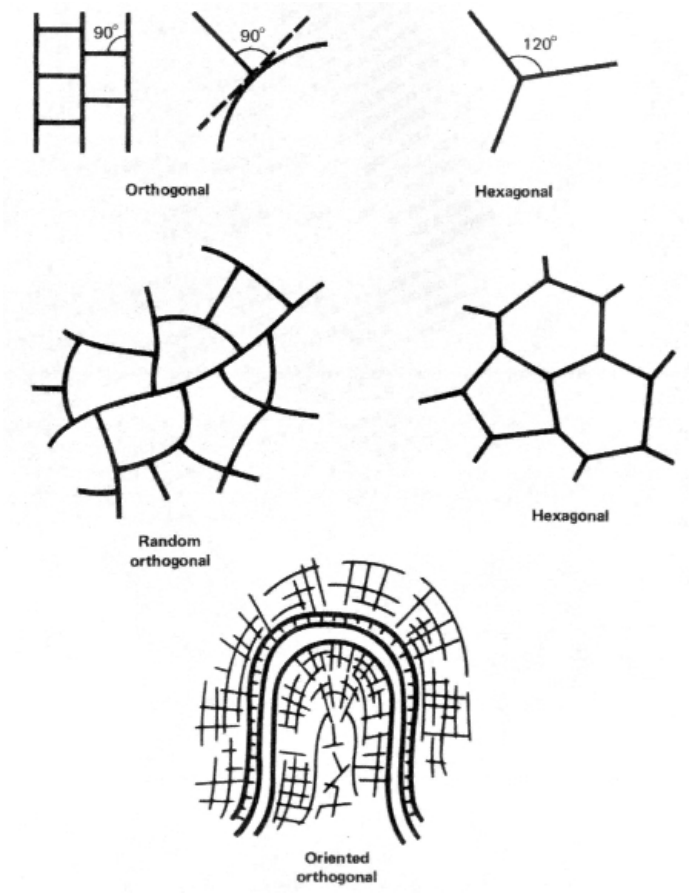

Figure 12: Orthogonal versus non-orthogonal classification scheme as proposed by Lachenbruch, 1965. After: French, 1996.

CHAPTER 5: METHODS

5.1 COLLECTION / SEARCH OF IMAGES

5.1.1 Martian Images

Images of Mars' surface have been collected at increasingly high resolution by a series of orbiters, from Mariner 4 in 1965 to, most recently, the Mars Orbiter Camera (MOC) on the Mars Global Surveyor which has continuously collected images since 1997. MOC collects both narrow and wide-angle images are collected in push-broom fashion, in which charge-coupled devices (CCDs) are in the form of 1-D detectors consisting of a single line of CCD elements. Numerous measurements of the CCD produces a 2-D image, in which the line array is scanned in the down-track direction by the motion of the spacecraft itself over the planet's surface (Caplinger, 1995). As a result, MOC images display much higher resolutions (~1.5-12.4 m/pixel) than is possible with framing systems. MOC imagery is freely distributed for scientific purposes from online databases provided by the Malin Space Science Systems (http://www.msss.com/moc_gallery/) and NASA's Planetary Image Atlas (http://pdsimg.jpl.nasa.gov/Atlas/).

To assemble a complete database of images of polygonal networks from Utopia Planitia, I examined all narrow-angle MOC images acquired from 09/1997 to 02/2003. This included all images obtained during the initial Mapping Phase of the mission (in which images are identified by a 3-character mission subphase descriptor designated M01-M23) those obtained during the Extended Mission Phase (designated E01-E23), and those obtained during the Relay Mission Phase that began January 1, 2003 (designated R01-R02).

The search region spanned the Casius region of Utopia Planitia, in which latitude ranges from 30º-65ºN, and longitude ranges from 240º-300ºW. Images are selected from the narrow angle gallery, referring to images acquired by the narrow angle camera system during the mapping phase of the Mars Global Surveyor (MGS) mission (Malin

et al., 2003). Image resolutions range from 1.5 to 12.4 metres per pixel, and selected images are downloaded in GIF, map-projected format, providing the best quality for analysis.

Image selection is further based on the following criteria, to ensure that only usable images are obtained. Only polygons displaying diameters less than 200m are included in this study (Figure 13), and all are located within Utopia Planitia on Mars' northern plains, specifically within the Casius region (30º-65ºN, 240º-300ºW). Selected images are in map-projected form, and images with errors or which displayed discontinuous or faint polygons were mapped, but not included in pattern analysis. All images available to date (January 2004) were considered, and include those released between September 1997 and February 2003.

Small-scale polygonal images referenced by other authors, including: Seibert and Kargel (2001), Kuzmin and Zabalueva (2003), Yoshikawa (2003), and Baker (2001), were verified and included where deemed appropriate. A total of 825 images were reviewed, 28 of which were selected for pattern analysis. Of these 28 images, 7 were previously identified by other authors. Appendix B contains the database of all images included for pattern analysis.

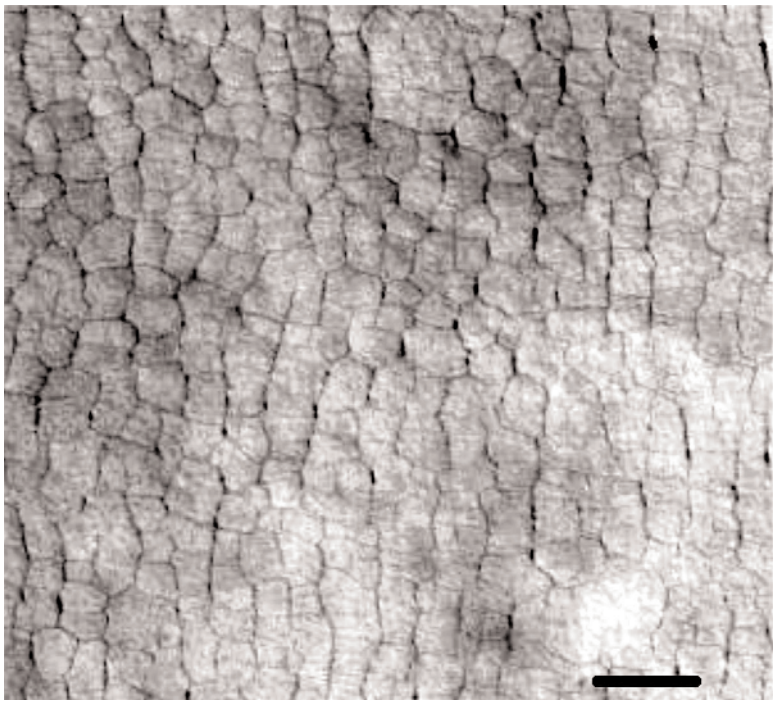

Figure 13: Example of small-scale polygons on Mars selected for pattern analysis in this study. Average polygonal diameter is ~80-90m. MOC image M01-01631. Scale bar = 250m.

5.1.2 Terrestrial Images

Terrestrial polygonal patterns used for comparison are taken from aerial photographs of the delta and mainland region located at the mouth of the Sagavanirktok River (Figure 14), where it empties into the Beaufort Sea near Prudhoe Bay, Alaska (70ºN-147ºW). Image resolution is 1.34 metres per pixel, and a total of 10 polygonal networks (Figure 15) were digitized and included in pattern analysis (Figure 16). Appendix A contains the terrestrial image database.

Prudhoe Bay is located on the north slope of Alaska, within the zone of continuous permafrost. It is located ~2092 kilometers south of the North Pole and 402 kilometers north of the Arctic Circle. Monthly temperature fluctuations (ºC) at Prudhoe Bay are listed in Table 2, and precipitation fluctuations (cm) in Table 3 (Western Regional Climate Center, 2003). Typical vegetation at Prudhoe Bay consists of moist

tundra, the dominant species consisting of grasses and moss cover with snow ranging from 5.0-16.0 cm deep (Western Regional Climate Center, 2003).

Figure 14: Region from which terrestrial polygonal patterns used for comparison are taken from. Location is at the mouth of the Sagavanirktok River where it connects to the Beaufort Sea, north of Prudhoe Bay, Alaska (70°N-147°W). After: Rand McNally Atlas, 2000.

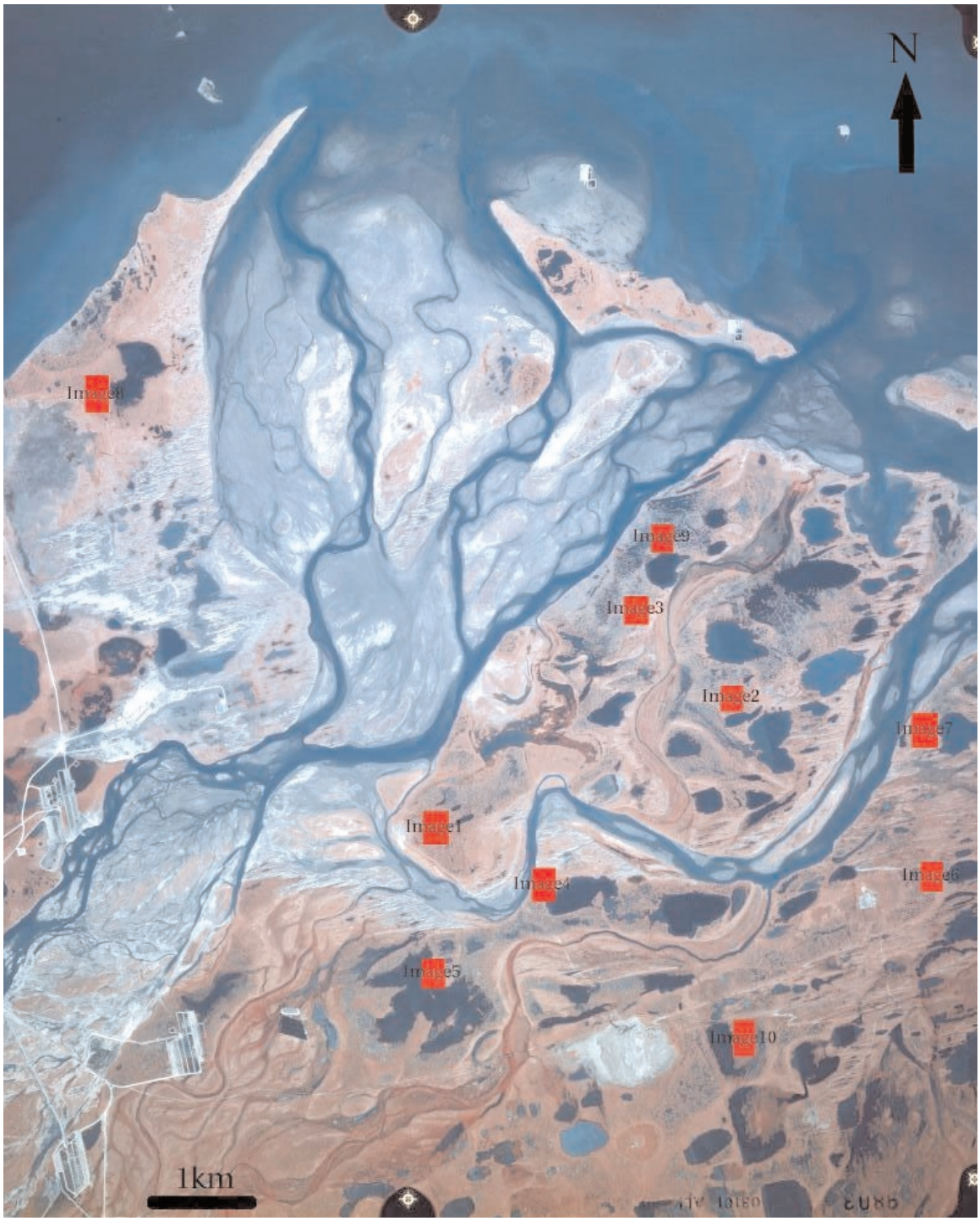

Figure 15: Aerial photograph from which terrestrial polygons were taken. Photograph displays the delta and mainland region located at the mouth of the Sagavanirktok River, where it empties into the Beaufort Sea, near Prudhoe Bay, Alaska.

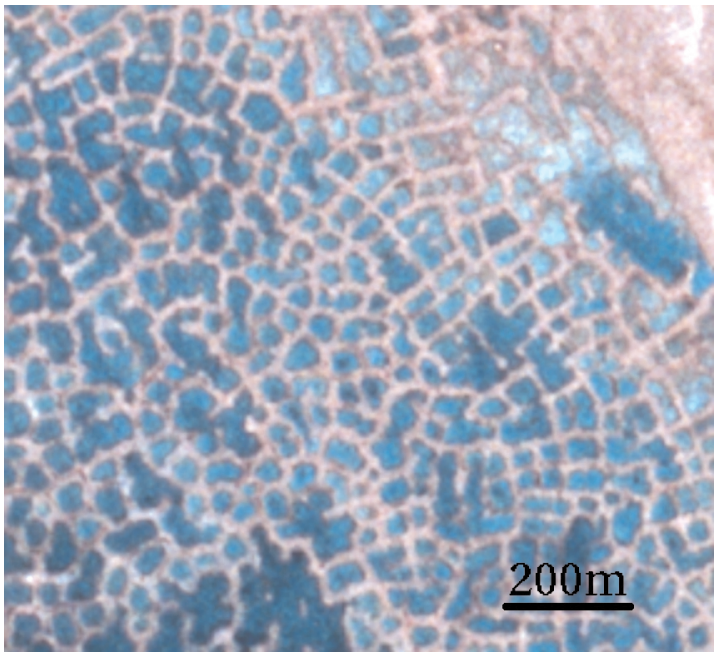

Figure 16: Example of terrestrial polygon digitized for pattern analysis. Average polygon diameter is ~53 m. Scale bar = 200m.

Month	Maximum Temperature (…C)	Minimum Temperature (…C)
January	-24.3	-31.1
February	-23.4	-31.3
March	-20.7	-29.1
April	-12.2	-20.4
May	-1.8	-7.2
June	7.3	0.4
July	13	4.3
August	10.6	3.1
September	3.5	-1.7
October	-6.1	-12.4
November	-17.3	-23.9
December	-21.4	-28.4
Annual	-7.7	-14.8

Table 2: Average maximum and minimum monthly temperature fluctuations (ºC) measured between 1986 – 1999. After: Western Regional Climate Centre, 2003.

Month	High (cm)	Low (cm)	Mean (cm)
January	1.98	0.00	0.51
February	1.85	0.00	0.43
March	0.89	0.00	0.36
April	0.81	0.00	0.20
May	0.94	0.00	0.23
June	4.09	0.08	0.99
July	3.12	0.66	1.73
August	5.89	0.94	2.90
September	3.10	0.48	1.55
October	2.06	0.08	0.97
November	1.70	0.00	0.46
December	1.14	0.00	0.51
Annual	18.82	7.37	10.82

Table 3: Annual, high, and low precipitation fluctuations (cm) at Prudhoe Bay, Alaska measured between 1986 – 1999. After: Western Regional Climate Centre, 2003.

The aerial photograph from which terrestrial images of polygons were selected, was taken using color-infrared film. This type of film has a yellow filter overlying the three emulsion layers in order to block ultraviolet (UV) and blue wavelengths. Once processed following exposure, the film produces yellow, magenta, and cyan dyes. Green vegetation (having a high reflection level of near-infrared wavelengths) appears red on the processed film; red objects (with very low near-infrared reflection) appear green; green objects (also with very low near-infrared reflection) appear blue; and blue objects (with very low near-infrared reflection) appear black (Carolina Map Distributors, 2003). The airphoto used is a USGS mapping photo with a 1:60000 scale.

5.1.3 Mudcrack Images

An additional set of images used for comparison are drawn from a desiccation crack experiment conducted at Dalhousie University in the summer of 2003. The mudcracks developed naturally in 10cm thick mud collected from the inter-tidal zone of the Minas Basin, Bay of Fundy, and dried in ambient conditions in a 119.4 cm x 119.4 cm plastic chamber. Images were collected by digital camera at 20 minute intervals; in total 7074 images were taken over a 8.5 week period, with the experiment ending when no new cracks opened, and no existing cracks propagated for a two week period. Images have a resolution of 0.002 m/pixel.

A total of 11 mud crack images were selected from the five series, chosen to represent the development of the pattern rather than at even time intervals. These were digitized and included in pattern analysis (Figure 17 A,B,C). Appendix B contains the mudcrack database.

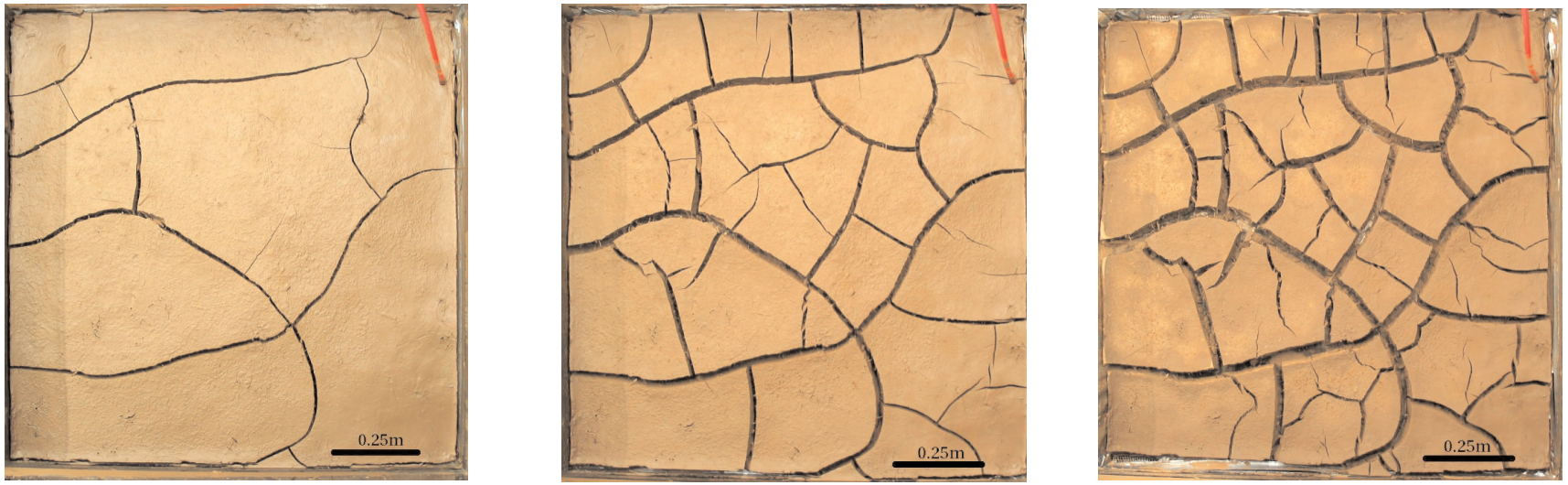

Figure 17 A, B, C: Example of sequential mud crack images digitized and included in pattern analysis. Scale bar = 0.2m.

5.2 DIGITIZING PROCESS

Selected images were scaled and enhanced to increase the ease with which digitizing was conducted. Image enhancements include adjusting the tonal range of images, i.e. contrast levels, saturation, and hue. The digitizing of terrestrial, Martian, and mudcrack images was preformed using Cracktrace, an open source program expressly designed for digitizing geomorphic patterns (Plug and Helmick, 2003). The majority of images were increased in size by a factor of two or three, depending on the image, effectively reducing the pixel size by 1/2 or 1/3 respectively. Cracktrace compensates for the change in ratio, by allowing the user to input scaled "x" and "y" values. Cracktrace generates a matrix file in which digitized line segments are represented in raster form, with the value of each element in the matrix crossed by a line segment set to the angle of the segment. The resulting matrix file is entered into the program Matlab, allowing for angle and spacing determinations, as described by Plug and Werner (2001).

5.3 STATISTICAL COMPARISION OF NETWORKS

The majority of research completed to date regarding small-scale polygonal patterns on Mars has focused on characterizing networks with respect to polygonal diameter, intersection types, and number of sides. Seibert and Kargel (2001) conducted a systematic analysis of small-scale polygons, noting average polygonal width and preferred orientation through the use of high-resolution MOC images. Yoshikawa (2003) preformed analysis on crack orientations, employing the nearest neighbor technique that produces a statistical description of patterns, independent of polygon size. Mellon (1997) produced a time-dependent viscoelastic model of thermal stress in an attempt to compare terrestrial and Martian patterns.

The method I have adopted follows that of Plug and Werner (2001) who measure spacing and relative orientation (angle) between successive fractures along randomly

selected sample lines. "Spacing" is the distance (measured along the sample line) between two successive intersections of the sample line and fractures. "Relative orientation" refers to the numerical value of the angle (ranging from -180º to 180º) between successive fractures. (Figure 18).

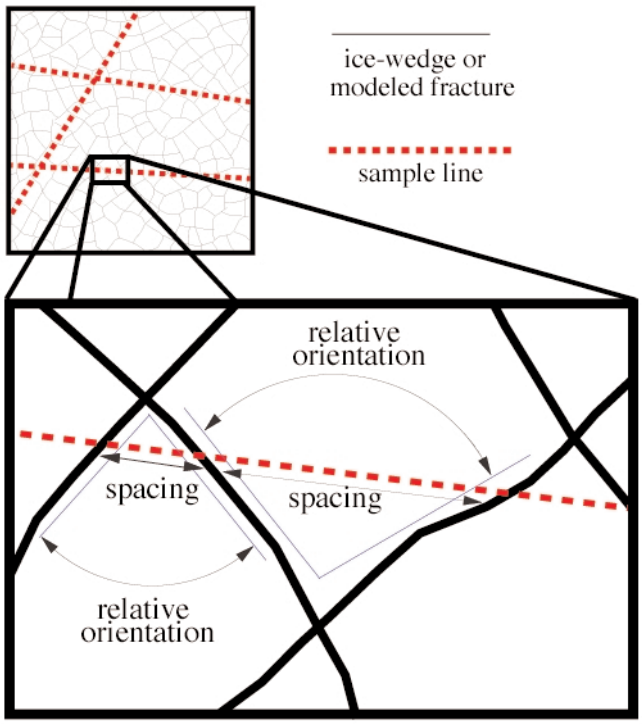

Figure 18: Spacing and relative orientation between fracture segments are measured along sample lines. After: Plug and Werner, 2001.

Error analysis was conducted by applying the Kolmogorov-Smirnov test to six images, each digitized by three separate individuals. Once digitized, the comparisons yield a probability (PKS) depicting the likelihood that the two sets of samples are not from different distributions. Values of PKS >0.1 indicate that borderline similarities exist between the digitized image sets, whereas PKS >0.2 suggests that the image sets are indistinguishable from one another. Results indicate that two of the three individuals conducted the digitizing process in a similar manner, as the mean of their PKS values is

>0.2 (0.3391). The third individual appears to have digitized in a different manner from the other two, as comparison of the individual's PKS values to those of the other individual's yields values of PKS <0.1, suggesting that notable difference exist among the two distributions. Results of error analysis can be found in Appendix C.

The Kolmogorov-Smirnov test is a goodness-of-fit test in which the difference between two distributions is characterized by the largest absolute differences in cumulative probability distributions. For two-dimensions, the cumulative probability distribution should be taken as the fraction of data contained within the four quadrants defined by the point (x, y), namely (x<X, y<Y), (x<X, y>Y), (x>X, y<Y), and (x>X, y>Y), (Peacock, 1983). The resulting statistic, *D,* is the maximum difference between the fraction of data contained in each distribution, (Smallwood, 1996). The normalization of statistic *D* by the square root of the number of observations ($Z = D\sqrt{N}$) yields a value for the test statistic *Z* (Plug and Werner, 2001). Comparison of *Z* to results determined by a Monte Carlo method which uses synthetic normal distributions, allows for the estimation of probability, P_{KS} (Smallwood, 1996). This probability (P_{KS}) refers to the likelihood that the two sets of samples are not from different distributions (Plug and Werner, 2001). For a binned distribution of 32 x 32 bins, $P_{KS} > 0.20$ suggests that no statistically significant difference exists between the two distributions, whereas $P_{KS} < 0.001$ implies that significant differences exist between the two distributions.

In addition to the use of Kolmogorov-Smirnov comparisons, two-dimensional distributions are shown as surface plots and are used to interpret planview characteristics of networks. Surface plots display the two-dimensional distributions of spacing and relative orientation between fractures (Figure 19), and are characterized by three values, displaying the degree to which successive fractures encountered along a sample line are orthogonal or parallel (Plug and Werner, 2001). The surface plots indicate the relative angle (degrees) and spacing (metres) between fractures. Orthogonal

intersections are represented by peaks in the distributions at +90ºand -90º, which extend out as ridges to the approximate value of spacing between parallel fractures, a value represented as a peak at 0º (Plug and Werner, 2001). Variations in the peak at 0º suggest a broad variety of polygon sizes (if the peak is stretched in the distance direction), or the increased disorganization of the network (if the peak is stretched in the angle direction). The width of the ridges is a measure of the degree of orthogonality of a network, with sharply peaked ridges corresponding to highly orthogonal and ordered networks, with neighboring fractures at ~ 90º to each other. Ridges which display sharp edges at small distances, but which widen toward larger distances are indicative of fractures in which

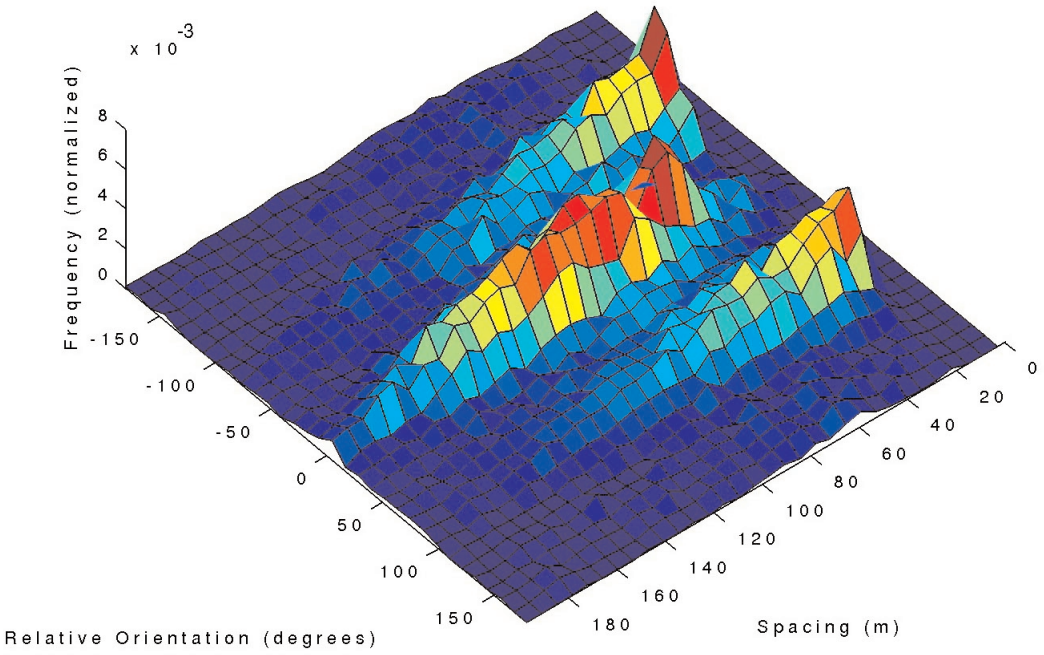

Figure 19: Two-dimensional distributions of spacing and relative orientation between fracture. MOC Image M04-03810.

orthogonal intersections occur where two fractures meet, but tend to deviate as the distance from the intersection increases. Broad ridges spanning 90º-120º suggest a network in which mixtures of orthogonal and hexagonal intersections occur together (Plug and Werner, 2001).

Two-dimensional distributions of angle and spacing are not sensitive to the

number of fractures at intersections, only to their relative orientations. To focus on intersection types, an additional method of comparison is applied to networks, discerning between three-way , four-way, and hexagonal intersections. For the purpose of classification, intersections are considered four-way if the spacing between opposing cracks of the intersection is <10% of the polygon diameter. Intersections are classified as non-orthogonal if the angle between the two fractures is ≤80º or >110º. This process is conducted manually, by counting the number and type of intersections present in the digitized images. This classification technique follows that of Yoshikawa (2003), but differs in that quantitative criteria are used to distinguish between intersection types. Here, the purpose of classifying intersections is to investigate developmental history of networks in the context of hypotheses for intersection types, as described in Chapter 4, section 4.2.2.

To investigate the overall absolute orientation of networks, the compass angle of each crack segment was automatically extracted from the digitized network. These values were binned into 10º wide bins and resultant distributions displayed as rose plots, with the concentric lines within the plot indicating the number of cracks in each bin. Pronounced peaks in rose plot distributions show dominant orientation of the networks, if any. For “random orthogonal” networks (terminology from Lachenbruch, 1965; French, 1996) rose plots display no strongly preferred orientation.

CHAPTER 6: RESULTS

6.1 INTRODUCTION

This chapter presents results of terrestrial, Martian, and mudcrack images included for pattern analysis. Polygonal networks are discussed with regards to variations in spacing, intersection type, and orientations, with a view to interpreting the origin of patterns, their spatial variability, and the information they hold on the substrate and climate history of the Utopia Basin. Complete results for networks are presented in Appendix B and images of networks in Appendix A. Here I focus on key results that differentiate networks and have the greatest significance for Mars' geological history.

6.2 QUALITATIVE DESCRIPTION OF MARTIAN NETWORKS

6.2.1 Distribution of Martian Polygonal Networks

A total of 28 Martian polygonal networks were digitized and included for pattern analysis. All are located within the Casius region of Utopia Planitia, between 30-65ºN latitude and 240-300ºW longitude. Polygonal networks are divided into five regions for ease of visualization and to organize presentation of results (Figure 20).

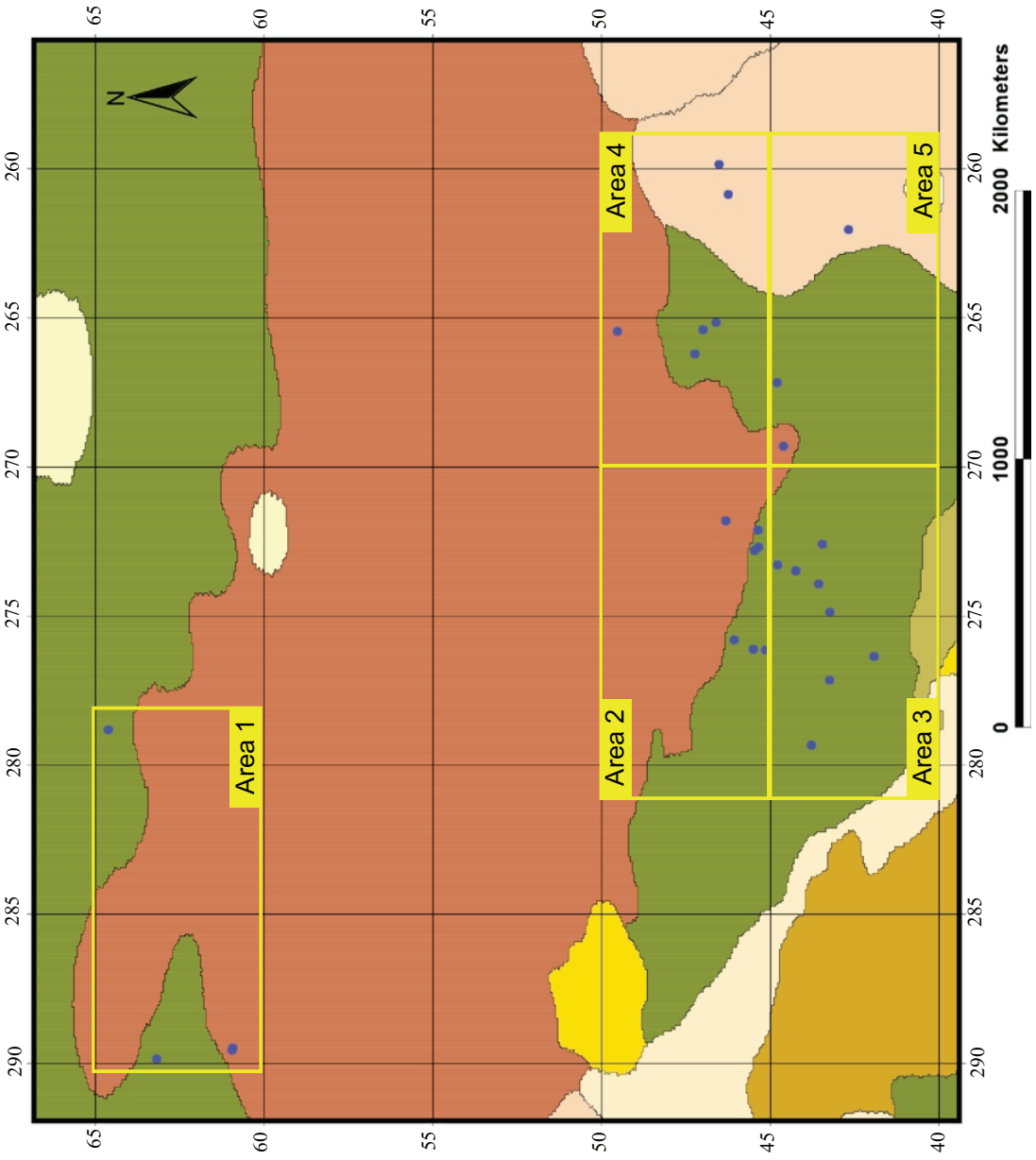

Figure 20: Division of polygonal networks into five regions within Utopia Planatia.

6.2.2 Region 1 Polygonal Networks

Region 1, located between 60-65ºN and 277-290ºW, contains four networks included in pattern analysis (Figure 21). The geological units in which networks reside are the Mottled Member (Hvm) and the Knobby Member (Hvk) of the Vastitas Borealis Formation, both of Hesperian age (Scott and Tanaka, 1986). The Vastitas Borealis Formation comprises subpolar plains deposits within the northern lowlands, its members distinguished by morphology and albedo contrast (Scott and Tanaka, 1986). The Mottled Member (Hvm), named for the mottled appearance of crater-ejecta blankets, displays higher albedo than adjacent terrain, and is interpreted as lava flows erupted from fissures, or alternatively deposits of alluvial or eolian origin (Scott and Tanaka, 1986). The Knobby Member (Hvk) is similar in appearance to the Mottled Member, but displays higher albedo and abundant small, dark, knob-like hills, some with summit craters (Scott and Tanaka, 1986), and generally interpreted to be of diverse origins including volcanic lava flows and recent eolian mantle. Knob-like hills may be small volcanoes, remnant highland terrain, or possibly ice-cored mounds similar to terrestrial pingos (Scott and Tanaka, 1986).

Measured diameters for polygons in Region 1 networks (Figure21) range from approximately 84 to151 metres, with greatest values drawn from networks E05-00113, E22-00059, and E03-02635 which appear poorly developed.

Image Number	*D* (meters)	Percentage of Orthogonal Intersections	Percentage of Non-Orthogonal Intersections	3-Way Intersections (%)	4-Way Intersections (%)
E05-00113	149.56	83.8	16.2	21.2	78.8
E22-00059	145.34	38.5	61.5	59.7	40.3
E03-02635	135.25	77.2	22.8	30.9	69.1
M19-00234	85.96	74.0	26.0	21.1	78.9

Table 4: Region 1 values of spacing, D, percentage of orthogonal and non-orthogonal intersections, and 3- and 4-way intersections.

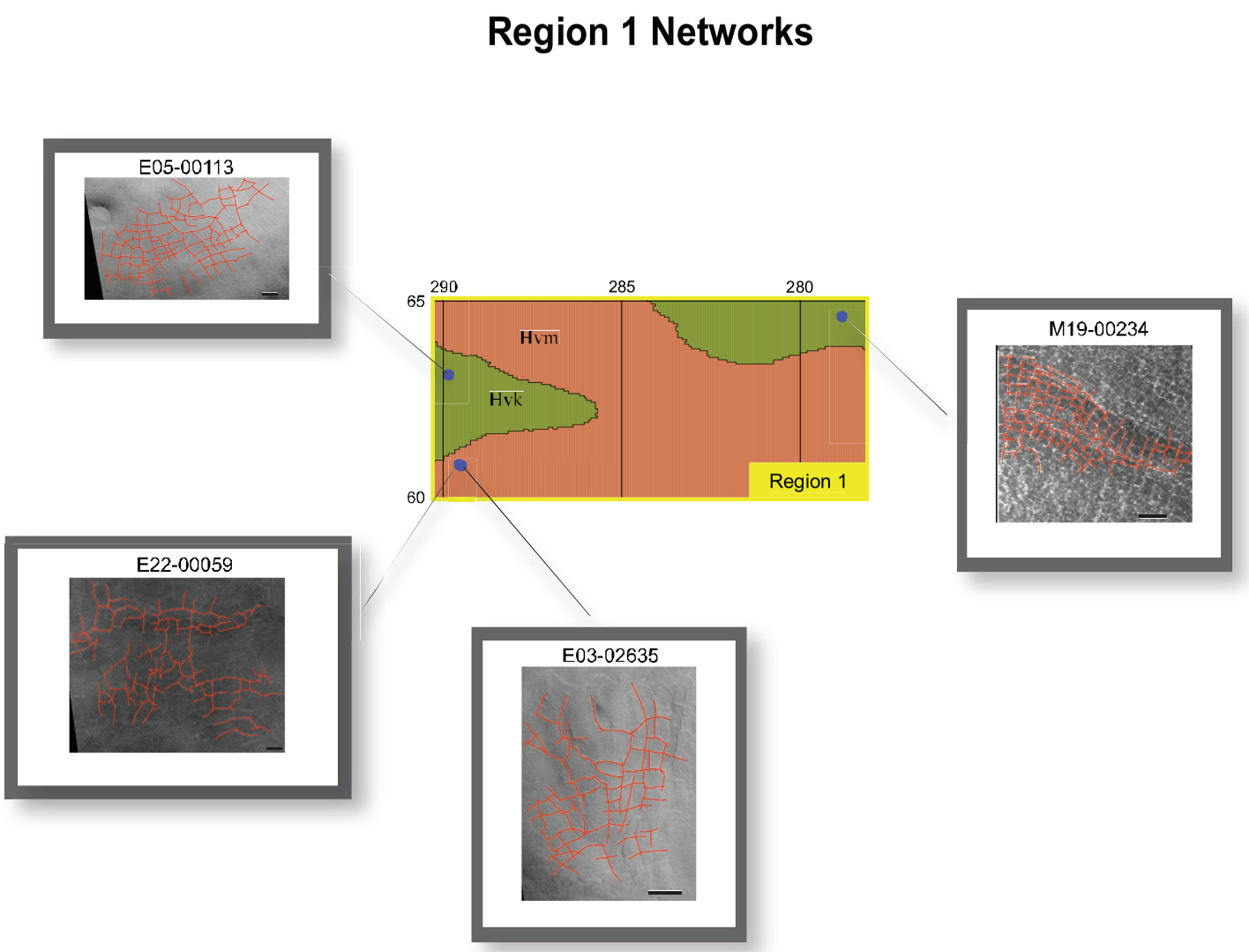

Figure 21: Region 1 networks, including MOC images E06-00113, E22-00059, E03-02835, and M19-00234.

Network M19-00234, located on a crater floor, is qualitatively distinct from other networks north of 60º latitude as its *D* value (Table 4) is considerably less. Smaller polygons are suggested to form in terrestrial ice wedge networks as a result of decreased depth of thermal tension and/or decreased crack depth, which results in narrower zones of stress relief and therefore less widely spaced cracks and polygons (Lachenbruch, 1962). Network M19-00234 displays a large percentage of 4-way intersections (78.9%), which form by multiple fracturing events. This network also appears visually similar to the "oriented orthogonal" systems of Lachenbruch (1965), which are thought to result from horizontal stress differences generated by horizontal thermal gradients.

Network M19-00234 is located at a higher latitude (66.16ºN, 278.81ºW) than other networks included in this study. In models of tensile stress for seasonal cooling (Mellon, 1997) there is a latitudinal dependence in peak tensile stress, with greater stress at high latitudes. Under elevated tensile stress new fractures may further subdivide polygons, resulting in a network with a smaller characteristic diameter. However, this is an improbable explanation for the smaller *D* values of this network as its location is only ~2-5 degrees latitude greater than other networks in Region 1, too small to display significant variation in maximum tensile stress. An alternative explanation is that this crater floor network may have developed in significantly different substrate, such as breccia or ash fall dust as is suggested by the darker appearance of its surface. Consequent variation in rheological properties may be reflected in the character of the resulting polygonal pattern.

The absolute orientation of network M19-00234 follows a band of lower albedo, approximately 325 m across, similar to some terrestrial networks which follow shorelines as a result of stress differences generated by horizontal thermal gradients near edges of bodies of water (Lachenbruch, 1962). For network M19-00234, absolute orientation may have followed lateral migration of a cooling front of a molten rock

Region 1 Surface Plots

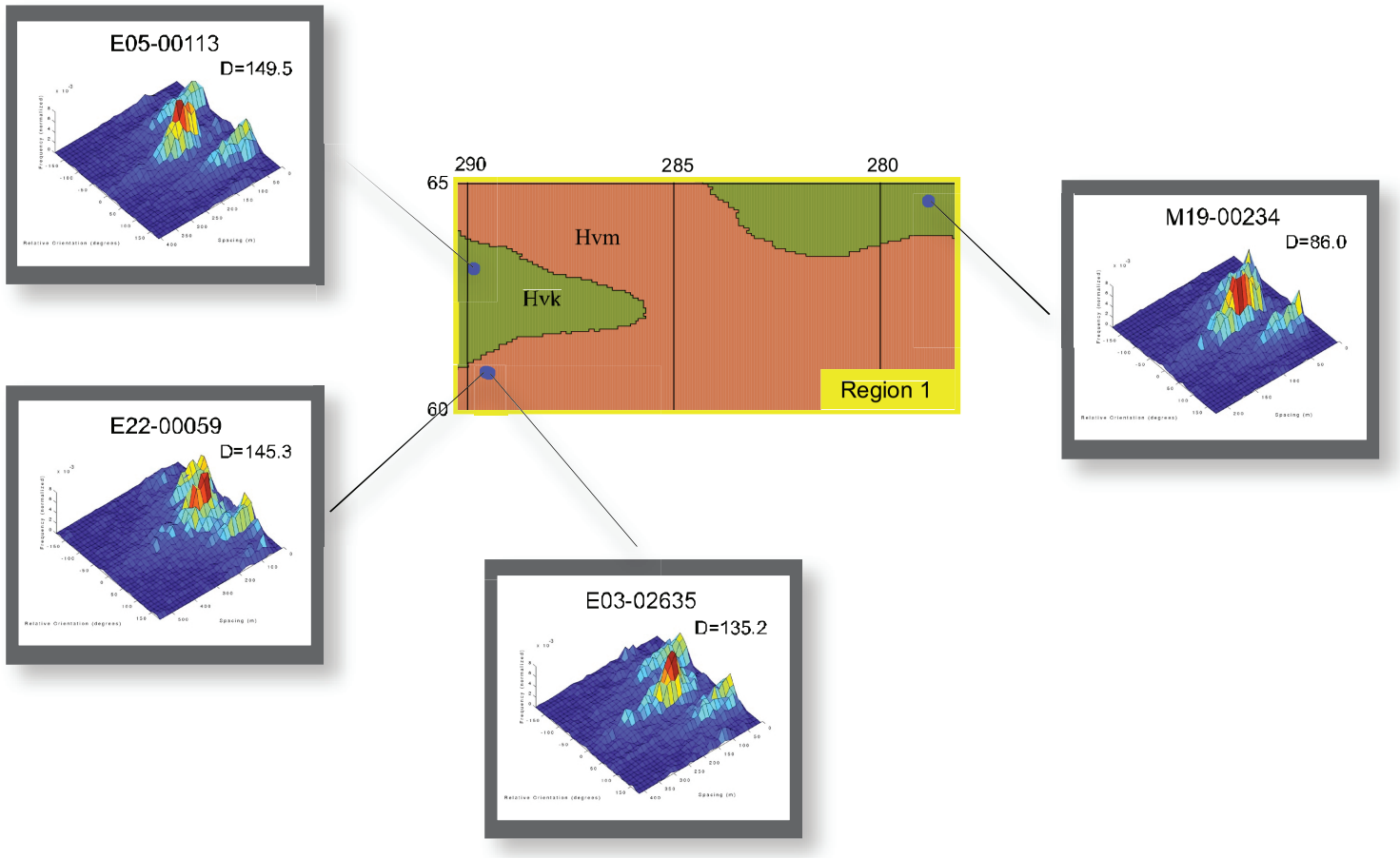

Figure 22: Region 1 surface plots, including MOC images E06-00113, E22-00059, E03-02835, and M19-00234.

following crater impact.

Networks E05-00113, E22-00059, and E03-02635, also located in Region 1, display larger spacings, (149.56, 145.34, and 135.25 respectively), indicative of (compared to M19-00234) lower maximum stress, substrate with higher tensile stress, deeper fractures, or lesser time for network development. Figure 22 displays the two-dimensional surface plots associated with each network in Region 1.

Networks E05-00113, E22-00059, and E03-02635 display larger spacing values (149.56, 145.34, and 135.25 respectively), indicative of (compared to M19-00234) lower maximum stress, substrate with higher tensile stress, deeper fractures, or lesser time for network development. These networks also display a greater percentage of 4-way intersections, indicative of multiple fracturing events, thought to occur in response to seasonal changes in climate.

Networks E05-00113, E22-00059, and E03-02635 are relatively unclear in MOC images. Therefore, an alternative explanation for their larger *D* value is that they are incompletely exposed, possibly as a result of insufficient sublimation occurring at this latitude, which exposes networks through the release of volatiles. At latitudes greater than 30º sublimation rates are dependant upon obliquity (Carr, 1996). A current increase in obliquity affecting higher latitudes might result in exposure of more fractures in Region 1 if they are present, and therefore a decrease in characteristic fracture spacing, *D*. The lack of other evidence for thermokarst in Region 1, compared to other regions, is consistent with the hypothesis that Region 1 networks are not fully exposed by sublimation and collapse of troughs over a wedge. Discerning between hypotheses for largely reduced network spacing and organization is revisited in Chapter 7, Discussion.

A notable feature of Region 1 is that it lacks evidence of thermokarst, a term applied to the process of ground ice melting (irrespective of origin) accompanied by subsidence or collapse of the ground surface (French, 1996). Within the Utopia basin, polygons are commonly associated with depressions interpreted as thermokarst pits, an

occurrence suggesting their formation at a time when ground ice was stable (Seibert and Kargel, 2001).

Notably, Region 1 networks lack a dominant orientation (Figure 23). In contrast to more southerly regions described below, Region 1 networks can be classified as random orthogonal (with the exception of local orientation within the crater floor network, as described above).

Networks E05-00113, E03-02635, and M19-00234 display the greatest percentage of orthogonal versus non-orthognal intersections within Region 1, with network values ranging from 38.5-83.8% and 16.2-61.5% respectively (Table 4). Networks E05-00113 and E03-02635 consist of predominantly 4-way intersections, whereas E22-00059 display a greater number of 3-way intersections (59.7%) for which various mechanisms of formation have been described (Section 4.2.2).

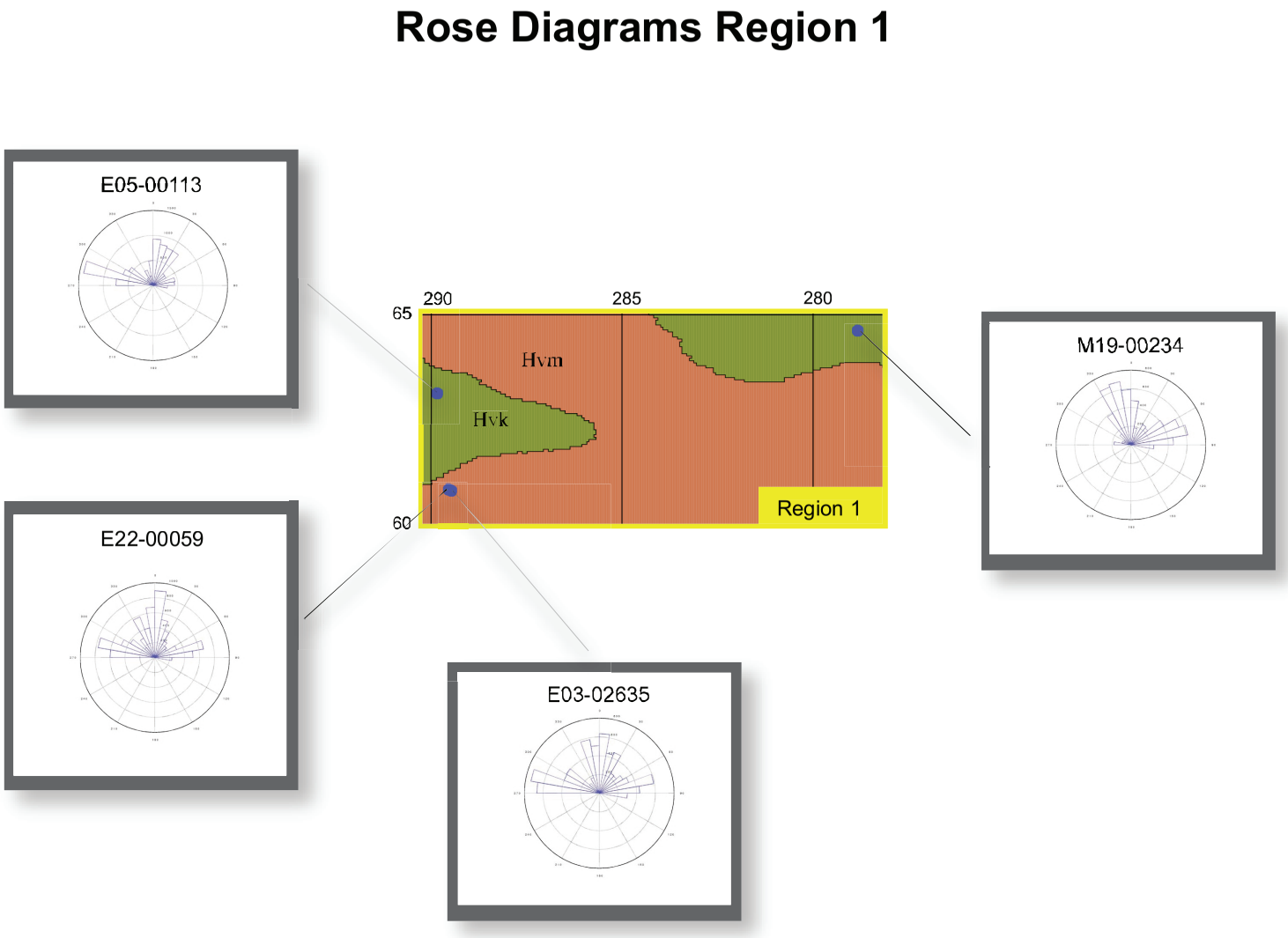

Figure 23: Region 1 rose diagrams, including MOC images E06-00113, E22-00059, E03-02835, and M19-00234.

6.2.3 Region 2 Polygonal Networks

Region 2, located between 45-50ºN and 270-281ºW, consists of seven networks, which were included in pattern analysis. As with Region 1, networks are located within the Mottled Member (Hvm) and Knobby Member (Hvk) of the Vastitas Borealis Formation (Scott and Tanaka, 1986). The measured diameters for polygons in these networks range from approximately 55-130 metres (Table 5).

Image Number	*D* (meters)	Percentage of Orthogonal Intersections	Percentage of Non-Orthogonal Intersections	3-Way Intersections (%)	4-Way Intersections (%)
M08-07602	129.52	74.6	25.4	29.9	70.1
M01-04558	124.72	74.0	26.0	34.6	65.4
M04-02704	87.21	74.8	25.2	47.1	52.9
M03-04331	81.61	75.1	24.9	40.5	59.5
M04-01631	98.90	79.7	20.3	30.6	69.4
M19-01326	55.03	61.1	38.9	44.4	55.6
M03-05694	58.16	66.8	33.2	33.3	66.7

Table 5: Region 2 values of spacing, D, percentage of orthogonal and non-orthogonal intersections, and 3- and 4-way intersections.

Five networks are distinguished from the other two by greater characteristic spacing, *D*, and by more pronounced trough development (Figure 24 area 2 networks). These include networks M08-07602, M01-04558, M04-02704, M03-04331, and M04-01631. The surface plots Figure 25 show especially large spacings of networks M08-07602 and M01-04558, represented as large peaks at 0º. A decrease in surface plot peaks at 0º reflects the smaller spacings of other networks in this region, possibly suggesting that recent climate change, as a result of variations in obliquity, caused an increase in sublimation and exposure of fractures.

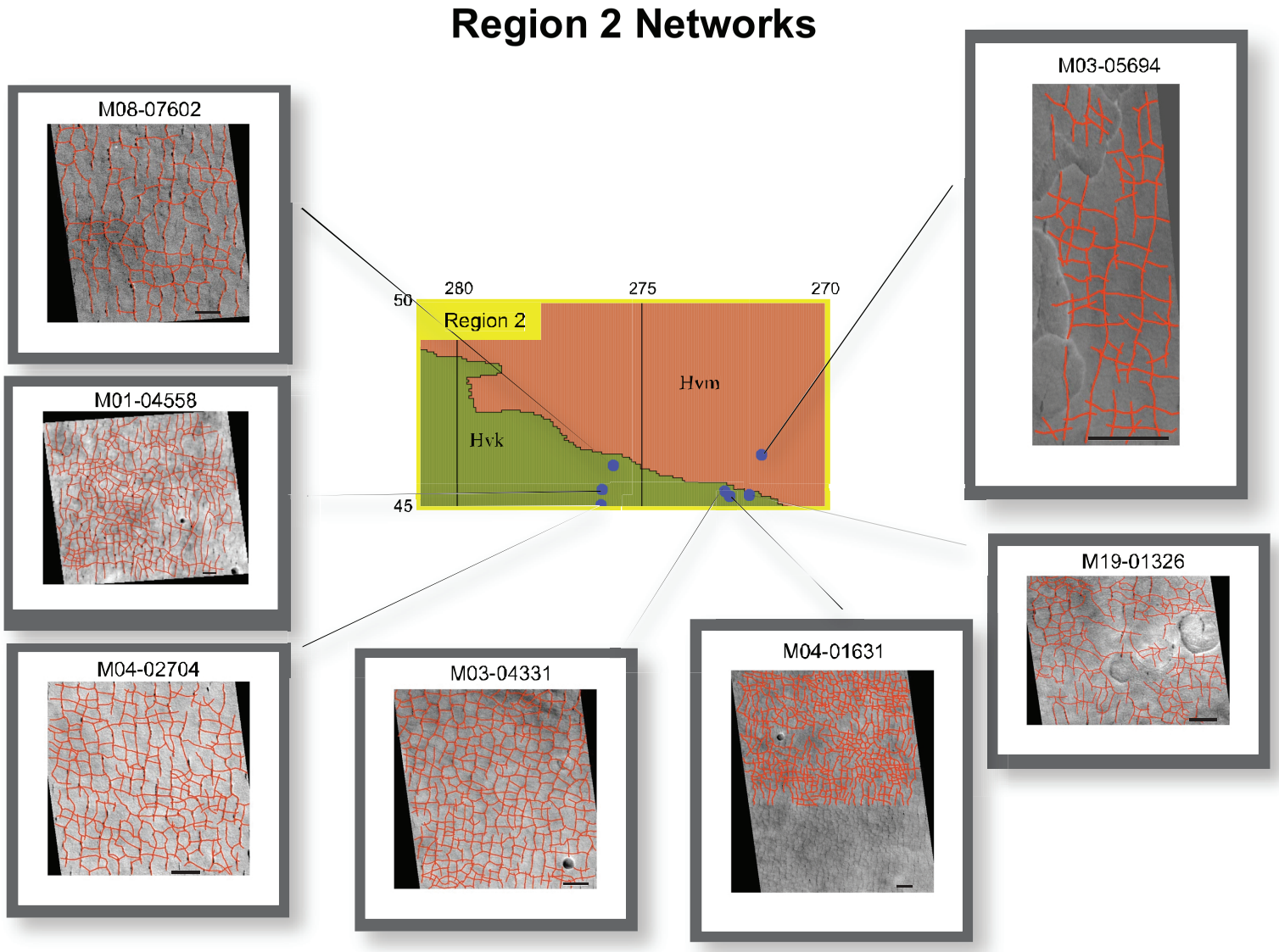

Figure 24: Region 2 networks, including MOC images M06-07602, M01-04558, M04-02704, M03-04331, M04-01631, M19-01326, and M03-05694.

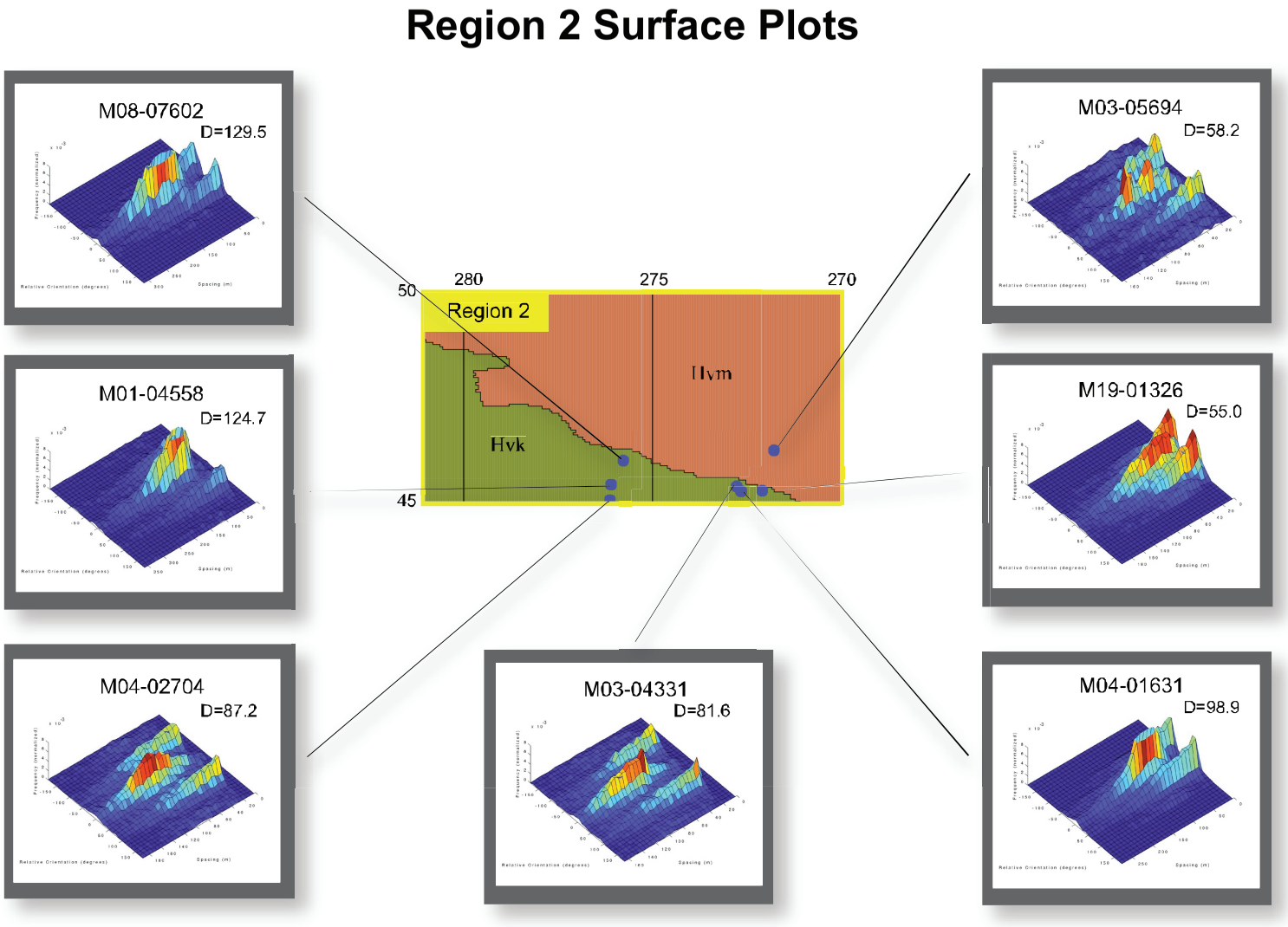

Figure 25: Region 2 surface plots, including MOC images M06-07602, M01-04558, M04-02704, M03-04331, M04-01631, M19-01326, and M03-05694.

Networks M19-01326 and M03-05694 have small characteristic spacing, but poorly developed troughs. Accompanying these networks are widespread, larger features thought to be indicative of thermokarst processes, including raised plateaus outlined by a jagged escarpment, which appear similar to escarpments formed by backwearing and downwearing in terrestrial permafrost regions. Irregular hollows surrounding the plateaus have been suggested to be similar to terrestrial alases that form by removal of ground ice by erosion and sublimation along the escarpments (Carr, 1996). It is difficult to determine whether the networks predate the thermokarst features, as cross-cutting relationships are very different between networks M19-01326 and M03-05694. In the former, polygonal networks are absent beyond the edge of the plateaus, where in the latter polygonal networks are superposed on plateaus. As a result of this diverse relationship, I suggest that the event of polygon formation was, at least, coeval with thermokarst processes at some point in Mars' history. Costard and Kargel (1995) report the association of polygons in the Utopia basin with anomalous scalloped depressions believed to form by thermokarst. An example of such a feature, thought to be indicative of thermokarst, is seen in Figure 26 (M03-05694 with network).

Network M03-05694 is located within the Mottled Member (Hvm) of the Vastitas Borealis Formation, and is less well developed than the networks located in the Knobby Member (Hvk). As such, network M03-05694 more closely resembles networks E22-00059 and E03-02635 of Region 1.

Networks within the Knobby Member displays higher albedo levels (0.275), which relate to the lower thermal inertias (~2.5 x 10^{-3} cal cm^{-2} $s^{-1/2}$) occurring in this unit. Values of thermal inertia, which essentially imply surface materials present (i.e. fine or coarse grained), only apply to the upper few centimeters of the material, and do not pertain to materials at greater depth. This suggests that the majority of Region 2 networks which are located in the Knobby Member may be overlain by fine-grained sediment, and possibly underlain by consolidated strata cemented by ground ice. As

previously stated, Mellon (1997) suggests that at Martian latitudes poleward of 20º-30º, tensile stresses would become high enough to fracture ice-cemented ground to a depth of 1.5m or less. Fracture strain in neighboring overlying layers would add to the imposed stress, causing fractures to propagate to deeper depths. This may explain the increased development of networks in Region 2.

Networks M04-02704, M03-04331, and M04-01631 display the greatest percentage of orthogonal versus non-orthogonal intersections within Region 2, with network values ranging from 61.1-79.7% and 20.3-38.9% respectively (Table 5). All networks of Region 2 display a greater percentage of four-way intersections, indicating their development over multiple fracture events.

The polygonal networks of Region 2 display a pronounced N-NE orientation in the absolute orientation of cracks (Figure 27). Various mechanisms have been proposed to explain the formation of this N-S orientation including: large scale bending of the Utopia basin, an E-W oriented anisotropic stress produced by a nearby water body or topographic slope, or pre-existing planes of weakness in a N-S trending direction.

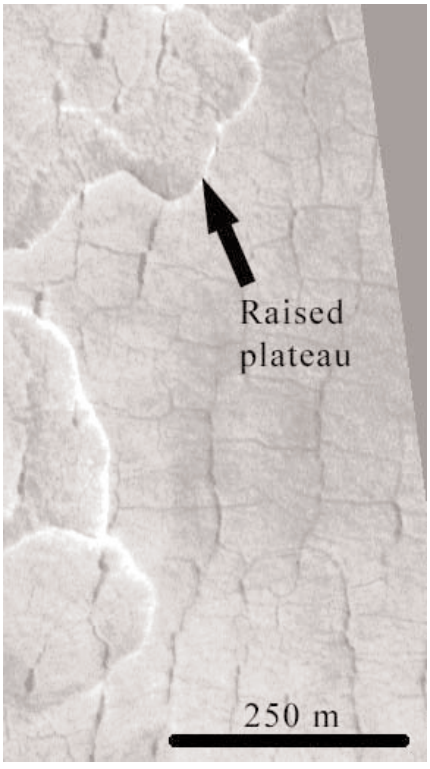

Figure 26: Example of perceived thermokarst feature on Mars. MOC image M03-05694.
Scale = 250 m

Rose Diagrams Region 2

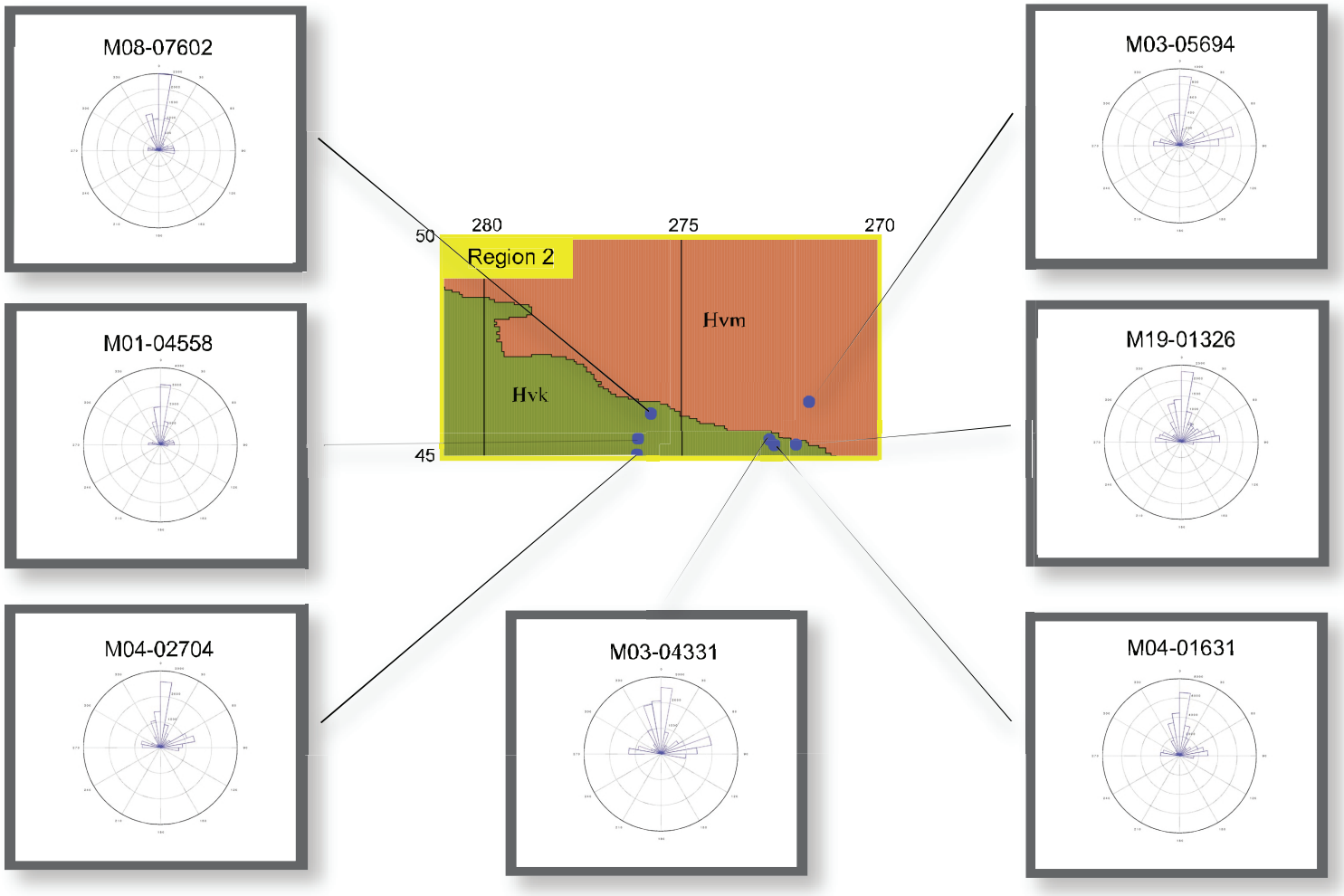

Figure 27: Region 2 rose diageams, including MOC images M06-07602, M01-04558, M04-02704, M03-04331, M04-01631, M19-01326, and M03-05694.

These hypotheses are revisited in Chapter 7, Discussion.

6.2.4 Region 3 Polygonal Networks

Region 3, located between 40-45ºN and 270-281ºW, holds eight networks included in pattern analysis (M04-03810, M08-03534, M22-02520, M04-04181, E23-01288, M23-00151, M09-03407, and M01-00582) (Figure 28 area 3 networks). All are within the Knobby Member (Hvk) of the Vastitas Borealis Formation (Scott and Tanaka, 1986). Values of *D* for these range from 41to122 metres (Table 6), with two of the displaying well developmed, deep troughs.

Image Number	*D* (meters)	Percentage of Orthogonal Intersections	Percentage of Non-Orthogonal Intersections	3-Way Intersections (%)	4-Way Intersections (%)
M04-03810	84.48	66.4	33.6	47.1	52.9
M08-03534	108.17	60.4	39.6	25.7	74.3
M22-02520	122.09	64.8	35.2	44.5	55.5
M04-04181	41.52	56.2	29.1	48.3	51.7
E23-01288	88.84	25.4	74.6	28.3	71.7
M23-00151	78.92	78.5	21.5	22.7	77.3
M09-03407	104.41	62.2	37.8	26.9	73.1
M01-00582	110.63	64.4	35.6	45.2	54.8

Table 6: Region 3 values of spacing, D, percentage of orthogonal and non-orthogonal intersections, and 3- and 4-way intersections.

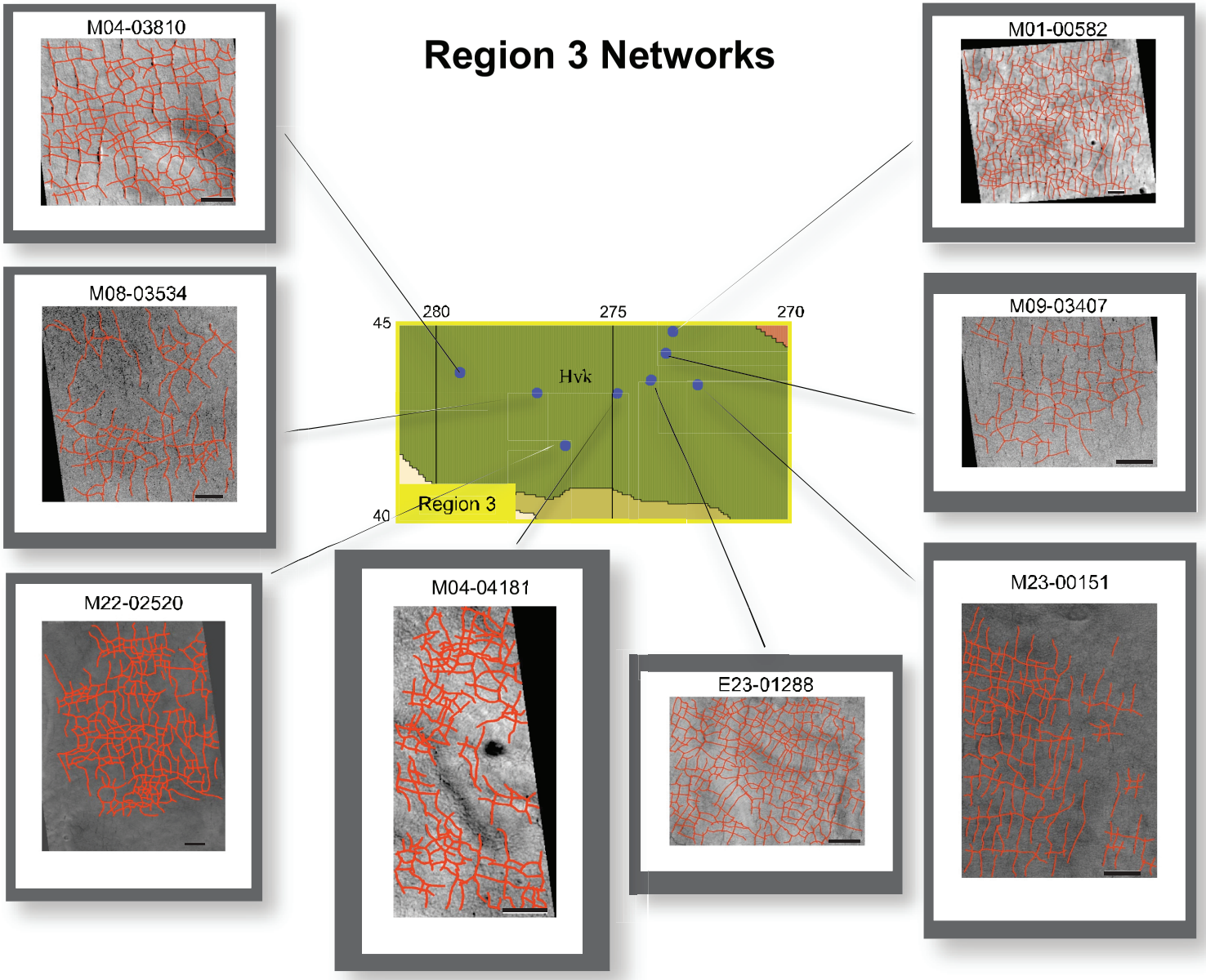

Figure 28: Region 3 networks, including MOC images N04-03810, M08-03534, M22-02520, M04-04181, E23-01288, M23-00151, M09-03407, and M01-00582.

Figure 29 displays two-dimensional surface plots associated with each network in Region 3. The surface plots display the relatively large spacings of networks M08-03534, M22-02520, M09-03407, and M01-00582 (represented as large peaks at 0º), and the smaller spacings of networks M04-03810, M04-04181, E23-01288, and M23-00151.

Networks M22-02520, M04-04181, and M23-00151 are poorly to moderately developed, and display features indicative of thermokarst processes similar to those observed in Region 2. A coeval relationship between polygonal networks and thermokarst features appears to exist in this region as well. Networks M04-03810 and M01-00582 display scalloped depressions believed to form by thermokarst, and the presence of these features further suggests the presence of an ice-rich ground layer at some point during the Martian history.

Network M23-00151 displays the greatest percentage of orthogonal versus non-orthogonal intersections within Region 3, with network values ranging from 56.2-78.5% and 21.5-74.6% respectively (Table 6). Intersections are predominantly four-way for all networks, indicating multiple fracture events.

The networks of Region 3 display a pronounced N-S orientation in the absolute orientation of cracks Figure 30, for which various mechanisms of formation have been proposed and will be revisited in Chapter 7.

Region 3 Surface Plots

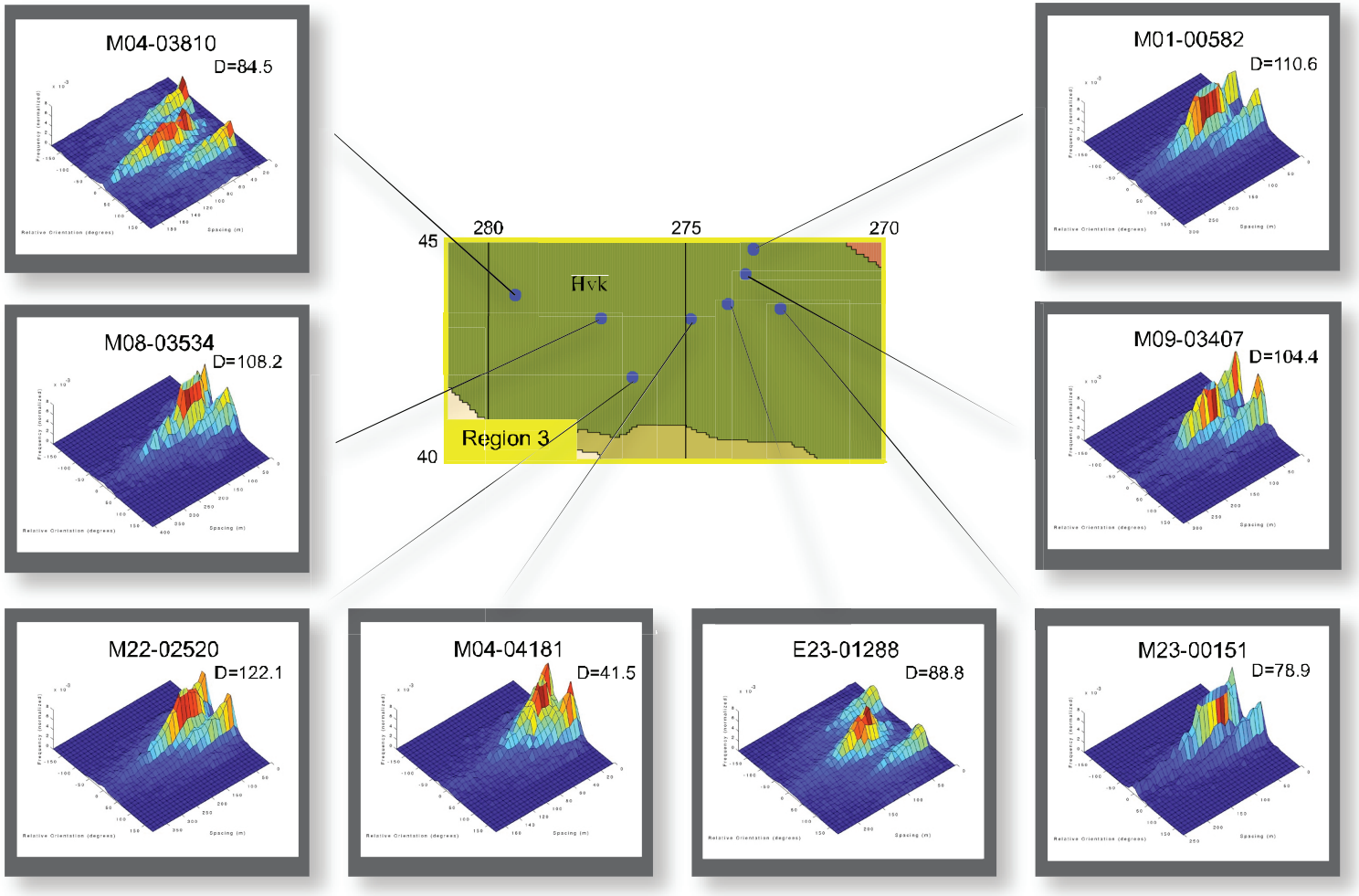

Figure 29: Region 3 surface plots, including MOC images N04-03810, M08-03534, M22-02520, M04-04181, E23-01288, M23-00151, M09-03407, and M01-00582.

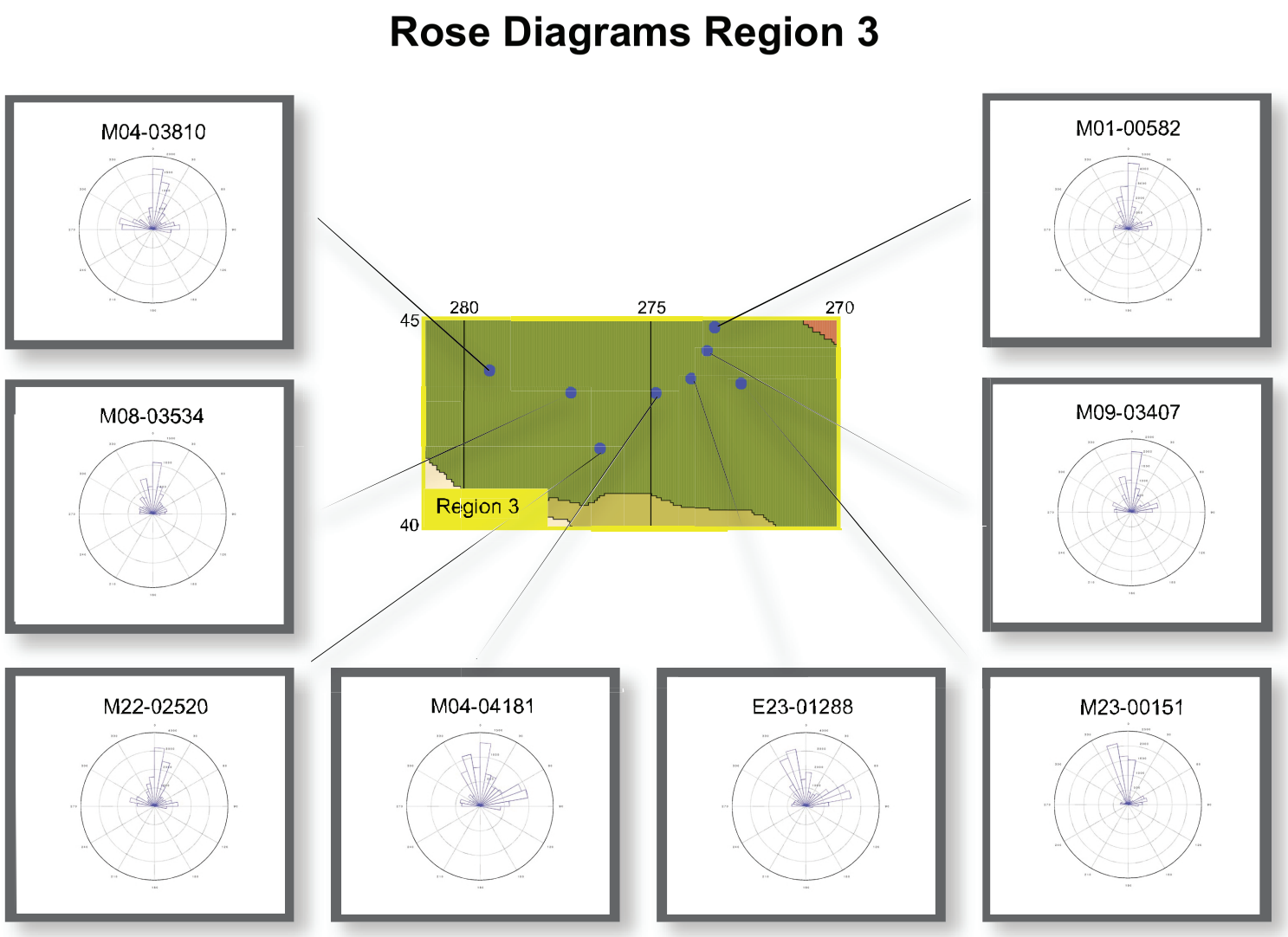

Figure 30: Region 3 rose diagrams, including MOC images N04-03810, M08-03534, M22-02520, M04-04181, E23-01288, M23-00151, M09-03407, and M01-00582.

6.2.5 Region 4 Polygonal Networks

Region 4, located between 45-50ºN and 270-259ºW, consists of six networks included in pattern analysis (Figure 31). Three networks are located within the Knobby Member (Hvk), one within the Mottled Member (Hvm), and two within the Grooved Member (Hvg) of the Vastitas Borealis Formation (Scott and Tanaka, 1986). The Grooved Member (Hvg) occurs as isolated patches throughout the lowland plains, and is characterized by curvilinear and polygonal patterns of grooves and troughs, interpreted to consist of similar material as the Mottled Member, with patterns being the result of tectonism, compaction, or periglacial processes (Scott and Tanaka, 1986).

Image Number	*D* (meters)	Percentage of Orthogonal Intersections	Percentage of Non-Orthogonal Intersections	3-Way Intersections (%)	4-Way Intersections (%)
M22-01173	52.95	70.4	29.6	35	65
M23-01857	69.89	70.3	29.4	20.2	79.8
M02-03335	80.36	53.6	46.4	25.3	74.7
M04-00990	52.72	58.8	41.2	41.9	58.1
M23-00078	106.15	77.5	22.5	38.7	61.3
M00-00215	57.76	51.9	48.1	44.4	55.6

Table 7: Region 4 values of spacing, D, percentage of orthogonal and non-orthogonal intersections, and 3- and 4-way intersections.

Characteristic spacing for polygons in these networks ranges from 52 to106 metres, with the majority tending towards smaller diameters (Table 7).

Networks M22-01173, M23-01857, M02-03335, M04-00990, and M00-00215 have small spacings, whereas network M23-00078 is considerably larger (Figure 32). As previously stated, smaller spacings may suggest that recent climate change, as a reult of variations in obliquity, caused an increase in sublimation and exposure of fractures.

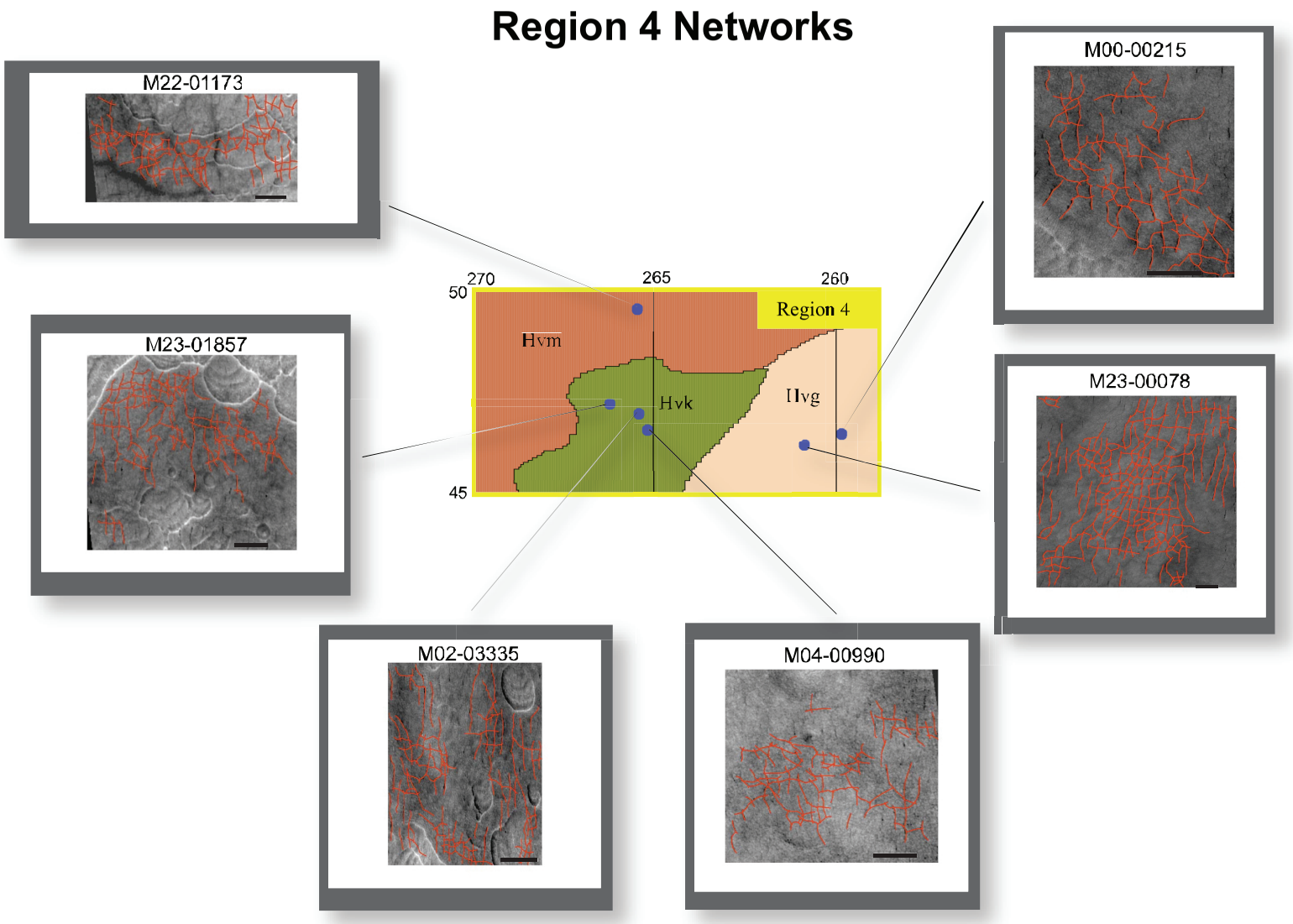

Figure 31: Region 4 networks, including MOC images M22-01173, M23-01857, M02-03335, M04-00990, M23-00078, and M00-00215.

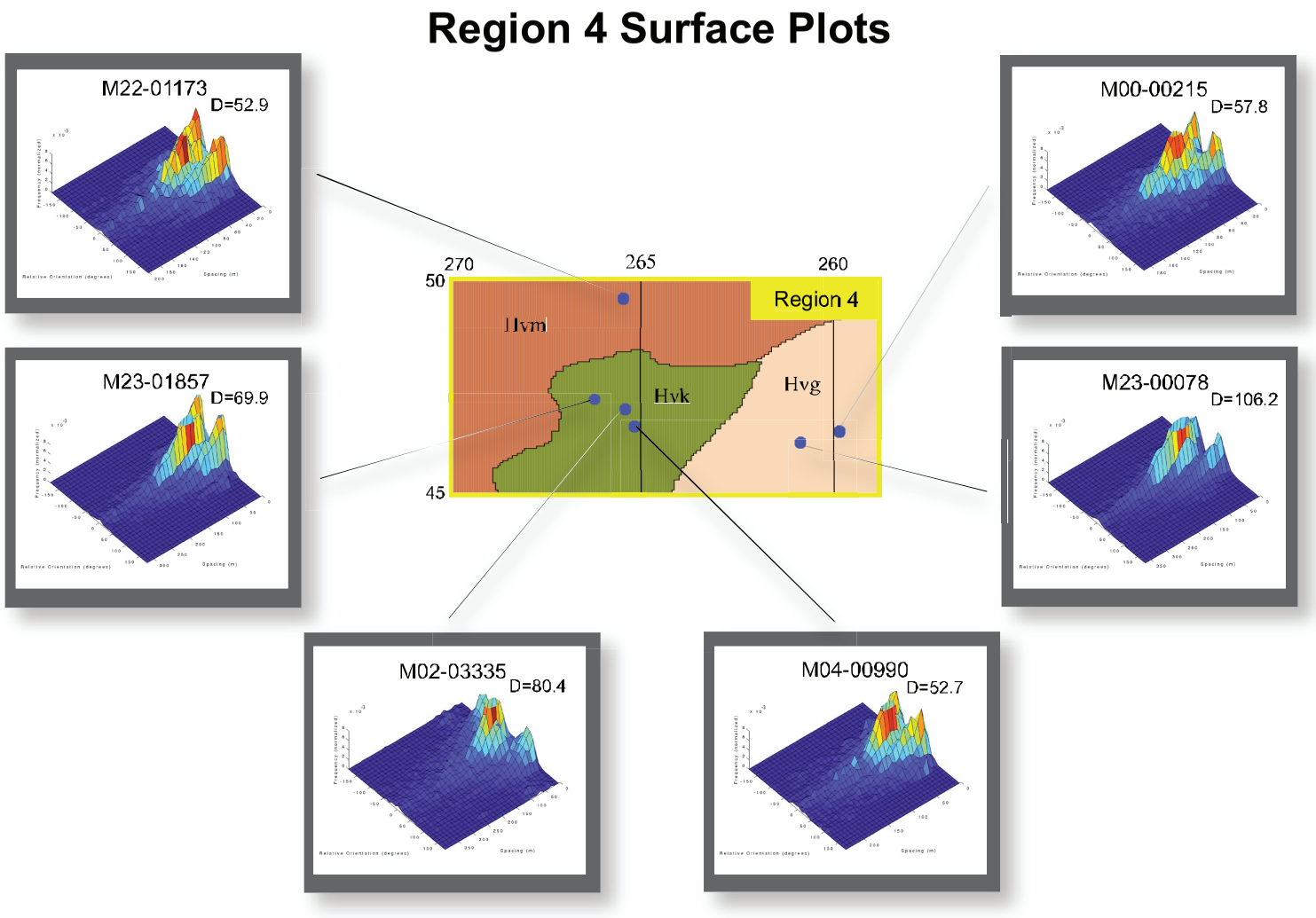

Figure 32: Region 4 surface plots, including MOC images M22-01173, M23-01857, M02-03335, M04-00990, M23-00078, and M00-00215

All networks in this area appear poorly developed, with the exception of M23-00078 which is moderately developed. Networks display features indicative of thermokarst processes similar to those observed in Regions 2 and 3. A coeval relationship between polygonal networks and thermokarst features appears to exist in this area as well.

Networks M23-01857, M02-03335, and M23-00078 display the greatest percentage of orthogonal versus non-orthogonal intersections within Region 4, with network values ranging from 51.9-77.5% and 22.5-48.1% respectively (Table 7). Intersections among fractures are predominantly four-way, although three-way intersections are also present.

Region 4 networks generally display a pronounced N-S orientation in the absolute orientation of cracks (Figure 33). This is consistent with other southerly regions (i.e. Regions 2-5).

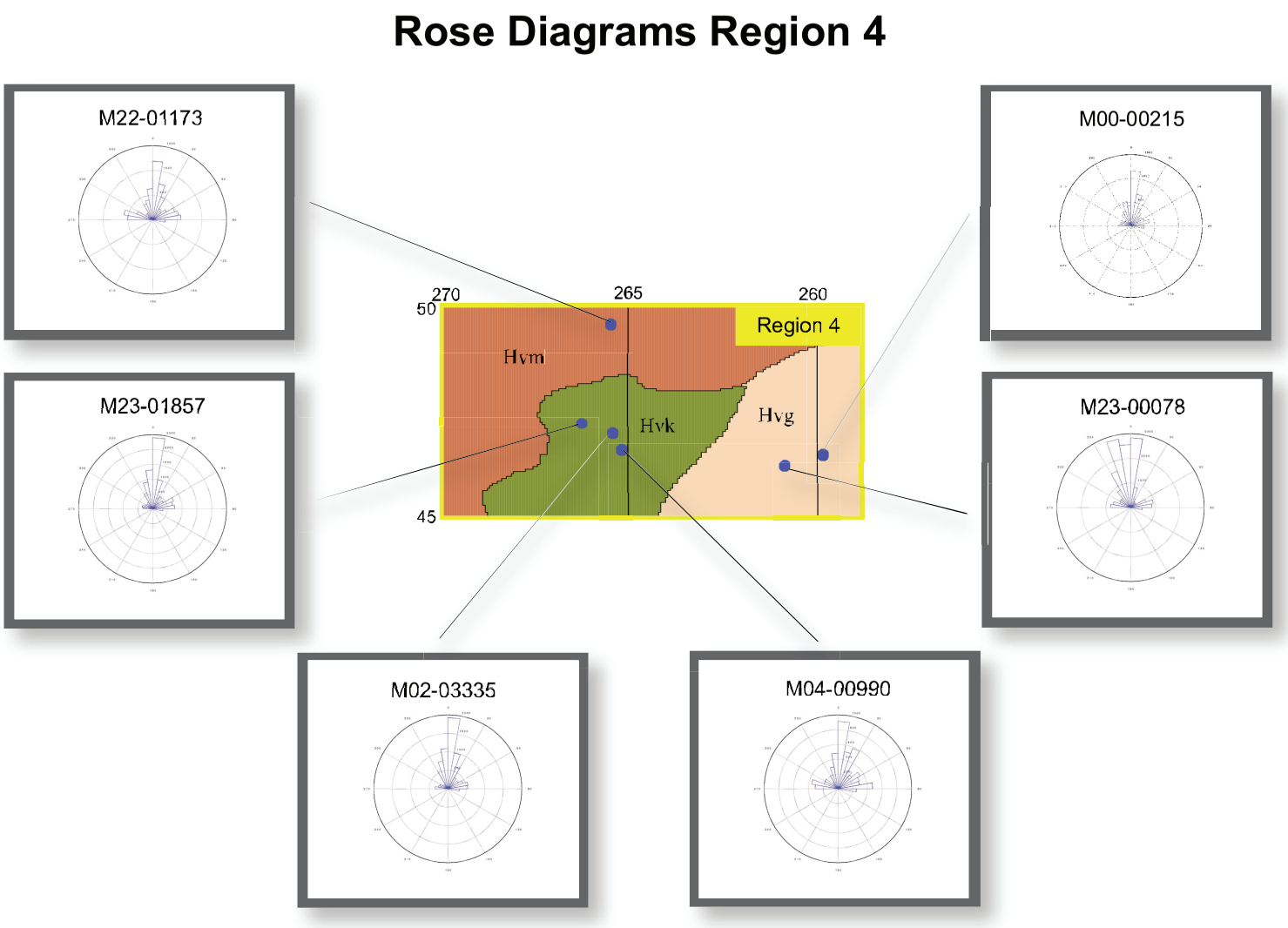

Figure 33: Region 4 rose diagrams including MOC images M22-01173, M23-01857, M02-03335, M04-00990, M23-00078, and M00-00215

6.2.6 Region 5 Polygonal Networks

Region 5, located between 40-45ºN and 270-259ºW, consists of three networks included in pattern analysis (Figure 34). One is located within the Knobby Member (Hvk), one within the Mottled Member (Hvm), and one within the Grooved Member (Hvg) of the Vastitas Borealis Formation (Scott and Tanaka, 1986). Measured diameters for the polygons in these networks range considerably from approximately 49 to104 metres (Table 8).

Image Number	*D* (meters)	Percentage of Orthogonal Intersections	Percentage of Non-Orthogonal Intersections	3-Way Intersections (%)	4-Way Intersections (%)
M19-01929	103.74	79.2	20.8	49.6	50.4
M02-02863	81.61	75.7	24.3	40.3	59.7
R02-00014	49.69	67.3	32.7	41.7	58.3

Table 8: Region 5 values of spacing, *D,* percentage of orthogonal and non-orthogonal intersections, and 3 and 4-way intersections.

Network M19-01929 exists within the Knobby Member (Hvk) and displays the largest spacing among fractures. This is similar to networks in other regions, in which *D* values generally appear greatest for networks developed in the Knobby Member.

Figure 35 displays two-dimensional surface plots associated with each network in Region 5. The surface plots display the high degree of variation among spacings of networks M19-01929, M02-02863, and R02-00014, which appears to correlate with the degree of network development. Network M19-01929 has large spacings and appears well developed, M02-02863 displays moderate spacing and development, and R02-00014 is poorly developed with small spacings.

Region 5 Networks

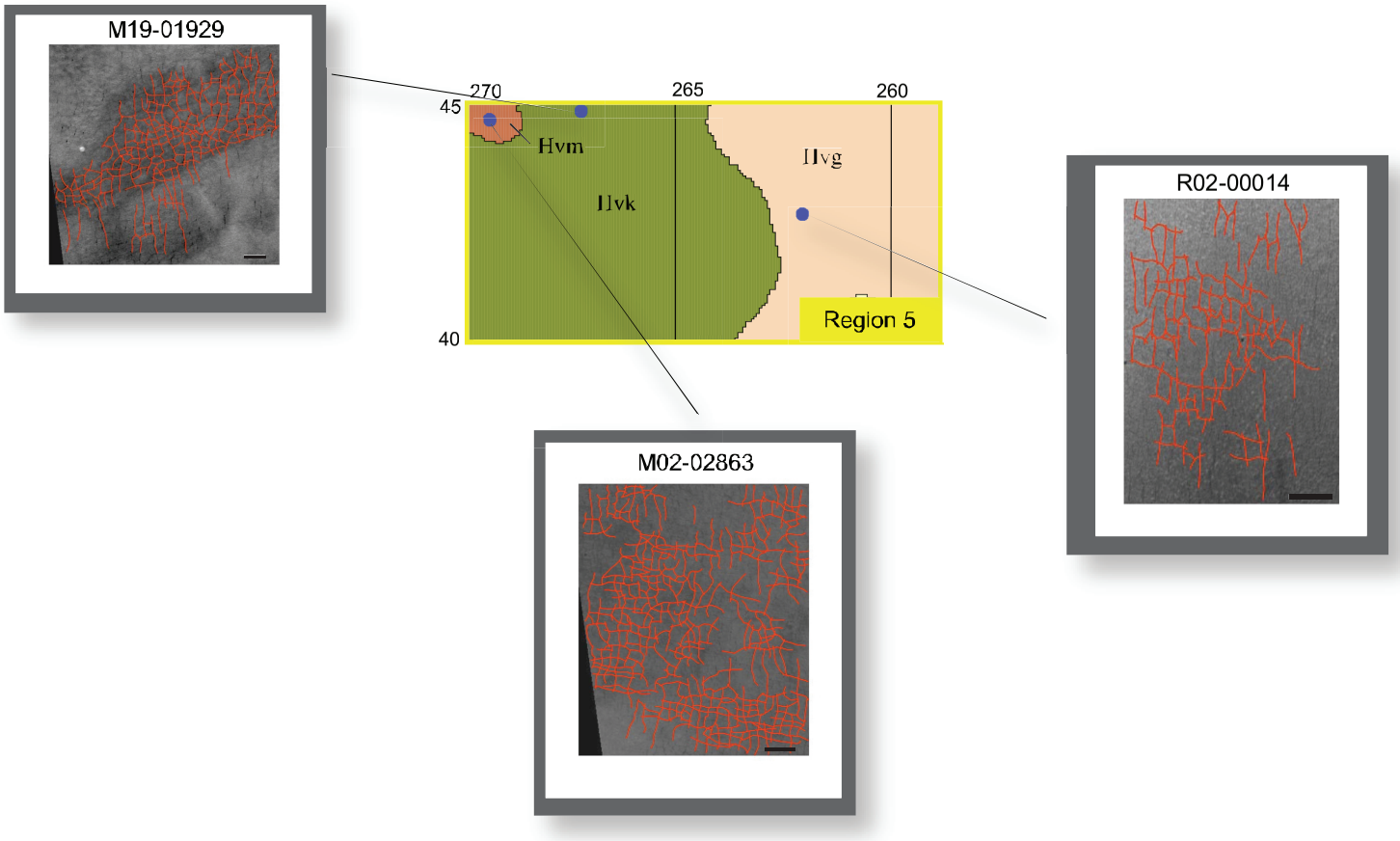

Figure 34: Region 5 networks, including MOC images M19-01929, M02-02863, and R02-00014.

Region 5 Surface Plots

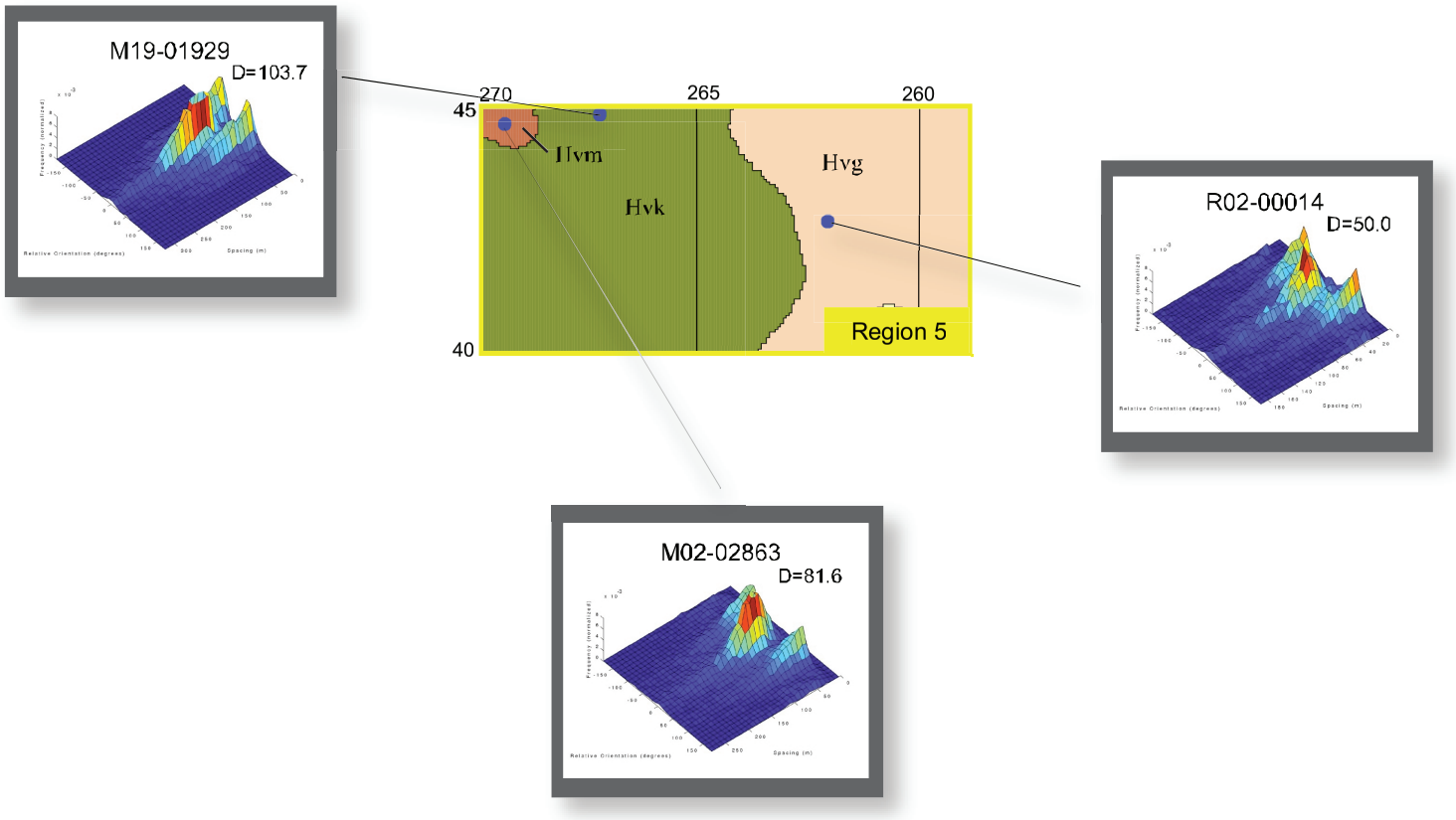

Figure 35: Region 5 surface plots, including MOC images M19-01929, M02-02863, and R02-00014.

Networks M19-01989 and M02-02863 display features indicative of thermokarst, similar to those observed in Regions 2, 3, and 4. A coeval relationship between polygonal networks and thermokarst features appears to exist in this region as well.

Network M19-01929 displays the greatest percentage of orthogonal versus non-orthogonal intersections within Region 5, with network values ranging from 67.3-79.2% and 20.8-32.7% respectively (Table 8). Intersections occur as both four-way and three-way, with neither being distinctively more abundant than the other. This may correspond to the varying degrees of network development suggested by spacing values.

The polygonal networks of Region 5 also display pronounced N-S orientation in the absolute orientation of cracks, as is noted in Figure 36.

Rose Diagrams Region 5

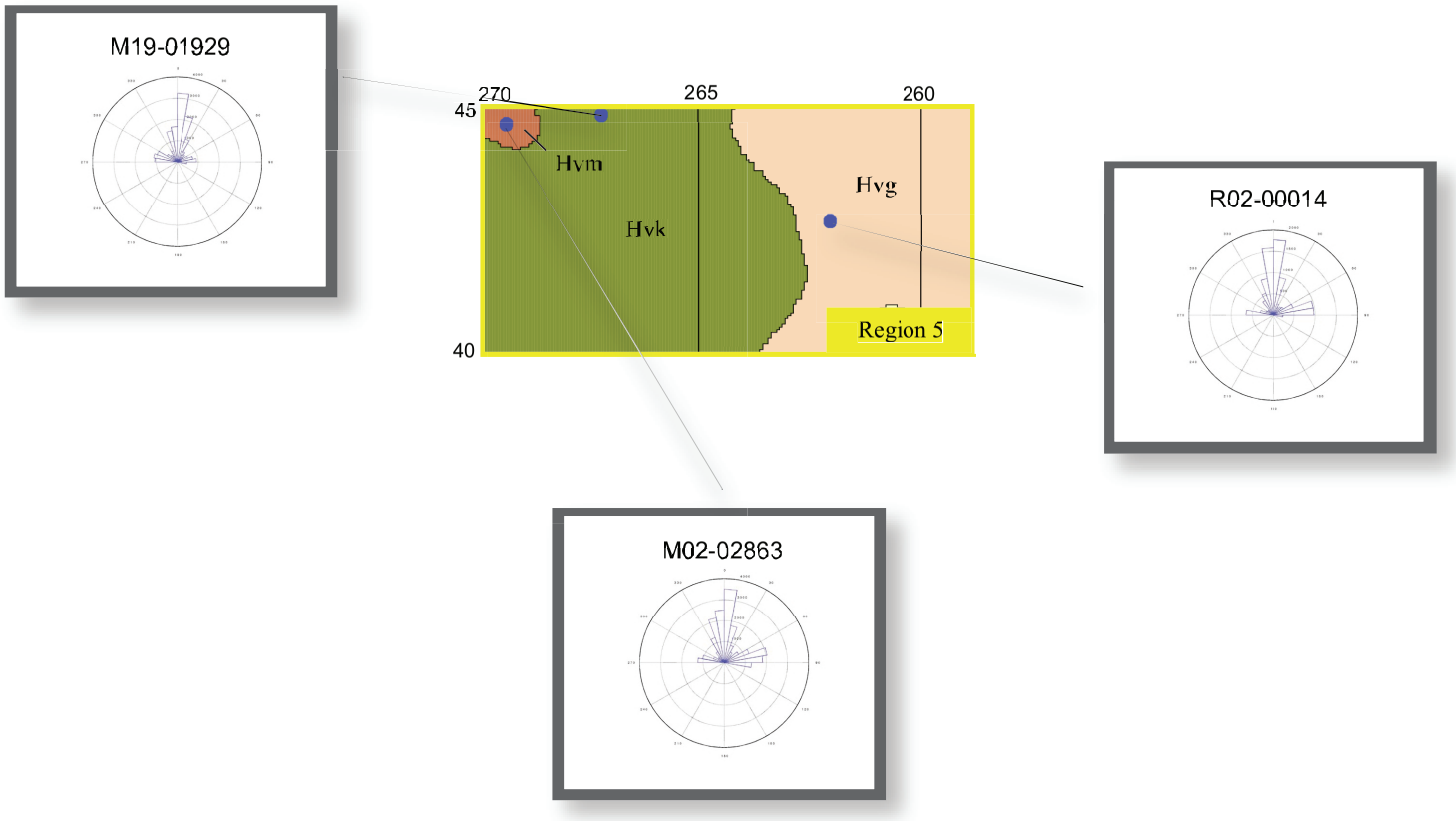

Figure 36: Region 5 rose diagrams, including MOC images M19-01929, M02-02863, and R02-00014.

6.3 QUALITATIVE DESCRIPTION OF TERRESTRIAL NETWORKS

6.3.1 Distribution and Characteristics of Terrestrial Networks

Terrestrial polygonal patterns included in pattern analysis were taken from aerial photographs of the delta and mainland region located at the mouth of the Sagavanirktok River (Figure 14), where it empties into the Beaufort Sea, near Prudhoe Bay, Alaska (70ºN-147ºW). Image resolution is 1.34 metres per pixel, and a total of 10 polygonal networks were digitized and included in pattern analysis, (Figure 15). Appendix A contains all relevant data pertaining to these images, and the images themselves can be found in Appendix B.

Average polygon diameters for terrestrial networks range from ~10-21 m, with an average measured diameter of 15.01 m. Values for spacing, *D*, percentage of orthogonal and non-orthogonal intersections, and 3- and 4-way intersections are given in Table 9.

Image Name	*D* (meters)	Percentage of Orthogonal Intersections	Percentage of Non-Orthogonal Intersections	3-Way Intersections (%)	4-Way Intersections (%)
En_image1	12.08	58.9	41.1	47.4	51.9
En_image2	14.83	61.3	38.7	47.2	52.8
En_image3	15.80	80.3	19.7	40.8	59.2
En_image4	11.93	66.3	33.7	45.5	54.5
En_image5	11.98	66.6	33.4	45.1	54.9
En_image6	18.08	62.3	37.7	43.2	56.8
En_image7	14.25	83.4	16.6	54.5	45.5
En_image8	15.29	69.4	30.6	37.3	62.7
En_image9	13.03	75.9	21.1	45.7	54.3
En_image10	12.41	72.2	27.8	46.4	53.6

Table 9: Terrestrial values of spacing, *D,* percentage of orthogonal and non-orthogonal intersections, and 3 and 4-way intersections.

Complete sets of images displaying networks digitized, corresponding surface plots, and rose diagrams relating to terrestrial networks are located in Appendix B. Terrestrial networks generally are well developed, with exceptions occurring where standing bodies of water exist (Figure 38).

Two-dimensional surface plots corresponding to digitized terrestrial networks display similar values of spacing, *D*, among networks, represented by peaks at 0º. Many of these peaks appear stretched in the direction of relative orientation, indicating an increase in disorganization of the networks (Figure 39). Orthogonal intersections are represented by peaks in the distributions at +90º and -90º, in which the width of the ridges is a measure of the degree of orthogonality of a network. Figure 40 displays sharply peaked ridges corresponding to a highly orthogonal and ordered network. Conversely, the majority of terrestrial networks display ridges with sharp edges at small distances, but which widen toward larger distances (Figure 39). Ridges such as these are indicative of fractures in which orthogonal intersections occur where two fractures meet, but tend to deviate as the distance from the intersection increases.

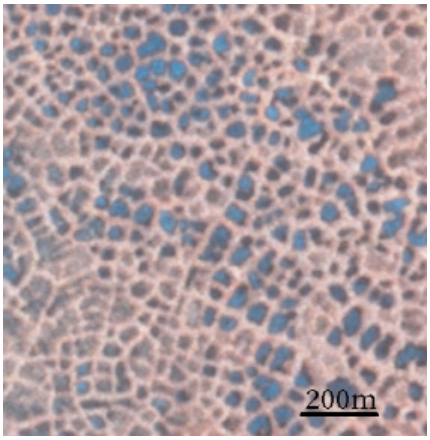

Figure 37: Example of terrestrial network located near Prudhoe Bay, Alaska. Scale = 250m.

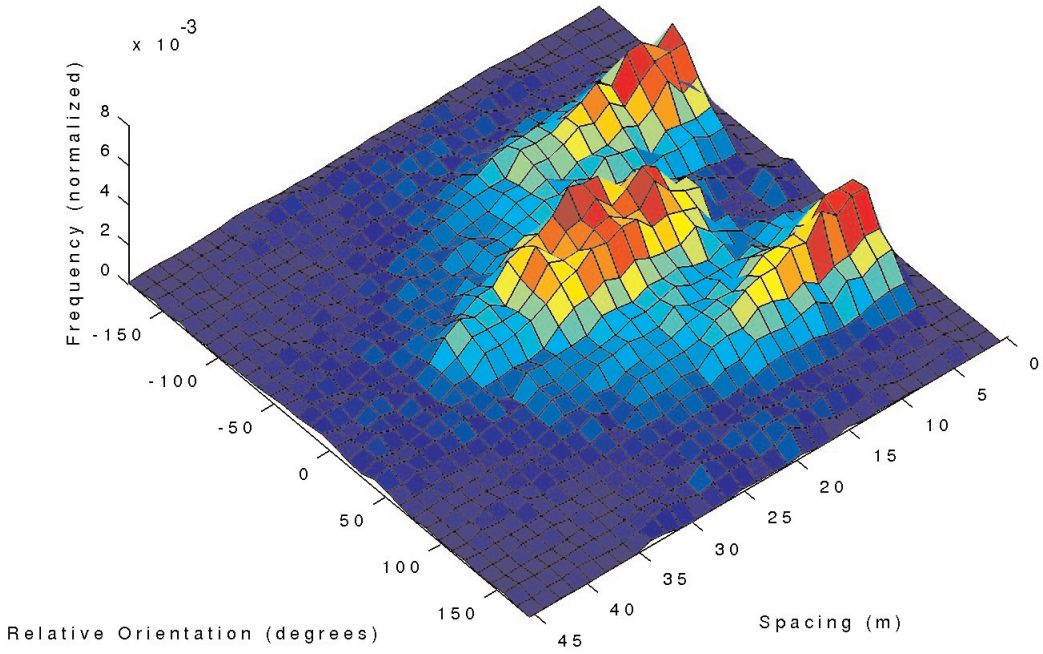

Figure 38: Example of two-dimensional surface plot, indicating spacing and relative orientation for a terrestrial network. Source: Earth_Image6.

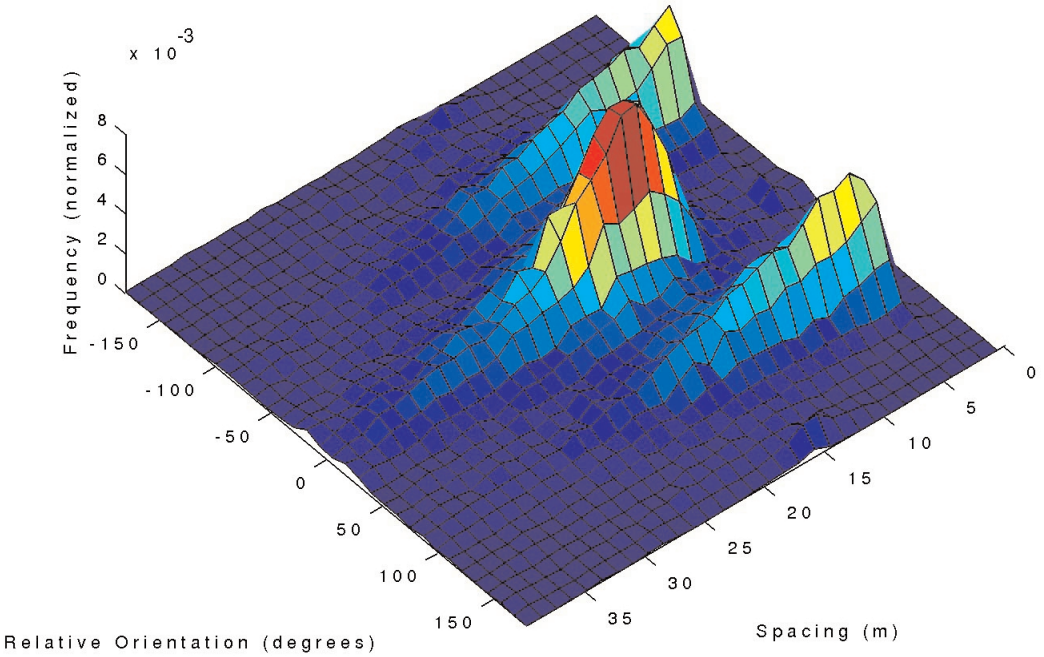

Figure 39: Example of two-dimensional surface plot, indicating spacing and relative orientation. Notice stretched appearance of peaks in the direction of relative orientation, indicating an increase in disorganization of the networks.

Terrestrial networks also display an abundant of both three- and four-way intersections, the combination of which suggests periods of multiple fracturing (possibly as a result of seasonal changes in climate), as well as single events.

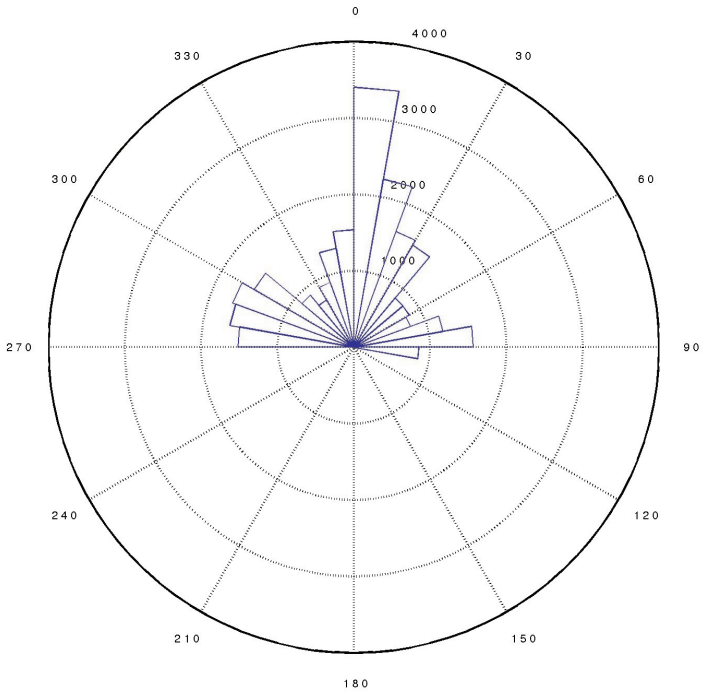

Figure 40: Example of rose diagram displaying absolute orientation. Source: Earth_Net9

Terrestrial networks appear to lack a preferred orientation, except in the case of networks 7 and 9 which display a general N-S orientation (Figure 40). These two networks are located in the vicinity of shorelines, which may be contributing to the development of this orientation. A similar explanation was suggested earlier for the formation of N-S orientations in Martian networks.

Image Name	*D* value (meters)	Percentage of Orthogonal Intersections	Percentage of Non-Orthogonal Intersections	3-Way Intersections (%)	4-Way Intersections (%)
20030806	0.29	81.8	18.1	90	10
20030812	0.25	81.8	18.2	95	5
20030818	0.20	85.3	14.7	97	3
20030824	0.17	88.1	11.9	98	2
20030901	0.14	72.7	27.3	98	2
20030905	0.13	71.5	28.5	96	4
20030910	0.13	70.5	29.5.	92	8
20030915	0.12	64.9	35.1	93	7
20030920	0.12	62.1	37.9	92	8
20030925	0.12	61.1	38.9	90	10
20030929	0.12	60.1	39.9	90	10

Table 10: Mudcrack values of spacing, *D,* percentage of orthogonal and non-orthogonal intersections, and 3 and 4-way intersections.

6.4 QUALITATIVE DESCRIPTION OF MUDCRACK NETWORKS

6.4.1 Characteristics of Mudcrack Networks

A total of 11 mud crack images were digitized and included for pattern analysis, with image resolutions of ~0.002 metres per pixel. Appendix A contains all relevant data pertaining to these images, and the images themselves can be found in Appendix B.

Average polygon diameters for mudcrack networks range from ~0.21-0.64 m, with an average measured diameter of 0.30 m. Values for spacing, *D*, percentage of orthogonal and non-orthogonal intersections, and 3- and 4-way intersections are given in Table 10.

Two-dimensional surface plots corresponding to digitized mudcrack networks display similar values of spacing, *D*, among networks, represented by peaks at 0º. The peaks appear extremely stretched in the direction of relative orientation, indicating a large degree of disorganization among the networks (Figure 41). Orthogonal intersections are represented by peaks in the distributions at +90ºand -90º, in which the width of the ridges is a measure of the degree of orthogonality of a network. Figure 42 displays ridges with sharp edges at small distances, but which widen toward larger distances. Ridges such as these are indicative of fractures in which orthogonal intersections occur where two fractures meet, but tend to deviate as the distance from the intersection increases. This is consistent with the work of Lachenbruch (1962) who suggests that desiccation polygons in mud are generally of the orthogonal type, but may display convex bends in the primary fracture leading to their confusion with non-orthogonal intersections.

Intersections within the mudcrack networks are almost entirely three-way, suggesting the formation of the network during a single event, such as an abrupt change in climate. Mudcrack networks appear to develop a moderate N-S orientation throughout their development; however, this is a function of the small size (119.4 cm x 119.4 cm) of the plastic chamber in which the mudcracks developed, and is not related to an anisotropic stess.

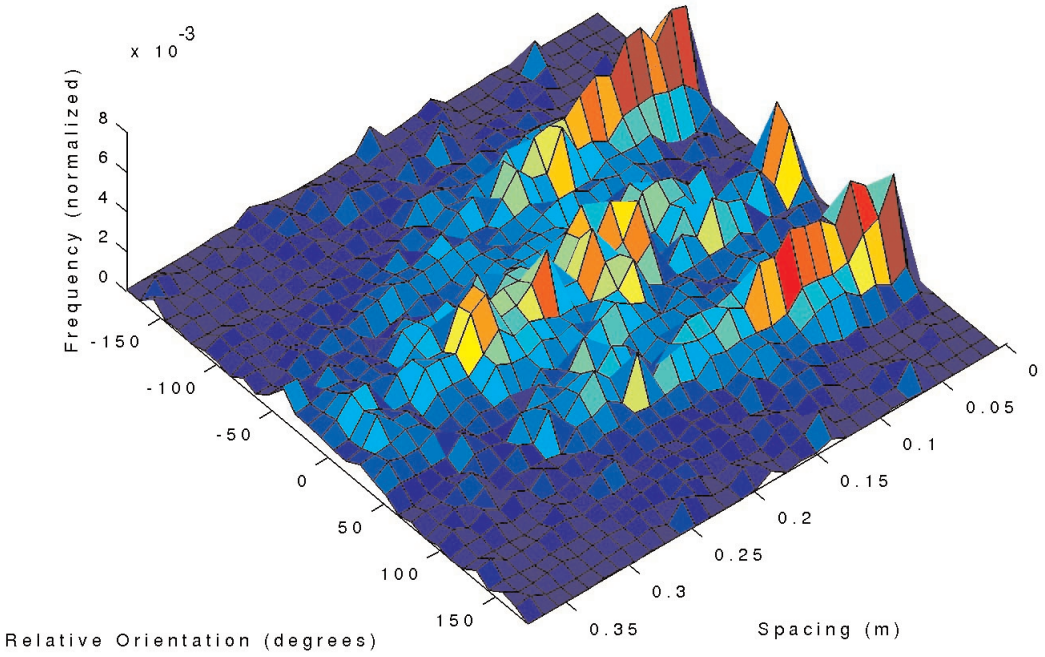

Figure 41: Example of two-dimensional surface plot for mudcrack network. Notice that peaks appear extremely stretched in the direction of relative orientation, indicating a large degree of disorganization among the networks. Image: 20030824.

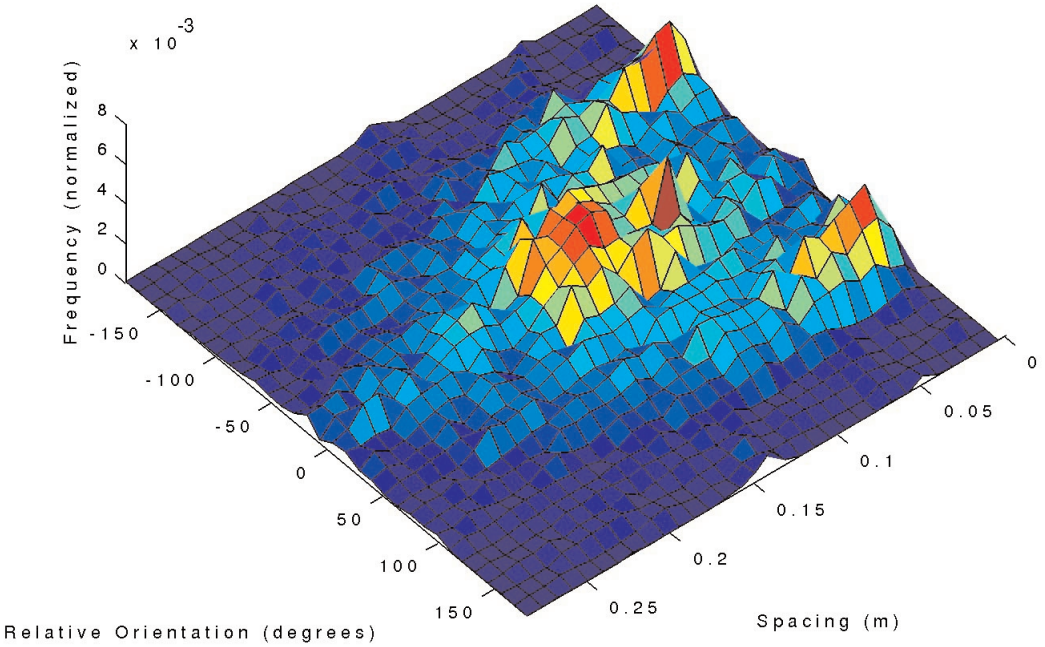

Figure 42: Two-dimensional surface plot displaying ridges with sharp edges at small distances, but which widen toward larger distances. Ridges are indicative of fractures in which orthogonal intersections occur where two fractures meet, but tend to deviate as the distance from the intersection increase. Image: 20030915.

CHAPTER 7: DISCUSSION

7.1 DISCUSSION OF MARTIAN POLYGONAL NETWORKS

7.1.1 Variations in Spacing, *D*

In a qualitative sense, for a field of closed polygons, network spacing is the typical diameter of polygons. Variations in network spacing, D, of Mars networks may be affected by a combination of factors including: strain rate, Martian temperature, tensile stress, and composition and rheology of subsurface materials. Variations in network spacing may be related to a linear relationship between stress reduction and fracture spacing, in which each crack is associated with a zone of stress relief (Lachenbruch, 1962). Within this zone, stresses are reduced below the tensile strength and cracking ceases, whereas beyond this zone near-surface ground stresses exceed the tensile strength and subsequent cracks develop. As such, the spacing of cracks, D, should be related to the width of the zone of stress relief for a single fracture. Larger polygons would thus tend to form as a result of increased depth of thermal tension and/or increased crack depth, resulting in wider zones of stress relief and therefore wider spaced cracks and polygons (Lachenbruch, 1962). In contrast to this, Plug and Werner (2001) suggest that spacing between fractures is nonlinearly dependent on the length scale of stress reduction and fracture spacing, a more complex relationship that arises out of the dynamics of multiple interactive fractures, including suboptimal placement of fractures and propagation, which can carry fractures into zones where stress is too low for a new fracture to initiate. This model suggests that fracture spacing may only be weakly dependent on fracture depth in frozen ground when depths exceed ~5 m (Plug and Werner, 2001).

The large spacings, D, for Martian networks likely reflects a deeper propagation of fractures associated with a longer period of fracture development.

7.1.2 Orthogonal versus Non-orthogonal Intersections

The relative orientation of fractures in Martian networks is predominantly orthogonal, as is indicated by surface plots. Manual measurements of orthogonal and non-orthogonal intersections in Martian networks support this conclusion, with all but two networks displaying a significantly greater number of orthogonal intersections. Similar results have been noted for a subset of polygonal patterns in Utopia Kuzmin et al., (2002).

Tension cracks preferentially propagate in the direction perpendicular to maximum tension. As such, the sequential emplacement of fractures results in the tendency of a new fracture to bend towards the normal of a pre-existing fracture, forming an orthogonal intersection. Parallel orientation is dependent on the emplacement of two orthogonal fractures, and as such the resulting networks should always have a greater degree of orthogonality than parallelism (Plug and Werner, 2001). This appears to be the case in the majority of Martian networks, suggesting a similar origin of tension cracking caused by thermal contraction of the surface.

7.1.3 Three-Way and Four-Way Intersections

Four-way intersections are suggested to form from three-way orthogonal intersections, which experience a reversal in fracture order during a subsequent winter (Plug and Werner, 2002). As a result, a previously arrested fracture may continue to propagate across a polygon, forming a four-way orthogonal intersection. Alternatively, a four-way intersection may develop in response to a directional change in tensile loading, in which two new fractures develop from an irregularity along a pre-existing fracture. The new fractures propagate at orthogonal intersections to the pre-existing fracture, but in opposite directions (Plug and Werner, 2001). The latter proposed mechanism is thought to be unlikely to occur, as four-way intersections are not observed in studies of initial fracture pattern growth in permafrost (Mackay, 1986).

Both Martian and terrestrial networks display a large percentage of four-way intersections. The formation of four-way intersections as a result of multiple fracturing events has been attributed to the effects of seasonal climate change on Earth. The large number of orthogonal intersections, leads to the suggestion that networks formed in response to seasonal changes, not by a single fracture event such as a climate change.

Conversely, three-way intersections form in response to a single event, such as an abrupt change in climate. Mud desiccation crack networks may be an example of a consist almost entirely of three-way intersections, suggesting that they formed by a mechanism dissimilar to Martian networks.

7.1.4 North-South Network Orientation

With the exception of Region 1, networks in this study have a preferred North-South orientation displayed in the rose diagrams for Martian networks. Possible mechanisms for the formation of this orientation are varied and include: large scale bending of the Utopia basin, an E-W oriented anisotropic stress produced by a nearby water body or topographic slope, or pre-existing planes of weakness in a N-S trending direction.

The suggested mechanism of bending of the Utopia basin is proposed by Yoshikawa (2003) to explain the strongly oriented N-S networks observed in the Utopia Planitia Basin. Yoshikawa (2003) presents a two layered model in which the upper layer, consisting a Vastitas Borealis Formation (Hvk-Hvm) material, is cracked as a result of uplift or submergence of an underlying basin. The resulting fractures are generally oriented N-NNE, and parallel the basin contour line which tends NNW. This mechanism of orientation formation favours a tectonic origin for the polygons, however tectonic activity has ceased to exist on Mars since the early Hesperian or possibly Noachian time. If the oriented cracks are the result of tectonic processes this would imply that they are considerably older than their appearance suggests.

The development of an E-W oriented anisotropic stress may also be responsible for the generation of the N-S orientation. Drawing from the example of terrestrial networks, Lachenbruch (1962) states that as stress relief on the surface ranges from a maximum in the direction perpendicular to a fracture to a minimum in the direction parallel to the fracture, stress anisotropy exists. The anisotropic stress represents an appreciable horizontal stress difference, and may be generated by nonuniform horizontal thermal gradients, possibly over a large area. Lachenbruch (1962) employs as an example a nearby water body where horizontal temperature changes, and therefore horizontal stress differences are significant. The axes of minimum and maximum horizontal tension correspond with the normal and tangent to the shoreline respectively. The water body acts as a heat source, lessening the stress perpendicular to the shoreline. If the shoreline were to recede, the first contraction cracks to form would be oriented normal to the shoreline and axis of maximum horizontal stress. Therefore, if an E-W trending shoreline were to recede, one would expect N-S oriented fractures to develop.

A similar mechanism involving large bodies of water may explain the preferred N-S orientation of Martian networks. Baker et al. (1991) have proposed a model in which a northern ocean termed the Oceanus Borealis, repeatedly formed and dissipated during the Hesperian and Amazonian as a result of large floods. It is suggested that the end of the Noachian marked a time in which Mars' climate was much like it is today, possibly consisting of a thick permafrost layer overlying a water-rich upper crust. Episodic volcanic activity within Tharsis resulted in widespread melting of ground ice, thus releasing large amounts of water in the form of floods (Baker et al., 1991). Numerous, and possibly simultaneous floods would have led to the formation of large oceans. Linear features have been noted in the northern plains and interpreted as ancient shorelines, supporting the hypothesis of large bodies of water being present in post-Noachian times. Once the oceans formed, water would infiltrate into the surface, and atmospheric CO_2 would dissipate, causing the Martian climate to return to

conditions similar to present. The infiltrated water may still be present today beneath the surface in the form of ground ice, thus supporting the hypothesis that small-scale polygonal patterns on Mars are similar to terrestrial polygonal patterns that form by thermal contraction cracking.

Head et al., (1999) studied two contacts previously mapped by Parker et al. (1993) who interpreted the contacts to represent shorelines and two separate highstands of a northern polar ocean. Head et al., (1999) suggested that if these contacts represent ancient shorelines, they should exist as equipotential lines (i.e. a surfaces representing the edge of a level surface). Investigation of these surface and plotting of the elevations revealed that contact 2 of Parker et al., (1993) closely approximates an equipotential line with an elevation range of ~4.7 km. MOLA data displays the relatively smooth surface of the northern lowlands, which would correspond with sedimentation below a shoreline.

Head et al., (1999) also suggest that the total volume represented by the topography below contact 2 (~1.4 x 10^7 km^3) is approximately equal to the predicted volume of material which flowed through the Chryse outflow channels (~0.6 x 10^7 km^3).

Experimental sequential flooding of the northern lowlands lead Head et al., (1999) to produce maps displaying where water would accumulate, and how oceans would evolve with changes in depth (Figure 43). If these shorelines were to recede, they would likely do so in a manner following the reverse order of the filling sequence. Regional slope maps compiled by Head et al., (1999) display linear slope changes within the Utopia basin, which parallel topographic contours and occur near or below contact 2. As such, Head et al., (1999) concludes that MOLA data provide evidence for large standing bodies of water to have existed in the northern lowlands during Martian history.

It is not unreasonable to assume that these ancient shorelines may have retreated

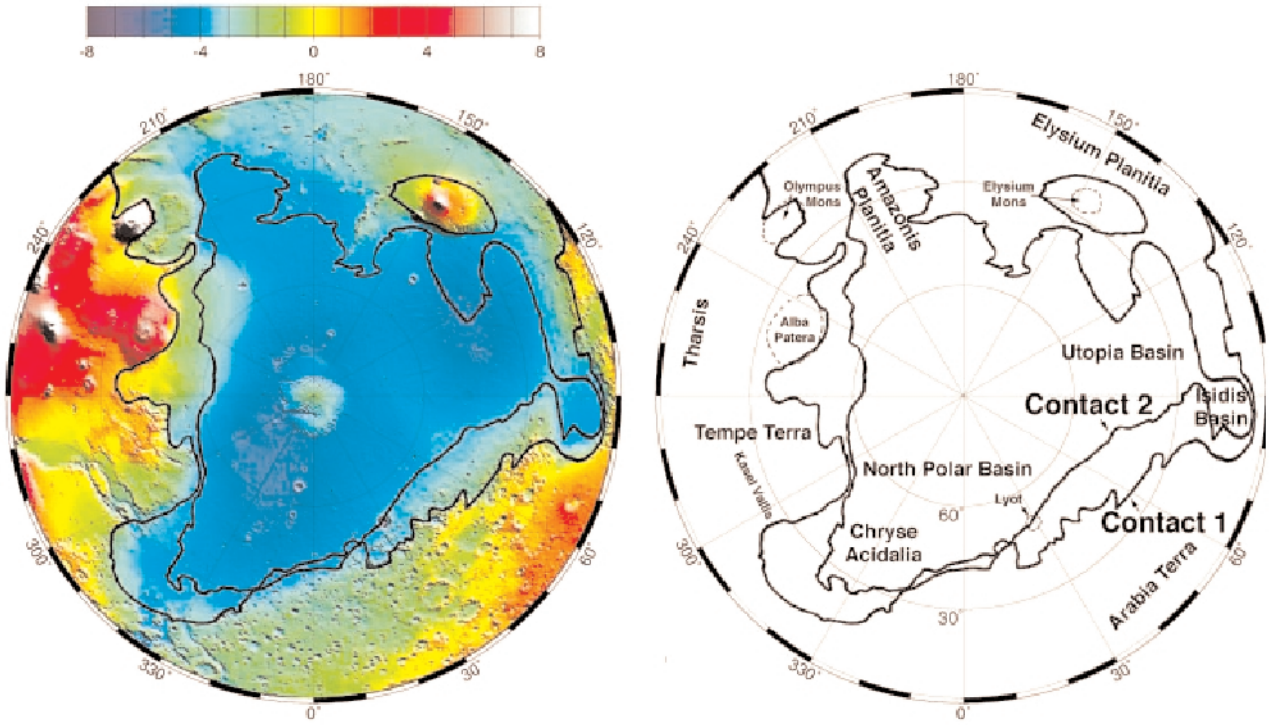

Figure 43: Schematic representation of Oceanus Borealis, which is suggested to have repeatedly formed and dissipated during the Hesperian and Amazonian as a result of large floods. After: Baker et al., 1991.

in a similar manner to terrestrial shorelines as described by Lachenbruch (1962). As such, an E-W oriented Martian shoreline would result in the initiation of perpendicular oriented fractures displaying a N-S orientation, as is observed in the polygonal networks on Mars. However, this hypothesis poses a problem similar to that of tectonics being responsible for the observed orientation. The presence and retreat of large bodies of water and associated fractures in post-Noachian time, would also suggest that the cracks are considerably older than their appearance suggests.

An apparently E-W oriented anisotropic stress responsible for the generation of a N-S orientation of fractures, may also be the result of a global topographic slope on the Martian surface. A pole-to-pole slope of 0.036º exists and results in the south pole having and elevation ~6 km higher than the north pole (Cattermole, 2001). This global slope is suggested to have been present throughout most of Martian history, and may be responsible for the transport of water on the surface and subsurface. Through the use of high resolution MOLA maps (Figure 2) it has been determined that the northern hemisphere is relatively smooth within the mid- to high latitudes, displaying an elevation of approximately – 4 ± 3km poleward of 50ºN. An overall southward slope of 0.056º exists within the northern hemisphere. Compressive stresses acting on the slope serve to counteract tensile stresses in the downslope direction, while maintaining tensile stresses in the horizontal (across slope) axes. As such, initial fractures will preferentially occur in an orientation perpendicular to the horizontal tensile stresses, i.e. a northward dipping slope will result in initial fractures oriented N-S, as in the case of polygonal networks on Mars.

An additional hypothesis is that in which pre-existing planes of weakness exist in a N-S trending direction within the fracturing material. This results in the material, not the stress, causing the preferred orientation.

7.1.5 Network Exposure

Variations exist with regard to the relative ease with which polygonal networks can be seen in MOC images. Networks appearing faint in images or less well developed (such as in Area 1) may be the result of insufficient sublimation occurring at the particular latitude, which exposes networks through the release of volatiles. At latitudes greater than 30º sublimation rates are dependant upon obliquity (Carr, 1996). At the current Martian obliquity of 25.19º, the rate of sublimation at soil depths greater than 1 m becomes negligible. It is only at high obliquities that significant sublimation occurs at high latitudes, and even this occurs at rates as low as 10-5 to 10-6 cm/yr. Yoshikawa (2003) suggests that Martian polygonal networks likely formed during a period of obliquity of ~32º, when ground ice would have been stable globally. A current increase in obliquity affecting higher latitudes would result in the propagation of more fractures, and therefore a decrease in fracture spacing, D, in networks such as Region 1.

7.1.6 Thermokarst Features

Features indicative of thermokarst are noted in images located in areas 2-5, but do not appear evident in images of area 1 (north of 60º latitude).

Thermokarst related features include depressions interpreted as thermokarst pits, and raised plateaus outlined by jagged escarpments. The presence of features possibly formed by thermokarst processes, further suggests the presence of an ice-rich ground layer at some point during the Martian history, thus supporting a hypothesis for the development of fractures by thermal contraction crack mechanisms.

It is difficult to determine whether or not the networks predate the thermokarst features, as cross-cutting relationships vary significantly. I suggest that the event of polygon formation was, at least, coeval with thermokarst processes at some point in Martian history.

7.2 COMPARISON OF MARTIAN AND TERRESTRIAL NETWORKS

7.2.1 Qualitative Comparison

Martian networks range in polygonal diameter from measured values of 29.83-150.72 metres, whereas terrestrial polygons range from 10.85-21.01 metres. Both display predominantly orthogonal intersections with values for orthogonality, O, on the order of 60.89-63.03.

Two-dimensional surface plots corresponding to digitized Martian and terrestrial networks display values of spacing, D, on the order of 41.52-145.34 and 11.92-18.08 respectively. D values are represented by peaks at 0º, most of which appear stretched in the direction of relative orientation in both Martian and terrestrial networks. Stretching of these peaks indicates an increase in disorganization within the networks. Orthogonal intersections are represented by peaks in the distributions at +90º and -90º, in which the width of the ridges is a measure of the degree of orthogonality of a network. The majority of Martian networks display sharply peaked ridges corresponding to highly orthogonal and ordered networks, whereas the majority of terrestrial networks display ridges with sharp edges at small distances, but which widen toward larger distances. Ridges such as these are indicative of fractures in which orthogonal intersections occur where two fractures meet, but tend to deviate as the distance from the intersection increases.

With the exception of Area 1, Martian polygonal networks have a preferred North-South orientation, whereas terrestrial networks appear to lack a preferred orientation, except in the case of networks 7 and 9. Various mechanisms are suggested to explain the Martian orientation including: large scale bending of the Utopia basin, an E-W oriented anisotropic stress produced by a nearby water body or topographic slope, or pre-existing planes of weakness in a N-S trending direction. Terrestrial networks that display a preferred N-S orientation are located in the vicinity of shorelines, possibly suggesting a similar mode of formation between terrestrial and Martian orientations.

Both terrestrial and Martian networks largely consist of four-way intersections, which form as a result of multiple fracturing events, attributed to the effects of seasonal climate change on Earth. As such, the similarities among networks leads to the suggestion that four-way intersections on Mars may also form in response to seasonal changes.

CHAPTER 8: CONCLUSIONS

The intent of this thesis was to investigate the distribution of small-scale polygons within the Utopia Planitia region of Mars as a function of surface properties, and test the hypothesis that Mars and terrestrial polygonal patterns are quantitatively similar and, by inference, have formed by similar mechanisms.

My results are consistent with the view that Martian patterns likely formed by the sequential emplacement of fractures, similar to the manner in which terrestrial networks develop. Martian networks display a tendency towards orthogonality, in which intersections are predominantly four-way. This is similar to measured values for terrestrial networks, but unlike features displayed by experimental mudcrack networks, thus suggesting that Martian patterns do not likely form by desiccation processes.

Martian networks display a strong north-northeast orientation over large regions, approximately parallel to the regional topographic slope into the Utopia basin. This is similar to the orientation of networks that develop in the vicinity of receding water bodies in terrestrial environments. As such, I conclude that the development of a predominant N-S orientation is related to the development of an E-W oriented anisotropic stress in both Martian and terrestrial environments.

The formation of networks through multiple fracturing events suggests that effects of seasonal climate change may influence the development of both terrestrial and Martian networks.

Remote sensing evidence, such as that provided by the Mars Orbiter Laser Altimeter and thermal emission spectrometer, suggest that material present at or near the Martian surface is not unlike the material within which terrestrial networks form (i.e. ice-rich, fine-grained). As such, tensile strength and other rheological characteristics are likely similar between terrestrial and Martian environments of formation.

APPENDIX A

APPENDIX A

Mars
E03_02635 Latitude - 61.98ºN Longtitude - 289.48ºW

Original Image

Digitized Image

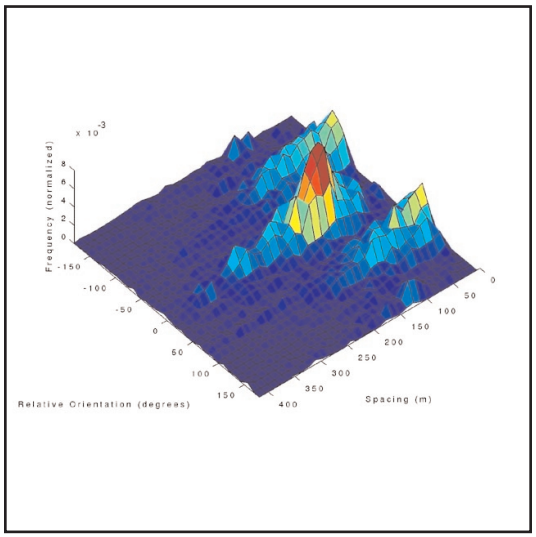

Surface Map

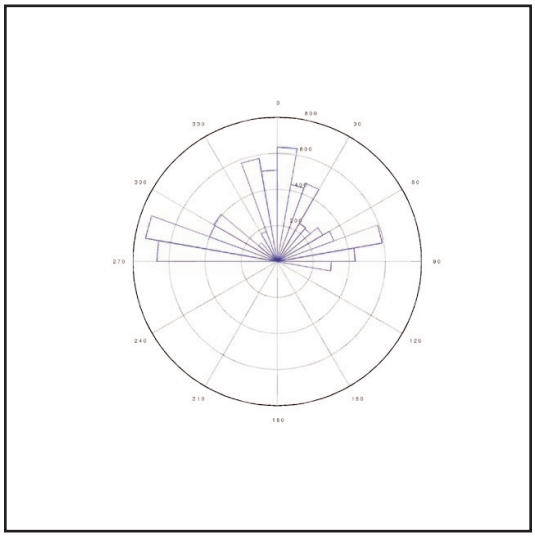

Rose Diagram

APPENDIX A

Mars
E05_00113 Latitude - 65.54ºN Longtitude - 289.86ºW

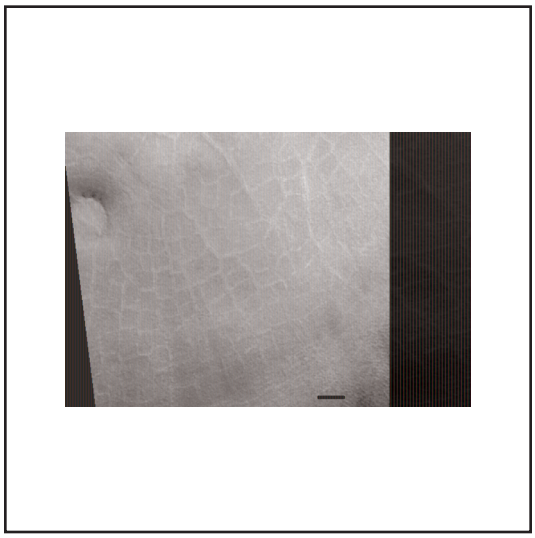

Original Image

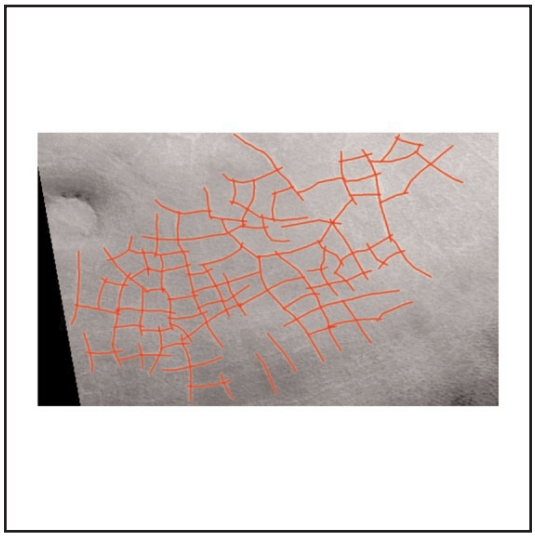

Digitized Image

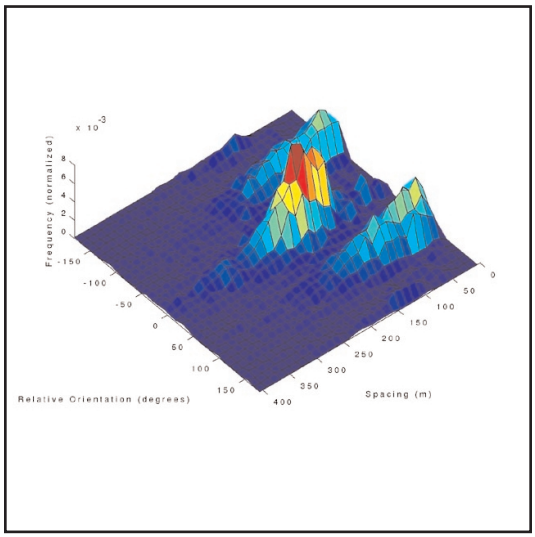

Surface Map

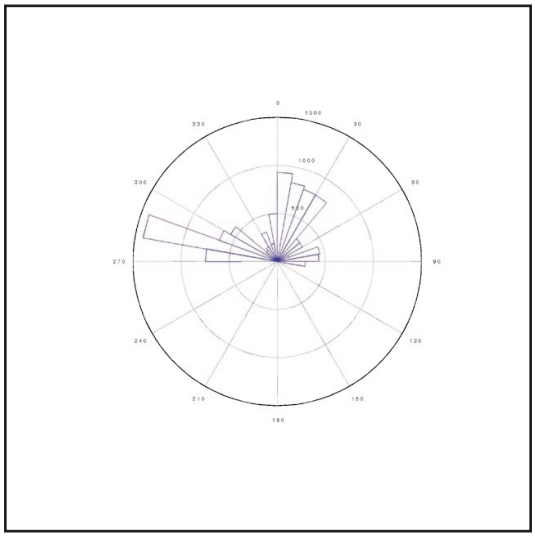

Rose Diagram

APPENDIX A

Mars
E22_00059 Latitude - 62.00ºN Longtitude - 289.55ºW

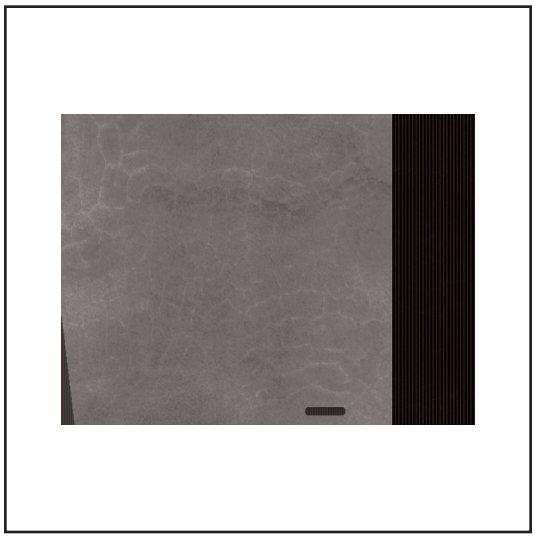

Original Image

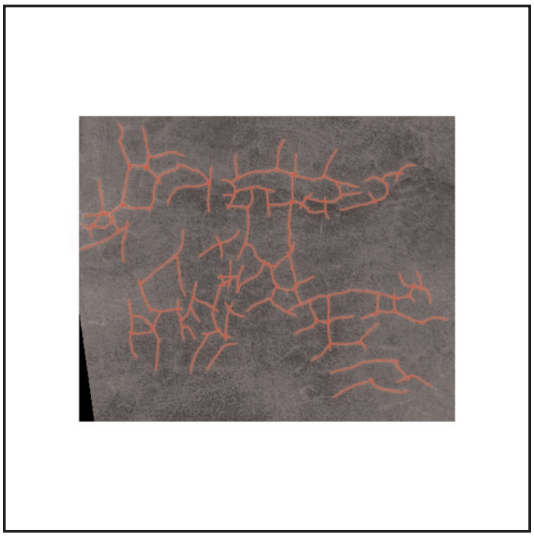

Digitized Image

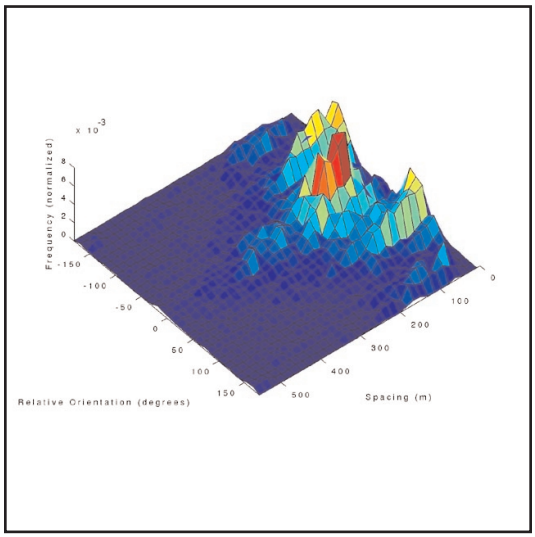

Surface Map

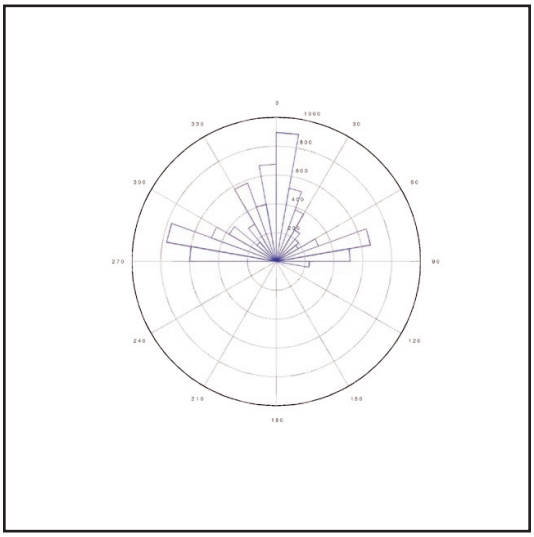

Rose Diagram

APPENDIX A

Mars
E23_01288 Latitude - 42.31°N Longtitude - 273.92°W

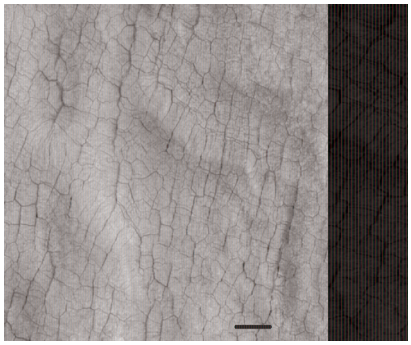

Original Image

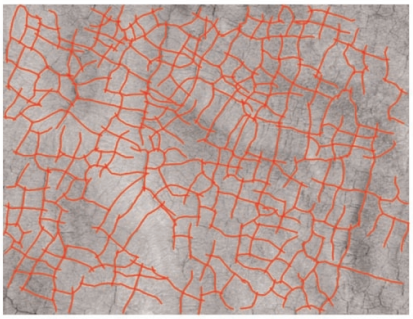

Digitized Image

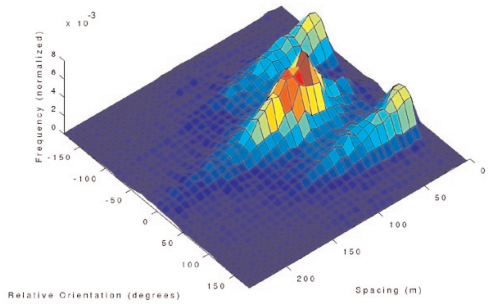

Surface Map

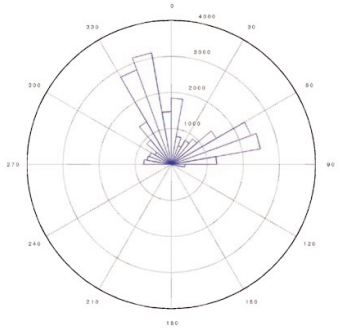

Rose Diagram

APPENDIX A

Mars
M00_00215 Latitude - 45.65ºN Longtitude - 259.84ºW

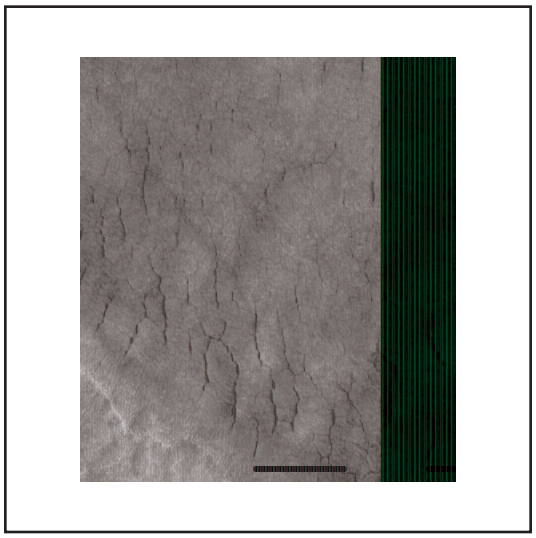

Original Image

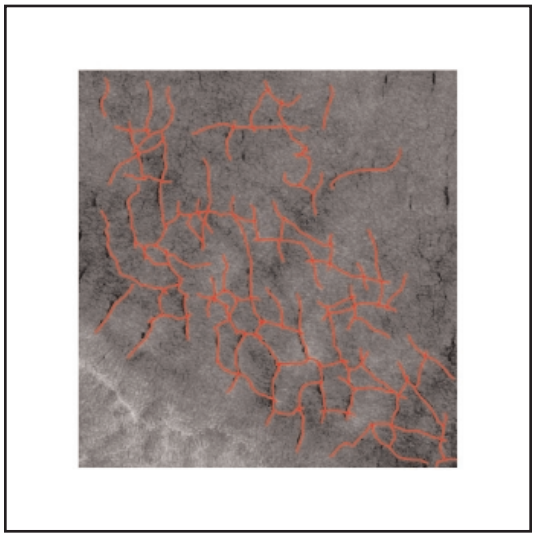

Digitized Image

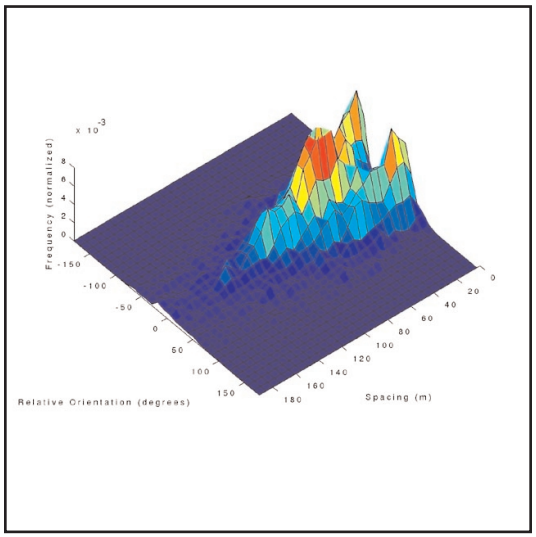

Surface Map

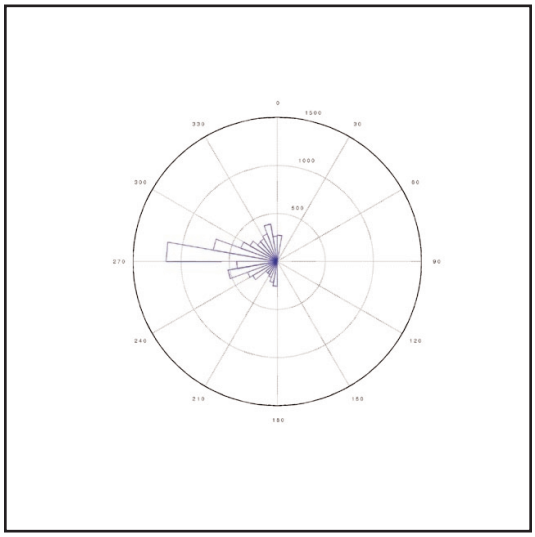

Rose Diagram

APPENDIX A

Mars
M01_00582 Latitude - 43.69ºN Longtitude - 273.28ºW

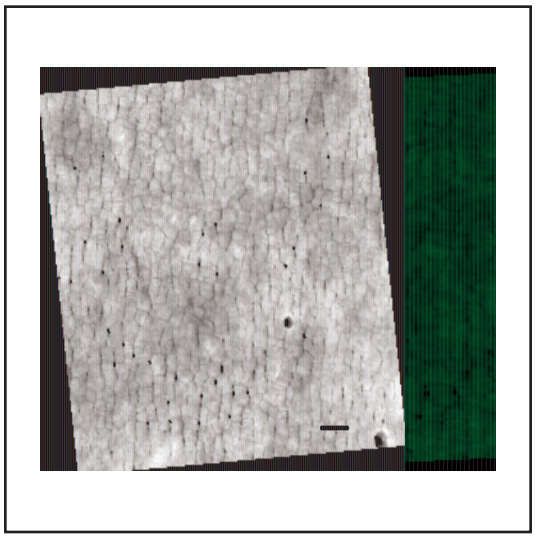

Original Image

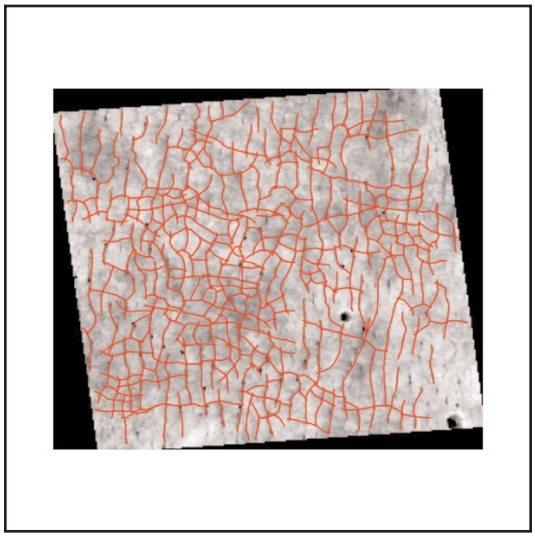

Digitized Image

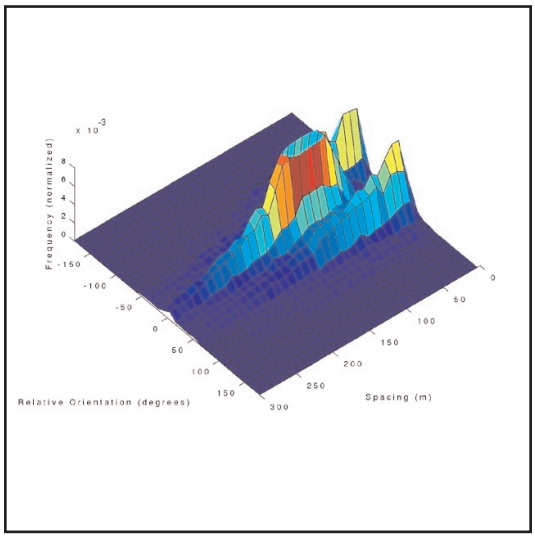

Surface Map

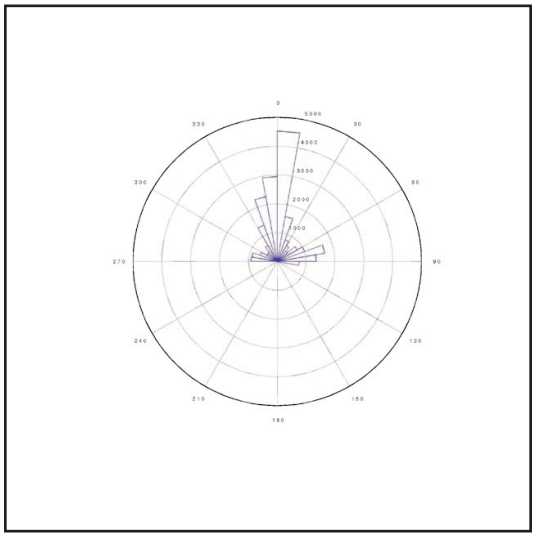

Rose Diagram

APPENDIX A

Mars
M01_04558 Latitude - 44.50ºN Longtitude - 276.11ºW

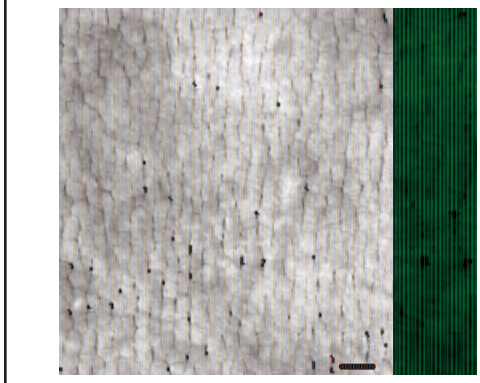

Original Image

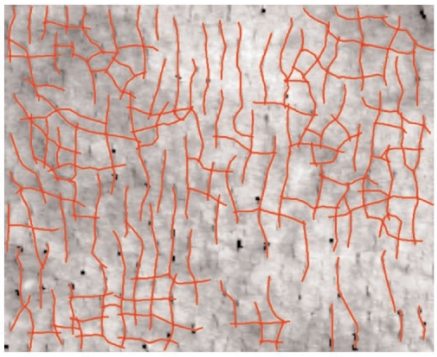

Digitized Image

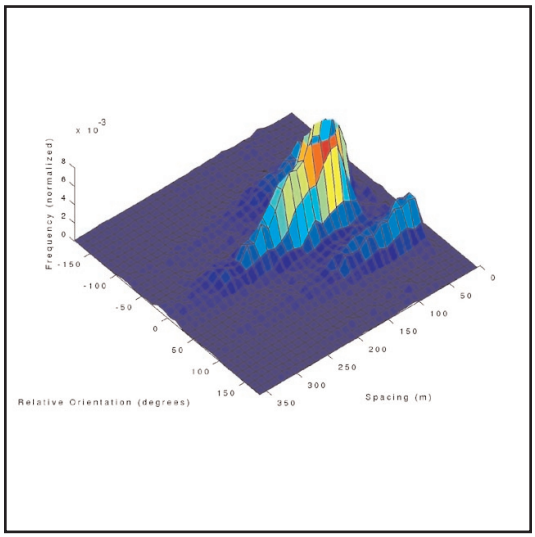

Surface Map

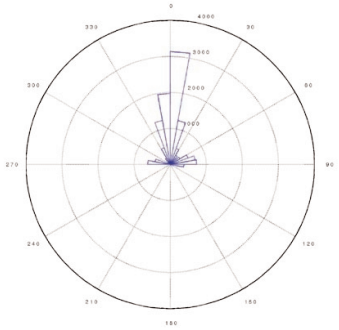

Rose Diagram

APPENDIX A

Mars
M02_02863 Latitude - 43.50ºN Longtitude - 269.30ºW

Original Image

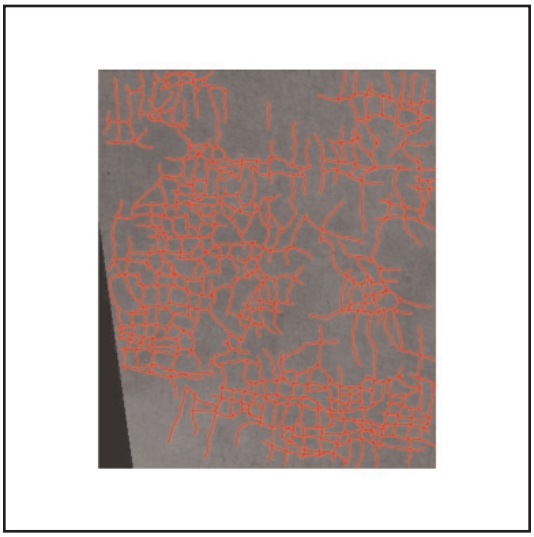

Digitized Image

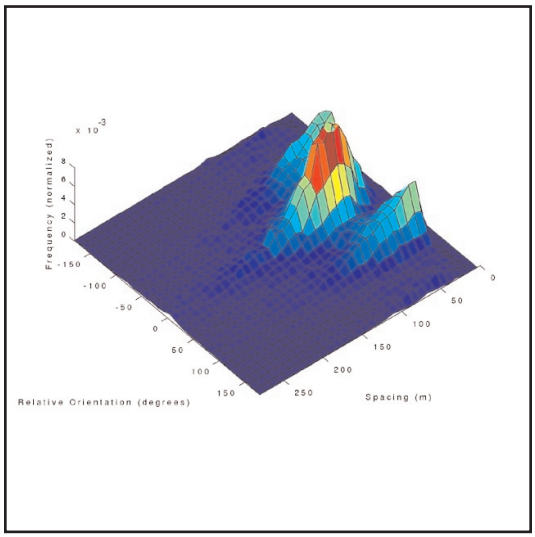

Surface Map

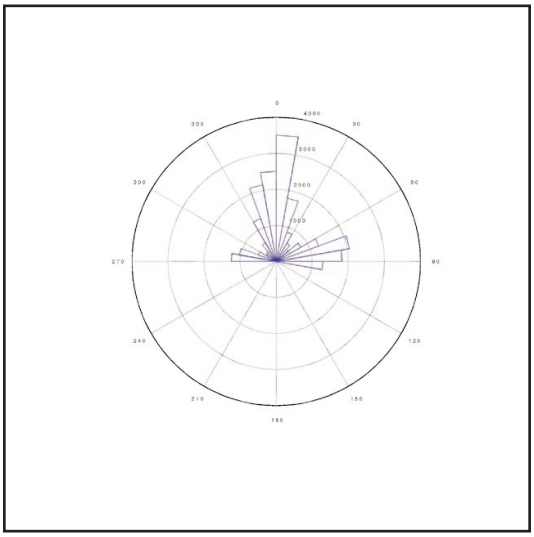

Rose Diagram

APPENDIX A

Mars
M02_03335 Latitude - 46.19ºN Longtitude - 265.39ºW

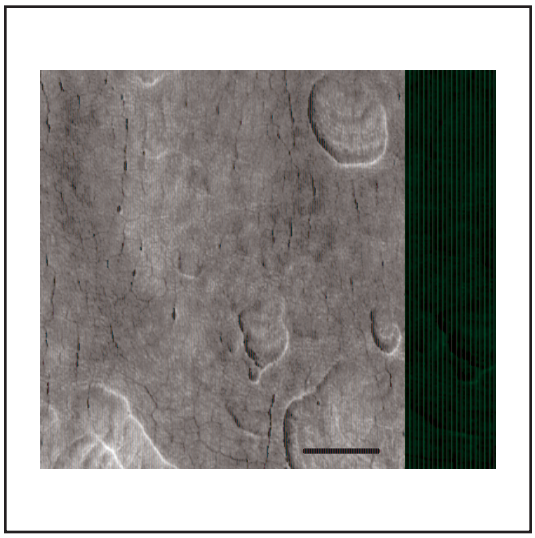

Original Image

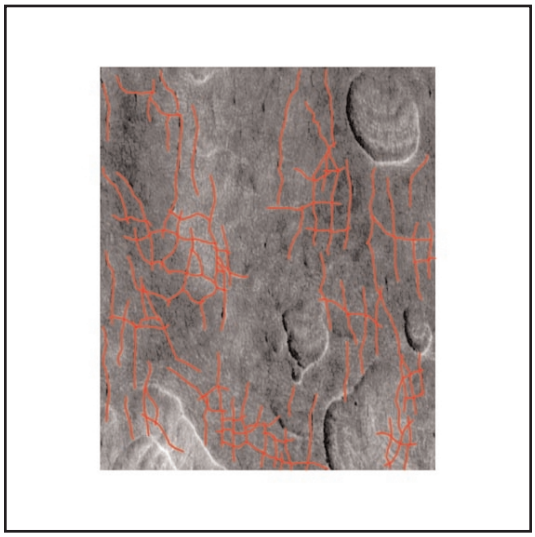

Digitized Image

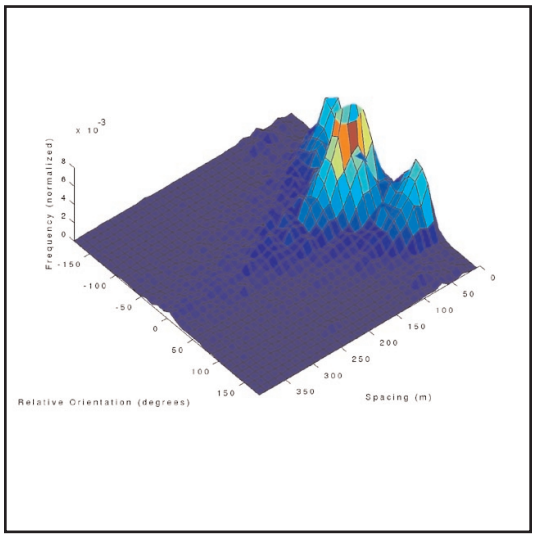

Surface Map

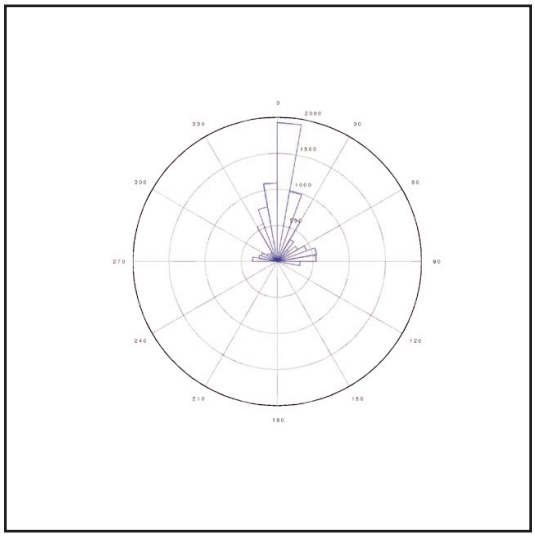

Rose Diagram

APPENDIX A

Mars
M03_04331 Latitude - 44.46ºN Longtitude - 272.80ºW

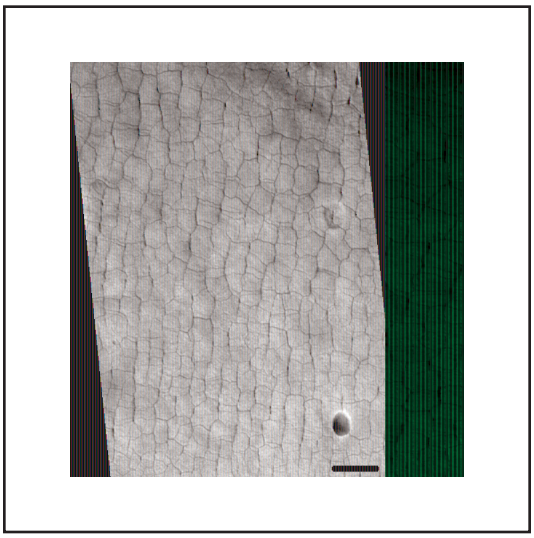

Original Image

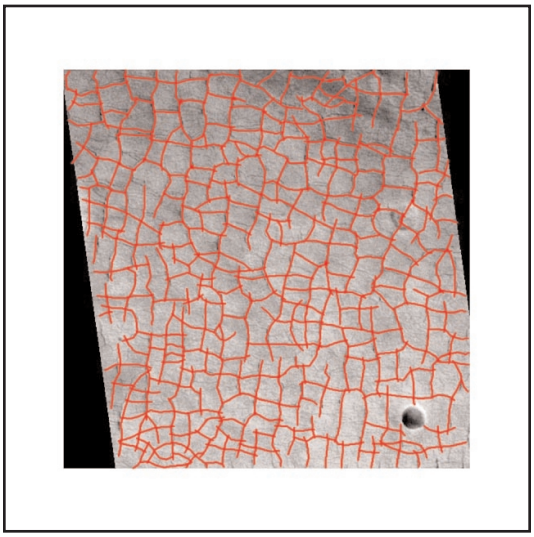

Digitized Image

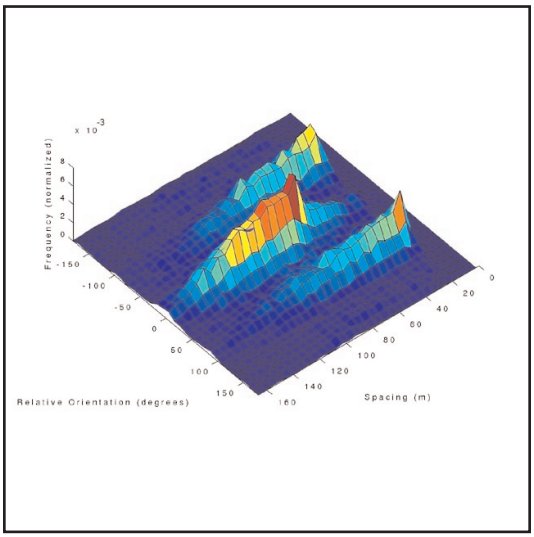

Surface Map

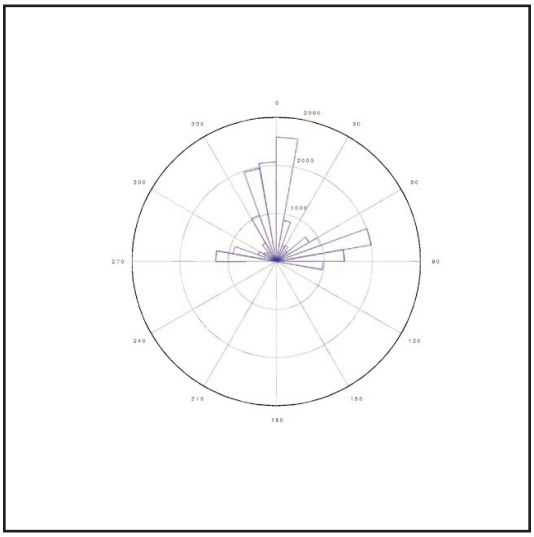

Rose Diagram

APPENDIX A

Mars
M03_05694 Latitude - 45.43ºN Longtitude -271.80ºW

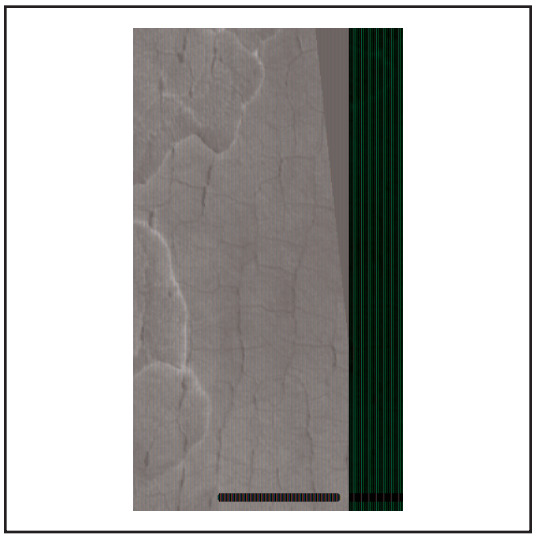

Original Image

Digitized Image

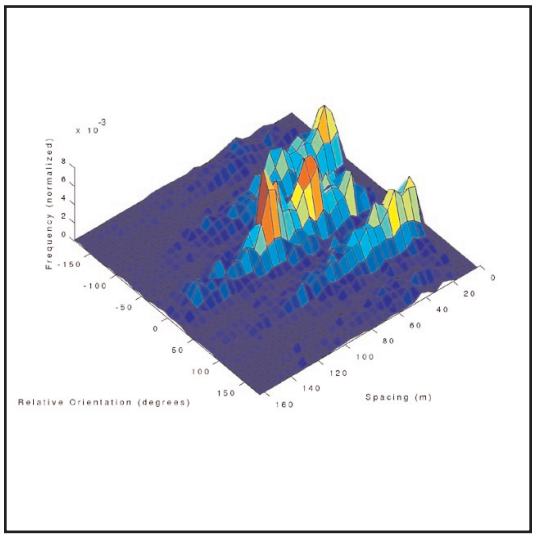

Surface Map

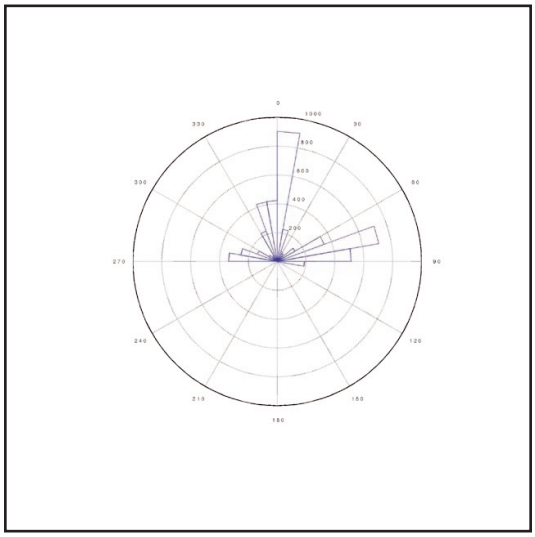

Rose Diagram

APPENDIX A

Mars
M04_00990 Latitude - 45.75ºN Longtitude - 265.15ºW

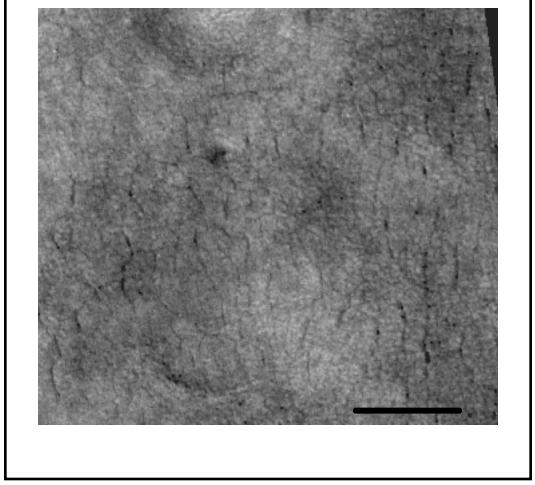

Original Image

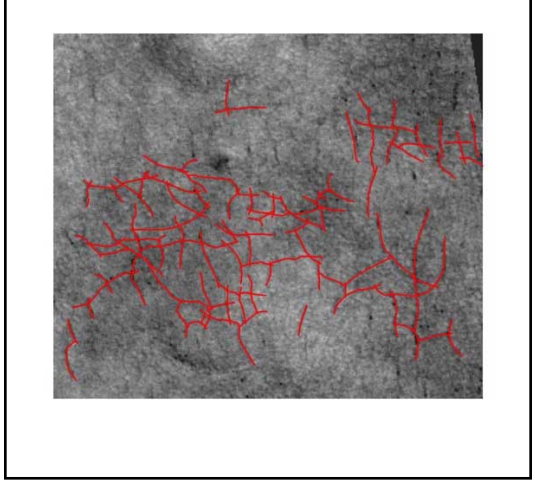

Digitized Image

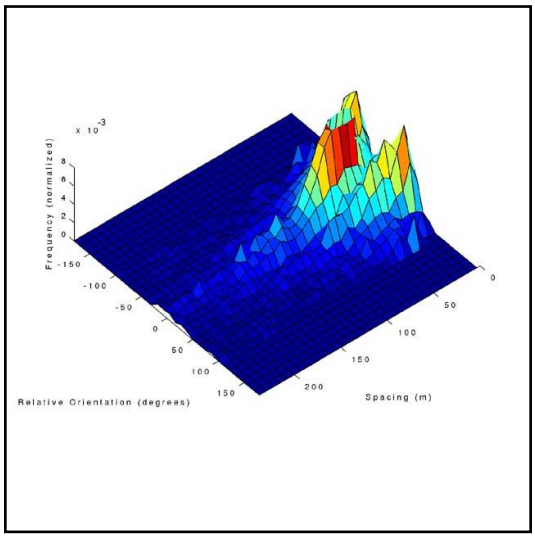

Surface Map

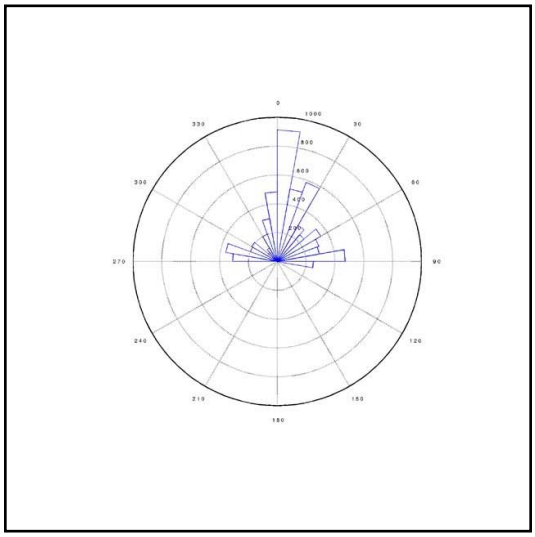

Rose Diagram

APPENDIX A

Mars
M04_01631 Latitude - 44.33ºN Longtitude - 272.68ºW

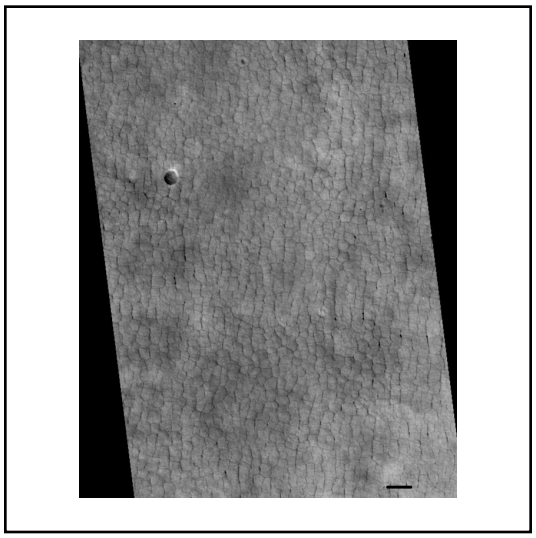

Original Image

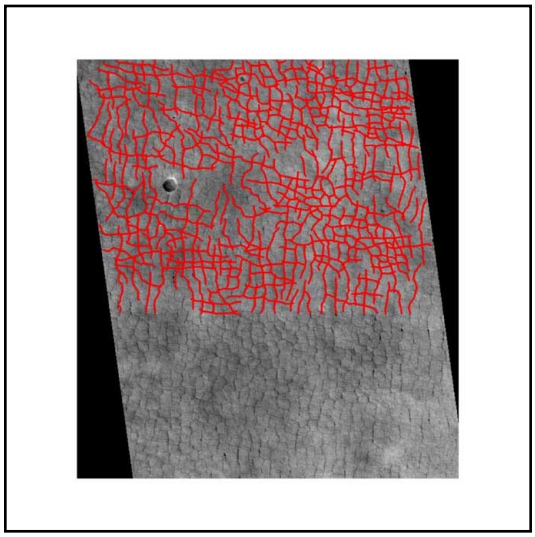

Digitized Image

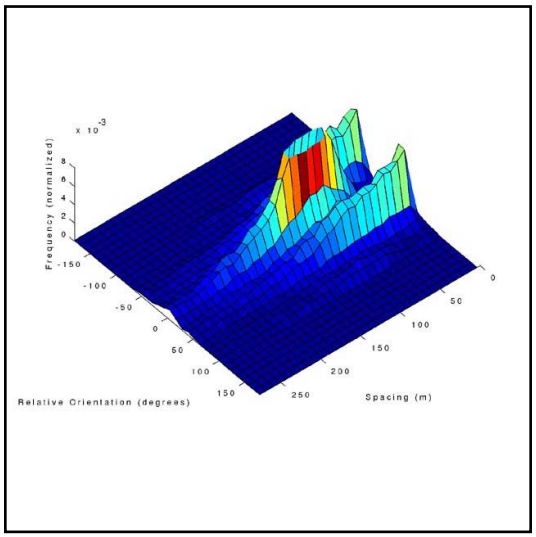

Surface Map

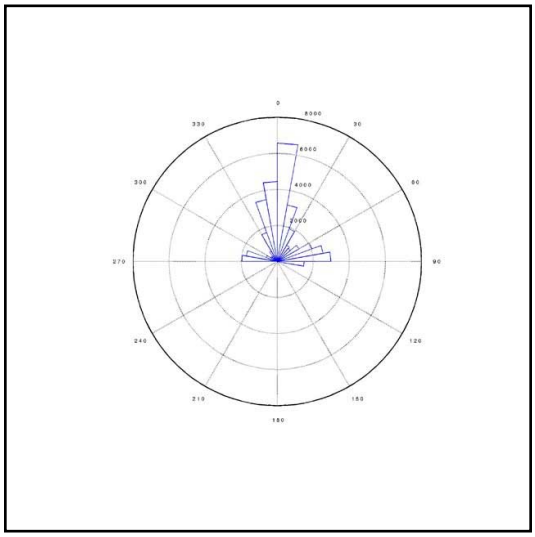

Rose Diagram

APPENDIX A

Mars
M04_02704 Latitude - 44.09ºN Longtitude - 276.14ºW

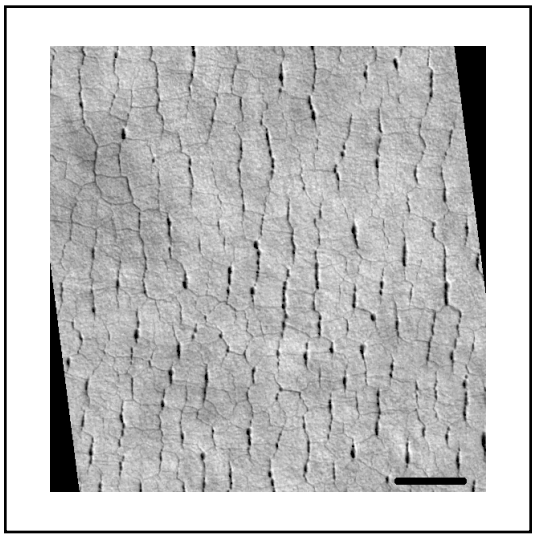

Original Image

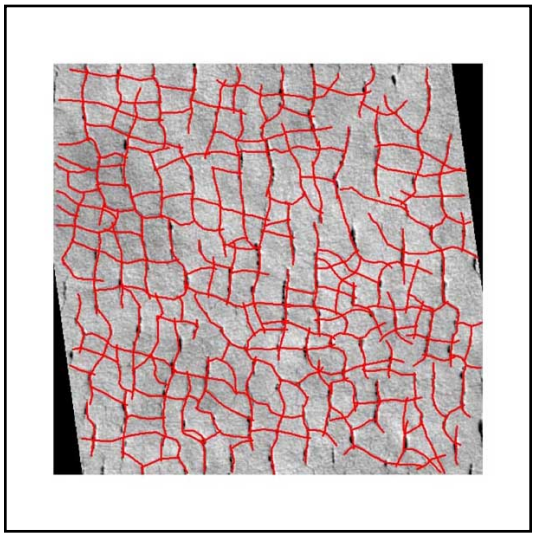

Digitized Image

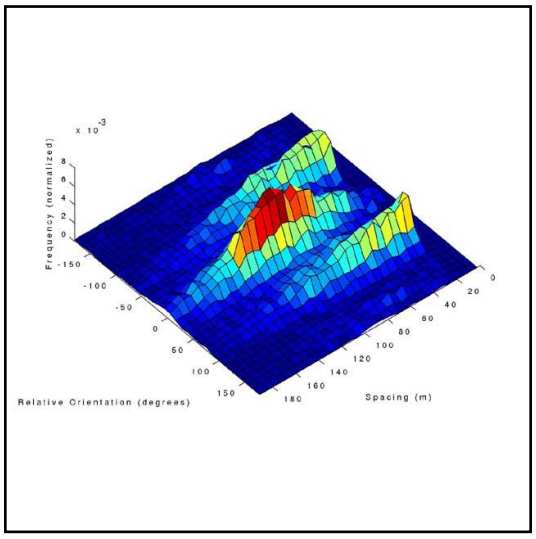

Surface Map

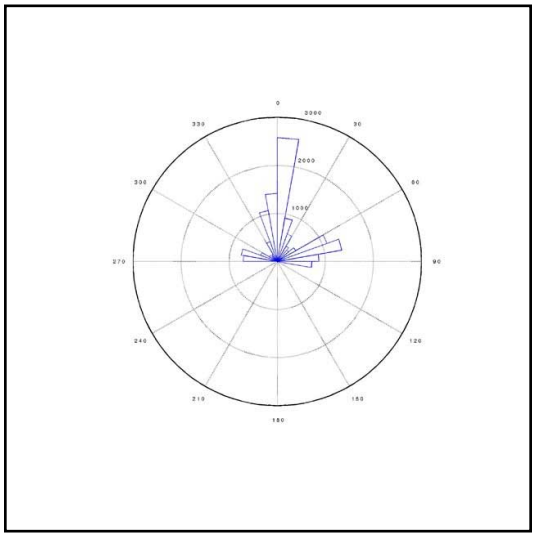

Rose Diagram

APPENDIX A

Mars
M04_03810 Latitude - 42.56ºN Longtitude - 279.32ºW

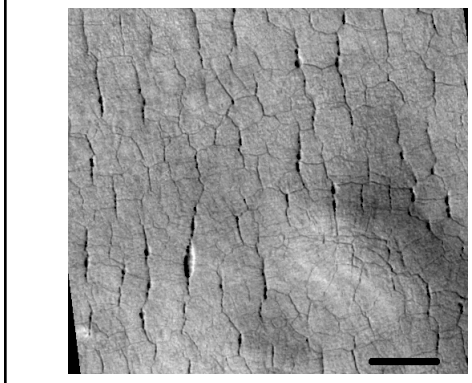

Original Image

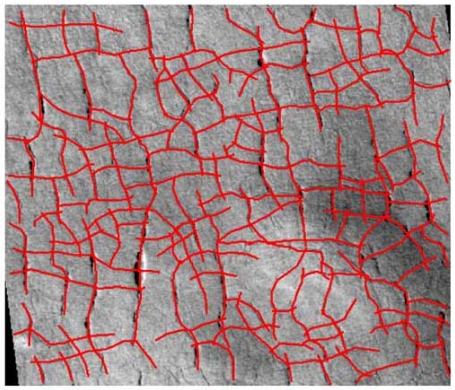

Digitized Image

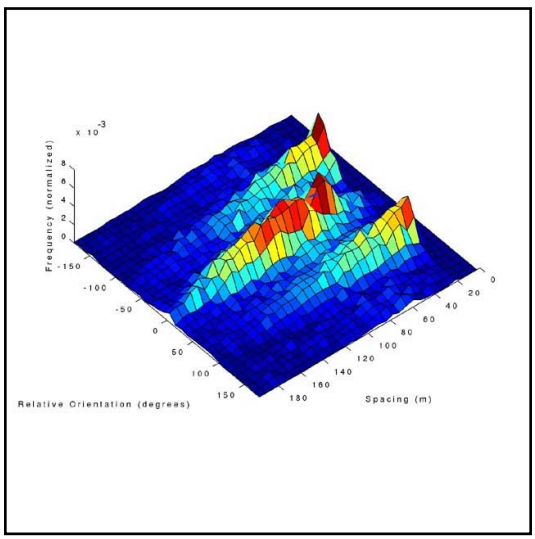

Surface Map

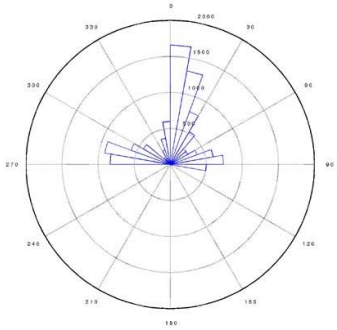

Rose Diagram

APPENDIX A

Mars
M04_04181 Latitude - 41.93ºN Longtitude - 274.87ºW

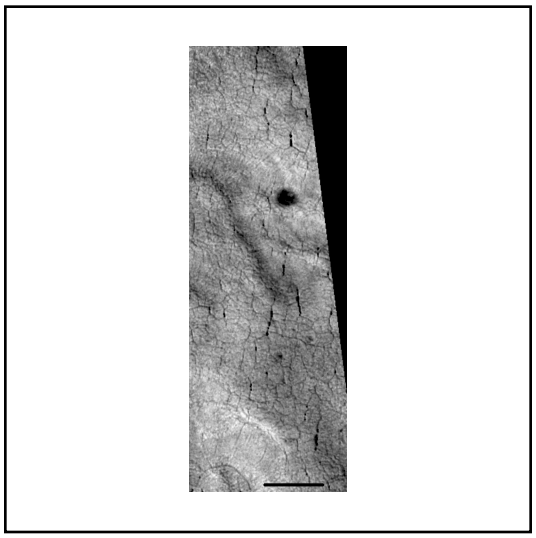

Original Image

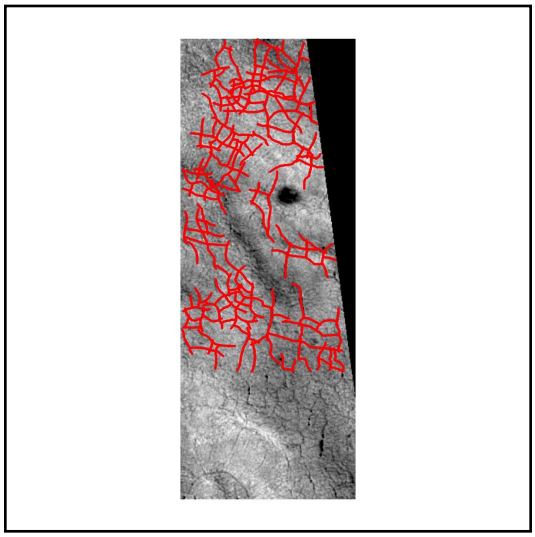

Digitized Image

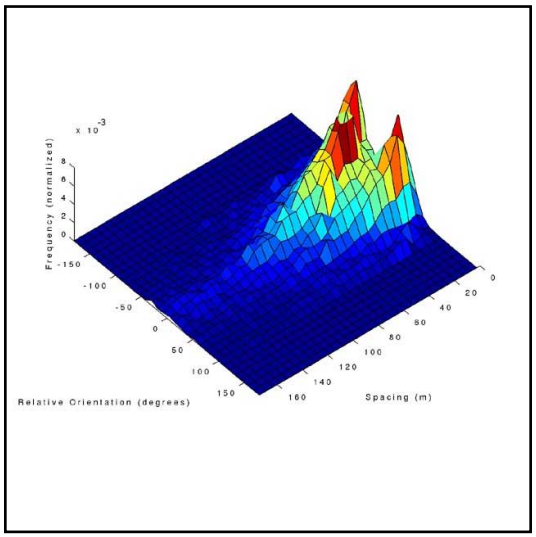

Surface Map

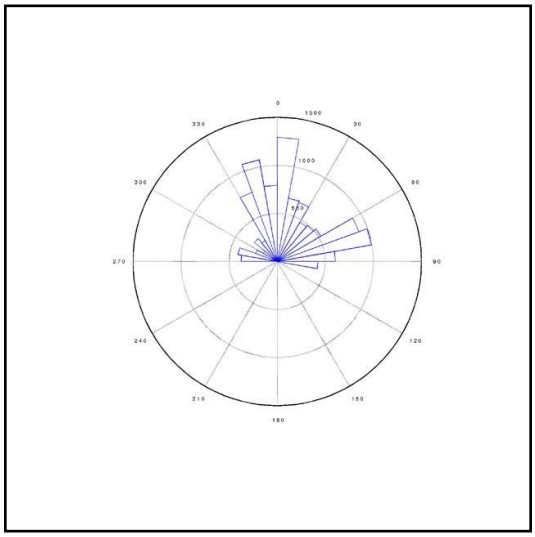

Rose Diagram

APPENDIX A

Mars
M08_03534 Latitude - 41.95ºN Longtitude - 277.15ºW

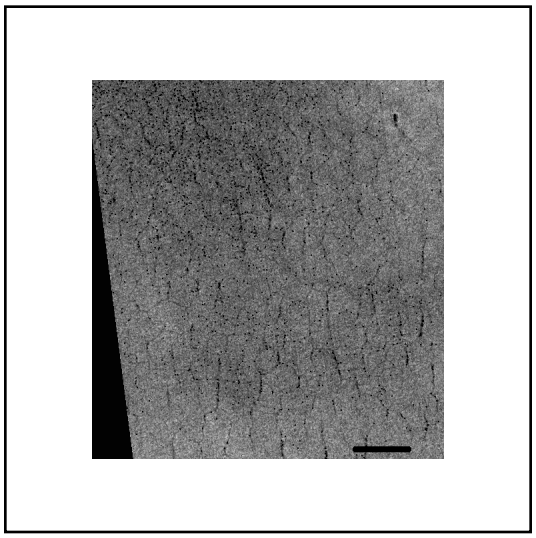

Original Image

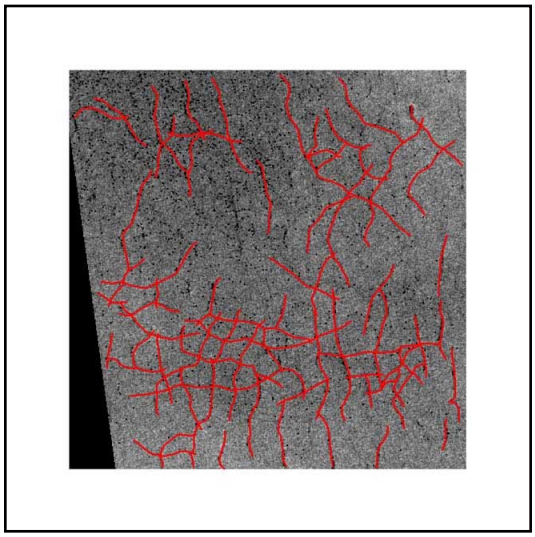

Digitized Image

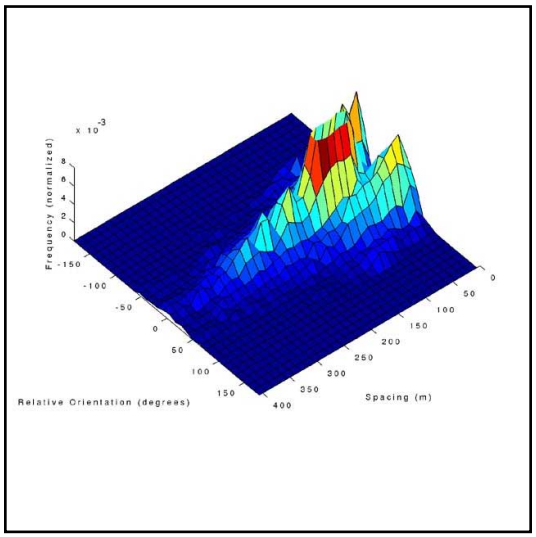

Surface Map

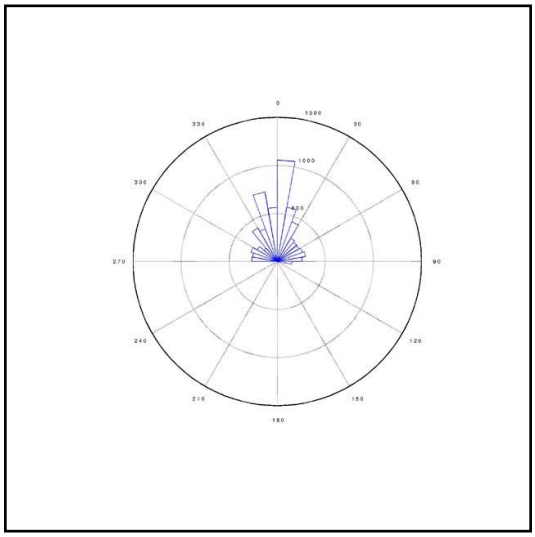

Rose Diagram

APPENDIX A

Mars
M08_07602 Latitude - 45.14ºN Longtitude - 275.80ºW

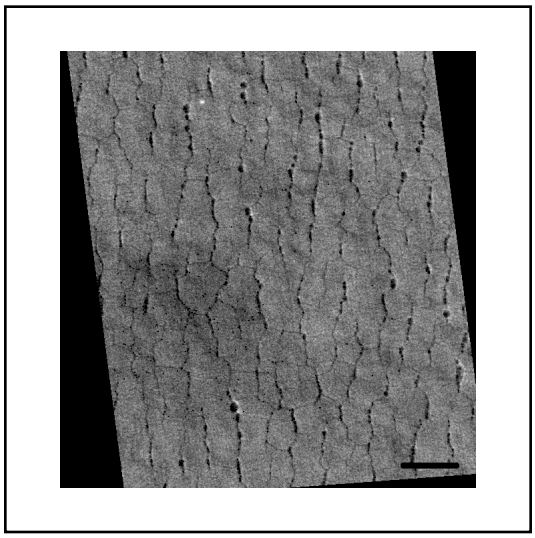

Original Image

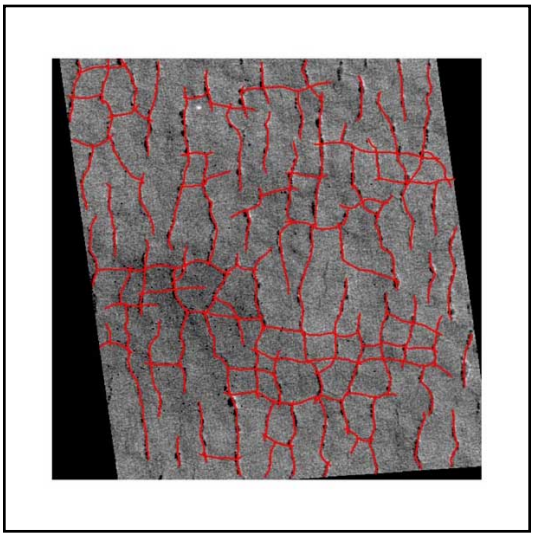

Digitized Image

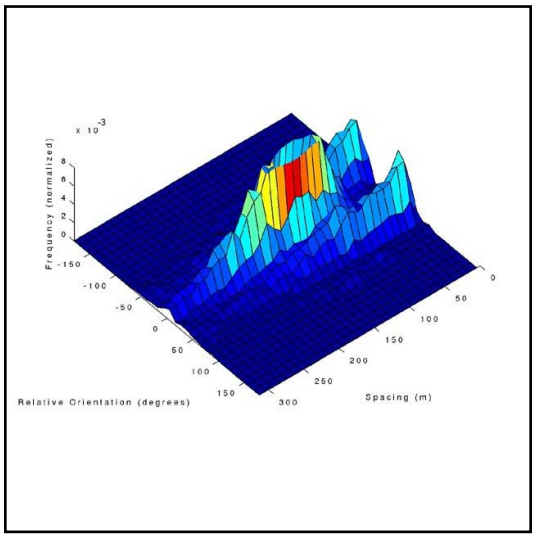

Surface Map

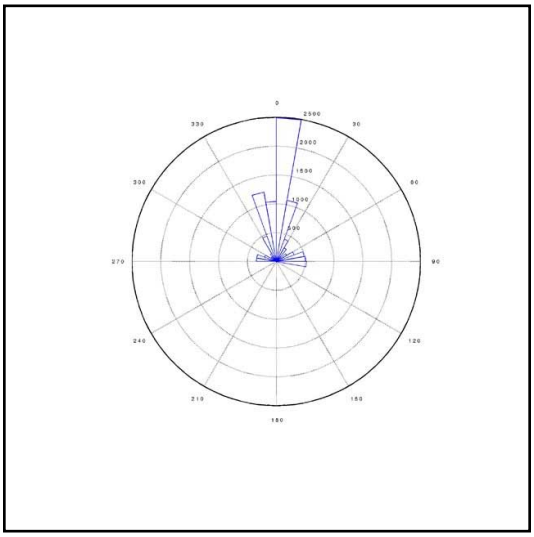

Rose Diagram

APPENDIX A

Mars
M09_03407 Latitude - 43.09ºN Longtitude - 273.48ºW

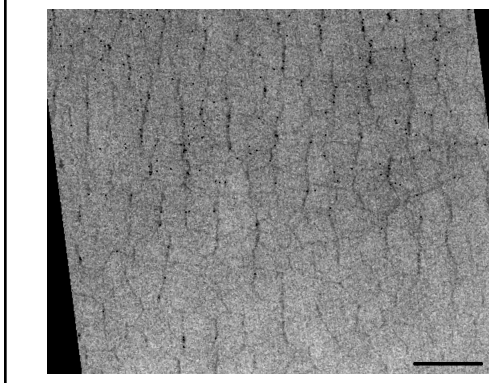

Original Image

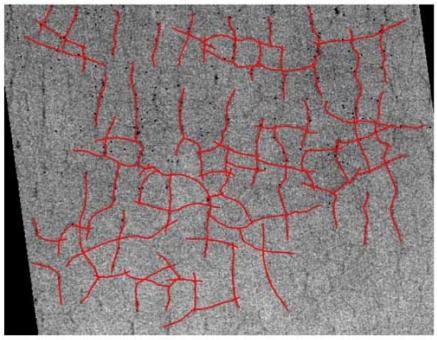

Digitized Image

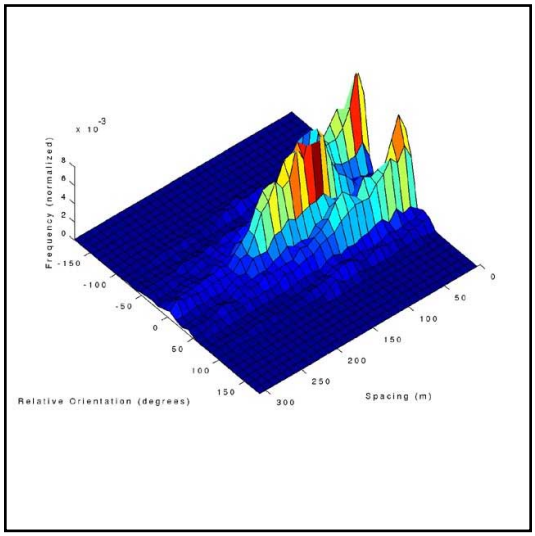

Surface Map

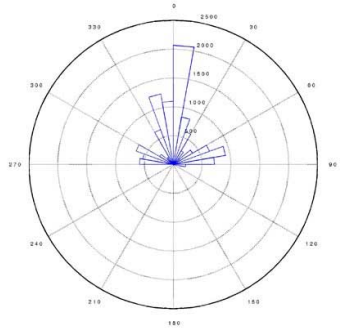

Rose Diagram

APPENDIX A

Mars
M19_00234 Latitude - 66.16ºN Longtitude - 278.81ºW

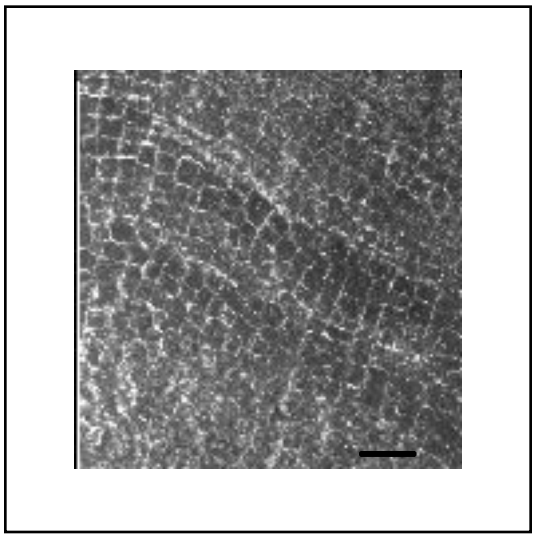

Original Image

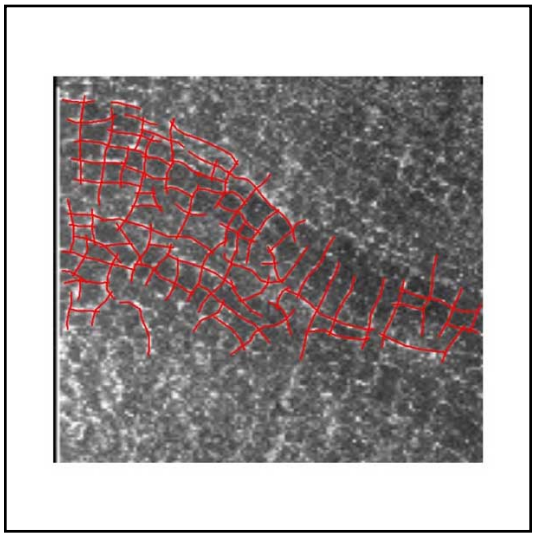

Digitized Image

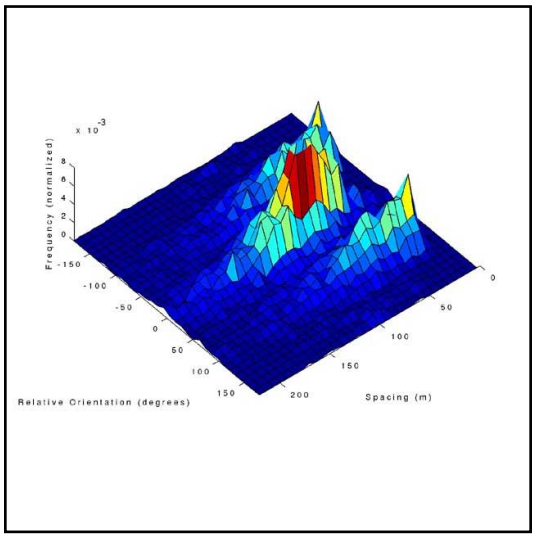

Surface Map

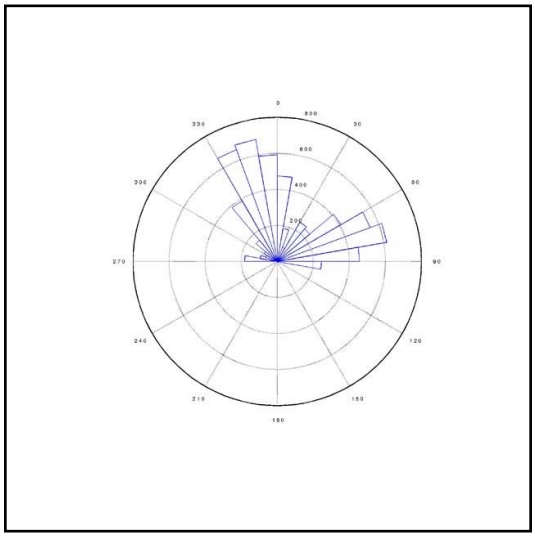

Rose Diagram

APPENDIX A

Mars
M19_01326 Latitude - 44.35ºN Longtitude - 272.11ºW

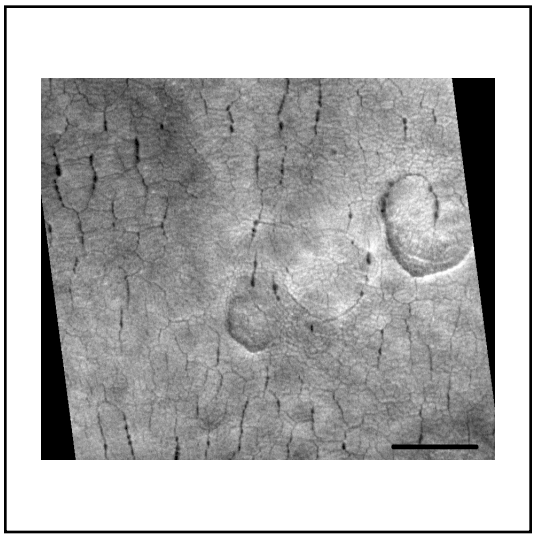

Original Image

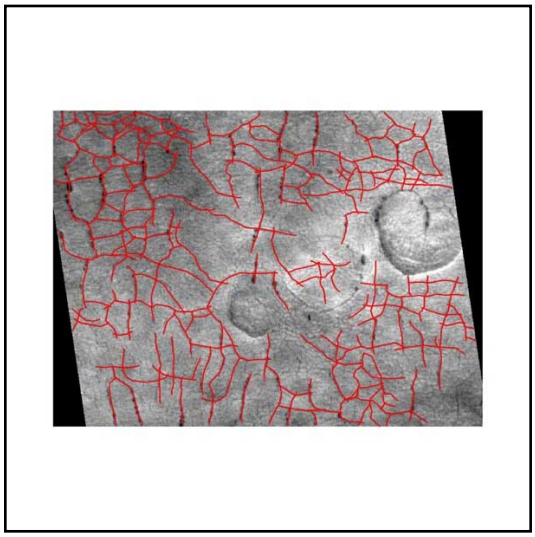

Digitized Image

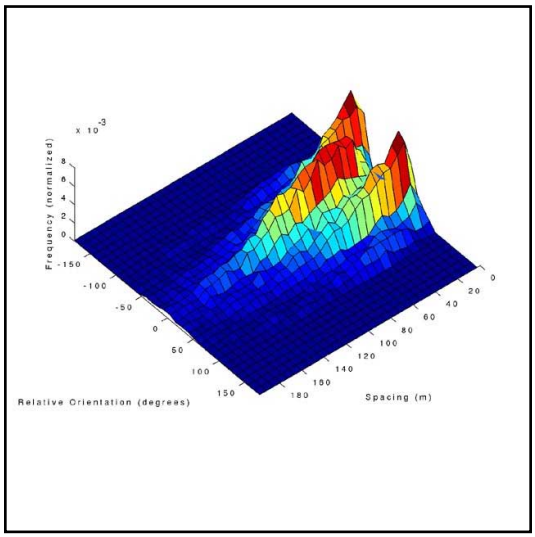

Surface Map

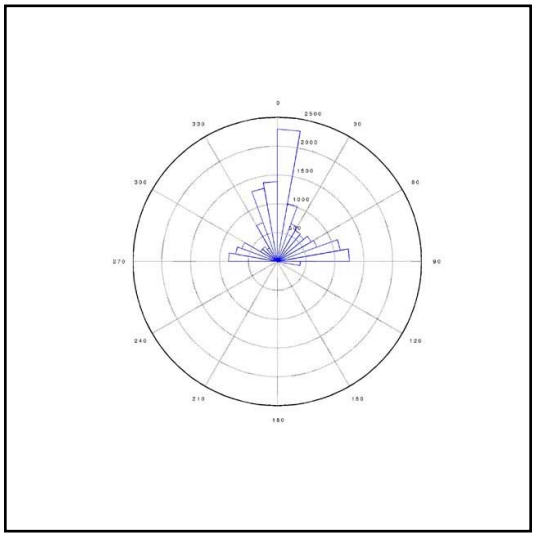

Rose Diagram

APPENDIX A

Mars
M19_01929 Latitude - 43.71ºN Longtitude - 267.16ºW

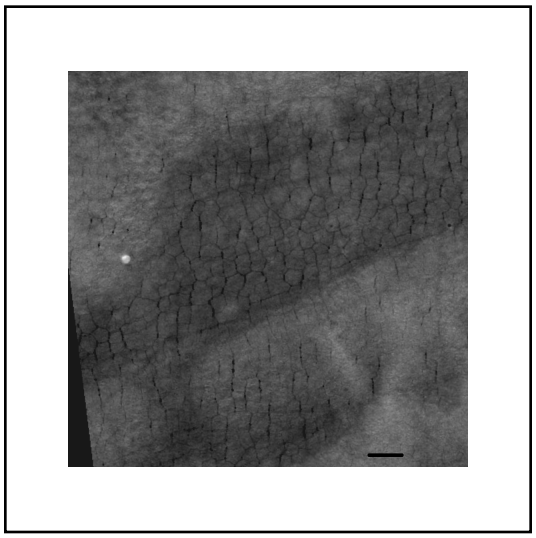

Original Image

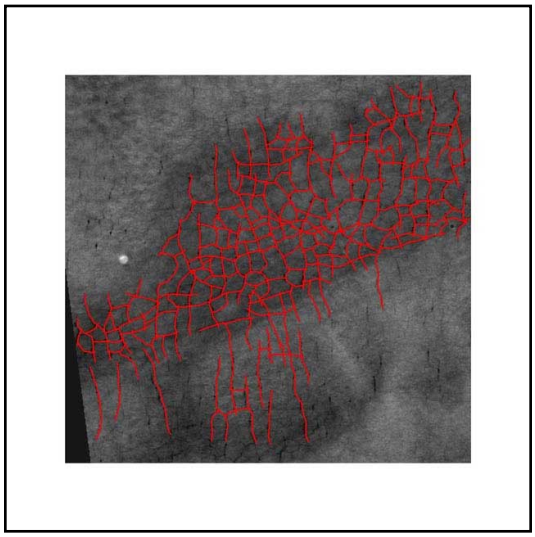

Digitized Image

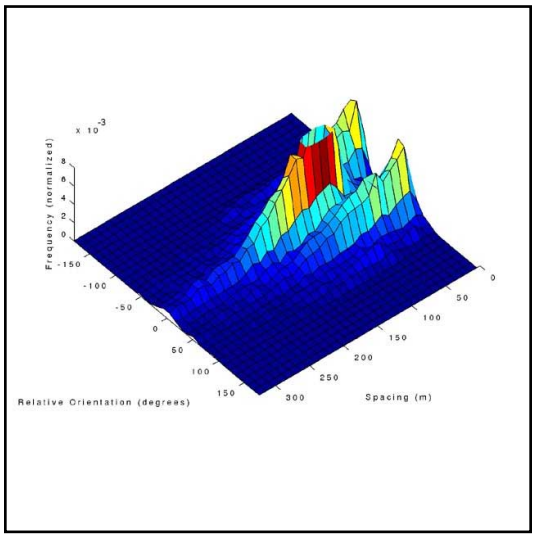

Surface Map

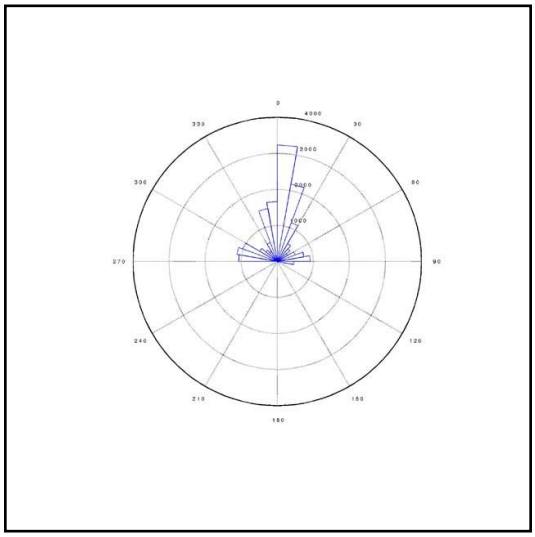

Rose Diagram

APPENDIX A

Mars
M22_01173 Latitude - 49.07ºN Longtitude - 265.44ºW

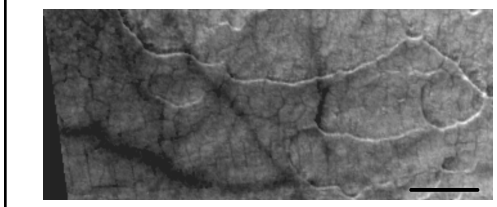

Original Image

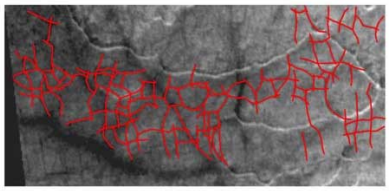

Digitized Image

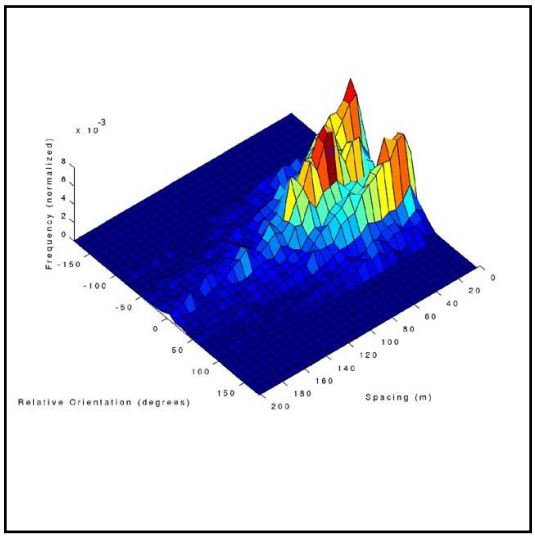

Surface Map

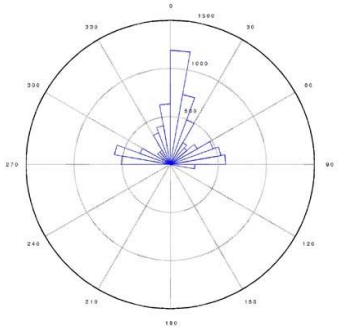

Rose Diagram

APPENDIX A

Mars
M22_02520 Latitude - 40.46ºN Longtitude - 276.35ºW

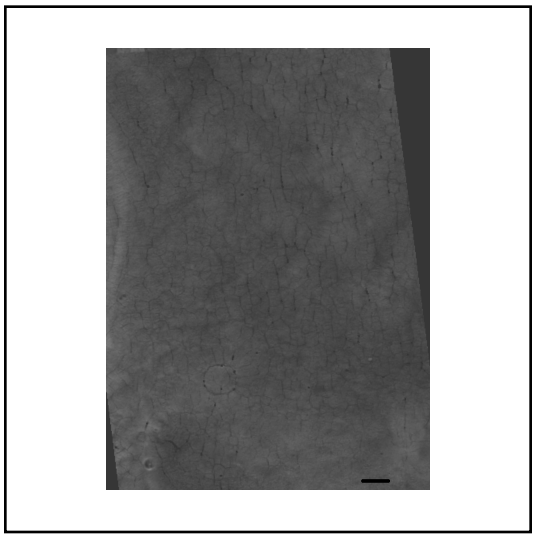

Original Image

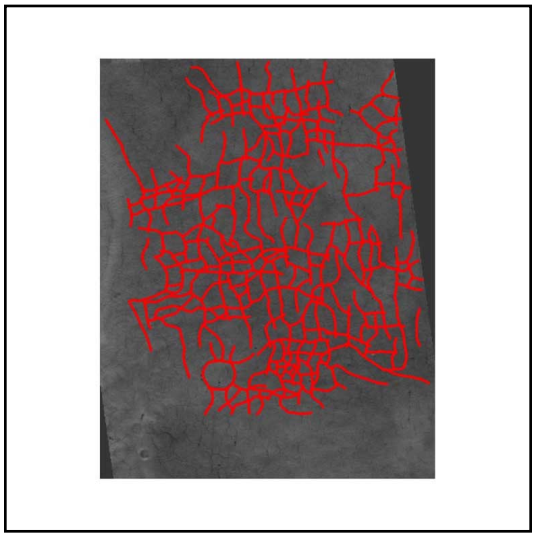

Digitized Image

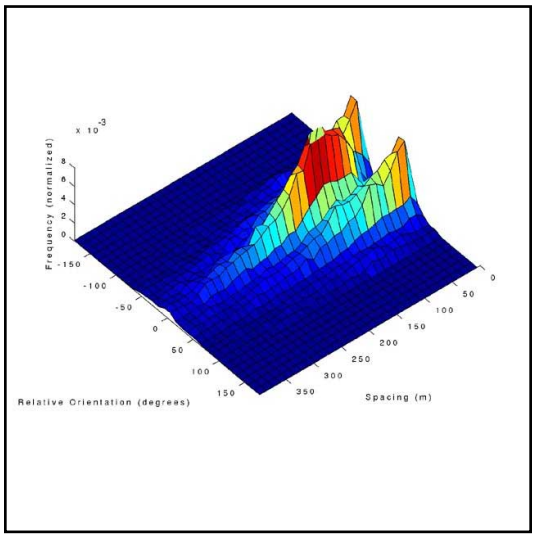

Surface Map

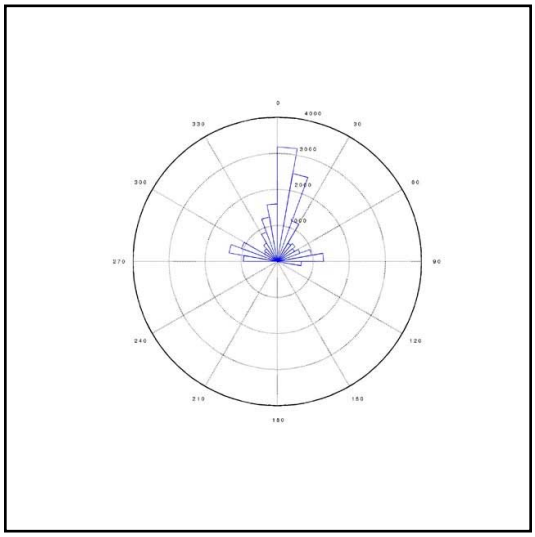

Rose Diagram

APPENDIX A

Mars

M23_00078 45.35ºN000000 Longtitude - 260.85ºW

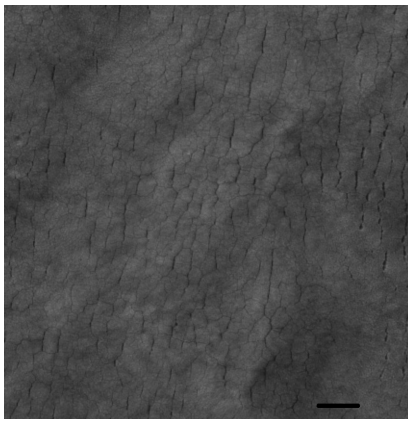

Original Image

Digitized Image

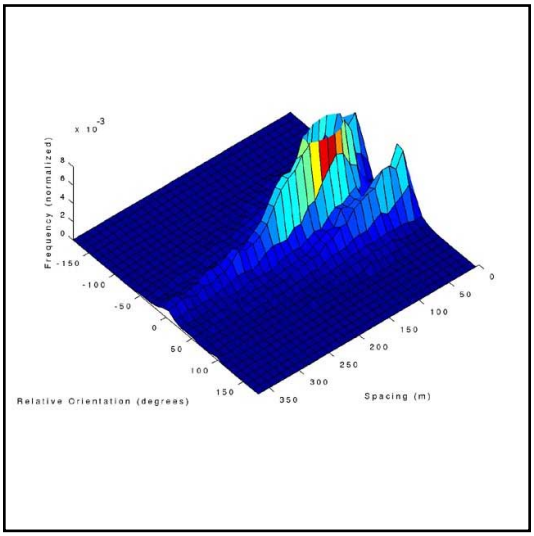

Surface Map

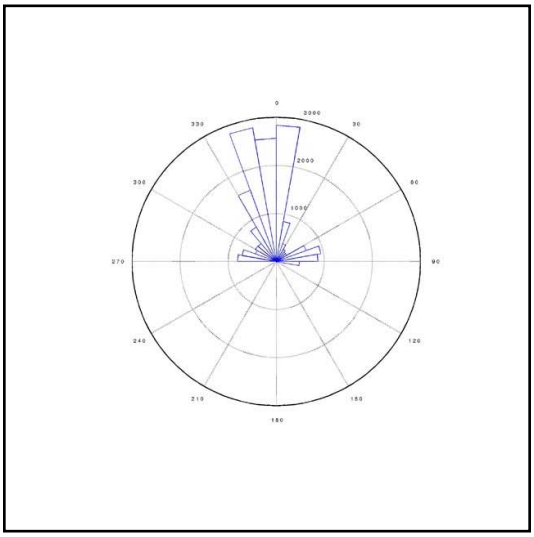

Rose Diagram

APPENDIX A

Mars
M23_00151 Latitude - 42.19ºN Longtitude - 272.59ºW

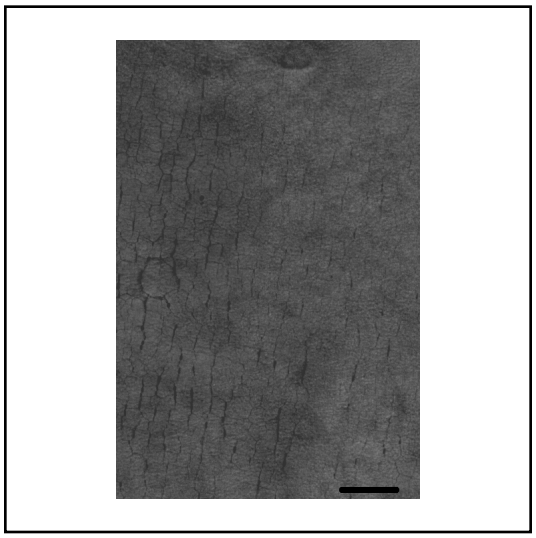

Original Image

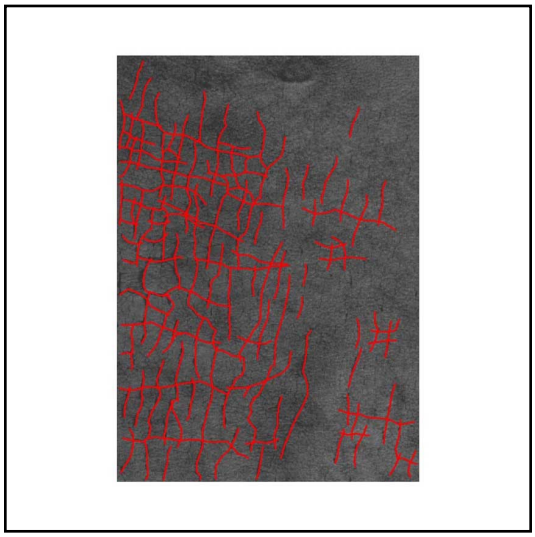

Digitized Image

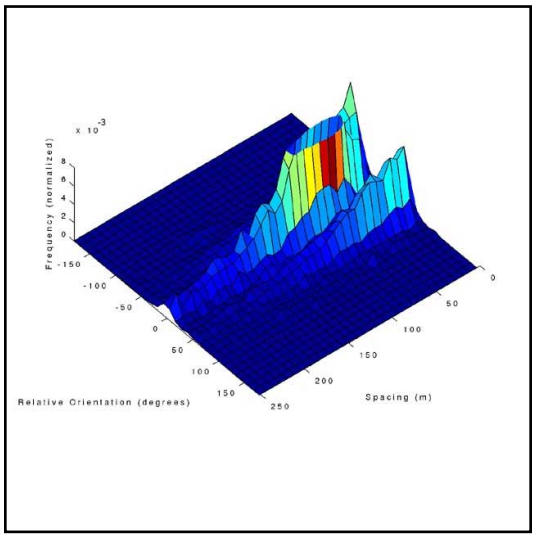

Surface Map

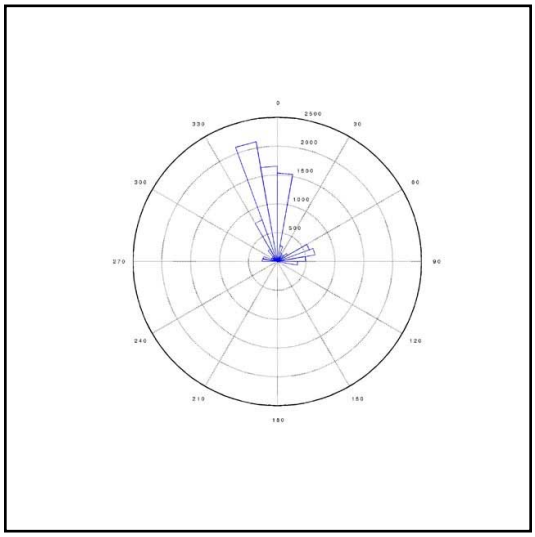

Rose Diagram

APPENDIX A

Mars
M23_01857 Latitude - 46.47ºN Longtitude - 266.20ºW

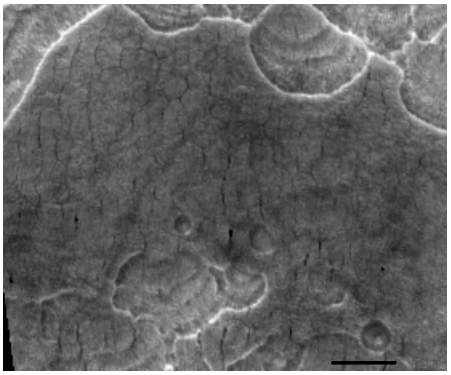

Original Image

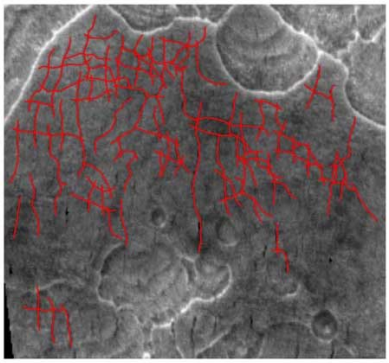

Digitized Image

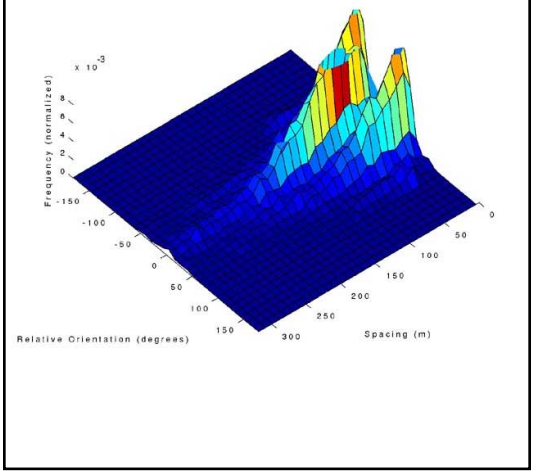

Surface Map

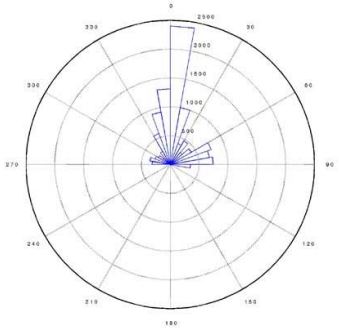

Rose Diagram

APPENDIX A

Mars
R02_00014 Latitude - 41.31ºN Longtitude - 262.03ºW

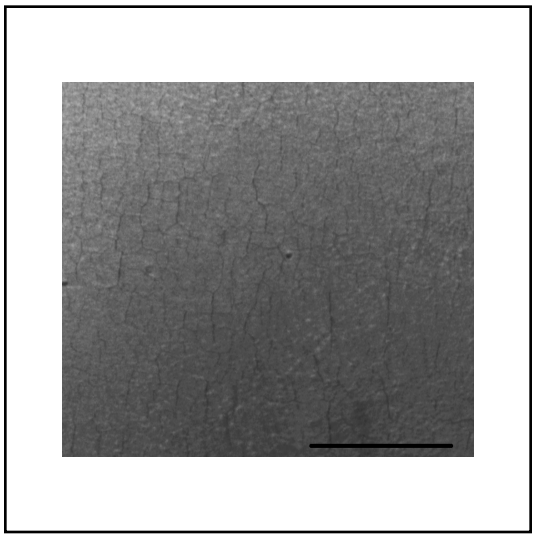

Original Image

Digitized Image

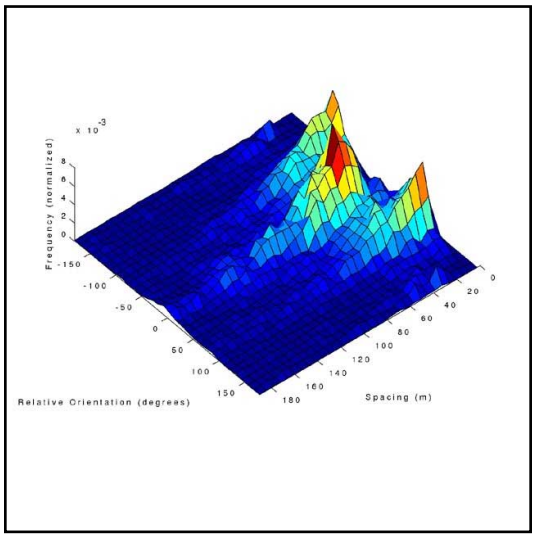

Surface Map

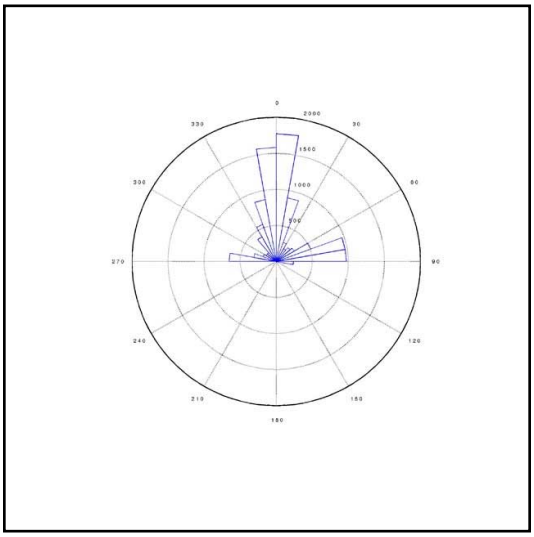

Rose Diagram

APPENDIX A

Terrestrial
EARTH_1

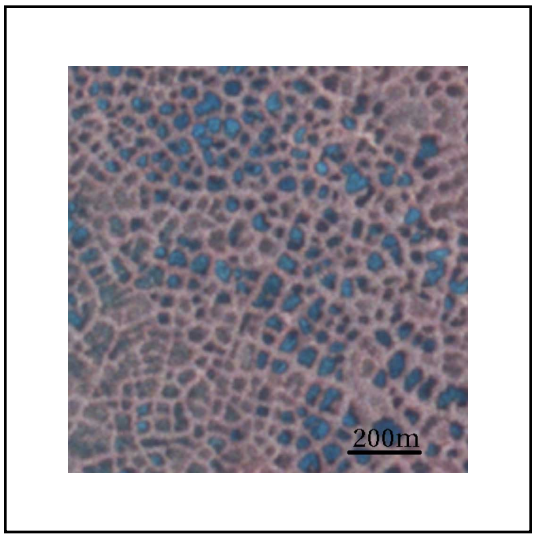

Original Image

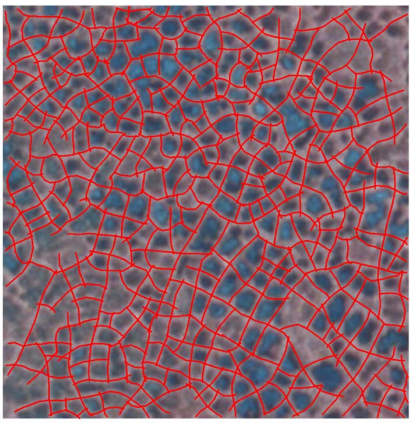

Digitized Image

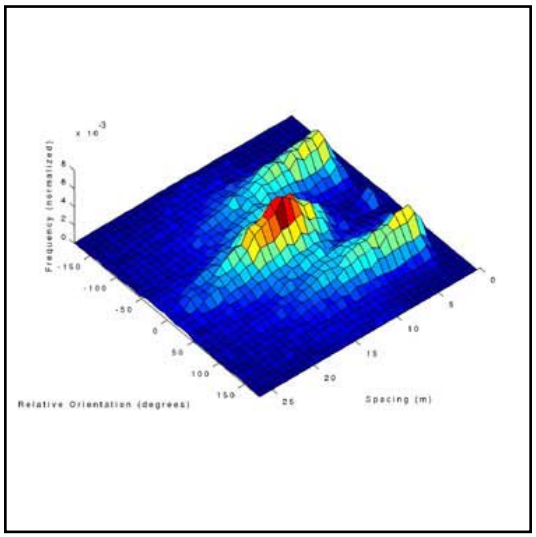

Surface Map

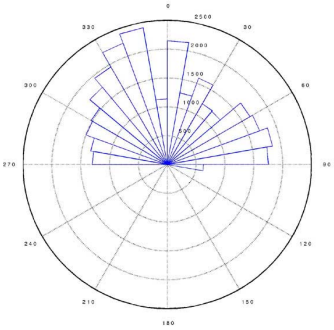

Rose Diagram

APPENDIX A

Terrestrial
EARTH_2

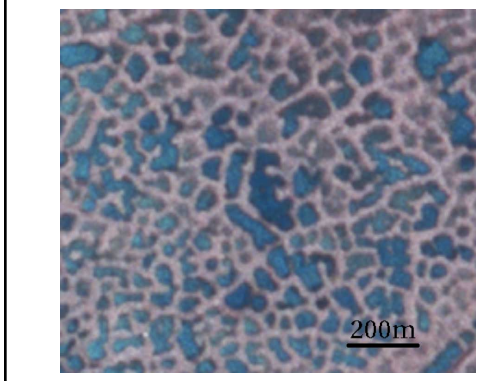

Original Image

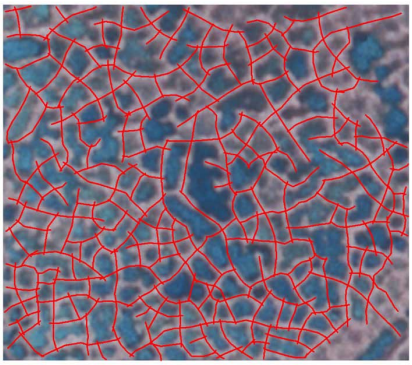

Digitized Image

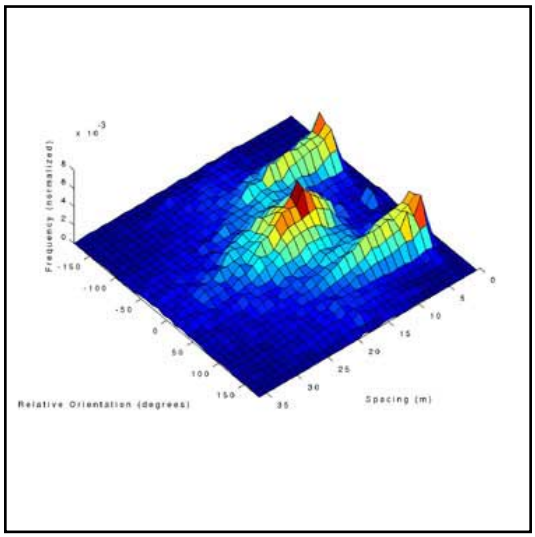

Surface Map

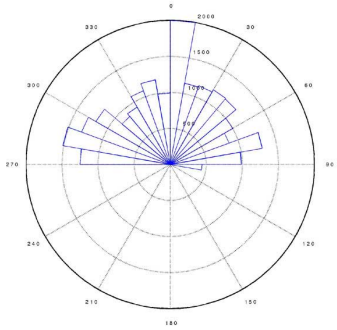

Rose Diagram

APPENDIX A

Terrestrial
EARTH_3

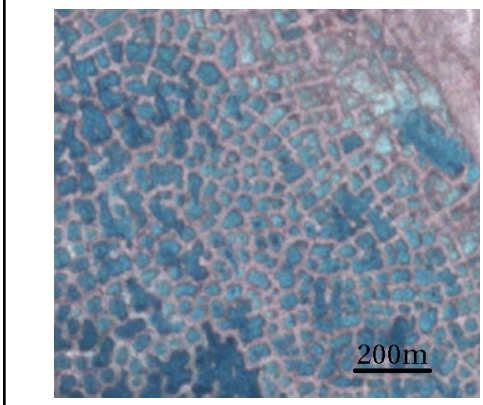

Original Image

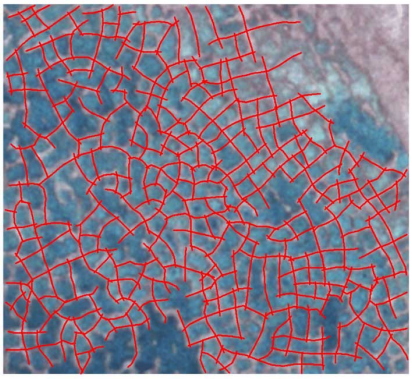

Digitized Image

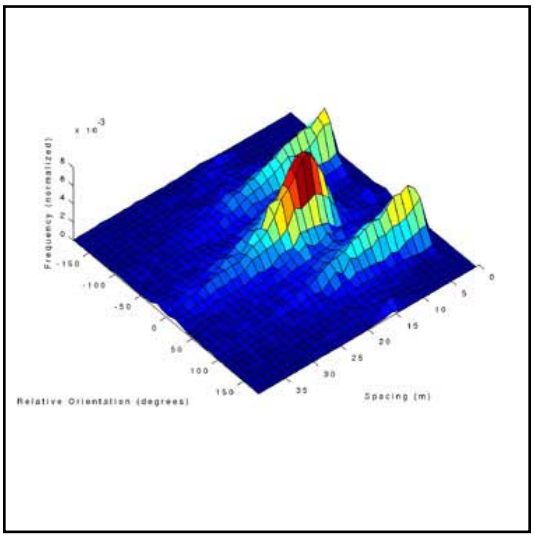

Surface Map

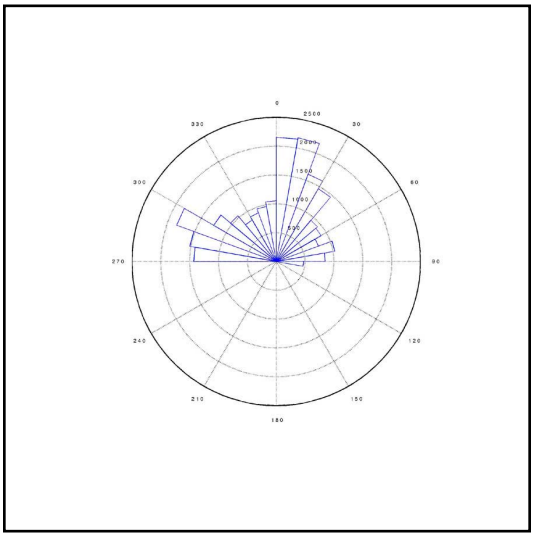

Rose Diagram

APPENDIX A

Terrestrial
EARTH_4

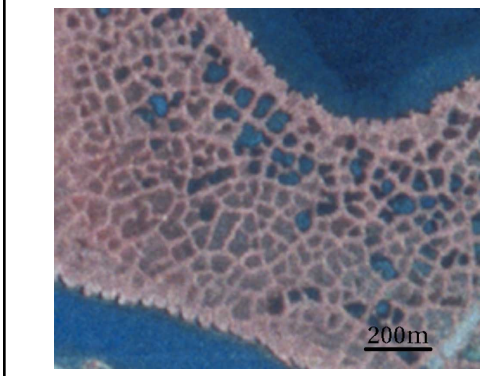

Original Image

Digitized Image

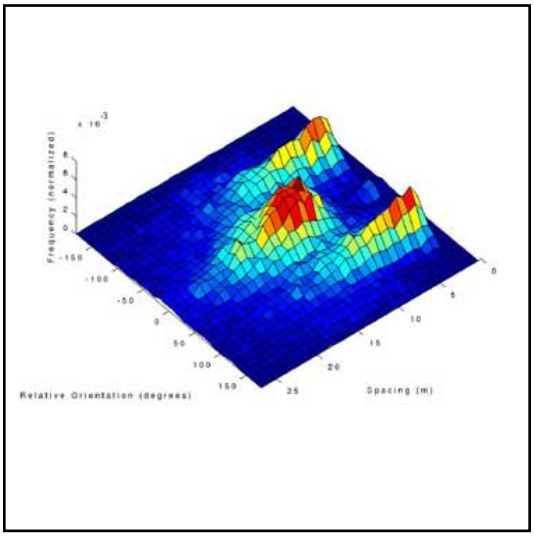

Surface Map

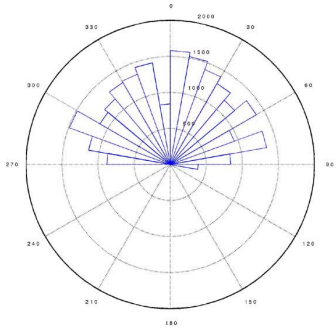

Rose Diagram

APPENDIX A

Terrestrial
EARTH_5

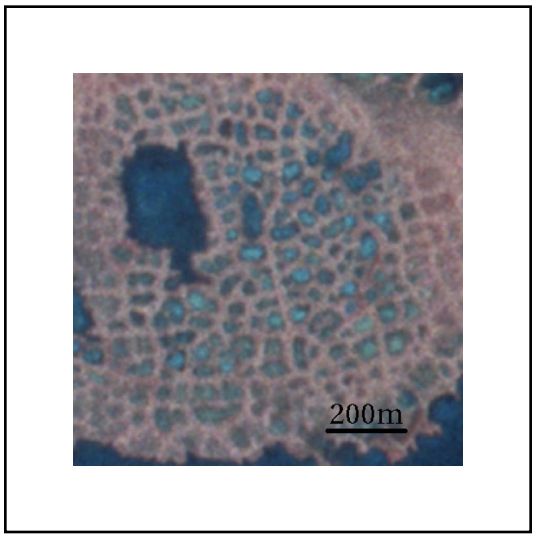

Original Image

Digitized Image

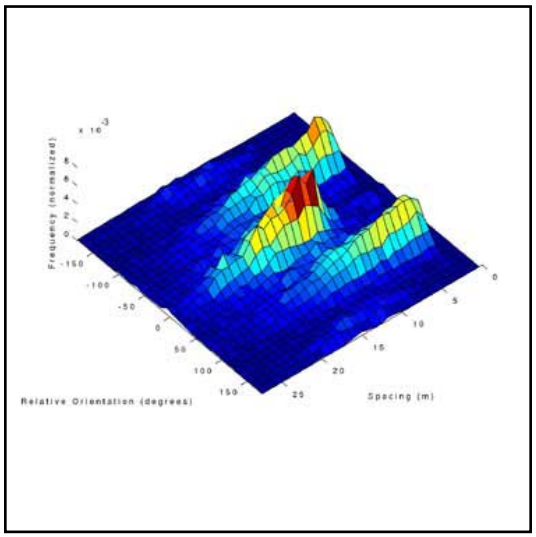

Surface Map

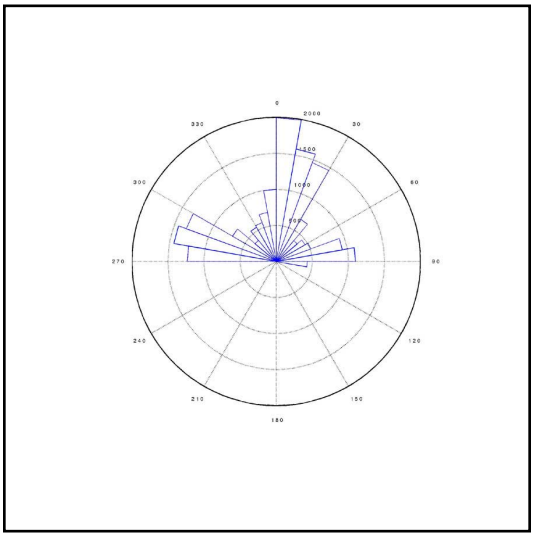

Rose Diagram

APPENDIX A

Terrestrial
EARTH_6

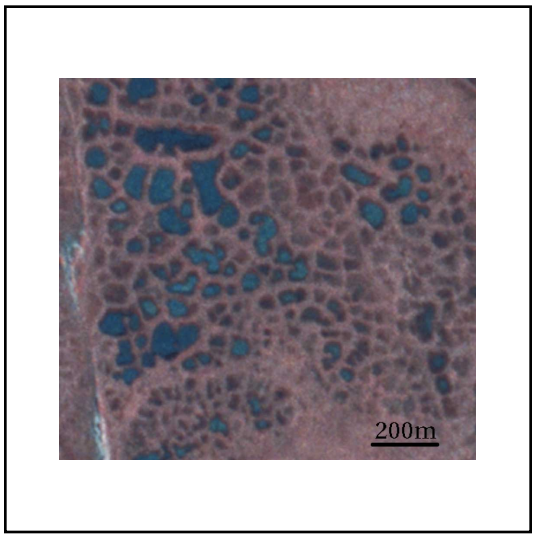

Original Image

Digitized Image

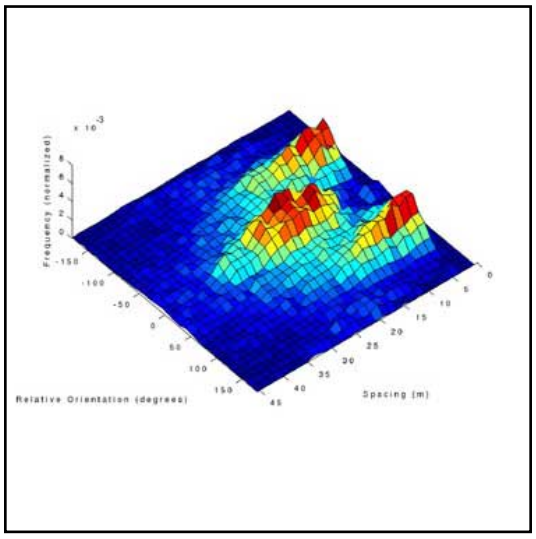

Surface Map

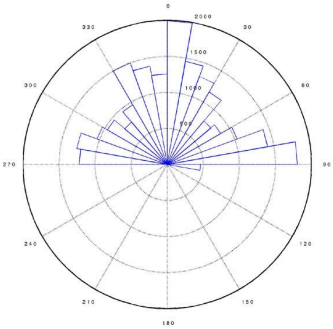

Rose Diagram

APPENDIX A

Terrestrial
EARTH_7

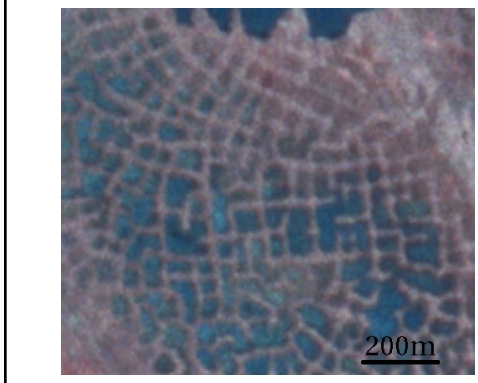

Original Image

Digitized Image

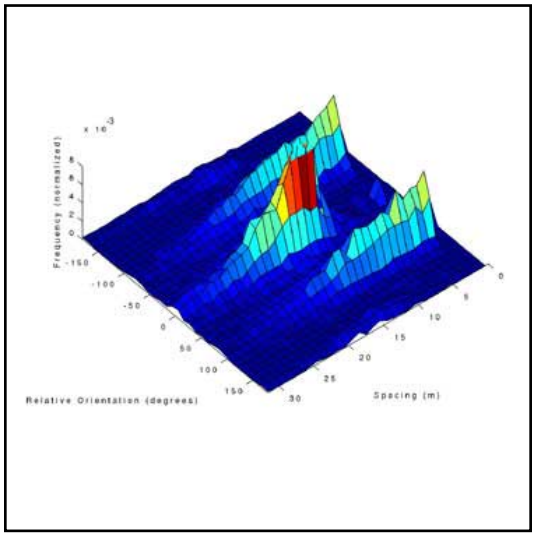

Surface Map

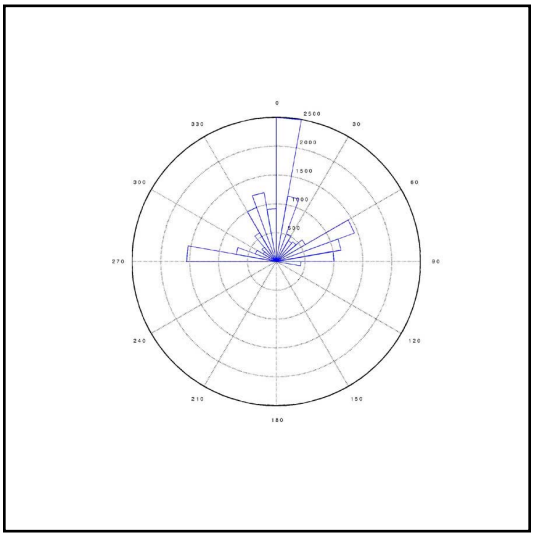

Rose Diagram

APPENDIX A

Terrestrial
EARTH_8

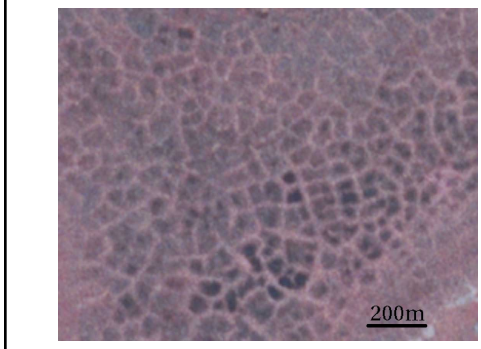

Original Image

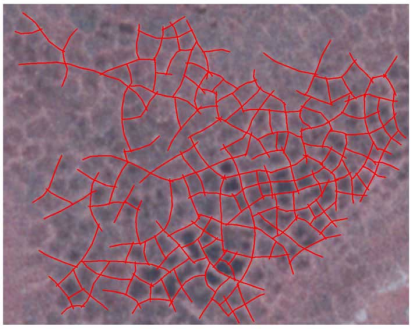

Digitized Image

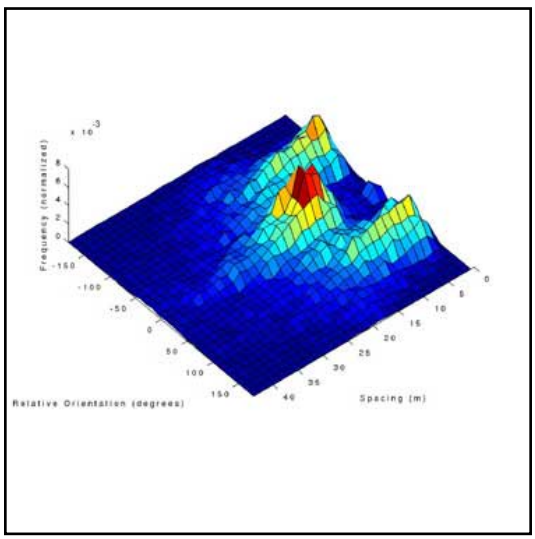

Surface Map

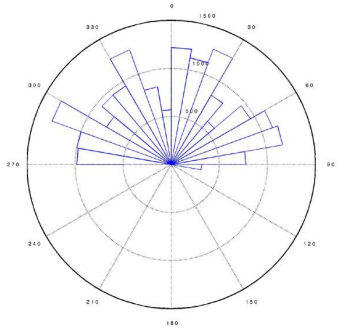

Rose Diagram

APPENDIX A

Terrestrial
EARTH_9

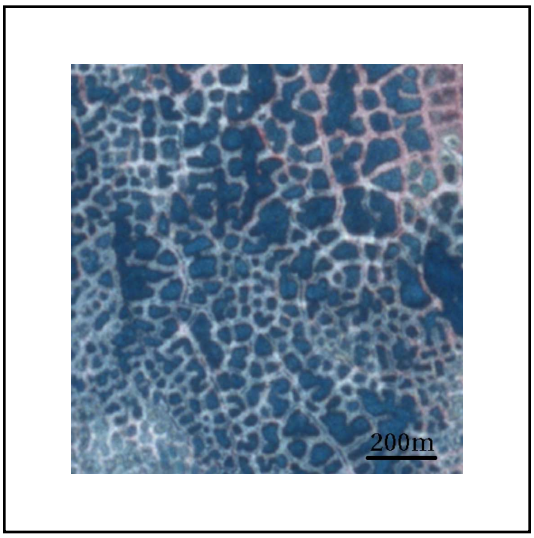

Original Image

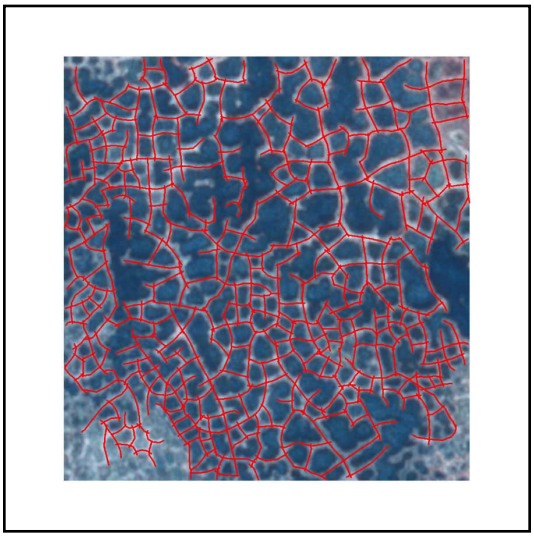

Digitized Image

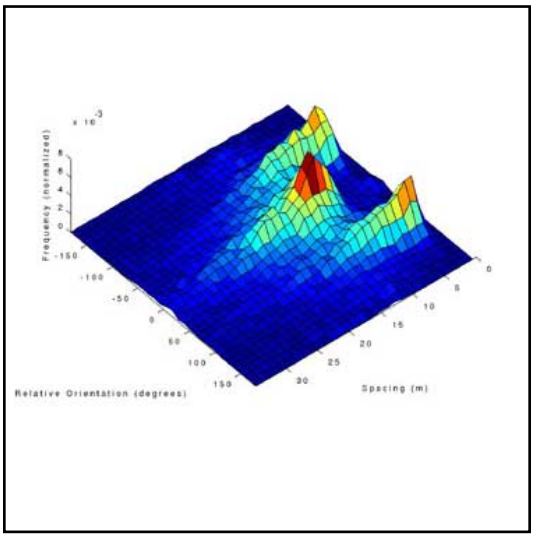

Surface Map

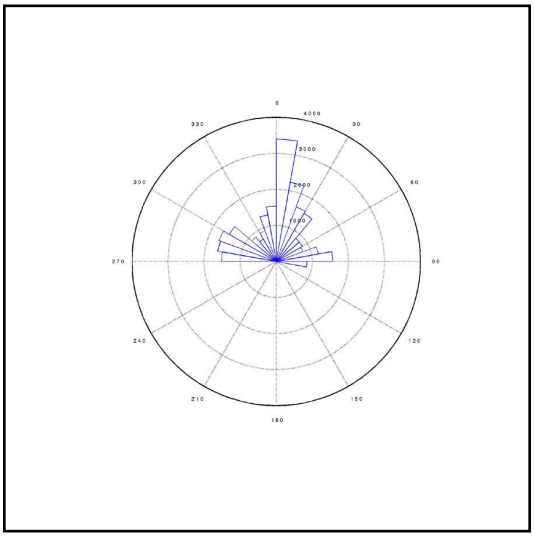

Rose Diagram

APPENDIX A

Terrestrial
EARTH_10

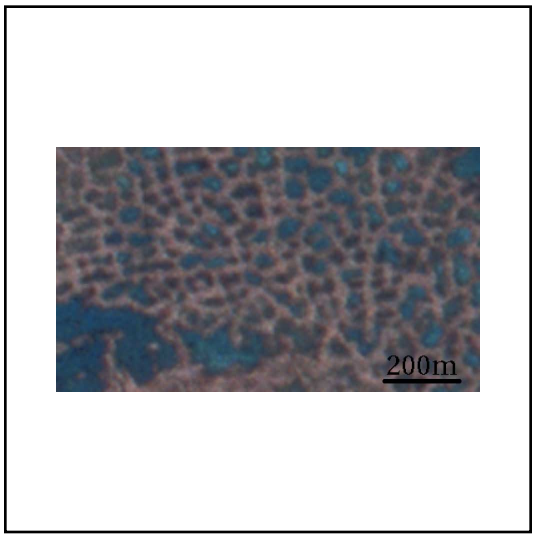

Original Image

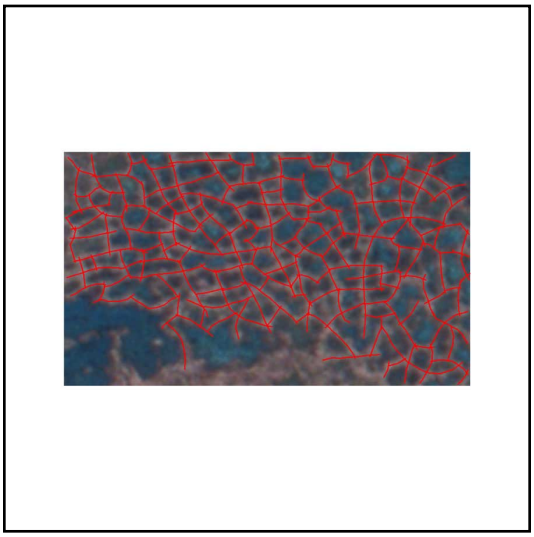

Digitized Image

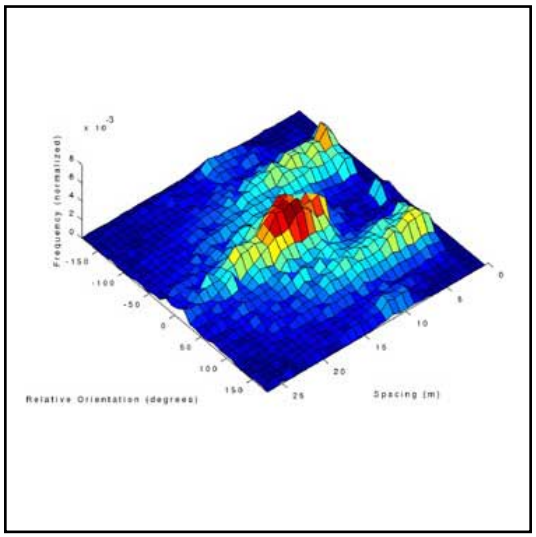

Surface Map

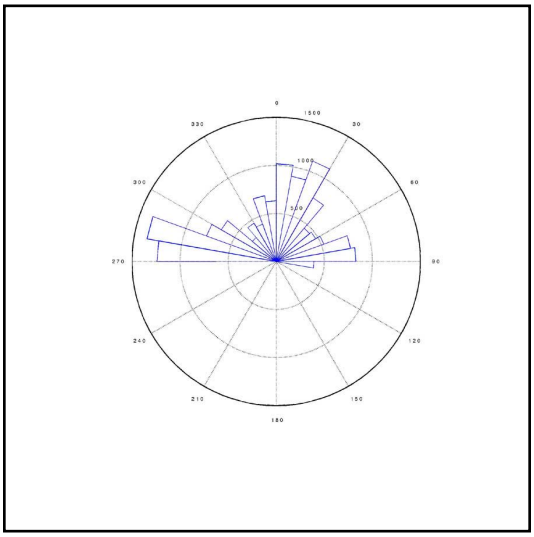

Rose Diagram

APPENDIX A

Mudcrack
20030806

Original Image

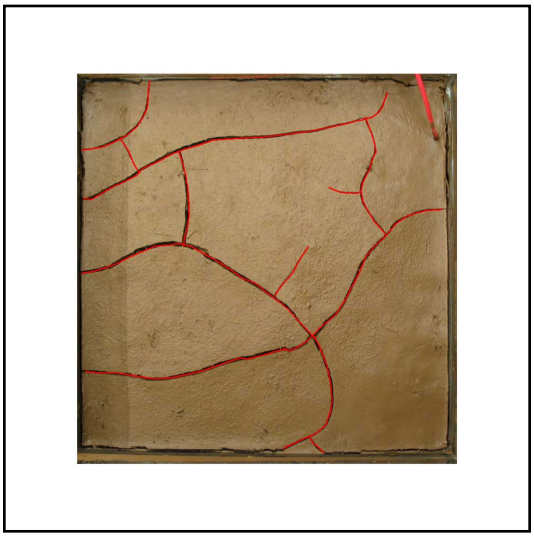

Digitized Image

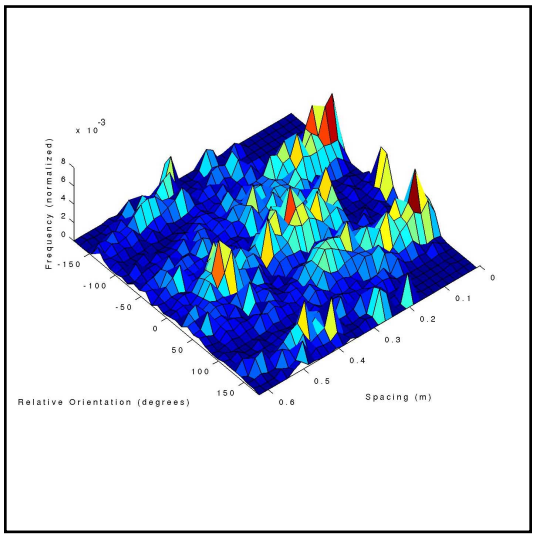

Surface Map

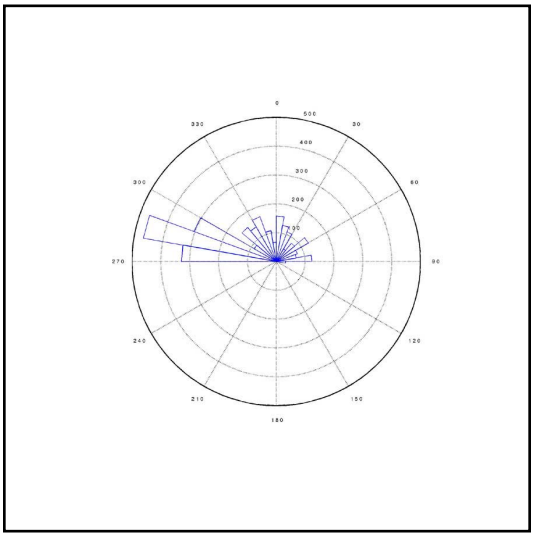

Rose Diagram

APPENDIX A

Mudcrack
20030812

Original Image

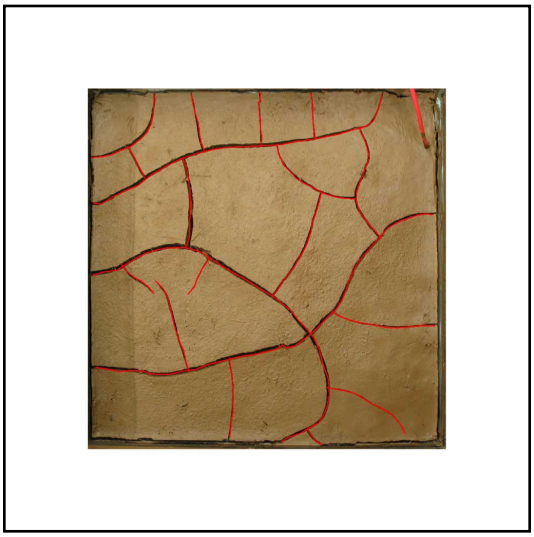

Digitized Image

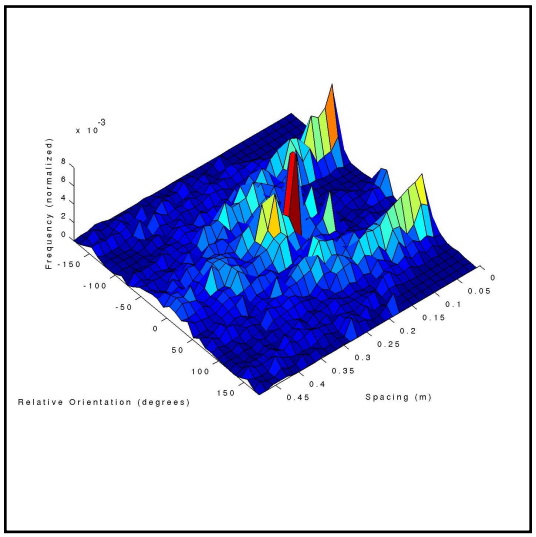

Surface Map

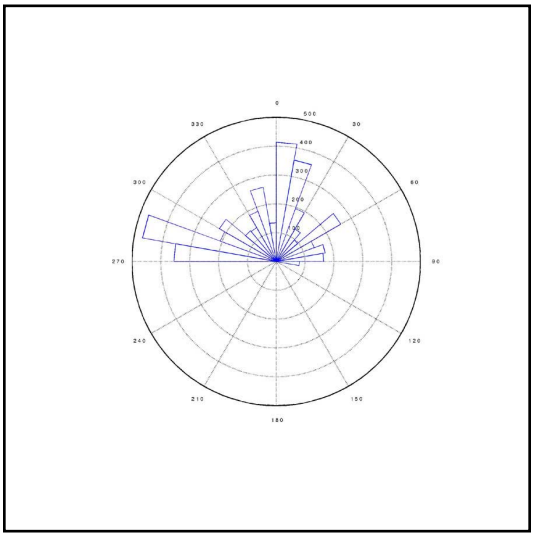

Rose Diagram

APPENDIX A

Mudcrack
20030818

Original Image

Digitized Image

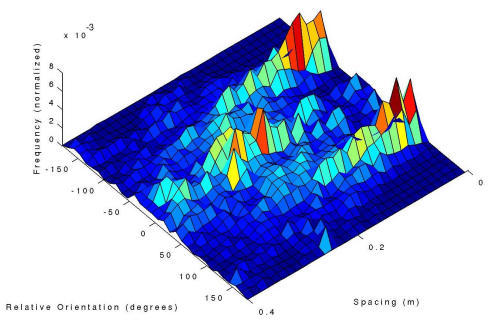

Surface Map

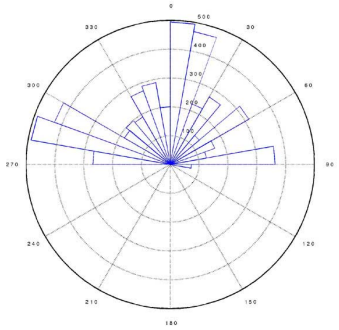

Rose Diagram

APPENDIX A

Mudcrack
20030824

Original Image

Digitized Image

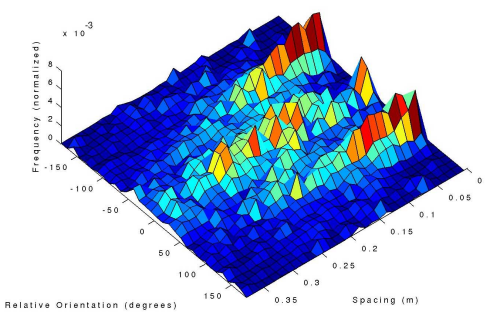

Surface Map

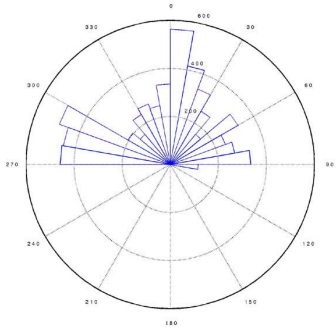

Rose Diagram

APPENDIX A

Mudcrack
20030901

Original Image

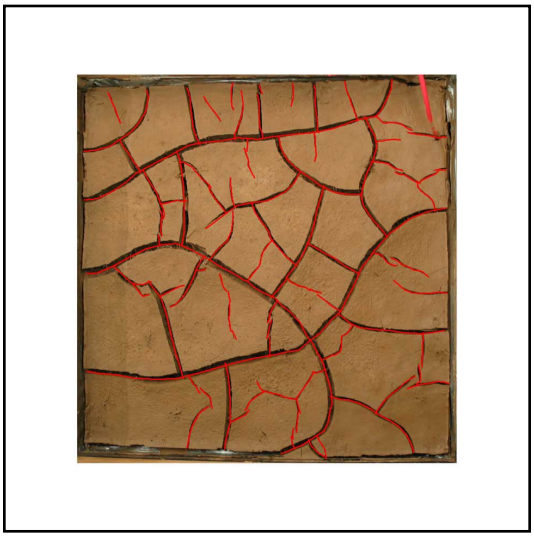

Digitized Image

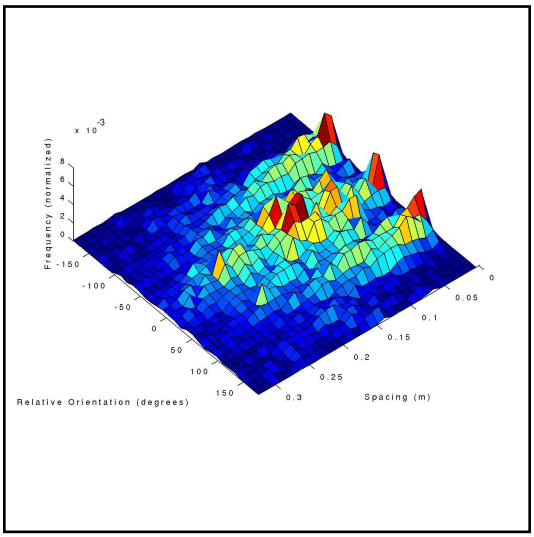

Surface Map

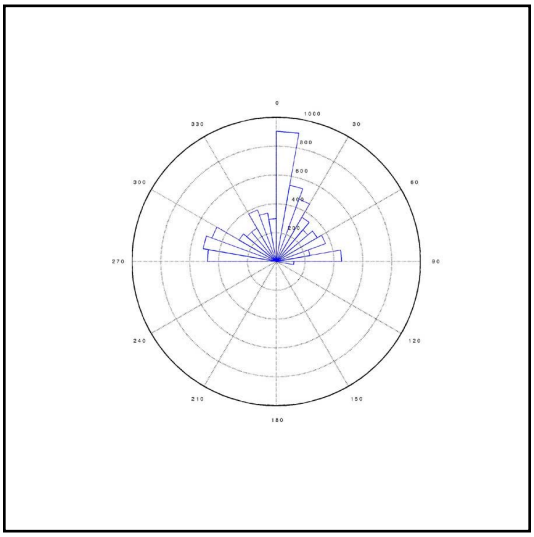

Rose Diagram

APPENDIX A

Mudcrack
20030905

Original Image

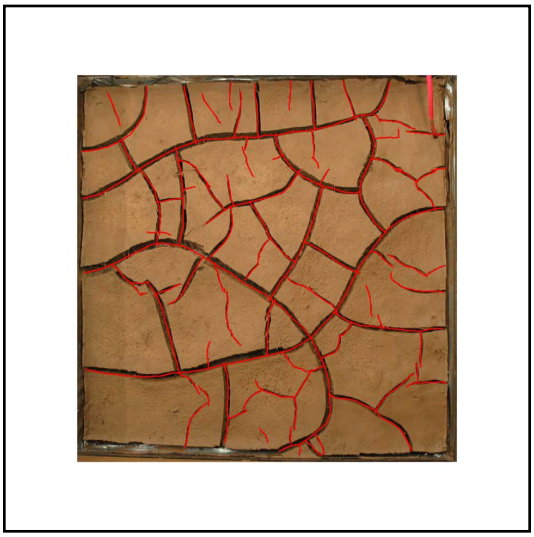

Digitized Image

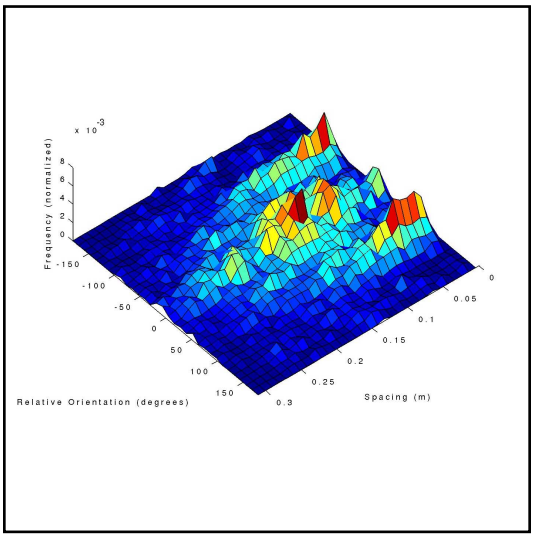

Surface Map

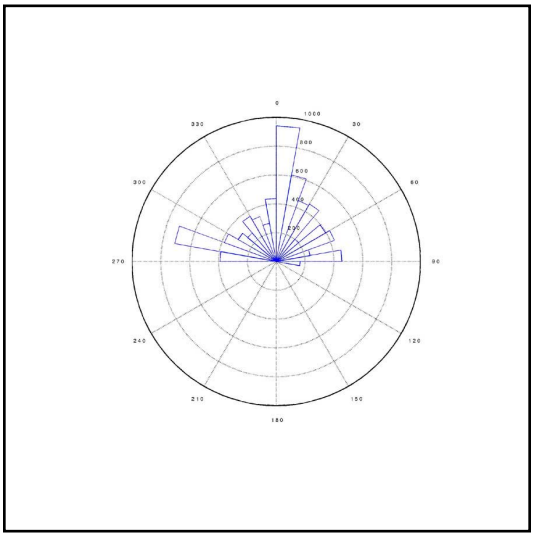

Rose Diagram

APPENDIX A

Mudcrack
20030910

Original Image

Digitized Image

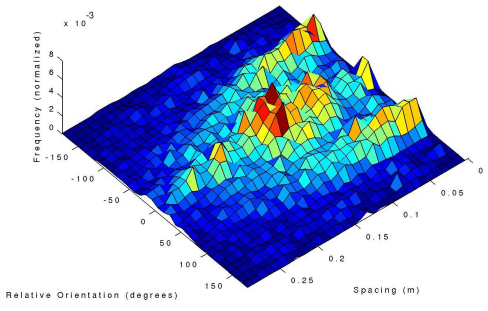

Surface Map

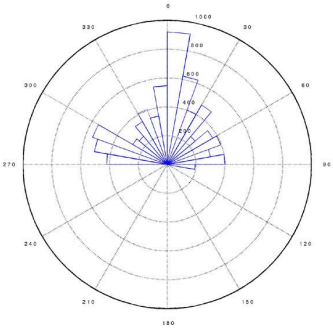

Rose Diagram

APPENDIX A

Mudcrack
20030915

Original Image

Digitized Image

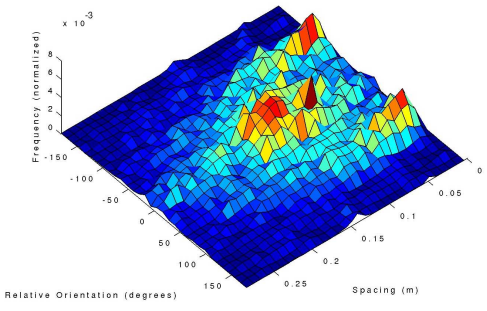

Surface Map

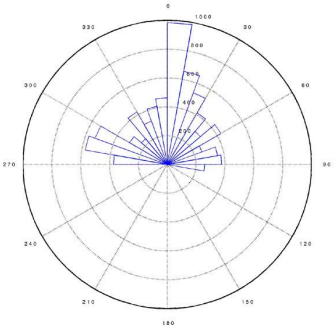

Rose Diagram

APPENDIX A

Mudcrack
20030920

Original Image

Digitized Image

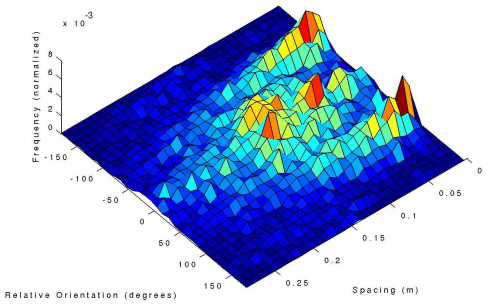

Surface Map

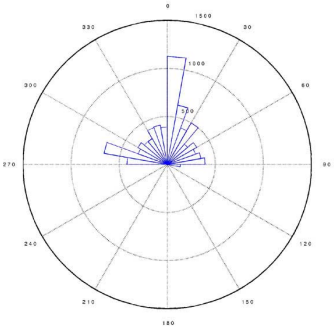

Rose Diagram

APPENDIX A

Mudcrack
20030925

Original Image

Digitized Image

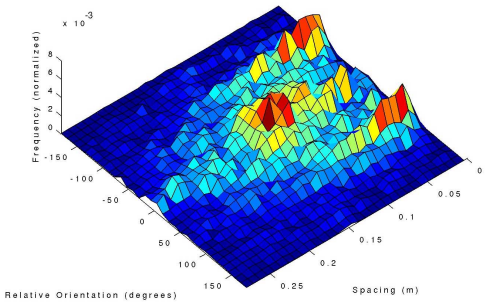

Surface Map

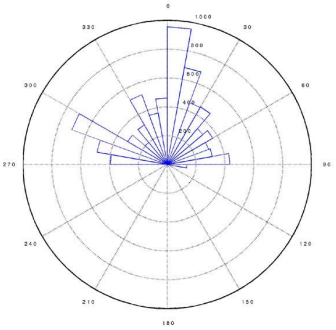

Rose Diagram

APPENDIX A

Mudcrack
20030929

Original Image

Digitized Image

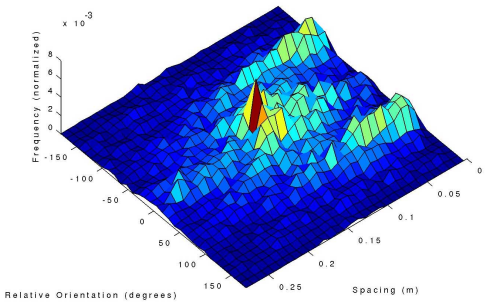

Surface Map

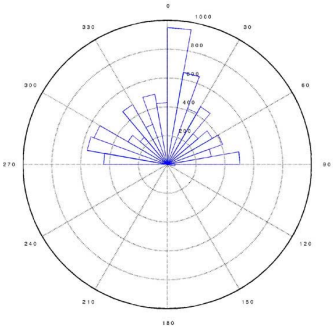

Rose Diagram

APPENDIX B

Mars Database

Sheet1

MOC Image ID	Centre Latitude	Centre Longitude	Area	Scaled Pixel Width (m/pixel)	Pixel Aspect Ratio	Image Width (pixels)	Image Height (pixels)	Spacecraft Altitude (km)	Fraction of Image	Map Projected	Diameter (m)	New Diameter (m)	Other Landforms	Clarity	Troughs
E22-00059	62.00°N	289.55°W	Casius	4.99	1.07	672	6144	427.25	5%	Y	277.8	105.63		20%	
E23-01288	42.31°N	273.92°W	Casius	4.87	0.89	672	11136	415.11	80%	N	414	106.31		70%	
R02-00014	41.31°N	262.03°W	Casius	1.62	1.56	2048	3968	414.98	10%	Y		47.5		15%	
Mars Processnet Database															
E05-00113	64.54°N	289.86°W	Casius	6.4	0.89	512	4864	429.93	20%	Y		141.44	floor of crater	90%	
E03-02635	61.98°N	289.48°W	Casius	4.77	1.12	672	6784	427.6	25%	Y		150.72	floor of crater	90%	
M19-00234	66.16°N	278.81°W	Casius	12.73	0.89	256	14592	427.72	30%	Y?	405	84.27	well developed	95%	
M19-01929	43.71°N	267.16°W	Casius	6.19	0.96	512	4736	414.3	85%	Y	217	121.67	well developed	90%	Y
M23-01857	46.47°N	266.20°W	Casius	6.23	1.16	512	4224	417.22	40%	Y	201	77.33	not well developed	80%	Y
M22-01173	49.07°N	265.44°W	Casius	4.69	1.15	672	1792	418.88	30%	Y	138	70.4	middle of image somewhat developed	70%	
M23-00078	45.35°N	260.85°W	Casius	6.23	0.93	512	11904	416.77	40%	N	179	97.13	somewhat developed	65%	Y
M22-02520	40.46°N	276.35°W	Casius	7.71	0.94	384	7040	412.48	20%	Y	215	123.82	somewhat developed	65%	Y
M23-00151	42.19°N	272.59°W	Casius	3.09	0.94	512	8064	413.96	30%	N	74	60.45	somewhat developed	75%	
M19-01326	44.35°N	272.11°W	Casius	1.55	0.93	768	1536	414.46	90%	Y	57	82.93	well developed	90%	Y
M08-07602	45.14°N	275.80°W	Casius	3.1	0.93	512	2432	414.62	95%	Y	126	122.97	somewhat developed	100%	Y
M09-03407	43.09°N	273.48°W	Casius	3.09	0.94	512	2432	413.2	95%	Y	197	97.5	somewhat developed	90%	Y
M08-03534	41.95°N	277.15°W	Casius	3.08	0.94	512	2432	412.06	80%	Y	104	103.85	somewhat developed	85%	Y
M04-01631	44.33°N	272.68°W	Casius	6.19	0.9	512	12160	414.26	100%	Y	201	99.59	only jpg available	100%	
M01-00582	43.69°N	273.28°W	Casius	12.36	0.94	256	256	413.52	95%	Y	346	111.38	well developed	100%	Y
M04-04181	41.93°N	274.87°W	Casius	3.08	0.94	512	2432	412.41	30%	Y	104	59.75	well developed	90%	
M04-00990	45.75°N	265.15°W	Casius	3.08	0.95	512	2432	415.58	70%	Y		55.6	somewhat developed	85%	
M00-00215	45.65°N	259.84°W	Casius	1.54	1.41	1024	6144	412.56	40%	Y	57	60.25	somewhat developed	70%	
M02-02863	43.50°N	269.30°W	Casius	6.19	0.93	512	8064	413.92	80%	Y	152	94.86	well developed	75%	Y
M02-03335	46.19°N	265.39°W	Casius	3.11	1.39	1024	3200	416.01	70%	Y	89	53.07	somewhat developed	80%	Y
M01-04558	44.50°N	276.11°W	Casius	12.39	0.93	256	256	414.62	90%	Y	307	108.07	well developed	90%	
M04-02704	44.09°N	276.14°W	Casius	3.09	0.95	512	2432	413.91	95%	Y	77	100.43	well developed	95%	Y
M04-03810	42.56°N	279.32°W	Casius	3.09	0.95	512	2432	412.72	70%	Y	95	100.65	well developed	90%	Y
M03-04331	44.46°N	272.80°W	Casius	3.09	0.94	512	2432	413.33	80%	Y	110	109.7	well developed	95%	Y
M03-05694	45.43°N	271.80°W	Casius	1.55	1.4	512	12160	414.02	30%	Y	53	64.17	not well developed	80%	Y

Mars Database

Comments	Set	Ratio	X-axis (m/pixel)	Y-axis (m/pixel)	Digitized	Development	Matlab Complete	Processnet Complete	D value	O value	P value	Number Orthogonal	Number Non-orthogonal	3-Way	4-Way
	Aug.02-Feb.03	2	2.5	2.67	Y	Developed network	N	Y	145.3444	61.3065	3.2086	85	136		
In 5th frame, GIF not map projected	Aug.02-Feb.03	2	2.44	2.17	Y	Developed network	N	Y	88.8408	63.0254	2.3491	645	250		
Unclear	Aug.02-Feb.03	2	0.81	1.26	Y	somewhat developed	N	Y	49.6908	63.0254	20.9932	204	99		
Map projection is sinusoidal, using 289.86 degrees W as prime meridian	Feb.01-July01	2	3.2	2.8	Y	Different looking	N	Y	149.459	62.1545	3.0481	290	56		
Map projection is sinusoidal, using 289.48 degrees W as prime meridian	Feb.01-July01	2	2.4	2.7	Y		N	Y	135.2462	63.0254	20.764	176	52		
jpg only available	Sept.00-Jan.01	4	3.18	2.83	Y	Developed network	Y	Y	85.9593	62.8191	28.8198	194	68		
	Sept.00-Jan.01	2	3.1	3	Y	Developed network	Y	Y	103.7448	63.0254	0.8824	416	109		
	Sept.00-Jan.01	4	1.6	1.8	Y	Moderately developed	Y	Y	69.8863	63.0254	1.1574	271	113		
	Sept.00-Jan.01	3	1.6	1.8	Y	Moderately developed	Y	Y	52.9462	63.0254	0.974	240	101		
not map projected	Sept.00-Jan.01	2	3.1	2.9	Y	Moderate-well developed	Y	Y	106.1508	63.0254	1.0886	382	111		
	Sept.00-Jan.01	2	3.9	3.6	Y	Developed network	Y	Y	122.0912	63.0254	0.8594	429	233		
not map projected	Sept.00-Jan.01	1	3.1	2.9	Y	Moderate-well developed	Y	Y	78.9177	63.0254	0.9969	361	99		
	Sept.00-Jan.01	1	1.6	1.4	Y	Developed network	Y	Y	55.0318	63.0254	2.9221	336	214		
well documented	Sept.99-Feb.00	1	3.1	2.9	Y	Developed network	Y	Y	129.5222	63.0254	1.249	252	86		
	Sept.99-Feb.00	2	1.5	1.4	Y	Early stages of development?	Y	Y	104.4101	63.0254	1.1918	156	95		
	Sept.99-Feb.00	1	3.1	2.9	Y	Early stages of development?	Y	Y	108.1665	63.0254	1.0084	168	110		
only jpg available	Sept.97-Aug.99	2	3.1	2.8	Y	Very well developed network	Y	Y	98.902	63.0254	1.1001	898	229		
	Sept.97-Aug.99	3	4.1	3.9	Y	Developed network	Y	Y	110.6345	63.0254	1.1001	628	347		
	Sept.97-Aug.99	2	1.5	1.4	Y	Developed network	Y	Y	41.5217	63.0254	0.9969	288	118		
	Sept.97-Aug.99	2	1.6	1.5	Y	Poor image quality	Y	Y	52.7228	63.0254	0.9626	144	101		
	Sept.97-Aug.99	1	1.54	1.41	Y	Early stages of development?	Y	Y	57.7639	63.0254	1.1001	120	111		
only jpg available	Sept.97-Aug.99	2	3.1	2.88	Y	Developed network	Y	Y	81.6088	62.7847	1.4095				
	Sept.97-Aug.99	2	1.56	2.16	Y	Early stages of development?	Y	Y	80.3635	63.0254	1.0657	104	90		
	Sept.97-Aug.99	3	4.13	3.84	Y	Moderately developed	Y	Y	124.7225	61.9711	1.249				
One of the best pictures	Sept.97-Aug.99	1	3.09	2.94	Y	Developed network	Y	Y	87.2067	61.0429	1.2949				
One of the best pictures	Sept.97-Aug.99	1	3.09	2.94	Y	Developed network	Y	Y	84.4808	62.5441	1.1459				
	Sept.97-Aug.99	1	3.09	2.91	Y	Developed network	Y	Y	81.6088	62.5441	1.3751				
	Sept.97-Aug.99	1	1.55	2.17	Y	somewhat developed	Y	Y	58.1599	63.0254	0.9511				

Terrestrial Database

Earth Images Database															
Earth Image Name	**Image Width (pixels)**	**Image Height (pixels)**	**Scaled Pixel Width (m/pixel)**	**Pixel Aspect Ratio**	**Scaled-Ratio**	**X-Axis (m/pixel)**	**Y-Axis (m/pixel)**	**Diameter (m)**	**Digitized**	**Processnet Complete**	***D* value**	***O* value**	***P* value**		
en_image1.tif	848	864	1.341	1	4	0.335	0.335	10.85	Y	Y	12.0832	63.0254	1.673		
en_image2.tif	900	788	1.341	1	4	0.335	0.335	15.08	Y	Y	14.8349	63.0254	5.34		
en_image3.tif	852	777	1.341	1	3	0.447	0.447	17.97	Y	Y	15.8038	63.0254	3.518		
en_image4.tif	984	832	1.341	1	4	0.335	0.335	13.9	Y	Y	11.929	63.0254	5.2483		
en_image5.tif	752	756	1.341	1	4	0.335	0.335	15.63	Y	Y	11.9783	63.0254	8.0787		
en_image6.tif	963	882	1.341	1	3	0.447	0.447	21.01	Y	Y	18.0828	61.444	6.7151		
en_image7.tif	828	732	1.341	1	4	0.335	0.335	14.96	Y	Y	14.2523	63.0254	1.1459		
en_image8.tif	1092	864	1.341	1	4	0.335	0.335	14.18	Y	Y	15.293	63.0254	7.6891		
en_image9.tif	867	906	1.341	1	4	0.335	0.335	12.59	Y	Y	13.0349	61.9138	2.8075		
en_image10.tif	848	488	1.341	1	4	0.335	0.335	13.96	Y	Y	12.4131	60.894	5.9931		

Mud Database

Mudcrack Images Database							
Mudcrack Image Name	**Date Image Taken**	**Time Image Taken**	**Image Width (pixels)**	**Image Height (pixels)**	**X-Scaled Pixel Width (m/pixel)**	**Y-Scaled Pixel Width (m/pixel)**	**Pixel Aspect Ratio**
20030806	20030806	08hr-14min-32sec	690	708	0.001730145	0.001511139	~1
20030812	20030812	00hr-08min-30sec	686	690	0.001740233	0.001730145	~1
20030818	20030818	00hr-14min-20sec	687	698	0.0017377	0.001710315	~1
20030824	20030824	00hr-05min-26sec	668	686	0.001787126	0.001740233	~1
20030901	20030901	00hr-02min-34sec	677	692	0.001763368	0.001725145	~1
20030905	20030905	06hr-58min-20sec	675	687	0.001768593	0.0017377	~1
20030910	20030910	21hr-25min-08sec	680	683	0.001755588	0.001747877	~1
20030915	20030915	17hr-16min-10sec	668	678	0.001787126	0.001760767	~1
20030920	20030920	17hr-55min-14sec	663	680	0.001800603	0.001755588	~1
20030925	20030925	09hr-42min-34sec	660	684	0.001808788	0.001745322	~1
20030929	20030929	00hr-41min-36sec	671	683	0.001779136	0.001747877	~1

Mud Database

Scaled-Ratio	X-Axis	Y-Axis	Diameter (m)	Digitized	Processnet Complete	*D* value	*O* value	*P* value				
1	0.002	0.002	0.638 (only one polygon)	Y	Y	0.2872	58.9574	2.9335				
1	0.002	0.002	0.391	Y	Y	0.2419	62.0055	4.5722				
1	0.002	0.002	0.327	Y	Y	0.202	61.3982	3.3461				
1	0.002	0.002	0.281	Y	Y	0.1712	62.292	4.5149				
1	0.002	0.002	0.255	Y	Y	0.1385	60.4356	1.5126				
1	0.002	0.002	0.274	Y	Y	0.1297	61.0544	1.1918				
1	0.002	0.002	0.226	Y	Y	0.1261	62.693	1.6616				
1	0.002	0.002	0.255	Y	Y	0.1221	60.3668	1.5011				
1	0.002	0.002	0.212	Y	Y	0.1232	60.6419	2.7273				
1	0.002	0.002	0.232	Y	Y	0.1191	61.9138	2.9106				
1	0.002	0.002	0.238	Y	Y	0.1221	60.596	5.9588				

PKS Error Analysis Database

PKS ERROR ANALYSIS							
Image Name	TEA-BMS		TEA-SB		SB-BMS		
	PKS		PKS		PKS		
M0401631_region1_sc2	0.4140		0.2783		0.24863		
M0401631_sub6_sc2	0.2360		0.3560		0.12		
M0401631_sub14_scnor4	0.0566		0.4057		0.01195		
M1900234_region_sc2	0.0902		0.3686		0.12224		
M1901929_region1	0.0386		0.3289		0.10007		
M1901929_region4	0.0063		0.2970		0.0095777		
MEAN	0.1403		0.3391		0.1021		
STANDARD DEVIATION	0.1561		0.0473		0.0882		
*Notes							
three anonymous individuals: TEA, BMS, SB							
PKS = Probability							

APPENDIX C

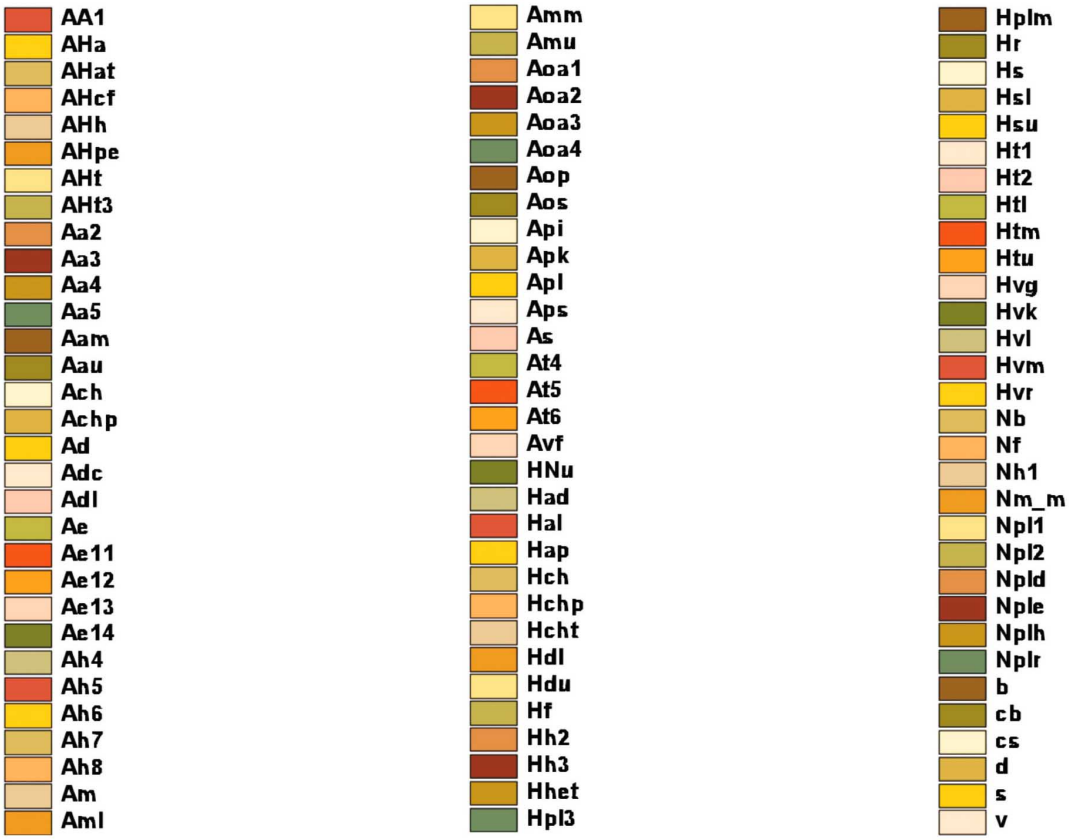

Legend Corresponding to Geology Map of Mars. After: Scott and Tanaka, 1986.

Stratigraphic Unit Descriptions to Accompany Mars Global Stratigraphy Map

SURFICIAL DEPOSITS

As **SLIDE MATERIAL:** Smooth to lobate flow material associated with some scarps and crater rims; especially well developed along channel walls in Deuteronilus Mensae region. Forms aprons along scarps and around knobs and mesas; may completely cover channel floors. Primarily equivalent to third type of slide material mapped by Scott and Tanaka (1986). No specific type area. **Interpretation**: Unconsolidated material, such as debris flows, resulting from mass wasting

Achu **YOUNGER CHANNEL AND FLOOD-PLAIN MATERIAL, UNDIVIDED:** In eastern equatorial part of map area; forms plain as wide as 600 km marked by dark, sinuous, intertwining albedo patterns; appears more mottled westward. Type areas (Scott and Tanaka, 1986): lat 15^{o} N., long 177^{o} (younger channel material) and lat 22^{o}N., long 171^{o} (flood-plain material). **Interpretation**: Fluvial deposits; distinct albedo patterns probably represent channels with bars and islands; mottled zones in western part may represent deposition from ponded terminus of fluvial system

Ad **DUNE MATERIAL:** Patches of barchan and other types of dunes on crater floors. Makes up part of dunes and dune-capped material (unit Ad) of south polar region (Tanaka and Scott, 1987). Type area: lat 48^{o} S., long 329^{o}. **Interpretation**: Sand deposited in areas of low wind strength

LOWLAND TERRAIN MATERIALS:

Consist of all plains-forming units between highland-lowland boundary scarp and north edge of map area, as well as materials of eastern volcanic assemblage.

Northern plains assemblage Materials deposited in widespread sheets on northern plains. Within each formation, members mapped on basis of morphology, albedo, and crater size-frequency distribution; some contacts approximately located. This assemblage postdates formation of highland-lowland boundary scarp (Scott, 1979).

Aps **SMOOTH PLAINS MATERIAL:** Forms patches and regions of flat, featureless plains;lightly cratered. Type area: lat 9^{o} N., long 222^{o}. **Interpretation:** Probably of diverse origin; many exposures probably consist of eolian deposits

AHpe **ETCHED PLAINS MATERIAL:** Occurs as patches in Elysium Planitia. Surface characterized by irregular mesas and pits. Type area: lat 15^{o}N., long 238^{o}. **Interpretation:** Plains deposits mantled by eolian material that has subsequently been eroded, possibly by wind

ARCADIA FORMATION: Forms low-lying plains (1) in Arcadia Planitia east of Phlegra Montes in east margin of map area and (2) in Acidalia Planitia as small patch in west margin. Common boundaries of older members mapped arbitrarily in places. Flows with lobate margins, ridges, and channels and small hills with summit craters visible in some areas. Members 2 and 5 as defined by Scott and Tanaka (1986) not present in map area. **Interpretation:** Mostly lava flows and small volcanoes

Aa4 Member 4 In Arcadia Planitia; overlies member 3. Type area: lat 45^{o} N., long 175^{o} (Scott and Tanaka, 1986)

Aa3 Member 3 In and north of Arcadia Planitia along east margin of map area. Flow fronts visible in places. Type area: lat 15^{o} N., long 155^{o} (Scott and Tanaka, 1986)

Aa1 Member 1 Near west and east borders of map area. Type area: lat 30^{o} N., long 40^{o} (Scott and Tanaka, 1986)

MEDUSAE FOSSAE FORMATION: **Occurs** near equator in eastern part of map area. Consists of extensive, relatively flat sheets, generally smooth to grooved and gently undulating; albedo moderate (Scott and Tanaka, 1986). Locally, where upper or middle member stripped by wind, underlying member shows lineations

Amu **Upper member:** Surfaces smooth, flat to rolling, light in color; sculptured into ridges and grooves in places; broadly curved margins, locally eroded into serrated scarps. Type area: lat 0^{o} N., long 160^{o} (Scott and Tanaka, 1986). **Interpretation:** Thick deposits of eolian sediments or volcanic pyroclastic deposits; wind eroded, particularly along margins, to form yardangs

Amm **Middle member:** Similar to upper member but in places surface is more rugged and eroded. Type area: lat 10^{o} N., long 160^{o} (Scott and Tanaka, 1986). **Interpretation:** Poorly to moderately indurated eolian or pyroclastic deposits; wind eroded, particularly along margins

Aml **Lower member:** Most widespread member in map area. Surfaces smooth to rough and highly eroded, darker than those of other members. One area centered at lat 1° S., long 182° contains long, broad troughs. Type area: lat 0° N., long 174° (Scott and Tanaka, 1986). **Interpretation:** Lava flows interbedded with eolian or pyroclastic deposits, in places heavily eroded

VASTITAS BOREALIS FORMATION Subpolar plains deposits of northern lowlands; members distinguished on basis of morphology and albedo contrast; placement of contacts locally arbitrary (Scott and Tanaka, 1986)

Hvm **Mottled member:** Major occurrence north of map boundary (Tanaka and Scott, 1987); extends as far south as about lat 430° N. Crater-ejecta blankets have higher albedo than adjacent terrain, giving mottled appearance. In places, gently rolling, closely spaced hills averaging 5 km in diameter can be distinguished. Type area: lat 550° N., long 40 (Scott and Tanaka, 1986). **Interpretation:** Possibly lava flows erupted from fissures, or of alluvial or eolian origin

Hvg **Grooved member:** Occurs as isolated patches in several areas of lowland plains; similar to mottled member but marked by curvilinear and polygonal patterns of grooves and troughs; closed polygons as wide as 20 km. Ridges present in center of some grooves, as at lat 53° N., long 295°. Type area: lat 45° N., long 15° (Scott and Tanaka, 1986). **Interpretation:** Material same as mottled member; patterns may be due to compaction, tectonism, or periglacial processes

Hvr **Ridged member:** Isolated patches in northern plains. Characterized by concentric, low ridges about 1 to 2 km wide; northwest of Deuteronilus Mensae, many ridges are within depressions. In Isidis basin, member displays low mounds, many of which are aligned. Type area: lat 38° N., long 33° (Scott and Tanaka, 1986). **Interpretation:** Material same as mottled member; unit appears to develop from erosion of surrounding units. Origin of ridges unknown but they may result from periglacial or erosional processes. Low mounds in Isidis basin may represent spatter cones along lines of vents

Hvk **Knobby member:** Similar in appearance to mottled member but generally has higher albedo and abundant small, dark, knoblike hills, some with summit craters. Crater ejecta have albedo similar to that of surrounding terrain. Type area: lat 55 °N., long 5 ° Scott and Tanaka, 1986). **Interpretation:** Plains of diverse origins (volcanic flows, eolian mantles); hills may be small volcanoes, remnants of highland terrain or of crater rims, or pingos

Eastern volcanic assemblage
Volcanoes and lava flows in Elysium region (Greeley and Spudis, 1981).

ELYSIUM FORMATION: Units associated with Elysium Mons.

Ael4 **Member 4:** Channel material. Type area: lat 36.9^{o} N., long 220^{o}. Interpretation: May be derived from lahars of members 1 and 3 (Christiansen and Greeley, 1981)

Ael3 **Member 3** Forms plains having rugged relief, hummocky surfaces; lobate deposits seen at high resolution. Type area: lat 43^{o} N., long 230^{o}. **Interpretation:** Of volcanic origin; flows possibly derived from Elysium Mons, possibly interfinger with member 1. Extensively modified by fluvial, eolian, and periglacial processes

Ael2 **Member 2:** Lobate deposits, with rilles, composing Elysium Mons edifice. Gradational with member 1. Type area: lat 25^{o} N., long 215^{o}. **Interpretation:** Lava flows displaying channels and partly collapsed lava tubes

Ael1 **Member 1:** Lobate, plains-forming deposits that radiate from Elysium Mons and overlie and embay Albor Tholus and Hecates Tholus Formations. Type area: lat 32.5^{o}N., long 214^{o}. **Interpretation:** Volcanic flows and related materials

AHat **ALBOR THOLUS FORMATION:** Material forming Albor Tholus; hummocky texture, more subdued near vent. Type area: lat 18^{o} N., long 210^{o}. **Interpretation:** Volcanic flows

Hhet **HECATES THOLUS FORMATION:** Forms Hecates Tholus; hummocky surface cut by many narrow, sinuous channels. Type area: lat 33^{o} N., long 209^{o}. **Interpretation:** Volcanic flows, some emplaced through lava channels

Hs **SYRTIS MAJOR FORMATION:** Plains-forming unit constituting Syrtis Major Planum. Characterized by many lobate deposits radiating generally from two irregular depressions (Nili Patera, centered at lat 9^{o} N., long 293^{o},and Meroe Patera, centered at lat 7^{o} N., long 291.5^{o}); flow fronts and margins clearly recognizable; mare-type ridges trend north-northwest; many light and dark "wind" streaks on plains deposits. Type area: lat 11^{o} N., long 295^{o}. **Interpretation:** Lava flows erupted with low effective viscosity from central vents; rheological properties similar to those of basaltic magmas

HIGHLAND TERRAIN MATERIALS: Rock units of moderate to high relief; dominate southern and near-equatorial parts of map area.

Ah8 **Knobby plains floor unit:** Floor material characterized by low knobs a few kilometers across. Type locality: lat 35°S., long 295. **Interpretation:** Possibly remnants of mantle that has been differentially eroded; knobs may be small cinder cones

Ah7 **Rugged floor unit:** Forms undulating terrain of rugged relief on a kilometer scale in western Hellas Planitia; one occurrence mapped. Type area: lat 42°S., long 310?. **Interpretation:** Eroded mantle of possible eolian origin overlying ridged plains material (unit Hr)

Ah6 **Reticulate floor unit:** Plains material characterized by reticulate pattern of ridges; one occurrence mapped. Type area: lat 36°S, long 301.5°. **Interpretation:** Plains material whose high-standing remnants result from differential erosion

Ah5 **Channeled plains rim unit:** Plains material on east rim of Hellas basin characterized by narrow, sinuous channels and slight to moderate relief; includes widespread mesas having irregular margins and a few small knobs. Appears to fill some craters. Type area: lat 43°S., long 264°. **Interpretation:** Mantle of volcanic or eolian deposits eroded possibly by a combination of fluvial and eolian processes. Channels may be fluvial or volcanic

Ah4 **Lineated floor unit:** Smooth plains material characterized by straight and curvilinear lineaments; one occurrence mapped. Type area: lat 34°S., long 295°. **Interpretation:** Possible mantle modified by local tectonic processes.

Hh3 **Dissected floor unit:** Smooth, rolling-plains material that has been deeply dissected to produce local rugged relief. Occurs in central part of Hellas Planitia. Type area: lat 40? S., long 289?. **Interpretation:** Sedimentary deposits modified by wind and minor fluvial activity; may include lava flows

Hh2 **Ridged plains floor unit:** Forms rolling smooth plains having sinuous to linear mare-type (wrinkle) ridges; occupies outermost Hellas Planitia as discontinuous concentric band. Type locality: lat 50°S, long 280°. **Interpretation:** Lava flows erupted with low effective viscosity; composition possibly basaltic

Nh1 **Basin-rim unit:** Material of the Hellas basin rim. Rugged, mountainous, heavily cratered, and modified by surficial processes, but intermontane patches have little relief. Type locality: lat 52°S., long 261°. **Interpretation:** Impact-generated unit of ancient Martian crust; consists of breccias and interbedded volcanic materials.

Plateau and high-plains assemblage
Forms ancient highland terrain and local tracts of younger deposits.

OLDER CHANNEL MATERIAL AND CHAOTIC MATERIAL

Hch **Older channel material:** Occurs mainly along boundary of northern highlands of Deuteronilus Mensae but also in other highland locations, including margin of Hellas basin. Channels generally steep sided, smooth floored, and abruptly terminated on up-slope end. Type area: lat 25^{o}N., long 60^{o} (Scott and Tanaka, 1986). **Interpretation:** May be mixture of channel deposits and mass-wasted materials; channels may have formed by sapping

Hcht **Chaotic material:** Forms semicircular patches of closely spaced knobs of similar heights; mapped near west map border just south of lat 40^{o}N. and near east border. Type area: lat 5^{o}S, long 27^{o} (Scott and Tanaka, 1986). **Interpretation:** Erosional remnants; not associated with channels within map area

Nm **MOUNTAINOUS MATERIAL:** Forms large, very rugged, isolated blocks. Scattered occurrences mostly around Hellas and Isidis basins. Equivalent in part to mountain material (mapped as "m") in south polar region (Tanaka and Scott, 1987). **Interpretation:**Mostly ancient crustal material uplifted during formation of impact basins

PLATEAU SEQUENCE: Forms rough, hilly, heavily cratered to relatively flat and smooth terrain covering most of highlands; occurs mostly in southern hemisphere.

Hpl3 **Smooth unit:** Forms flat, relatively featureless plains in southern highlands; locally embays other units of plateau sequence. Faults and flow fronts rare. Type area: lat 43^{o}S., long 105^{o} (Scott and Tanaka, 1986). **Interpretation:** Interbedded lava flows and sedimentary deposits of eolian or fluvial origin that bury most underlying rocks

Hplm **Mottled smooth plains unit:** Same as smooth unit but has mottled albedo patterns. Global occurrences only in southwestern part of map area. Type area: lat 38^{o}S., long 358^{o} **Interpretation:**Same as smooth unit except that wind-sorted sediments have produced mottled appearance

Npl2 **Subdued cratered unit:** Forms highland plains characterized by subdued and partly buried crater rims; fills some crater floors; flow fronts rare. Type area: lat 28^{o}S., long 162^{o} (Scott and Tanaka, 1986). **Interpretation:**Thin lava flows and sedimentary deposits that partly bury underlying rocks.

Npl1 **Cratered unit:** Widespread in southern highlands; highly cratered, uneven surfaces of generally moderate, locally high relief; fractures and channels common. Type area: lat 45°S., long 148° (Scott and Tanaka, 1986). **Interpretation:**Materials formed during period of high impact flux; probably a mixture of volcanic materials, erosional products, and impact breccia

Npld **Dissected unit:** Similar in occurrence and appearance to cratered unit but more highly dissected by small channels, channel networks, and troughs. Gradational with cratered unit; placement of contact based on abundance of channels. Type area: lat 45°S., long 70° (Scott and Tanaka, 1986). **Interpretation:** Origin same as that of cratered unit but material more highly eroded by fluvial processes

Nple **Etched unit:** Similar to cratered unit but deeply furrowed by sinuous, intersecting, curved to flat-bottomed grooves, producing an etched or sculptured surface; commonly forms small mesas having irregular margins; craters and other depressions filled with smooth deposits. Occurs in several places on cratered plateaus, but is most extensive and well developed northwest of Syrtis Major Planum. Type area: lat 45°N., long 55° (Scott and Tanaka, 1986). **Interpretation:** Cratered unit that has been partly mantled by deposits of possible eolian origin and dissected by eolian erosion, decay and collapse of ground ice, and minor fluvial activity

Nplr **Ridged unit:** Resembles and is locally gradational with ridged plains material (unit Hr) where units adjoin, but ridges generally larger and farther apart, intervening areas rougher and more densely cratered. Type area: lat 15°S., long 163° (Scott and Tanaka, 1986). **Interpretation:** Flood-lava flows; ridges due to faulting, folding, or volcanic processes

Nplh **Hilly unit:** Rough, hilly, fractured material of moderately high relief. Type area: lat 12° S., long 174° (Scott and Tanaka, 1986). Forms complete or partial rims of Isidis and some other ancient basins. **Interpretation:** Ancient highland rocks and impact breccia generated during period of heavy bombardment

HNu **UNDIVIDED MATERIAL:** Forms closely spaced, conical hills a few kilometers across whose distribution indicates that they are remnants of numerous craters. Unit also forms rugged terrain on margins of cratered plateaus and isolated remnants (as west of Orcus Patera near east map border). Gradational with knobby plains material (unit Apk) where units adjoin, but hills are more closely spaced, larger, and occupy more than about 30 percent of area. No specific type area. **Interpretation:** Most hills are eroded remnants of ancient cratered terrain produced by mass-wasting processes, possibly as result of removal of ground ice; some hills may be erosional remnants of intrusive bodies (Greeley and Guest, 1978). Material may include some units of plateau sequence

HIGHLAND PATERAE

AHt **Tyrrhena Patera Formation:** Material forming Tyrrhena Patera; seen on high-resolution images to consist of several members (Greeley and Spudis, 1981), including a highly dissected basal member. Type locality: lat 22º S., long 254º. **Interpretation:** Volcanic materials erupted serially, including early-stage pyroclastic material and later lava flows

AHa **Apollinaris Patera Formation:** Material composing Apollinaris Patera. Consists of several members including deposits dissected by channels, some of which flowed over a basal scarp; forms a large fanlike feature on southeast flank. Type area: lat 9º S., long 186º. **Interpretation:** Material of multiple-stage eruptions forming shield volcano (Greeley and Spudis, 1981)

AHh **Hadriaca Patera Formation:** Material of Hadriaca Patera. Consists of smooth floor material in central depression, locally ridged along margin, surrounded by material dissected radially to depression. Type area: lat 31º S., long 268º. **Interpretation:** Material of central-vent volcano formed by multiple eruptions; possible pyroclastic deposits indicate explosive activity (Greeley and Spudis, 1981)

Had **Amphitrites Formation, dissected member:** Forms shieldlike deposit along north edges of Malea Planum (near south map border). Consists of deeply etched, ridged, lobate deposits and superposed crater material; sinuous furrows, ridges, and scarps trend toward Hellas Planitia. Type area: northern Malea Planum. **Interpretation:** Ridged plains material (unit Hr) modified by fluvial channeling

MATERIALS OCCURRING THROUGHOUT MAP AREA

Apk **KNOBBY PLAINS MATERIAL:** Extensive in northern lowlands where it forms moderately to lightly cratered, generally smooth plains; several isolated occurrences in cratered highlands. Conical hills or knobs occur at irregular intervals; mare-type (wrinkle) ridges locally present. Where adjacent to undivided material (unit HNu), units are intergradational, but knobs in knobby plains unit are smaller and spaced farther apart. Type area: lat 22º N., long 263º. **Interpretation:** Probably of diverse origins but appears to have formed mainly by erosion of older units. Knobs are probably erosional remnants but some may be volcanic. Intervening plains may be erosional surfaces or may consist of eolian, mass-wasted, or volcanic materials

Hr **RIDGED PLAINS MATERIAL:** Characterized by broad planar surfaces, rare lobate deposits, and long, parallel, linear to sinuous mare-type (wrinkle) ridges about 30 to 70 km apart. Forms plains within and outside craters throughout

plateau area and lowland plains north of Orcus Patera (near east map border). Locally gradational with ridged plateau material (unit Nplr) where units adjoin. Type area: Lunae Planum, lat 10º N., long 65º (Scott and Tanaka, 1986). **Interpretation:** Extensive lava flows erupted with low effective viscosity from many sources at high rates; ridges either volcanic constructs or compressional features

c , s **IMPACT-CRATER MATERIALS:** Yellow indicates materials of superposed craters greater than about 100 km across; brown indicates materials of partly buried craters greater than about 150 km across. May include rim crest (hachured), central ring (inner circular feature, also hachured), and central peak. Hachures also denote impact-basin rims. Symbol "c" denotes crater-rim and ejecta material. Symbol "s" and orange color denote smooth floor material; within mapped crater material, only patches larger than 30 km across are shown; elsewhere, only patches larger than about 80 km across are shown. Linear dot pattern denotes secondary craters outside crater aprons. **Interpretation:** Units resulting from impact cratering, but smooth-floor material may be of volcanic, eolian, or fluvial origin

LOWLAND TERRAIN MATERIALS

Consist of all plains-forming units between the highland-lowland boundary scarp and the north edge of the map area, exclusive of materials of the western volcanic assemblage on the Tharsis swell.

Northern plains assemblage

Materials deposited in widespread sheets on northern plains. Within each formation, members mapped at places on basis of crater density; these contacts are approximately located. Assemblage postdates highland-lowland boundary scarp (Scott, 1979).

ARCADIA FORMATION: Forms low-lying plains in Arcadia, Amazonis, and Acidalia Planitiae. Embays highland margins and partly buries outflow channels of Kasei, Shalbatana, Simud, Tiu, and Ares Valles. Members distinguished on basis of morphology, albedo, and crater density; common boundaries of older members mapped arbitrarily at places. Flows with lobate margins and small hills with summit craters visible in many places. High-resolution pictures show that sources of some flows are small cratered cones. **Interpretation:** Mostly lava flows and small volcanoes

Aa5 **Member 5:** Relatively small areal extent. Dark, fresh-appearing flows; few superposed impact craters. Type area: lat 47º N., long 30º

Aa4 **Member 4:** In Arcadia Planitia underlies member 5 and has similar appearance; one other occurrence in channel system of Chryse Planitia. Type area: lat 45º N., long 175º

Aa3 **Member 3:** Forms smooth plains west of Olympus Mons aureoles; embays both the aureoles and fractured terra of Acheron Fossae. Flow fronts visible in places. Type area: lat 15º N., long 155º

Aa2 **Member 2:** Underlies members 3, 4, and 5 in Arcadia Planitia. Includes many small (<10-km-diameter) structures resembling volcanoes and cinder cones. Curved concentric ridges visible on surfaces of flows. Type area: lat 45º N., long 155º

Aa1 **Member l:** Widespread in Chryse and Amazonis Planitiae. Mare-type (wrinkle) ridges common. Type area: lat 30º N., long 40º

MEDUSAE FOSSAE FORMATION- Consists of extensive, relatively flat sheets, generally smooth to grooved and gently undulating; deposits appear to vary from soft to indurated; albedo moderate. Occurs near equator in western part of map area. Total thickness may exceed 3 km

Amu **Upper member:** Discontinuous but widespread deposits extend from south of Olympus Mons westward across Amazonis Sulci to map boundary. Smooth, flat to rolling, light-colored surfaces; sculptured into ridges and grooves in places (as in Medusae Fossae); broadly curved margins, locally serrated. Type area: lat 0º N., long 160º. **Interpretation:** Nonwelded ash-flow or ash-fall tuff or thick accumulation of eolian debris; wind eroded, particularly along margins

Amm **Middle member:** Similar to upper member but in places (as at Memnonia Sulci) surface appears rougher, more deeply eroded; cut by scarps of Gordii Dorsum and transected in type area by intersecting joint sets. Type area: lat 10º N., long 160º. **Interpretation:** Welded and nonwelded pyroclastic rocks or layers of relatively soft to indurated eolian deposits

Aml **Lower member:** Two small occurrences in western map area. Surfaces smooth to rough and highly eroded, darker than those of other members. Type area: lat 0ºN., long 174?. **Interpretation:** Lava flows interbedded with pyroclastic rocks or eolian deposits

VASTITAS BOREALIS FORMATION: Subpolar plains deposits of northern lowlands. Its four members distinguished on basis of morphology or albedo contrast; placement of contacts locally arbitrary

Hvm **Mottled member:** Major occurrence north of map boundary (Tanaka and Scott, unpub. data, 1985); extends as far south as topographic reentrants between Acidalia and Chryse Planitiae where appears windswept. Crater-ejecta blankets have higher albedo than adjacent terrain; lobate flow fronts visible; some small

hills present. Type area: lat 55º N., long 40º. **Interpretation:** Possibly consists of lava flows erupted from fissures and small volcanoes or of alluvial and eolian deposits. Mottled appearance due to contrast between generally low albedo of plains and brightness of small hills and impact-crater aprons

Hvg **Grooved member:** Similar to mottled member in Acidalia Planitia but marked by curvilinear and polygonal patterns of grooves and troughs; closed polygons as wide as 20 km. Type area: lat 45º N., long 15º. **Interpretation:** Material same as mottled member; patterns may be due to compaction or to tectonic or ground-ice phenomena

Hvr **Ridged member:** Three small occurrences of mottled plains characterized by concentric pattern of low, narrow ridges about 1 to 2 km wide. Type area: lat 38º N., long 33º; other two outcrops near lat 54º N., Iong 176º. **Interpretation:** Material same as mottled member; origin of ridges unknown but they may be periglacial structures or channel-meander features accentuated by differential erosion

Hvk **Knobby member:** Similar in appearance to mottled member but generally has higher albedo and abundant small, dark, knoblike hills, some with summit craters. Type area: lat 55º N., long 5º. **Interpretation:** Material same as mottled member; hills may be small volcanoes or remnants of highland terrain or crater rims

Channel-system materials

Deposited in outflow channels and on flood plains; exhibit both depositional and erosional features. Interpretation: Channel and flood-plain materials of alluvial origin; some surfaces sculptured by flood waters. Chaotic material formed by disruption of terrain by ground-water release.

Ach, Achp **YOUNGER CHANNEL AND FLOOD-PLAIN MATERIALS:** Along western margin of map area, form plain as wide as 200 km marked by dark, sinuous, intertwining channels with bars and islands; fill small channels in Arcadia Planitia, along north edge of Tempe Fossae, and in Ophir and Candor C hasmata. Crater counts and superposition relations indicate Amazonian age. Type areas: lat 15º N., long 177º (unit Ach) and lat 22º N., long 171º (unit Achp)

Hch, Hchp, Hcht **OLDER CHANNEL, FLOOD-PLAIN, AND CHAOTIC MATERIALS:** Mainly between Valles Marineris and Chryse Planitia, also in other highland locations. Channel deposits longitudinally striated; teardrop-shaped channel bars large and well developed. Flood-plain material occurs adjacent to channels and in lowland plains below channel mouths, smooth and featureless. Chaotic material occurs at source areas and along margins of channels and within some chasmata and craters; generally a mosaic of highland

blocks in depressions. Type areas: lat 25º N., long 60º (unit Hch); lat 27º N., long 53º (unit Hchp); lat 5º S., long 27º (unit Hcht)

HIGHLAND TERRAIN MATERIALS

Rock and rock-tectonic units of moderate to high relief; dominate southern and near-equatorial parts of map area. Volcanic mountains and associated lava flows of Tharsis region, although not typical of highland terrain, are included in this physiographic classification because they are superposed on highland terrain or form high plains and locally rugged topographic features.

Western volcanic assemblage

Volcanoes and lava flows in Tharsis region of Mars (Schaber and others, 1978; Scott and others, 1981).

THARSIS MONTES FORMATION: Includes large volcanic shields and associated lava flows of Arsia Mons, Pavonis Mons, and Ascraeus Mons; lava flows similar in morphology to terrestrial basalts (Schaber and others, 1978)

At6 **Member 6:** Fresh-appearing lava flows form smooth, fan-shaped arrays on flanks of Arsia, Pavonis, and Ascraeus Montes, flows probably originate from fissures along major structural trends. Flanks of these volcanoes exhibit grabens, some concentric. Member also includes most recent fill within central calderas of Tharsis Montes. Type area: lat 5º S., long 117º

At5 **Member 5:** Widespread around Tharsis Montes volcanoes. Overlies parts of channel and flood-plain deposits (units Hch, Hchp) of Kasei Valles; contact with upper member (unit Hsu) of Syria Planum Formation northwest of Echus Chasma poorly resolved. At places forms elongate, light-colored flow lobes with abundant dark wind streaks. Cut by few faults. Type area: lat 20º S., long 120º

At4 **Member 4:** Exposed mostly northeast and southwest of member 5. Consists of overlapping light flows with dark wind streaks similar to those of member 5; flows elongate on steep upper slopes, broad on gentler lower slopes. High-resolution images show pressure ridges concentric with lobate flow fronts; minor faulting. Type area: lat 15º S., long 135º

AHt3 **Member 3:** Makes up central shields of Arsia, Pavonis, and Ascraeus Montes and embays highland terrain west of Arsia Mons and along northwest side of Claritas Fossae, where light and dark flows common. Fewer lobate fronts, pressure ridges, and dark streaks but more faults than in members 4 and 5. Type area: lat 27º S., long 127º

Ht2 **Member 2:** Occurs in southern and northeastern parts of Tharsis region; embays highland terrain of Tempe Fossae. Composed of relatively smooth flows having broad frontal lobes; fractures and faults common in places. Type area: lat 33º S., long 135º

Ht1 **Member 1:** Scattered outcrops in southern Tharsis region. Generally forms rough, hummocky surface; mare-type (wrinkle) ridges in places; faults and fractures common locally. Type area: lat 30? S., long 120º

OLYMPUS MONS FORMATION: Includes young lava flows extruded from fissures in plains east of Olympus Mons, young shield lavas of the volcano, and aureole deposits surrounding the volcano. Interpretation of aureoles: Formed by gravity spreading of materials forming a larger, earlier Olympus Mons; alternatively, could be ash or lava flows (see text)

Aop **Plains member:** Embays basal scarp of Olympus Mons and overlaps shield member. Consists of many overlapping smooth lava flows ranging in shape from narrow tongues to broad lobes; flows appear to be extruded from faults and fissures below scarp on southeast side of Olympus Mons. Type area: lat 20º N., long 125º

Aos **Shield member:** Lava flows form complex, finely textured, interfingering tongues and lobes. Channels and levees extend down flanks of Olympus Mons and across prominent basal scarp on north, east, and south sides, collapse pits common. Type area: lat 15º N., long 135º

Aoa4 **Aureole member 4:** Uppermost of a series of aureole units around Olympus Mons that formed prior to or contemporaneously with the volcano's basal scarp. Forms broad, semicircular, flat lobes; corrugated, cut by numerous faults that formed scarps and deep troughs and grabens. Type area: lat 25º N., long 145º

Aoa3 **Aureole member 3:** Forms two lobes; similar to but underlying member 4. Type area: lat 28º N., long 134º

Aoa2 **Aureole member 2:** Forms three lobes; similar to members 3 and 4; underlies member 3 in relatively small area on southwest side of Olympus Mons; on east side occurs as islands surrounded by plains member. Type area: lat 14º N., long 143º

Aoa1 **Aureole member 1:** Forms widespread basal aureole; overlaps younger and older fractured materials (units Hf and Nf). Resembles younger aureole members but smoother and more degraded by wind. Type area: lat 15º N., long 147º

AHcf CERAUNIUS FOSSAE FORMATION: A series of overlapping flows whose surfaces are relatively smooth and even toned to mottled and streaked; trends northeast across older fractured material (unit Nf) in Ceraunius Fossae; channels with levees occur in places. Type area: lat 23º N., long 115º. **Interpretation:** Lava flows, most of which originated from fissures

SYRIA PLANUM FORMATION: Volcanic flows of intermediate age that originated from crestal area and flanks of topographic high in northern Syria Planum and Noctis Labyrinthus

Hsu **Upper member:** Partly encircles crest of topographic high. Consists of both long narrow lava flows and sheet flows that have prominent lobes mottled light and dark; pit craters common. Relatively smooth around Valles Marineris. Covers some fault systems of Claritas Fossae but cut by few others in Noctis Labyrinthus. Flows probably extruded from calderas near summit of Syria Planum and from fissures; gradational with lower member. Boundary with ridged plains material (unit Hr) not clearly defined, placed where member appears to overlap ridges. Type area: lat 15º S., long 100º

Hsl **Lower member:** Similar to upper member but more highly cratered and faulted. Type area: lat 25º S., long 90º

ALBA PATERA FORMATION: Forms low shield and extensive lava flows of Alba Patera volcano

Aau **Upper member:** Covers large area within and around central calderas; lava flows completely or partly bury most ring and radial structures; channels with levees common along crests of flows. Type area: lat 40º N., long 110º

Aam **Middle member:** Encircles crestal region and upper member; occurs as low radial ridges with summit channels and as long narrow tongues with leveed channels. Highly faulted but buries many grabens in older fractured material (unit Nf). Type area: lat 40º N., long 118º

Hal **Lower member:** Covers broad area around north and west flanks of Alba Patera. Flow fronts less distinct than those of younger members. Extends into plains region; appears to be overlapped in places by lowermost member (unit Aa1) of Arcadia Formation but most of boundary indistinct. Type area: lat 35º N., long 125º

Plateau and high-plains assemblage
Forms ancient highland terrain and local tracts of younger deposits.

SURFICIAL DEPOSITS
Slide material of three types°

As (1) In Valles Marineris and other chasmata as rotational slide deposits from canyon walls, surfaces hummocky near crown scarp; distal parts commonly lobate, longitudinally striated, with long runout. Type area: lat 9° S., long 72°. **Interpretation:** Gas- or water-lubricated slides and debris flows
(2) Mostly on northwest flanks of Olympus Mons and largest volcanoes of Tharsis Montes as fanlike corrugated sheets as wide as 600 km that appear to override topographic obstacles without deflection of internal structure; source areas hummocky, contain small hills and circular depressions. Type area: lat 5° S., long 125°. Interpretation: Volcanic-debris avalanches resulting from either slope failure or explosive volcanism; alternatively, may be recessional moraines of former local ice caps
(3) Along scarps of Charitum Montes and Mareotis Fossae as smooth, sloping aprons with steep, high edges. No specific type area. Interpretation: Debris aprons produced by mass wasting and slow, glacierlike flow of ice-rich plateau material

Ae **Eolian deposits:** Form broad level plains chiefly on aureole deposits of Olympus Mons. Surfaces locally appear rough, deeply etched, and striated in directions of prevailing winds. Type area: lat 15° N., long 145°

VALLES MARINERIS INTERIOR DEPOSITS:Materials within Valles Marineris and associated canyons, excluding walls and mapped landslides and channel materials

Avf **Floor material:** Occurs along canyon floors as smooth to hummocky and rugged material of low relief. No specific type area. **Interpretation:**Mixture of landslides and debris flows from canyon walls, eolian material, volcanic deposits, and channel and possibly lacustrine deposits

Hvl **Layered material:** Thinly bedded dark and light materials visible in high-resolution pictures on floors of several canyons. Forms platforms and hills of moderate to high relief. Type area: lat 7° S., long 48°. **Interpretation:** Volcanic or lacustrine material or both, deposited during intermediate to late stages of canyon development

PLATEAU SEQUENCE: Forms rough, hilly, heavily cratered to relatively flat and smooth terrain covering most of highlands, which are dominant in southern hemisphere. Several units represent transitional stages modified by erosional or depositional processes

Hpl3 **Smooth unit:** Forms large areas of flat, relatively featureless plains in southem highlands; locally embays other units of plateau sequence. Faults and flow fronts

rare. Type area: lat 43º S., long 105º. **Interpretation:** Thick interbedded lava flows and eolian deposits that bury most of underlying rocks

Npl2 **Subdued cratered unit:** Forms plains (mostly in highlands) marked by subdued and partly buried old crater rims. Flow fronts rare. Type area: lat 28º S., long 162º. **Interpretation:** Thin interbedded lava flows and eolian deposits that partly bury underlying rocks

Npl1 **Cratered unit:** Most widespread unit in southern highlands; locally extensive in northern plains. Highly cratered, uneven surface of moderate relief; fractures, faults, and small channels common. Type area: lat 45º S., long 148º. **Interpretation:** Materials formed during period of high impact flux; probably a mixture of lava flows, pyroclastic material, and impact breccia

Npld **Dissected unit:** Similar in occurrence and appearance to cratered unit but more highly dissected by small channels and troughs. Type area: lat 45º S., long 70º. **Interpretation:** Origin same as that of cratered unit but more eroded by fluvial processes

Nple **Etched unit:** Similar to cratered unit but deeply furrowed by sinuous, intersecting, curved to flat-bottomed grooves that produce an etched or sculptured surface. Type area: lat 45º N., long 55º. **Interpretation:** Cratered unit that has been degraded by wind erosion, decay and collapse of ground ice, and minor fluvial processes

Nplr **Ridged unit:** Resembles ridged plains material (unit Hr) where units adjoin, but ridges generally larger and farther apart, intervening areas rougher and more densely cratered. Type area: lat 15º S., long 163º. **Interpretation:** Most ridges due to normal faulting but others may be volcanic constructs or compressional features

Nplh **Hilly unit:** Rough, hilly material that resembles in part basement complex (unit Nb) and older fractured material (unit Nf), but relief is gentler and faulting less intense. Type areas: lat 12º S., long 174º and Nereidum and Charitum Montes surrounding Argyre Planitia. **Interpretation:** Ancient highland volcanic rocks and impact breccia uplifted by tectonism and impact-basin formation during period of heavy bombardment

Hr **RIDGED PLAINS MATERIAL:** Major occurrences cover an area of about 4,000,000 km2 extending from Solis Planum to Tempe Fossae. Characterized by broad planar surfaces with flow lobes visible in places and long, parallel, linear to sinuous mare-type (wrinkle) ridges; ridges about 30 to 70 km apart. Type area: Lunae Planum, lat 10º N., long 65º. **Interpretation:** Extensive flows of low-viscosity lava erupted from many sources at high rates, ridges either volcanic constructs or compressional features (see text)

TEMPE TERRA FORMATION: Interpreted to consist of intermediate-age lava flows extruded from small shield volcanoes, fissures, and depressions on Tempe Terra plateau. All members exhibit lobate scarps that may be edges of flows

Htu **Upper member:** Smooth, light-colored, partly mottled material that embays hilly, mountainous, and fractured terrain of highlands; small (<10-km-diameter) shield volcanoes visible in high-resolution pictures; few faults and fractures; embayed by a lower member (unit Ht2) of Tharsis Montes Formation and by lower member (unit Hal) of Alba Patera Formation. Type area: lat 36º N., long 86º

Htm **Middle member:** Similar to upper member but faults, fractures, and collapse depressions common. Type area: lat 42º N., long 80º

Htl **Lower member:** Smooth to rough, uneven surfaces; small faults and collapse depressions common. Overlaps hilly and cratered units (units Nplh, Npl1) of plateau sequence but is embayed by upper and middle members of Tempe Terra Formation. Type area: lat 39º N., long 84º

HIGHLY DEFORMED TERRAIN MATERIALS: The origin and composition of these rock units are only surmised because multiple sets of fractures and grabens have obscured original characteristics. The units are interpreted to consist of impact breccia interlayered with volcanic flows and to intergrade locally

Hf **Younger fractured material:** Occurs mostly around Valles Marineris and Syria and Sinai Plana and northwest of Pavonis Mons. Forms relatively smooth, raised surfaces of moderate relief with fractures, grabens, and collapse depressions. Overlies other highly deformed terrain materials but is embayed and partly covered by Syria Planum Formation and other younger rock units. Type area: lat 5º S., long 103º

Nf **Older fractured material:** similar to fractured material but widespread, has greater relief, is more highly deformed, and faults are more complexly oriented; impact-crater outlines largely destroyed. Type area: lat 20º S., long 109º

Nb **Basement complex:** Undifferentiated material characterized by highly complicated structure and prominent relief. Most common in Claritas and Mareotis Fossae areas. Type area: lat 28º S., long 100º

HNu **UNDIVIDED MATERIAL:** Forms hills and small knobs adjacent to highland-lowland boundary scarp that extend almost to north map border. Also forms walls and interior mountains in Valles Marineris and associated canyons and channels, as well as hummocky terrain and scarps along edges of Chryse and Acidalia Planitiae. No specific type area. **Interpretation:** Erosional remnants

and exposures of plateau sequence, highly deformed terrain materials, ancient crater rims, and some other materials that are older than surrounding rock units

NORTH POLAR REGION

Northern plains assemblage
Materials deposited in widespread sheets on northern plains. Boundaries between rock units commonly not well defined, in places indicated by dashed contact.

ARCADIA FORMATION: Smooth, sparsely cratered; lobate fronts visible in places. Embays all neighboring units. (Members 2, 4, and 5 (units Aa2, Aa4, and Aa5) mapped to south, not present in map area.) Interpretation: Lava flows and sediments from local sources

Aa3 **Member 3:** Forms isolated patches along edge of map area between long 170° and 180°

Aa1 **Member 1:** Forms low-lying plains surrounding Alba and Tantalus Fossae

Aps **SMOOTH PLAINS MATERIAL:** Forms two areas of smooth, sparsely cratered plains north of crater Lyot near edge of map area (long 315° to 340°) and near knobby, undivided material at long 193°. **Interpretation:** Probably of diverse origin, but may primarily consist of eolian deposits

VASTITAS BOREALIS FORMATION: Subpolar plains deposits. Type areas designated in western equatorial region (Scott and Tanaka, 1986)

Hvm **Mottled member:** Characterized by high-albedo crater deposits superposed on low-albedo, smooth-plains deposits; occurs along more than half of edge of map area; gradational with other members, particularly with knobby member. **Interpretation:** Lava flows, possibly erupted from fissures and small volcanoes, or alluvial or eolian deposits. Mottled appearance due either to relatively fresh, light-colored material exposed during impact-crater excavation or to high-albedo eolian debris trapped within crater ejecta

Hvg **Grooved member:** Marked by grooves forming polygonal pattern; polygons commonly 5 to 20 km across; small patch at lat 80° N., long 60° in mouth of Chasma Boreale; eroded on south side. **Interpretation:** Degraded lava flows or sediments; grooves may be lava-cooling, periglacial, tectonic, dessication, or compaction phenomena

Hvr **Ridged member:** Scattered occurrences mostly in western longitudes; gradational with knobby, mottled, and smooth members; in places embayed by

Arcadia Formation. Ridges about 1 to 2 km wide and several to tens of kilometers long commonly form polygons 5 to 20 km across; ridge patterns in some southern outcrops are arcuate or concentric, as at lat 56º N., long 173º. **Interpretation:** Degraded lava flows or sediments; ridge pattern may be formed by intrusion of viscous lava in grooves of grooved member or by remnants of dikes on a stripped surface; concentric ridges may result from scarp retreat caused by periglacial or erosional processes

Hvk **Knobby member:** Characterized by abundant, kilometer-size, dark, knoblike hills spaced generally a few kilometers apart and commonly grouped into linear chains. Occurs in broad circumpolar belt; interknob areas gradational with mottled and ridged members. **Interpretation:** Knobs probably small volcanoes and highly degraded remnants of highland material (unit HNu), crater rims, and older plains material. Interknob plains probably degraded lava flows or sediments

Channel-system and eolian materials

Depositional and erosional units within channels and plains, and dune deposits.

Ach **YOUNGER CHANNEL MATERIAL:** Smooth, sparsely cratered material within part of channel along edge of map area at long 58º; channel originated from Tempe Fossae region to south (Scott and Tanaka, 1986). Superposed on flood-plain material and mottled and knobby members of Vastitas Borealis Formation. Interpretation: Recent fluvial material

Adc **CRESCENTIC DUNE MATERIAL:** Forms individual and linked crescentic dunes; individual dunes as large as several kilometers across. Occurs along most of edge of Planum Boreum. **Interpretation:** Active barchan dunes made up of sand-size particles consisting of mineral grains or dust and ice aggregates. Occurrence indicates areas of moderate sand accumulation or erosion

Adl **LINEAR DUNE MATERIAL:** Forms linear, ripplelike patterns of dunes in north polar erg in Arion Planitia and near mouth of Chasma Boreum; wavelength of ripples about 1 to 2 km. **Interpretation:** Forms relatively stable, mature dune field; dune orientations controlled by oscillating wind directions. Presence indicates regime of large sand accumulations in topographic lows

Am **MANTLE MATERIAL:** Smooth to hummocky deposit, as much as several hundred meters thick; surrounds most of Planum Boreale; extent of unit may vary seasonally. Mapped only north of lat 66º N., where thick enough to obscure features characteristic of members of Vastitas Borealis Formation. **Interpretation:** Eolian deposits derived from seasonal frost and dust accumulation and perhaps erosion of polar layered deposits, polar dunes, and subpolar plains materials

Hchp **FLOOD-PLAIN MATERIAL:** Smooth, moderately cratered material with longitudinal albedo streaks; occurs at edge of map area at long 60º, adjacent to younger channel material; forms north tip of flood-plain deposits along west edge of Acidalia Planitia; embayed by member 1 of Arcadia Formation. **Interpretation:** Deposits from fluvial channels south of map area (Scott and Tanaka, 1986)

Western volcanic assemblage

ALBA PATERA FORMATION

Hal **Lower member:** Forms gently sloping plateau that emerges from Vastitas Borealis Marked by degraded lobate flow fronts and small impact craters; displays grabens a few kilometers across and tens to hundreds of kilometers long; embayed by member 1 of Arcadia Formation. To south, unit covers broad region containing most of Alba and Tantalus Fossae; north edge of region extends into map area. Previously mapped as cratered and fractured plains material (Dial, 1984). **Interpretation:** Older, highly degraded lava flows originating from Alba Patera and surrounding fractures

Plateau and high-plains assemblage

Consists of ancient highland terrain and local tracts of younger deposits that stand relatively high.

POLAR DEPOSITS

Api **Polar ice deposits:** Residual polar cap of high-albedo material imaged in late spring and summer (Ls=92 to 154), 1977; occurs on high surfaces of Planum Boreum, in irregular patches north of lat 70º N. between longs 10º and 270º, and on crater floors. **Interpretation:** Photometry and infrared thermal mapping indicate water-ice and dust composition (Kieffer and others, 1976). Covered by CO2 frost that extends continuously as far south as lat 65º N. during winter. Some outlier deposits may be wind-streaked material composed mainly of ice or frost

Apl **Polar layered deposits:** Form Planum Boreum and nearby mesas south of Chasma Boreale; smooth, uncratered; moderate albedo; Planum Boreum cut by troughs in swirl pattern; troughs expose alternating light and dark layers tens of meters thick, some unconformable; total thickness estimated at 4 to 6 km (Dzurisin and Blasius, 1975) or 1 to 2 km (Wu and others, in press). Composite age of deposits uncertain. **Interpretation:** Deposits of mixed ice and dust. Light and dark layering caused by variation in dust-to-ice ratio; reflects long-term

REFERENCES

Baker, V. R., Water and the Martian Landscape, *Nature*, ***412***, 2001.

Baker, V. R., Strom, R. G., Gulick, V. C., Kargel, J. S., Komatsu, G., and Kale, V. S., Ancient oceans, ice sheets and the hydrological cycle on Mars, *Nature,* ***352,*** pp. 589-594, 1991.

Black, R. F., Permafrost-A Review, *Bulletin of the Geological Society of America, 65*, pp. 839-856, 1954.

Black, R. F., Periglacial features indicative of permafrost: Ice and soil wedges, *Quaternary Research., 6*, pp. 3-26, 1976.

Boynton, W. V., Feldman, W. C., Squyres, S. W., Prettyman, T., Bruckner, J., Evans, L. G., Reedy, R. C., Starr, R., Arnold, J. R., Drake, D. M., Englert, P. A. J., Metzger, A. E., Mitrofanov, I., Trombka, J. I., d'Uston, C., Wanke, H., Gasnault, O., Hanara, D. K., Janes, D. M., Marcialis, R. L., Maurice, S., Mikheeva, I., Taylor, G. J., Tokar, R., and Shinohara, C., Distribution of hydrogen in the near-surface of Mars: Evidence for subsurface ice deposits, *Sciencexpress,* zdoi;10.1126/science.1073722, 2002.

Caplinger, M., Mars Observer Camera Ground Data System Overview, Malin Space Science Systems, Inc. (San Diego, California, U.S.A.; http://www.msss.com/mars/observer/camera/papers/gds_papers/GDS_overview/GDSoverview.html), 1995.

Carolina Map Distributors., (Waynesville, NC.; http://www.carolinamapdistributors.com/products/aerial/cir.htm), 2003.

Carr, M. H., *Water on Mars*, pp. 229, Oxford University Press, New York, NY., 1996.

Cattermole, P.J., *Mars: The Mystery Unfolds*, pp. 186, Oxford University Press, New York, NY., 2001.

Clifford, S. M., A model for the hydrologic and climatic behavior of water on Mars, *Journal of Geophysical Research*, ***98***, pp. 10, 973-11, 016, 1993.

Clifford, S. M., A pore volume estimate of the Martian megaregolith based on a lunar analog, *Lunar Planetary Science Institute Contribution,* ***441***, pp. 46-48, 1981.

Costard, F. M., and Kargel, J. S., Outwash Plains and Thermokarst on Mars, *Icarus*, ***114,*** pp. 93-112, 1995.

Davis, N., *Permafrost: A Guide to Frozen Ground in Transition*, University of Alaska Press, Fairbanks, Alaska., 2001.

De Pater, I., and Lissauer, J. J., *Planetary Sciences*, pp. 523, Cambridge University Press, Cambridge, UK., 2001.

Fanale, F. P., Salvail, J. R., Zent, A. P., and Postawko, S. E., Global distribution and migration of sub-surface ice on Mars, *Icarus*, ***67,*** pp. 1-18, 1986.

Feldman, W. C., Prettyman, T. H., Maurice, S., Plaut, J. J., Bish, D. L., Vaniman, M. T., Mellon, M. T., Metzger, A. E., Squyres, S. W., Karunatillake, S., Boynton, W. V., Elphic, R. C., Funsten, H. O., Lawrence, D. J., and Tokar, R. L., The global distribution of near-surface hydrogen on Mars, *Journal of Geophysical Research – Planets*, 2003.

Ferrians, O., Kachadoorian, R., and Green, G. W., Permafrost and related engineering problems in Alaska, *United States Geological Survey*, *Professional Paper 678*, pp. 37, 1969.

French, H. M., *The Periglacial Environment, 2nd ed.*, Addison Wesley Longman Limited, Essex, England, 1996.

Head, J. W., Heisinger, H., Ivanov, M. A., Kreslavsky, M. A., Pratt, S., and Thomson, B. J., Possible Ancient Oceans on Mars: Evidence from Mars Orbiter Laser Altimeter Data, *Science, **286**,* pp. 2134-2137, 1999.

Head, J. W., Mustard, J. F., Kreslavsky, M. A., Milliken, R. E., and Marchant, D. R., Recent Ice Ages on Mars, *Nature, **426**,* pp. 797-802, 2003.

Heisinger, H., and Head, J. W., Characteristics and origin of polygonal terrain in southern Utopia Planitia, Mars: Results from Mars Orbiter Laser Altimeter and Mars Orbiter Camera data, *Journal of Geophysical Research, **105**, No. E5,* pp. 11, 999 – 12, 022, 2000.

Jakosky, B. M., and Carr, M. H., Possible precipitation of ice at low latitudes of Mars during periods of high obliquity, *Nature, **315**,* pp.559-561, 1985.

Jakosky, B. M., and Farmer, C. B., The seasonal and global behavior of water vapour in the Mars atmosphere: Complete global results of the Viking atmospheric water vapour detector experiment, *Journal of Geophysical Research, **87**,* pp.2999-3019, 1982.

Jakosky, B. M., and Haberle, R. M. / Kieffer, H. H. et al., eds., The seasonal behaviour of water on Mars, pp. 969-1016, *Mars*, University of Arizona Press, Tucson, 1992.

Kuzmin, R. O., Ershow, E. D., Komarow, I. A., Kozlov, A. H., and Isaev, V. S., The Comparative Morphometric Analysis of Polygonal Terrain on Mars and the Earth High Latitude Areas, *Lunar and Planetary Science*, ***33***, 2002.

Kuzmin, R. O., and Zabalueva, E. V., Polygonal terrains on Mars: Preliminary Results of Global Mapping of their Spatial Distribution, *Lunar and Planetary Science,* ***34,*** 2003.

Lachenbruch, A. H., Mechanics of Thermal Contraction Cracks and Ice-Wedge Polygons in Permafrost, Geological Society of America, Special Paper Number 70, Waverly Press, Baltimore, Maryland, pp. 69, 1962.

Leffingwell, E. K., Ground-ice wedges, the dominant form of ground-ice on the north coast of Alaska, *Journal of Geology,* ***23,*** pp. 635-654, 1915.

Leovy, C., Weather and Climate on Mars, *Nature,* ***412,*** pp. 245-249, 2001.

Lucchitta, B. K., Mars and Earth: Comparison of Cold-Climate Features, *Icarus,* ***45,*** pp. 264-303, 1981.

Mackay, J. R., The world of underground ice, *Annals, Association of American Geographers*, *62*, pp. 1-22. 1972.

Mackay, J. R., The first 7 years (1978-1985) of ice wedge growth, Illisarvik experimental drained lake site, western Arctic coast, *Canadian Journal of Earth Sciences, **23**,* pp. 1782-1795, 1986.

Malin Space Science Systems, Inc., (San Diego, California, U.S.A.; http://www.msss.com/newhome.html).

Masson, P., Carr, M. H., Costard, F., Greeley, R., Hauber, E., and Jaumann, R., Geomorphologic Evidence for Liquid Water, *Space Science Reviews, **96**,* pp. 333-364, 2001

Mellon, M. T., Small-scale polygonal features on Mars: Seasonal thermal contraction cracks in permafrost, *Journal of Geophysical Research, **102**, No. E11,* pp. 25, 617-25, 638, 1997.

Mellon, M. T., Jakosky, B. M., Keiffer, H. H., and Christensen, P. R., High-Resolution Thermal Inertia Mapping from the Mars Global Surveyor Thermal Emission Spectrometer, *Icarus, **148**,* pp. 437-455, 2000.

Muller, S. W., Permafrost or permanently frozen ground and related engineering problems, *U.S. Geological Survey Special Report, Strategic Engineering Study 62, 2nd ed.,* pp. 231, 1945.

Mustard, J. F., Cooper, C. D., and Rifkin, M. K., Evidence for recent climate change on Mars from the identification of youthful near-surface ground ice, *Nature, **412**,* 2001.

Mutch, T. A., Arvidson, R. E., Binder, A. B., Guinness, E. A., and Morris, E. C., The Geology of the Viking Lander 2 Site, *Journal of Geophysical Research,* ***92****, No. 28,* pp. 4452-4467, 1977.

NRC Canada., *Glossary of permafrost and related ground-ice terms*, Natural Resources Canada, Technical Memorandum 142, Ottawa, Ontario, 1988.

Parker, T. J., Gorsline, D. S., Saunders, R. S., Pieri, D. C., Schneeberger, D. M., Coastal geomorphology of the Martian northern plains, *Journal of Geophysical Research,* ***98****,* pp. 11061, 1993.

Peacock, J. A., Two-dimensional goodness-of-fit testing in astronomy, *Mon. Not. R. astr. Soc.,* ***202****,* pp. 615-627. 1983.

Péwé, T. L., *Ice-Wedges in Alaska – Classification, Distribution, and Climatic Significance*. Proceedings, 1st International Permafrost Conference, National Academy of Science, National Research Council of Canada, Publication 1287, pp. 76-81, 1966.

Péwé, T. L., *Quaternary Geology of Alaska*. USGS Professional Paper 935, Washington, D.C., U.S. Government Printing Office, pp. 145, 1975.

Pihlainen, J. A. and Johnston, G.H. *Guide to a Field Description of Permafrost*, National Research Council of Canada, Associate Committee on Now and Soil mechanics, Technical Memorandum 79, National Research Council Publication 7 576. 1963.

Plug, L. J., and Helmick, C., Cracktrace, (http://panorama.earthsciences.dal.ca), 2003.

Plug, L. J., and Werner, B. T., Fracture Networks in Frozen Ground, *Journal of Geophysical Research, **106**, No. B5,* pp. 8599-8613, 2001.

Plug, L. J., and Werner, B. T., Nonlinear dynamics of ice-wedge networks and resulting sensitivity to severe cooling events, *Nature, **417***, pp. 929-933, 2002.

Putzig, N. E., Mellon, R. E., and Arvidson, R. E., Thermophysical properties of the Martian south polar region, Sixth International Mars Conference, Abstract 3173, Lunar and Planetary Institute, Houston, Texas, Thermal inertia, 2003.

Scott, D. H. and Carr, M.H., *Geological Map of Mars*, Miscellaneous Investigation Series, Map I-1083, United States Geological Survey, Flagstaff, Arizona, 1978.

Seibert, N. M, and Kargel, J. S., Small-scale Martian Polygonal Terrain: Implication for liquid surface water, *Geophysical Research Letters, **28**, No. 5,* pp. 899-902, 2001.

Scott, D. H., and Tanaka, K. L., *Geological map of the western equatorial regions of Mars*, U.S. Geological Survey Miscellaneous Investigation Series, Map I-1802-A, 101-105, 1986.

Smallwood, R. H., A two-dimensional Kolmorogov-Smirnov test for binned data, *Phys. Med. Biol, **41**,* pp. 125-135, 1996.

Tanaka, K. L., The Stratigraphy of Mars, Proceeding of the Seventeenth Lunar and Planetary Science Conference, Part 1, *Journal of Geophysical Research, **91**, No. B13,* pp. E139-E158, United States Geological Survey, Flagstaff, Arizona, USGS mapping photo, 1986.

Western Regional Climate Center; (http://www.wrcc.dri.edu/index.html), 2003.

Williams, P. J., and Smith, M. W., *The Frozen Earth: Fundamentals of Geocryology*, Cambridge University Press, Cambridge, UK., pp. 306, 1989.

Yoshikawa, K., Origin of the polygons and the thickness of Vastitas Borealis Formation in Western Utopia Planitia on Mars, *Geophysical Research Letters, **30**, No. 12, 1603*, 2003.